Development of a High-Performance Pressure Swing Sorption Process for Natural Gas Dehydration

A Thesis Submitted to the College of

Graduate and Postdoctoral Studies

in Partial Fulfillment of the Requirements

for the Degree of Doctor of Philosophy

In the Department of Chemical & Biological Engineering

University of Saskatchewan

Saskatoon, Saskatchewan, Canada

By

Saeed Ghanbari

Permission to Use

In presenting this thesis/dissertation in partial fulfillment of the requirements for a Postgraduate degree from the University of Saskatchewan, I agree that the Libraries of this University may make it freely available for inspection. I further agree that permission for copying of this thesis/dissertation in any manner, in whole or in part, for scholarly purposes may be granted by the professor or professors who supervised my thesis/dissertation work or, in their absence, by the Head of the Department of Chemical and Biological Engineering or the Dean of the College of Graduate and Postdoctoral Studies in which my thesis work was done. It is understood that any copying or publication or use of this thesis/dissertation or parts thereof for financial gain shall not be allowed without my written permission. It is also understood that due recognition shall be given to me and to the University of Saskatchewan in any scholarly use which may be made of any material in my thesis/dissertation.

Requests for permission to copy or to make other uses of materials in this thesis/dissertation in whole or part should be addressed to:

Dean

College of Graduate and Postdoctoral Studies

University of Saskatchewan

116 Thorvaldson Building, 110 Science Place

Saskatoon, Saskatchewan S7N 5C9 Canada

Abstract

Natural gas is an important energy source for industry, transportation, and homes. It is also used as a chemical feedstock in the manufacturing of plastics and other commercially important organic chemicals. The presence of water in natural gas not only substantially decreases the heating value of natural gas, but also damages the transportation pipeline by corrosion and methane hydrate formation. To dehydrate natural gas, technologies such as absorption, adsorption, condensation, and supersonic separation have been developed. Despite satisfactory results from these technologies, problems with pollution and high processing costs still exist. In this research project, a new pressure swing sorption process for dehydration of gases using biosorbents was developed, which is efficient, environmentally friendly, and economically favorable. Biosorbents were made from flax shives and oat hulls, which had high water vapor sorption capacity and selectivity compared to numerous commercial adsorbents. Six-step and four-step PSA cycles were designed and dual-column pressure swing experiments were conducted. The process worked for over 450 cycles without observable degradation and pipeline-quality dry gas was achieved. Equilibrium and kinetic modeling were performed to further investigate the water vapor sorption characteristics and mechanisms. In addition, the properties of the biosorbents such as sorption capacity, selectivity, pore size and pore volume distributions, surface functional groups, packing and true densities, thermal stability, and biopolymer/elemental compositions were determined. Furthermore, a life cycle assessment was performed to compare the environmental impacts of biosorbent production with those of molecular sieves production. The results showed that both the PSA process and the biosorbents developed in this work are environmentally friendly and efficient, and have a potential for industrial applications such as dehydration of natural gas, biogas, syngas, and air. The value propositions of the developed process are efficient gas dehydration with low negative environmental impacts and a potential market for agricultural residues as industrial biosorbents in this process.

Acknowledgements

Dedication

To my family for their unconditional love and sacrifices for me to achieve my goals.

Table of Contents

List of Figures

List of Tables

Abbreviations and Nomenclature

Abreviations

ADS	Adsorption or sorption step
ATR	Attenuated total reflectance
BE	Binding energy (eV)
BET	Brunauer–Emmett–Teller
BJH	Bopp-Jancso-Heinzinger
BTEX	Benzene, toluene, ethylbenzene and xylene
DFT	Density functional theory
DPR	Depressurization step
FE-SEM	Field emission scanning electron microscopy
FT-IR	Fourier transform infrared spectroscopy
FWHM	Full width at half max
GAB	Guggenhein, Anderson, and de Boer
GC	Gas chromatography
GHG	Greenhouse gas
ID	Identification number
ISAT	Ideal adsorbed solution theory
LCA	Life cycle assessment
LNG	Liquefied natural gas
MS	Molecular sieves
MOF	Metal organic framework
MTZ	Mass transfer zone
NG	Natural gas
NGL	Natural gas liquids
NREL	National renewable energy laboratory
OBOGS	On-board gas generation system
ODE	Ordinary differential equation
P&ID	Piping and instrumentation
PDE	Partial differential equation
PE	Pressure equalization step
PID	Proportional, integral, derivative control
PR	Pressurization step

PSA	Pressure swing adsorption
PSD	Particle size distribution
Pt	Single score unit in LCA
Re	Reynolds number
REG	Regeneration step
RH	Relative humidity (%)
SAPO	Silico aluminate phosphates
SD	Standard deviation
SEM	Scanning electron microscopy
SPSS	Statistical package for social science
SSE	Sum of squared errors in curve fitting
TCD	Thermal conductivity detector
TEG	Triethylene glycol
TGA	Thermo gravimetric analysis
TSA	Temperature swing adsorption
USD	US dollar
VPSA	Vacuum pressure swing adsorption
XPS	X-ray photoelectron spectroscopy

Nomenclature

<u>English Letters</u>

a	Specific surface area of the adsorbent particle (m^2/m^3)
a_m	Molecular projected surface (m^2)
At%	Percentage of atoms on the surface
b	Surface affinity (pa^{-1})
c_a	Model parameter in GAB isotherm (pa)
c_{FW}	Model parameter in Fowler-Guggenhein isotherm
C 1s	Carbon peak in the XPS spectrum
Ca 2p	Calcium peak in the XPS spectrum
C^*	Solid-gas gas phase concentration (mol/ m^3 bed void volume)
C_{gi}	Concentration in the gas phase for component i (mol/m^3 bed void volume)

C_{in}	Concentration in the feed gas (mol %)
C_{vg}	Specific gas phase heat capacity at constant volume (MJ/kmol·K)
C_{ps}	Specific heat capacity of adsorbent (MJ/kg·K)
Co	Initial concentration in the bed (mol/ m^3 bed void volume)
d	Excess heat of liquefaction (kJ/mol)
D_B	Bed diameter (m)
e	Bed voidage (m^3 void/m^3 bed)
e_m	Interparticle voidage (m^3 pore/m^3 particle)
E_a	Activation Energy (kJ/mol)
f_{eq}	Isotherm equation
H	Height of the column (m)
k	Surface affinity parameter in GAB isotherm (pa^{-1})
k_f	Boundary layer mass transfer coefficient (m/s)
k_{LDF}	Linear driving force mass transfer coefficient (1/s)
$\dot{m}_i$	Mass flow rate of component i (g/hour)
Mg 2s	Magnesium peak in the XPS spectrum
M	Mean molecular weight (g/mole)
n	Model parameter in Redhead isotherm
$\dot{n}_c$	Molar flow rate of carrier gas (mol/s)
$\dot{n}_m$	Molar flow rate of methane (mol/s)
$\dot{n}_w$	Molar flow rate of water vapor (mol/s)
$\mathbb{N}_a$	Avogadro number
N 1s	Nitrogen peak in the XPS spectrum
N	Number of sites in multi-site Langmuir isotherm
O 1s	Oxygen peak in the XPS spectrum
P_s	Vapor pressure at a reference temperature (kPa)
P_t	Total pressure of the column (absolute, kPa)
p	Partial pressure of water (kPa)
$\bar{\bar{q}}_i$	Loading on solid adsorbent in the kinetic model (mol/kg)
q^*	Loading on solid adsorbent at equilibrium with the gas phase (mol/g)
q	Experimental water vapor sorption capacity (gram water/gram adsorbent)
q_m	Monolayer sorption capacity (gram water/gram adsorbent)

Q	Standard heat of sorption (kJ/mol)
r	Radial particle coordinate in a cylindrical adsorbent (m)
r_p	Particle radius (m)
R	Universal gas constant (J/mol·K)
t_b	Breakthrough time
t_s	Stoichiometric time
T	Temperature (K)
T_0	Reference Temperature (K)
u_f	Interstitial velocity (m/s)
v_g	Superficial velocity (m/s)
V_F	Flow rate of feed gas (L/min)
V_R	Regeneration gas (L/min)
x_w	Mole fraction of water vapor
x	Relative partial pressure
Y	Mole fraction of water vapor
w	Lateral interactions among adsorbed molecules on the surface (J/mol)
Z	Axial coordinate in bed (m)

Greek Symbols

α	Statistical significance level
Δ	Difference in quantities
ΔH°	Standard heat of sorption (kJ/mol)
μ	Gas phase dynamic viscosity (kg/m/s)
ρ_g	Molar gas phase density (mol/m^3)
ρ_s	Density of solid adsorbent (kg/m^3)

Chapter 1.   Introduction and Literature Review

1.1   Introduction

1.1.1   Research Motivation

Natural gas (NG) entrapped in underground reservoirs is one of the major sources of energy.[1] According to a report from the National Energy Board, Canadian marketable natural gas production is predicted to slightly increase from 416,106 m³/d (14.7 Bcf/d) in 2014 to 489,247 m³/d (15.6 Bcf/d) in 2020. NG is water contaminated during the wellbore production as the gas emerges from reservoirs.[2] Furthermore, NG, mainly comprised of methane, can form hydrates under specific thermodynamic conditions (pressure and temperature) that are suitable for hydrate formation. In addition, the presence of water vapor in NG significantly decreases its heating value. Therefore, natural gas dehydration is mandatory. Several processes were applied in industry for natural gas dehydration including glycol systems, calcium chloride, and temperature swing adsorption.[3] Each process has its own advantages and drawbacks. To be more specific, glycol systems were recently banned as a result of contaminations and environmental issues, while temperature swing adsorption (TSA) is energy intensive and produces considerable amounts of greenhouse gases as temperature is changed using steam or natural gas. Pressure swing adsorption process (PSA) avoids greenhouse gases because pressure is changed instead of temperature. Changing temperature typically involves the burning of fossil fuels. PSA process has not been successfully applied in natural gas dehydration as a result of the limitation of commercial adsorbents. Specifically, the regeneration properties and selectivity of adsorbents are key in natural gas dehydration.[4] Most commercial adsorbents are microporous/mesoporous materials and their regeneration requires external heating and elevated temperatures in addition to pressure change to remove the adsorbed water from their porous structure.[5] The solution could be a high-performance adsorbent that can be easily regenerated. In recent years, biosorbents have been widely used in wastewater treatment and gas/alcohol dehydration, and showed an excellent performance.[6-9] In recent papers by the author, biosorbents developed from flax shives and oat hulls showed a promising performance in natural gas dehydration.[7,10] The biosorbents showed a high performance in terms of sorption capacity, selectivity, and regeneration properties. In this thesis, the performance of these biosorbents in a pressure swing sorption process for natural gas dehydration was studied and various aspects of the process were compared to those of the applied dehydration processes in the industry. Flax shives and oat hulls were rarely studied for

natural gas dehydration and many aspects of the dehydration process such as sorption equilibrium and surface properties need to be studied. Most importantly, their performance in a continuous cyclic operation has not ever been studied. This work was performed to fill these knowledge gaps.

1.1.2 Knowledge Gaps

Based on the literature review, the following knowledge gaps were identified:

1) Among the current technologies for natural gas dehydration, the glycols-based processes cause contaminations and are not considered environmentally friendly. The condensation method is expensive and the operating and capital costs are high. The costly conventional solid adsorbents have moderate to low selectivity and require high regeneration temperatures. Therefore, it is necessary to explore novel cost-effective, high-performance, and environmentally friendly adsorbents.

2) Several agricultural by-products have been studied for alcohol dehydration and demonstrated promising potential for gas dehydration, but more detailed studies on gas dehydration such as natural gas or air have not been performed yet. Moreover, more insights to the sorption kinetic and equilibria must be provided.

3) The dehydration of multi-component gas systems using biosorbents has been reported in the literature; yet, limited knowledge is currently available on the dehydration of natural gas in a PSA system using biosorbents. More information is required in order to potentially implement these biosorbents in industry. The effect of other components such as N_2 or CO_2 on the dehydration of methane needs to be investigated.

4) For the rigorous design of the dehydration process in industry, PSA process under real conditions according to the industry requirements must be thoroughly investigated. Only few works were reported in the literature addressing the challenge of scaling up the PSA process from a lab scale to an industrial scale. In other words, the application of the PSA process using biosorbents in the industry is at their early stage.

5) Despite the development of numerous adsorbents for the PSA process in recent decades, the life cycle assessment of adsorbents' production has been rarely reported in the literature. It is currently unknown how the biosorbent production stands against that of the commercial adsorbents in terms of environmental damages and life cycle.

1.1.3 Hypothesis

It is hypothesized that flax shives and oat hulls can selectively sorb water over methane and dehydrate natural gas in a pressure swing sorption process. It is also hypothesized that they can be used repeatedly in sorption/desorption cycles with negligible degradation.

1.1.4 Research Objectives

The overall objective of this thesis was to develop a novel process for natural gas dehydration using biosorbents and to investigate the fundamentals of selective water sorption by biosorbents. The reason behind choosing biosorbents is the large quantity of adsorbent needed for a large-scale natural gas plant. Furthermore, the sustainable goal of converting wastes into useful materials for industries has been pursued for decades, which was another incentive for this research. In order to address the above-mentioned knowledge gaps, the following objectives are proposed:

1) To develop biosorbents and determine their characteristics for sorption of H_2O, CH_4 CO_2, and N_2 from the respective single component systems.
2) To determine the performance of methane dehydration using the biosorbents.
3) To determine the effect of operating parameters on the equilibria and kinetics of water vapor sorption.
4) To investigate the stable performance of a dual-column continuous PSA process.
5) To perform a life cycle assessment and investigate the environmental impacts of the PSA process and biosorbent production.

1.2 Literature Review

1.2.1 Applied Dehydration Processes in Industry

Natural gas is an important energy source for industry, transportation, and homes. It is also used as a chemical feedstock in the manufacturing of plastics and other commercially important organic chemicals. Natural gas contains primarily methane; however, it also contains varied amounts of water, carbon dioxide, and hydrocarbons, among other components. The presence of water in natural gas substantially decreases the heating value of natural gas.[4] In addition, natural gas must be dried before entering distribution pipelines to control corrosion and prevent the formation of solid hydrocarbon/methane hydrates.[3] To this end, technologies such as absorption, adsorption, condensation, and supersonic separation have been

developed.[3,4,11] As can be seen in Figure 1.1 the dehydration unit is an essential part of the natural gas processing plants.
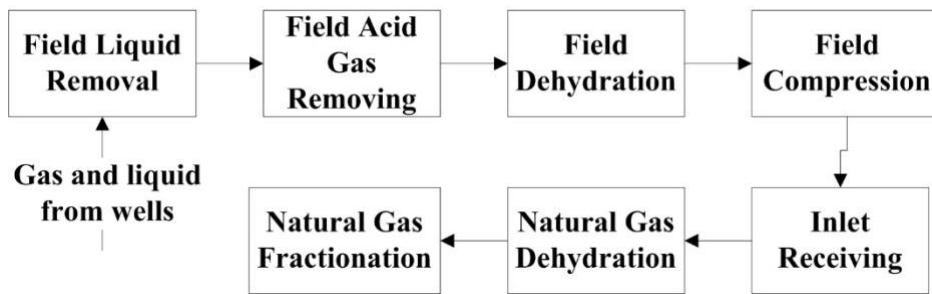
Figure 1.1: Overview of a natural gas processing plant[3].

Pressure swing adsorption (PSA) has been extensively used for air drying and gas separation since 1948 because the pressure can be changed easier and faster. Furthermore, the operating temperatures are lower than those of the temperature swing adsorption (TSA) process, and the control of PSA process is easier.[12] The main challenges in PSA process are selectivity of the adsorbents and gas compression or evacuation costs.[13-19]

Opportunities exist to further explore novel strategies, materials, and approaches for the dehydration of natural gas. In recent years, biosorbents demonstrated promising performance in the dehydration of alcohols.[8,9,20-26] Tajallipour et al. used canola meal to dehydrate ethanol and investigated the effect of operating parameters in ethanol dehydration a PSA process.[9] Ranjbar et al. demonstrated that canola meal was also able to dehydrate ethanol after protein extraction and had a higher selectivity towards water vapor compared to untreated canola meal.[8] The authors concluded that lignocellulose materials similar to canola meal have suitable surface functional groups for water (polar molecules) sorption. These promising results attracted the attention of the author to the potential application of biosorbents in natural gas dehydration. Flax shives and oat hulls, byproducts from agricultural industry, are lignocellulose materials; hence, they have the potential to be used in a PSA process to effectively dehydrate non-polar gases such as natural gas. However, to the best of the author's knowledge, the research has not been reported prior to this work. In recent decades, a number of successful systems have been designed and implemented.[27] The most strategic dehydration methods are absorption, adsorption, condensation, and supersonic separation. Eimer did a comprehensive review of glycol based absorption process.[2] Michal Netušil et al. investigated the advantages and drawbacks of the condensation method in detail.[11] In recent studies, new technologies using supersonic nozzles have been developed suggesting a new approach to gas dehydration, which is capable of selectively removing water from high-pressure natural gas streams with a

high recovery.[28,29] The shortcomings of each separation method, however, limit its application in industry. These limitations are discussed in the following paragraphs.

Referred to as the workhorse of the gas treating industry, absorption of H_2O is the first dehydration method ever applied in industry using triethylene glycol (TEG). Glycol based absorption process takes place in an absorption column where TEG and humid natural gas are brought in contact using trays or packings. The water rich glycol stream is regenerated in a distillation column and recycled back into the absorber column in a closed system with makeup glycol to account for losses in the system.[4] Numerous scholars have cited the operating issues in these columns such as high energy requirements of the process, glycol foaming and loss in the columns, and contaminations that are absorbed by glycol and accumulated in the system over time or released into the atmosphere.[4,11,27,29] According to the authors, energy costs (reboiler and condenser duty) account for more than 70% of the process total operating cost. Another inevitable issue in this process is contaminants in the glycol solution that cause fouling and corrosion in process equipment.[29] According to the author, salt build-up leads to precipitation in the regenerator where water content is at its lowest, which could not be even prevented using solution filters. Furthermore, FeS and Fe_2O_3 used in this process also cause corrosion issues.[30] The authors asserted that black solution was also caused by absorbed heavy hydrocarbons from the feed gas.

As for the condensation method, it employs gas cooling in order to turn water vapor into liquid water so that they can be separated from the gas phase as a liquid phase. This process is typically applied for simultaneous dehydration and Natural Gas Liquids (NGL) recovery.[3] Likewise, high operating costs is a disadvantage of this process, especially in large industrial plants. In addition, a considerable amount of methane hydrate inhibitors such as methanol must be used in the cryogenic operations.

Another method is adsorption of water by solid desiccants such as molecular sieve, silica gel, and alumina, which are commonly used in industry. In this method, single or multiple columns work periodically following the main procedure in a TSA process. While this method sounds superior to previous ones, the relative costs of the adsorbents and their regeneration process could be considered as one of the current challenges in industry. The recovery of these processes are very low and are preferably applied in cases were high purity products are desired.[3] Since these commercial adsorbents are microporous, water desorption during the regeneration step is diffusion-controlled and requires elevated temperatures.[5] In addition, the

adsorbents continuously experience significant temperature fluctuations during the cyclic operation in natural gas dehydration using TSA process and lose their adsorption properties over time.[3] That said, the development of cost-effective high-performance adsorbents and processes is necessary.

Overall, these challenges in the dehydration industries could be addressed by research and development. Absorption by TEG is nowadays the most widely used method, in which a dew point T_{dew} of around −10 °C (below natural gas pipeline specification) is usually achieved.[11] Adsorption, on the other hand, requires a higher capital investment and vast space for equipment and apparatus.[4] According to the literature, the capital cost of an adsorption system is 2 - 3 times higher than that of a glycol system.[31] As a result of complex cooling systems and operational problems associated with methane hydrates, the condensation method is mostly considered unfavorable from the standpoint of energy consumption. According to Karimi et al.[28], similar issue was found in the supersonic nozzles method, which is only applicable for small scale plants; nonetheless, high selectivity and recovery can be simultaneously achieved in these systems. Therefore, more research is required to explore a process or methodology by which high selectivity and recovery could be achieved at reduced costs. Among these methods, PSA and TSA have the most potential to meet the current industrial needs; yet many challenges need to be overcome to apply a new process in industry. This project was completed to fill some of these knowledge gaps and investigate the technical and economic feasibility of a PSA process for natural gas dehydration.

1.2.2   Pressure Swing Adsorption Process

Gas molecules are adsorbed either on the surface of adsorbents by physical or chemical bonds based on the functional groups on the surface of the adsorbents or inside the porous structure of adsorbents based on adsorption mechanisms such as micropore diffusion and capillary condensation.[5,32,33] The amount adsorbed and the selectivity of adsorbents toward different components in the gas phase depends on the thermodynamics and kinetics of the gas-solid system. That being said, adsorption can be categorized as equilibrium-controlled (separation is based on gas-solid equilibrium - a thermodynamic property) and kinetics-controlled (separation is based on different diffusion rates of the species inside the solid particles - a kinetic property).[33] The adsorption equilibrium is analyzed using isotherms at different pressures. Adsorption kinetics is also dependent on temperature and pressure in addition to the porous structure of adsorbents. Therefore, the adsorption capacity and

selectivity of adsorbents can be manipulated by controlling these operating parameters. On the other hand, some of these solid adsorbents must be frequently replaced with fresh adsorbents to achieve a required product purity. In industry, it is not reasonable to discard the adsorbent and use fresh adsorbent once they are saturated or degraded. For a continuous industrial process, a cyclic operation is performed by manipulating the adsorption equilibrium and/or kinetics, that is executed by changing either temperature or pressure.[5,33] The TSA and PSA processes were invented based on these principles. Cycle design is key to these processes and determines the efficiency and economics of the process. The PSA process is advantageous to the TSA process since changing pressure in general is easier and faster than changing temperature[5,33]; however, the regeneration properties of adsorbents is sometimes a big limitation as microporous adsorbents cannot be regenerated by just changing the pressure at low to moderate temperatures. Sometimes elevated temperatures are required to remove the adsorbed components and regenerate the adsorbents.[34]

The PSA process has been successfully applied for a large variety of applications over the years: air separation[35-37], on board gas generation system (OBOGS)[38], CH_4 upgrading[39-41], noble gas (He, Xe, Ar) purification, hydrogen purification[42,43], and so on. The PSA process is usually designed based on a popular cycle known as the Skarstrom, which is broadly used in industries, and was firstly employed for air drying.[33] This cycle is briefly described in the following paragraph. The following four steps make up the Skarstrom cycle: 1) pressurization, 2) feed or adsorption, 3) blowdown, and 4) purging. These four steps are applied in a cyclic operation to continuously run the process and separate the components. During the pressurization step, the column is pressurized to the desired level suitable for adsorption of target species, while the less selectively adsorbed species in the gas phase at the product's end is being enriched. Medium to high pressure adsorption happens during the feed or adsorption step delivering high-purity raffinate product. In the blowdown step, the column is depressurized to atmospheric pressure. During the purging step, which may be conducted under vacuum, desorption occurs at low pressures removing the gases present in the void volume of the column and the adsorbed species.[33] During the purge step, adsorbents are regenerated by feeding a stream (usually a part of the product of the adsorption step) to the column at lower pressure and recovering an output gas enriched in the adsorbed component.

Aiming to increase the productivity of the process, desorption under vacuum (vacuum pressure swing adsorption, VPSA) has been further developed.[37] In a VPSA unit, higher efficiency and product purity is traded for higher energy requirements and cost. In another

work, by adding a pressure equalization step in the basic Skarstrom cycle, the ESSO research successfully increased the recovery of the process.[39] In short, the research on improving this process is still ongoing and such new technologies hold promise for the natural gas dehydration industry. Pahinkar et al. developed a novel TSA process for natural gas upgrading.[44,45] They used micro-channels to enhance the heat transfer between the gas and solid adsorbents. In another work, Moreira et al. creatively combined the TSA and PSA processes and developed a cryogenic pressure-temperature swing adsorption process for natural gas upgrading.[46] They achieved high product purity and recovery; nonetheless, the process is very costly as a result of cryogenic operations and gas compression (80 bar) costs. The process seems impractical since natural gas typically emerges from the reservoir at a pressure between 35 to 60 bar.[3,4] Further gas compression to 80 bar in order to separate CO_2 is not a reasonable approach. Several works were published on biogas upgrading mainly focused on the separation of CH_4 and CO_2.[47-49] Carbon molecular sieves showed a great performance and seems to be the best adsorbent for this application. Augelletti et al. focused their work on the configuration of the PSA process to improve the product purity and recovery.[47] In a similar work, Yousef et al. managed to separate CO_2 from methane in a low temperature PSA process.[49]

A number of papers were published on the dynamic simulation and numerical modeling of PSA/TSA processes. Bhatt et al. used ASPEN Adsim and did a dynamic simulation of dual-reflux PSA process for the separation of CO_2 from N_2.[50] In another work, Erden et al. investigated the feasibility of high-purity CO_2 production from dilute feed streams.[51] Shi et al. focused their work on a detailed heat and mass transfer study of PSA process and used numerical math to model the process.[52] Their results provided valuable information about the PSA process and the transport phenomena.[50-52] Similarly, Kim et al. developed a model for CH_4/CO_2 separation in a PSA process and substantiated their experimental data using the model.[53] Feasibility study of natural gas dehydration in a PSA process, however, has not been reported in the literature.

1.2.3 Conventional Adsorbents

Adsorbents could be considered as the heart of the adsorption process.[54] To reach high product purity and recovery, adsorbents must have suitable surface properties and pore volume/size distribution.[5,32] Another desired property obviously is a long lifetime with a stable performance. It is not economically favorable to shut down the process in order to fill the adsorption columns with fresh adsorbents or run two duplicate systems in parallel. The most

common adsorbents used for dehydration are activated alumina, silica gel, and molecular sieves. A great deal of research has been done on the synthesis of advanced materials such as metal organic frameworks (MOFs) or silico aluminate phosphates (SAPOs)[55-60]; however, these adsorbents are so expensive and impractical for industrial applications. In addition, high temperatures are required to regenerate them, which adds a heavy economic burden to the process.[61] In addition, the technology for the large-scale production of these high-tech materials is still immature.

Silica gel is an excellent adsorbent for dehydration, which has been extensively used in dehydration industries.[62] The positive features of silica gel are high equilibrium capacity and moderate regeneration temperature (150-200 °C). Both natural and synthesized zeolites are considered as successful adsorbents for water adsorption in the literature.[57,63] Samira Karimi et al. investigated the water adsorption capacity of natural zeolite.[64] A bioethanol purification of 99.9% was achieved. Nonetheless, if one examines their process conditions, high-temperature regeneration and low selectivity were major drawbacks. Zeolite must be activated at a high temperature (300-400 °C) for at least 2-3 hours prior to adsorption under vacuum condition (p < 15 Pa).[65] Moreover, using synthesized zeolite in industry may add to the overall cost depending on the type of zeolite. In summary, despite the development of adsorbents to date, industry is still calling for cost-effective environmentally friendly adsorbents with a satisfactory performance.

1.2.4 Biosorbents

Agricultural by-products (or biomass) are mainly lignocellulose materials with useful properties, and a great deal of research has been performed to convert them into useful adsorbents for wastewater treatment and gas separation.[8,9] Numerous papers were published on their suitable properties for water vapor sorption and gas/alcohol dehydration.[7-10,20,24,27,66-69] Promising results were achieved using agricultural residue such as canola meal, flax shives, oat hulls, barley straw, and corn meal. However, one main concern about biomass material is their stability, especially at higher temperatures.

It has been numerously reported in the literature that lignocellulose materials similar to flax shives and oat hulls are mainly macroporous and have hydroxyl and carboxyl functional groups on their surface.[7,8,10,67] They are made of cellulose, hemicellulose, lignin, and a small percentage of protein and other compounds. Their suitable surface functional groups are related to these building blocks, the details of which have not been reported yet. In Saskatchewan,

which is ranked among the top Canadian provinces in agricultural industry, flax shives, oat hulls, and canola meal are easily available at a large scale and low price. According to the 2016 market reports in the industry, there is an enormous opportunity for the future of the biomass industry in Canada. The domestic biomass pellet market sharply progressed in the last two years. In summary, the lignocellulose materials demonstrated a great potential for natural gas dehydration; however, such investigation has not yet been performed. This research project was completed to fill this gap.

1.2.5 Equilibrium and Kinetic of Water Sorption

Equilibrium and kinetic of sorption are two critical factors affecting the performance of a sorption process. A significant deal of research has been performed to investigate the adsorption equilibria of water vapor, methane, and carbon dioxide on various types of zeolite molecular sieves[36,60,63,70-72], silica gel[60,62,73], alumina[74,75], and activated carbon[17,58,61,76-81]. Wang et al.[72] investigated the adsorption equilibrium of water vapor – carbon dioxide binary systems and concluded that the ideal adsorbed solution theory (ISAT) can better predict such binary systems with non-ideality than the Toth model. In another work, Wang et al.[60] focused their study on the adsorption equilibrium of pure components on silica gel granules. The authors found that silica gel adsorbs methane, carbon dioxide, and water vapor. They used the Toth isotherm to describe these systems and investigated the effect of temperature on the adsorption equilibrium. In a similar study, Desai et al.[74] did an extensive isotherm study on several grades of activated alumina. It was found out that the equilibrium behavior of the system and isotherm selection heavily depends on the nature of the adsorbents and the regeneration conditions. These studies suggest that the adsorption process can be improved by in-depth understanding of the adsorption equilibrium.

A great deal of research has been performed on the kinetic study of sorption process in packed beds.[15,82,83] Teo et al. investigated the kinetic of water adsorption on aluminum fumarate.[84] In a similar study, Jribi et al. examined the kinetic of CO_2 adsorption in a temperature swing adsorption process.[79] Both studies suggests that diffusion in the microporous structure of the adsorbents was the dominating mass transfer mechanism. Mrowiec et al. focused their study on the equilibrium and kinetic of water vapor adsorption by SiO_2-$CaCl_2$ composites.[73] They reported the effect of operating parameters on the overall mass transfer coefficient.[85] In another study, Liu et al. simulated the dehydration of isopropyl alcohol in a pressure swing adsorption process.[85] Similarly, linear driving force (LDF) model was used.

They studied the effect of cycle time, purge to feed ratio, and other parameters on the concentration and loading profiles. LDF kinetic model has been widely used in the modeling of adsorption processes in a packed column.[32,86,87] In numerous works, authors used this model to study the mass and heat transfer in swing adsorption processes for biogas upgrading, carbon capture, and methane purification.[17-19,88] Several authors also modified the common LDF model for a better prediction of their specific system.[76,81,89,90] It was reported in some works that their modified LDF model showed better agreement with experimental data. Several advanced kinetic models were discussed by Ruthven, which adds more complexity to the problem.[33] Overall, kinetic study provides information on the nature of the sorption process and assist engineers in the design and development of swing sorption processes.

It is to note that gas dehydration by lignocellulose materials could be involved in adsorption and/or absorption. Considering the nature of the biosorbents used in this work (flax shives and oat hulls), water removal by the biosorbents could be more reasonably considered to be "Sorption", which may include adsorption and absorption. This is a scientific term that has been widely used in the literature for the sorption of water vapor by cellulose, hemicellulose, pectin, and similar biopolymers, which are the main components in the composition of biosorbents and similar bio-based materials. Thus, this term "sorption" and its respectively derived term "sorb", and so on are used where applicable in the following chapters associated with the results and discussion about water vapor in this thesis. The term "adsorption" is used when discussing the nonpolar gases such as methane, carbon dioxide, nitrogen, and helium.

1.3   Thesis Layout

Starting with the theory, Chapter two explains the equilibrium and mass transfer theories related to this project. Chapter 3 illustrated the materials and methodologies that were used in this project for the experiments and the characterization of the biosorbent materials. Chapter 4 illustrated the preparations and characterization results of the biosorbents as one of the important components in the project. Next, the foundation of the work was reported in Chapter 5 where the sorption of natural gas components by flax shives and oat hulls (biosorbents) was investigated in single-component (water vapor, methane, carbon dioxide, nitrogen) and multi-component systems (e.g. methane and water vapor). The water vapor sorption capacities and selectivities at various operating conditions were determined using breakthrough curve experiments and mass balance in a single column apparatus. The

regeneration properties and stability of the biosorbent developed from flax shives were investigated. Furthermore, the effects of operating parameters on the performance of the flax shives were reported. A second material, oat hulls, is also investigated and compared with flax shives from different perspectives. Chapter 6 presents the water sorption isotherm modeling results. Isotherm data, and the analysis on the water vapor sorption mechanisms were reported in this chapter. Chapter 7 presents the kinetic modeling results where the experimental breakthrough curves were simulated using the linear driving force model and the values of mass transfer coefficients were reported and discussed. Based on the results achieved, a bench-scale system was built, continuous gas dehydration in a cyclic automated dual-column system under simulated industrial conditions was investigated, and the results were reported in Chapter 8. Different cycle designs were investigated and the effect of operating parameters on the process was determined. The stability and feasibility of natural gas dehydration in a PSA process were analyzed. Finally, Chapter 9 reports the life cycle assessment of this dehydration process. The focus of the life cycle assessment was on the environmental damages caused by the production of biosorbent, which were compared with those of molecular sieves production. The final chapter concludes the thesis and discusses the significant scientific findings, the limitations of this work, and future prospects of this project.

Chapter 2.   Theory

2.1   Sorption Isotherm Models

The equilibrium between gas-liquid-solid phases is a function of thermodynamics of the system, the properties of gas, liquid, and solid phases, and the chemical/physical interactions among molecules in these phases. Mathematically, this equilibrium is represented using isotherm models, each of which has been developed based on different assumptions for different gas-liquid-solid systems depending on their properties and conditions. Isotherm study is a useful mean to acquire information about a sorption system such as monolayer sorption capacity, surface affinity towards sorbates, heat of sorption, etc. In the water uptake of this work, water adsorption and absorption can take place at the same time and the portions of water adsorption and absorption can vary at different equilibrium water concentrations in the gas phase. In addition, the structures of natural materials flax shives and oat hulls used in this work are complex. These make it very challenging to quantify the portions of adsorption and absorption at each equilibrium data point. Thus, this work used the approach combining both adsorption and absorption capacities. Such methodologies and isotherm models have been popularly and commonly used to describe water sorption isotherms of lignocellulose materials such as cellulose, hemicellulose, corn starch, wheat starch, and several fruit peels. Such works have been reported in reputable journals and books.[32,103-105,118,121]

In this section, a number of sorption isotherm models for gas-solid sorption systems is illustrated, which was considered in this research and was fitted on the experimental data.

2.1.1   GAB Model

The GAB (Guggenhein, Anderson, and De Boer) model describes multilayer sorption isotherms (type II and type III) and was developed as a refinement of BET (Brunauer–Emmett–Teller) and Langmuir theories in order to extend the narrow validity range of the BET equation (relative partial pressure or p/p_s is between 0.05 to 0.35).[32] In the GAB model, it is postulated that the second layer and superior layers have identical state of sorbate molecules and the heat of sorption on the second and subsequent layers is lower than the heat of liquefaction. The isotherm constant, k, is introduced as a measure of chemical potential standard differentiation between molecules in the second layer and subsequent layers of sorbed atoms on the surface.[32] The shape of this isotherm is more convex than that of the BET equation in the high range of relative pressure, and its validity range is up to $p/p_s = 0.9$.[32] The model equation is shown below:

$$\frac{q}{q_m} = \frac{c_a k x}{(1 - kx)(1 + (c_a - 1)kx)} \tag{2.1}$$

where $x = p/p_s$ and the model parameters p, p_s, q, c_a, k, and q_m are the partial pressure, vapor pressure, sorption capacity, a model parameter, surface affinity, and monolayer sorption capacity, respectively. The GAB model provides information about the excess heat of liquefaction that the second and subsequent layers release during the multilayer sorption.[32] This excess heat d is associated with the constant k through Eq. 2.2:

$$k = \exp\left(\frac{d}{RT}\right) \tag{2.2}$$

Then d can be determined as follows.

$$d = RT \ln k \tag{2.3}$$

2.1.2 Redhead Model

The Redhead model has been successfully used to describe type II and type III isotherms such as the adsorption of argon on alumina, neopentane on silica, and nitrogen on anatase.[5,32] This type of isotherm describes multiplayer sorption. Similar to the BET and GAB models, the Redhead model provides the information of monolayer sorption capacity; however, it extends the narrow range of validity of the BET equation ($x = p/p_s$ between 0.05 to 0.35; where p is partial pressure and p_s is vapor pressure.).[32] Thus, it finds wide applications. This model has two fitting parameters compared to the GAB model with three parameters. Using the Redhead model, monolayer sorption capacity can be determined, based on which the specific surface area of a material can be determined.[5,32] The model is as follows:

$$\frac{q}{q_m} = \left[\frac{(2n - 1)x}{(1 - x)}\right]^{\frac{1}{n}} \tag{2.4}$$

where q and q_m are total and monolayer sorption capacities, respectively; x is relative partial pressure, p/p_s, and n is a model fitting parameter.

2.1.3 Fowler-Guggenhein Model

The Fowler-Guggenhein (F-G) model has been effectively used to describe Type I and linear isotherms. It was derived from the general Gibbs isotherm equation considering the van

der Walls equation of state to describe the surface or solid phase.[32] This model was also derived from the statistical thermodynamics approach by Rudzinski and Everett.[5,32] Importantly, this model considers lateral interactions among the sorbed atoms and can predict the two dimensional condensation. The model is as follows[32]:

$$bp = \frac{\theta}{1 - \theta} \exp\left(-c_{FW}\theta\right) \qquad (2.5)$$

where p is partial pressure of water vapor, b is surface affinity towards water vapor, c_{FW} is model parameter, and θ is the surface coverage. The model parameter c_{FW} can take a value from 0 to 7.[32] This parameter is related to the interactions among sorbed molecules through Eq. 2.6:

$$c_{FW} = \frac{zw}{R_g T} \qquad (2.6)$$

where z is the coordination number, w is the interaction parameter; R_g is the universal gas constant; and T is absolute temperature. The interaction parameter is a measure of interaction forces among the sorbed molecules on surface. A positive value for w indicates attraction among the sorbed molecules on the surface, while a negative value indicates repulsion. The value of this parameter can provide further information on the strength of these interactions and/or bonds among the sorbed molecules on the sorbent surface, while the surface affinity parameter (b) provides info on the interaction forces among the sorbed molecules and the surface of sorbent materials. Langmuir theory assumes that sorption is localized and the sorbed molecules on each cite do not interact with each other; however, the F-G model considers these interactions as an attempt to bring the model assumptions closer to the real situation with practical solids.

2.1.4   Linear Model

For an ideal surface in dilute systems, a linear relationship is assumed between the sorbed phase pressure and the number of molecules of sorbate adjacent to the surface according to the general Gibbs equation of state describing the sorbed phase.[32] In other words, the sorbed phase pressure is linearly proportional to the pressure in the gas phase adjacent to the surface at equilibrium. As this correlation is not useful as to relate to the sorption equilibrium data, the Gibbs equation of state[32] is integrated at constant temperature using the linear equation for the sorbed phase pressure. The result is the linear isotherm obtained for dilute systems correlating the sorbed amounts q and the partial pressure of sorbate p, the slope of which is called the

Henry constant, K_L.[32] A form of this linear isotherm is the simplest form of isotherm equations, which takes the following form[32]:

$$q = K_L p \tag{2.7}$$

The application of this isotherm is in dilute systems were the surface of the sorbent material shows ideal behavior. The standard heat of sorption can be determined using the van't Hoff equation based on equilibrium constants of b_1, and b_2 obtained at different temperature T_1 and T_2:

$$ln\frac{b_2}{b_1} = \frac{-\Delta H^{\circ}}{R}\left(\frac{1}{T_2} - \frac{1}{T_1}\right) \tag{2.8}$$

where R, and $-\Delta H^{\circ}$ are the ideal gas constant and standard heat of sorption, respectively. In this work, the Henry constant K_L obtained from the linear isotherm modeling results and were used instead of b values.

2.2 Mass Transfer and Dynamic Modeling

Molecules in the gas phase are transported from the gas phase to the outer surface of solid sorbent, and then within the porous structure of the particles, and finally onto the active surface of the sorbent material where sorption takes place. Mass transfer rates throughout this transport process is critical to the performance of sorption. To study the mass transfer, the linear driving force model was used to obtain useful information on the water vapor sorption by flax shives. The mass transfer coefficients are typically obtained and their values are discussed and used to investigate the sorption process. In the following sections, the model equations, assumptions, and parameters that were used in this research are illustrated.

2.2.1 Model Equations and Assumptions

To present the model equations, the common assumptions that have been extensively made in the literature are firstly presented[33]:

1) Isothermal system
2) Ideal gas law
3) No axial dispersion
4) Two component system (carrier gas and water vapor)
5) Linear and GAB isotherm models depending on the experimental conditions

16

6) Cylindrical shape for the biosorbent

The temperature of the water sorption column was controlled using an oil jacket. Thus the breakthrough experiments were performed under isothermal conditions and the effect of temperature on the sorption kinetic was investigated at different temperatures in aid of the modeling results. The maximum pressure in the experiments was 5 bars and the ideal gas law can be used. It is reported in the literature that mixing effects and axial dispersion are negligible when the height of a packed column L is larger than fifty times of the diameter of sorbent particle d_p (L> 50d_p).[33] That means axial dispersion is negligible if the column is long enough. In this work, the ratio of L/d is about 500 which is much higher than 50. Thus the assumption of negligible axial dispersion could be acceptable in this work. The flax shive particles are approximately cylindrical as seen in the photos and SEM images; hence, this particle shape was considered in the modeling.

The sorption process in packed beds is typically modeled by a system of coupled PDEs, ODEs, and algebraic equations. In his book, Ruthven[33] discussed the fundamentals of this process and derived all the equations governing the system. The PDE equation is gas phase mass balance taking the following form based on the above assumptions:

$$\frac{\partial C_{gi}}{\partial t} = -u_f \frac{\partial C_{gi}}{\partial z} - \frac{\rho_s}{e} \frac{\partial \bar{\bar{q}}_i}{\partial t} \tag{2.9}$$

where C_{gi} is the concentration of component i in the gas phase (mol/bed void volume), u_f is the interstitial velocity (m/s), $\bar{\bar{q}}_i$ is the average loading of the biosorbent (mol/kg biosorbent), e is the bed voidage, z is the axial distance (m), ρ_s is the bulk density of the biosorbent (kg/m^3), and t is time (s). The first term in the left-hand side of the equation is the accumulation term, the second term is the convention term, and the last one is the sorption term. The boundary and initial conditions for this PDE during the sorption step are:

$$C_{gi}\big|_{t=0} = C_o \,, C_{gi}\big|_{z=0} = C_{in} \ \ at \ \ t > 0 \tag{2.10}$$

The bed is initially free of moisture so C_o for water vapor is considered 10^{-6}. The concentration of methane and water vapor in the feed gas at $z = 0$ are known (C_{in}). The term $\frac{\partial \bar{\bar{q}}_i}{\partial t}$ represents the rate of sorption term in the equation, which is discussed in the next section.

2.2.2 Linear Driving Force Model for the Rate of Sorption

Since only water vapor was sorbed by the biosorbent, the subscript i was removed from the rate of sorption term (this term is assumed zero for methane). The linear driving force (LDF) is one of the most common expression used for the rate of sorption term in the equation because of its simplicity and reasonable results, which takes the following form[33]:

$$\frac{\partial \bar{\bar{q}}}{\partial t} = (1 - e)k_{LDF}(q^* - \bar{\bar{q}}) \tag{2.11}$$

where q^* is the biosorbent loading at equilibrium with the gas phase, and k_{LDF} is the effective mass transfer coefficient (1/s). This term will replace the sorption term in the right-hand side of Eq. 2.9. The term $(q^* - \bar{\bar{q}})$ is correlated with the respective water concentration term in the gas phase based on the suitable form of isotherm under different operating conditions.

2.2.3 Pressure Drop

Ergun equation is used to estimate the pressure drop along the axial coordinate.[5] This equation is also used to estimate the bed voidage at various operating conditions using the measured pressure drops from experiments.

$$\frac{\partial p}{\partial z} = -\mu u_f \frac{0.15(1 - e)^2}{4r_p^2 e^3} - 1.75 \times 10^{-3} M \rho_g u_f^2 \frac{(1 - e)}{2r_p e^3} \tag{2.12}$$

where μ is the viscosity of the gas phase, r_p is the particle radius, and M is the average molecular weight of atoms in the gas phase. The above-mentioned system of PDEs and ODEs was solved using finite difference numerical methods. The PDEs were converted into a system of coupled ODEs using the method of lines and ASPEN Adsim (Aspen Technology, Inc. Massachusetts, USA) solvers were used to solve the system of ODEs. Parameters estimation and optimization were performed using the line search method in the ASPEN Optimization toolbox. Sum of squared errors were minimized and R squared was used to check the goodness of fit.

Chapter 3.   Materials and Methods

The aim of this chapter is to illustrate all the materials and methodologies that were used in this research project to investigate the targeted knowledge gaps.

3.1   Biosorbents and Gases

The main biosorbent used in this work was flax shives, which were supplied from Schweitzer-Mauduit Canada, Inc., Winkler, Manitoba. Then, to investigate the effects of different batches of feedstocks and compare different agricultural byproducts, a new batch of flax shives was obtained from Biolin Research Inc. Saskatoon, Saskatchewan, and two batches of oat hulls (2017 and 2018) were provided by Richardson Milling Saskatoon, Saskatchewan. The samples were ground, oven dried at 105 °C for 24 hours, and sieved using standard Canadian Sieves. No chemical treatment was performed. Biosorbents with two different particle size ranges of 0.425 – 1.18 mm, and 1.18 - 3 mm were used in this work.

To compare the performance of these two types of biosorbents with commercial adsorbents, silica gel and molecular sieves were investigated. Commercial grade silica gel (Sigma-Aldrich, 5 mm beads, USA) and molecular sieve 3A (EMD Millipore, 5 mm beads, Ontario, Canada) particles were purchased. These adsorbents were dried in oven at 105 °C for 24 hours prior to packing into the column.

Ultra-High Purity (5.0) CH_4, CO_2, N_2, and He gases were purchased from Praxair Canada Co. Compressed air (laboratory grade 3.5) was also purchased from Praxair and used for air drying experiments.

3.2   Characterization of the Biosorbents

3.2.1   Particle Size Distribution

The particle size distribution of the biosorbents was measured by a particle size analyzer (Mastersizer 2000, Malvern Instruments, USA) via a laser diffraction method. The shives are cylindrical with a ratio of length to diameter being approximately 2. The shape factor was calculated by the device program based on the L/D ratio provided. Oat hulls are almost cylindrical as well; but their morphology is more amorphous than that of flax shives. Five grams of sample were loaded onto the feed chamber, and the feed injection rate was 1.6 g/s. Air was the gas used in the device to maintain a constant flow of particles through the analysis tube and sensor assembly. The particle size distribution was reported on a volume basis. In

addition, interparticle voidage and true density of the biosorbent were measured using Quantachrome multi pycnometer (Anton Paar USA Inc.). The bulk density of biosorbents were determined using ASTM D-1895.[91]

3.2.2 Composition of the Biosorbents

The ash, moisture, and volatile contents of flax shives were determined by proximate analysis according to the ASTM 3173-87 (2003), ASTM 3174-04 (2004), and ASTM D 3175-07 (2007) methods, and ultimate analysis using a PerkinElmer Elemental CHNS analyzer.[8,9]

3.2.3 Brunauer-Emmett-Teller (BET) Surface Area

The surface area of the biosorbents was analyzed by a commercial pore size analyzer (Micromeritics Inc. ASAP 2020) using nitrogen gas adsorption at liquid nitrogen temperature (74.15 K). The biosorbent particles (0.425-1.18 mm) were first degassed at 385 K under a vacuum of 500 µHg for 12 h. The specific surface area was determined by the BET method via standard nitrogen adsorption method.

3.2.4 Field Emission Scanning Electron Microscopy (FE-SEM)

The morphology of the biosorbents has a substantial effect on their sorption performance. Thus, it was analyzed by FE-SEM in this work. Hitachi SU8010 (Japan, Tokyo) ultra-high resolution (1.00 nm) FE-SEM was used to investigate the morphology and structure of the fresh and reused biosorbents after as many as 70 complete sorption-desorption cycles. Several images were taken at various magnifications. Five nanometer chromium was used to coat the biosorbents samples.

3.2.5 Optical Microscopy

Liquid water transport through flax shives was monitored using an Olympus BX51M optical microscope with a high-speed camera (Olympus K-TV0.63XC 7J19174, Tokyo, Japan) and a high-power illumination source (EXFO X-Cite series 120). For visualization, 5 µL of blue food dye (Assorted Food Colors & Egg Dye; McCormick & Co., Inc., Hunt Valley, MD) was mixed with 95 µL of deionized water. Then, 10 µL of the diluted blue dye solution was loaded to the edge of flax shive sample placed on glass slide substrates. The microscopic images were taken in time intervals over several minutes after initial addition of dyed water.

The water transport within flax shives was analyzed through optical microscopic images using ImageJ (NIH) software.

3.2.6   Fourier Transform Infrared (FT-IR) Spectroscopy

Surface functional groups are essential in the sorption process. Surfaces with different functional groups have affinity towards different components, which determines the selectivity of a sorbent towards a target component. Flax shives and oat hulls are novel sorbents for gas dehydration and limited information is available about their surface properties. FT-IR spectra of biosorbents were obtained with VERTEX 70/70v (BURKER Inc. Cincinnati, Ohio) using an attenuated total reflectance (ATR) sampling accessory. The sample was vacuum dried at 105 °C and 2 µm Hg. The spectra were recorded over the range of $4000 - 400$ cm^{-1}. Thirty two scans were performed with a resolution of 4 cm^{-1} and a corrected baseline. The peaks were identified using the IRbud commercial software.

3.2.7   X-ray Photoelectron Spectroscopy

In addition to the FT-IR spectroscopy, X-ray photoelectron spectroscopy (XPS) has widely been used to quantify the functional groups on the surface of the materials. In this work, an AXIS Supra photoelectron spectrometer (Kartos Analytical CO.) was used to obtain the XPS spectra of the biosorbents. Wide scans were performed at different spots with a spot size of 250 µm $\times$ 250 µm. The device was operated at a very low vacuum (approximately 3.12×10^{-10} kPa). The sample was vacuum dried at 105 °C and 2 µmHg for 48 hours in a sealed sample tube using ASAP 2020 (Micromeritics) system; and then were loaded onto a stainless steel stub. In order to minimize moisture sorption from air, the sample was quickly mounted on the device sampling and degassed under vacuum again for another 30 minutes.

3.3   Sorption Experiments

3.3.1   Single-Column Experiments

A cylindrical column was used to study the sorption of natural gas components by the biosorbents. In these single-column experiments, the effects of key process parameters on the system were analyzed. Figure 3.1 shows the schematic of a single-column apparatus used in the experiments. The flow rate and composition of feed gas were adjusted using mass flow controllers and pressure regulators connected to the gas cylinders. The feed gas was humidified in the humidifier column (E-1) containing deionized water and its relative humidity was

adjusted by mixing this humid gas with a portion of the dry gas using two metering valves (Figure 3.1, V-2, and V-4). The humidity of the gas was measured using high accuracy relative humidity (RH) sensors (Honeywell, US, HIH9000). The temperature of the feed gas in the pipelines was adjusted using heating tapes. Then, the wet feed gas was sent into a column with a height of 51 cm and inside diameter of 4.9 cm where sorption and desorption took place at high pressure and vacuum, respectively. Isothermal condition was maintained in the column using a jacket with oil circulation throughout the experiment. Two pressure transducers (Honeywell, US) and two temperature sensors (Honeywell, US) were installed to monitor pressure and temperature at the top and bottom of the column (I-6 and I-8, and I-5 and I-7). The gas composition of the outlet gas from the column was measured over time during the experiments using a gas chromatograph equipped with a thermal conductivity detector (TCD) (SRI-58424HQ000, SRI International), and water vapor was measured by another relative humidity sensor (Honeywell, US, HIH9000).
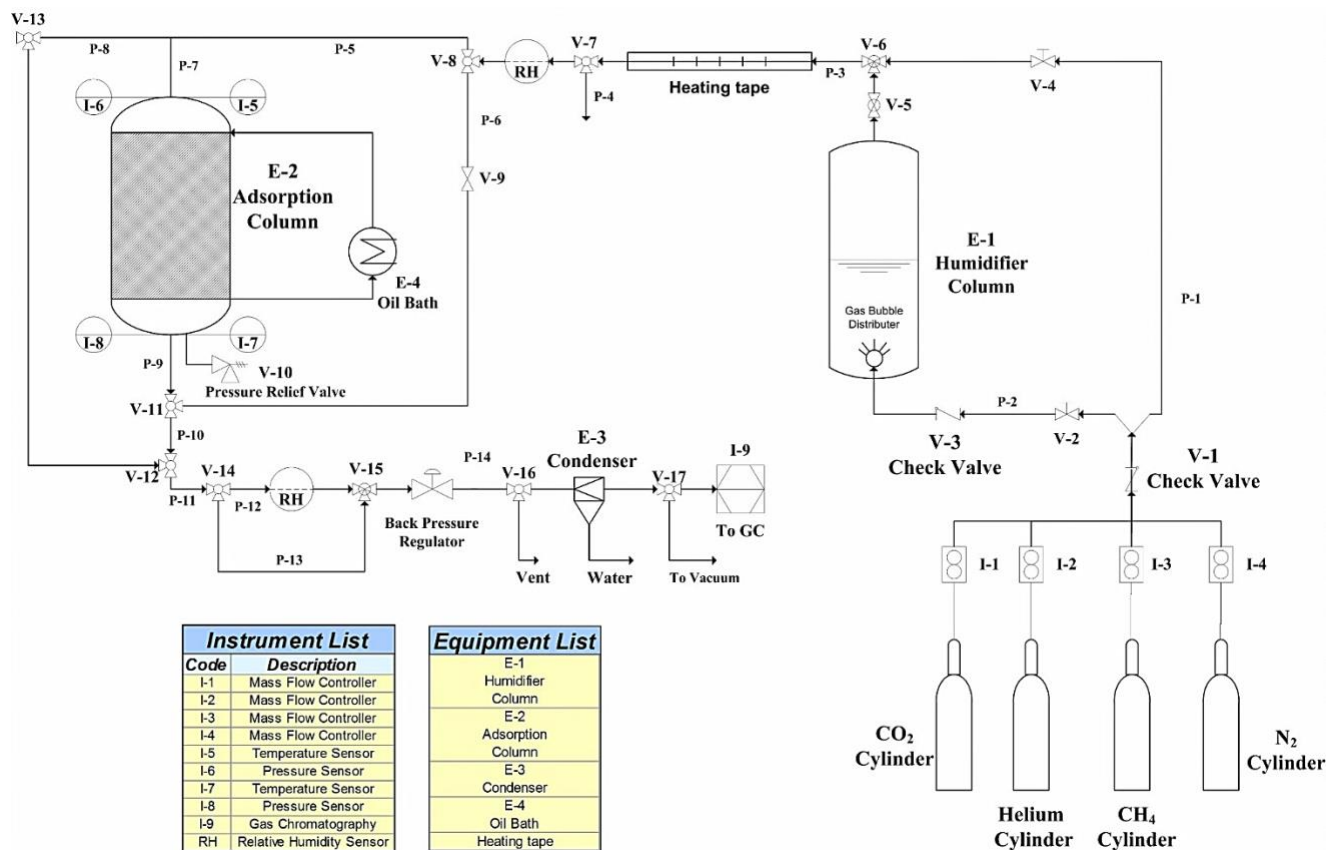
Figure 3.1: Schematic of the single-column experimental setup.

As can be noticed in Figure 3.1, all sensors were connected to a data acquisition and monitoring system in a computer. As the gas stream passes through the bed, water and/or other molecules are sorbed on the biosorbents over time, while unsorbed components of the gas leave

the column at the bottom. A back-pressure regulator was used to maintain a constant-pressure in the column. The sorption process was terminated when the mole fraction of species in the outlet gas was equal to 95 % of that in the inlet gas, which indicates a saturated bed by definition[5,8,9]. Once the bed was saturated, the column was regenerated under vacuum with nitrogen purged to the column. The mole fraction of water in the outlet was measured over time using the RH sensor and the bed was considered regenerated when the outlet humidity reached to almost zero percent. The analysis was started with single-component gas, namely methane, nitrogen, carbon dioxide, and water vapor. Helium was used as carrier gas. Later, binary and multi-component feed gases were investigated as well. Nonetheless, methane, the major component of natural gas, was chosen to investigate the capability of the biosorbents for dehydration of natural gas in a pressure swing sorption process later on in this work.

In contrast to previous works in the literature where it was assumed that the total flow rate of output gas from the column is the same as that in the inlet gas (carrier gas assumption) in order to do the mass balance, RH sensors allowed accurate measurements without such assumptions. The molar flow rate of water vapor is evaluated using the following equation[91]:

$$RH = \frac{P_t}{P_s} \times \frac{\dot{n}_w}{\dot{n}_w + \dot{n}_m + \dot{n}_c} \times 100 \tag{3.1}$$

where RH is the relative humidity measured by the RH sensors, P_s is the vapor pressure of water at the gas temperature, P_t is the total pressure of the column (absolute), $\dot{n}_w$ is the molar flow rate of water vapor, $\dot{n}_m$ is the molar flow rate of methane, and $\dot{n}_c$ is the molar flow rate of carrier gas (helium or nitrogen). Helium was first used as a carrier gas for methane or nitrogen adsorption experiments. Once it was confirmed that adsorption of nitrogen gas by flax shives was negligible, nitrogen gas was used as the carrier gas in the rest of experiments for methane dehydration and water sorption in the later stages. The molar flow rates of the carrier gas and methane in the inlet gas are known because they are adjusted using mass flow controllers, which is calculated using the ideal gas law under the operating conditions of each test. The carrier gas passes through the whole system and its molar flow rate in the outlet is equal to that in the inlet. Gas chromatography (GC) was used to measure the content of methane in the outlet over time; however, since methane is not adsorbed by biosorbents, the molar flow rate of methane in the outlet is the same as that in the inlet. Therefore, the only unknown in Eq. 3.1 is the molar flow rate of water vapor, which is calculated at every time step using the values recorded by RH, temperature, and pressure sensors at the top and bottom of the column. The

molar flow rate of water vapor is converted to mass flow rate; hence, the mass flow rates in the inlet and outlet of the column is known in every time interval during the experiment. In addition, the amount of water accumulating in the void space of glass beads and flax shives are negligible in comparison with that sorbed by flax shives. More details can be found in Appendix.

3.3.2   Continuous Dual-Column Pressure Swing Sorption Experiments

Based on the results achieved in the single-column experiments, a dual-column PSA system was established in order to investigate the cyclic performance of natural gas dehydration using the biosorbents. Figure 3.2 shows the P&ID of this setup (a picture is available in the supporting data). The data acquisition system is similar to that of the single-column setup; however, this dual-column setup is automated and controlled by a Labview program developed for this new process, which is capable of running a n-step swing sorption process (n = 4 or 6 in this work). The pressure of the columns and humidity of the feed gas were precisely controlled using two PID controllers. The columns dimensions are the same as those of the single-column setup (ID = 4.9 cm, H = 51 cm). Two temperature sensors were installed at the top and bottom of the column to record the cyclic temperature history of the columns over time. Pressures and humidity values were recorded using high accuracy pressures and humidity sensors.
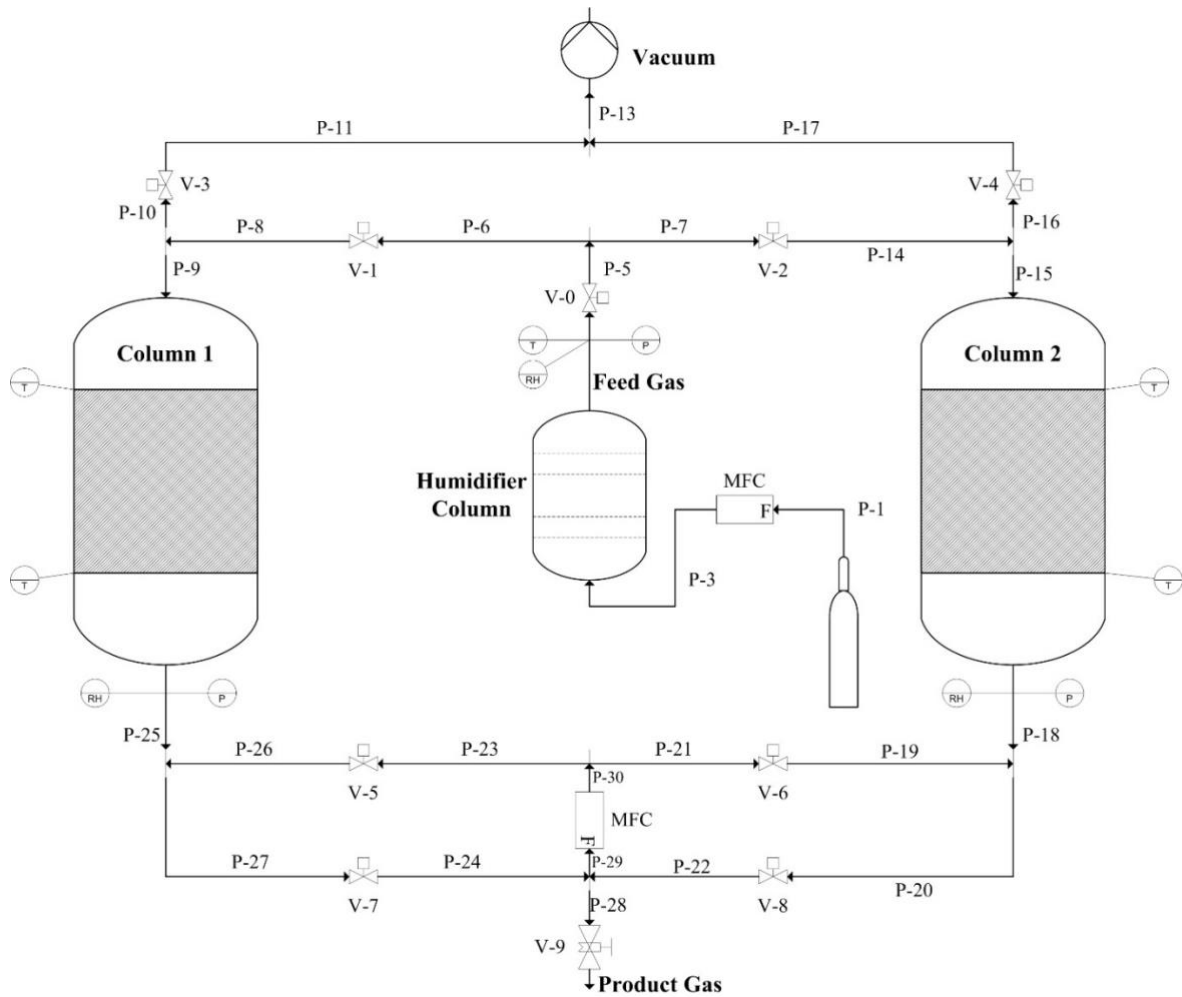
Figure 3.2: P&ID of the dual-column PSA process for natural gas dehydration; MFC: mass flow controller; RH: relative humidity.

3.3.3 Six and Four Step PSA Processes

As described in Figure 3.2, six-step and four-step PSA processes were established and operated. In the six-step dual-column PSA process, each bed undergoes the following steps: 1) pressurization (PR), sorption (ADS), pressure equalization (PE), depressurization (DPR), regeneration (REG), and pressure equalization (PE). These steps are repeated in a cyclic operation to achieve a continuous dehydration process. Table 3.1 summarizes these steps in this cyclic operation. The piping and instrumentation diagrams (P&ID) and steps of the process are shown in Figure A2 of Appendices. The six-step cycle was used in dual-column cyclic experiments at 300 kPa in Chapter 6.

Table 3.1: Configuration and steps in a six-step dual column PSA process for natural gas dehydration.

Cycle Step	1	2	3	4	5	6
Column 1	PR	ADS	PE	DPR	REG	PE
Column 2	DPR	REG		PR	ADS	

The four-step dual-column PSA process, which is also known as the vacuum swing adsorption (VSA) process, undergoes the same steps as those of the six-step PSA process, except for the PE steps, as shown in Figure A2 of Appendices. Table 3.2 shows these cyclic steps. This cycle design was used for experiments at atmospheric pressure in this work.

Table 3.2: Configuration and steps in a four-step dual column PSA process for natural gas dehydration.

Cycle Step	1	2	3	4
Column 1	PR	ADS	ADS	REG
Column 2	ADS	REG	PR	ADS

3.3.4   Experimental Design

Since the PSA process using biosorbents is new to the natural gas dehydration, the effect of operating parameters must be studied. The main operating parameters that affect the process are the pressure of the column, temperature of the column, input gas flow rate, and the humidity of the inlet gas (mole fraction of water vapor). To this end, a full factorial experimental design was done using the aforementioned four factors for the single-column experiments. Table 3.3 is a summary of this factorial design, which was later analyzed using statistical methods in order to find the main effects of and the interactions among the factors. The values of these parameters were determined based on the system limitations and/or industrial operation. Specifically, the temperature of sweet natural gas, which is the feed gas for the dehydration unit in the natural gas processing plants (see Figure 1.1) is between 35 to 38 °C. Hence, this temperature and room temperature were considered as the levels in the factorial experiment design. To consider the safety (explosive methane gas) and the limitations of the instruments available for this work, a pressure range of $101.3 - 300$ kPa was selected. The maximum water vapor mole fraction in a 100 % humid gas at 300 kPa and 24 °C is 0.0098. The water sorption capacity was calculated by water mass balance when the sorption reached equilibrium. Each experiment was performed in duplicates, and the results were presented as average plus standard deviation.

The flow rate of the carrier gas was adjusted based on the flow rate of gas during the sorption step (3 to 4.5 L/min at 46 kPa). This range was selected based on the mass flow meter operating range (0 – 5 L/min). Also, the regeneration gas to feed gas volumetric ratio of 1.5 is typically used in industry to ensure sufficient residence time for water sorption/desorption. Once the bed was approximately free of moisture, the bed was regenerated and ready for

26

another sorption experiment. To investigate the reusability and stability of the biosorbent, the biosorbent was repeatedly used in 70 completed sorption-desorption cycles. The dual-column experiments were based on simulated natural gas dehydration process in industry, the details of which are reported in Chapter 6.

Table 3.3: Factors considered in the full factorial experiment design.

Factors	Levels		
Pressure	P1 = 300.0 kPa	P2 = 101.3 kPa	
Temperature	T1 = 24 °C	T2 = 35 °C	
Gas flow rate	F1 = 2 L/min	F2 = 4 L/min	
Water vapor mole fraction in feed gas	C1 = 0.0098	C2 = 0.0083	C3 = 0.0068

3.4   Kinetic and Isotherm Modeling

Isotherm parameters and mass transfer coefficients are critical in the study of sorption processes. Linear and nonlinear isotherms were fitted on the respective experimental equilibrium data and the optimal fitted model parameters were obtained and reported. Each experimental isotherm was obtained at a specific temperature, total pressure, and total gas flow rate. The standard sum of squared errors minimization algorithm was used for the curve fitting. Each model provided a unique perspective and different information on the fundamentals and mechanisms of water sorption by the biosorbents. Likewise, kinetic studies were performed by fitting the linear driving force (LDF) model on the experimental breakthrough curves at various operating conditions. The system of partial/ordinary/algebraic equations were numerically solved using the finite difference method and ASPEN Adsorption solvers. The obtained mass transfer coefficients were reported and discussed in Chapter 7.

Chapter 4.   Preparation and Characterization of Biosorbents

In this chapter, the preparation of biosorbents from flax shives and oat hulls are illustrated and their properties are reported. To be more specific, compositions, elemental components, particle size and morphology, specific surface area, and surface functional groups were determined.

4.1   Preparation of the Biosorbents

The samples were ground, oven dried at 105 °C for 24 hours, and sieved using standard Canadian Sieves. No chemical treatment was performed. Biosorbents with two different particle size ranges of 0.425 – 1.18 mm, and 1.18 - 3 mm were used in this work.

4.2   Characterization of Biosorbent Developed from Flax Shives

4.2.1   Main Properties

Flax shives are categorized as a lignocellulose material, which is composed of cellulose, hemicellulose, lignin, and protein. Its main properties are summarized in Table 4.1. Based on previous studies, cellulose and hemicellulos impart suitable functional groups to the surface of the material for the sorption of polar molecules.[8,9,92,93] Since water is a polar molecule, and methane is nonpolar, it is hypostatized that flax shives can selectively separate water vapor from natural gas.

Table 4.1: Main properties of flax shives.

Biopolymers (reported by manufacturer, SWM Inc.)	Cellulose (%)	53.2
	Hemicellulose (%)	13.6
	Lignin (%)	20.5
	Protein (%)	3
Ultimate analysis (CHNS)	H (%)	6.21 ± 0.16
	N (%)	0.70 ± 0.01
	S (%)	0.07 ± 0.00
	C (%)	48.34 ± 0.09
Proximate analysis	Volatile content (%)	84.62 ± 0.19
	Ash content (%)	6.31 ± 0.36
	Moisture content (%)	4.33 ± 0.09
Bulk density (kg/m³)		155.2
BET surface area (N₂) (m²/g)		1.34 ± 0.07

4.2.2   Particle Size Distribution

The approximate size range of the flax shive particles was 425-1180 μm, which is the size distribution of flax shives used in the majority of experiments. Particles were approximately cylindrical or needle shape. The particle size distribution of the particles was further measured by a particle size analyzer and is presented in Figure 4.1. The average diameter was 1097 μm. According to the results, 10 % of the population have a diameter smaller than 750 μm, and 90 % have a diameter smaller than 2561 μm.
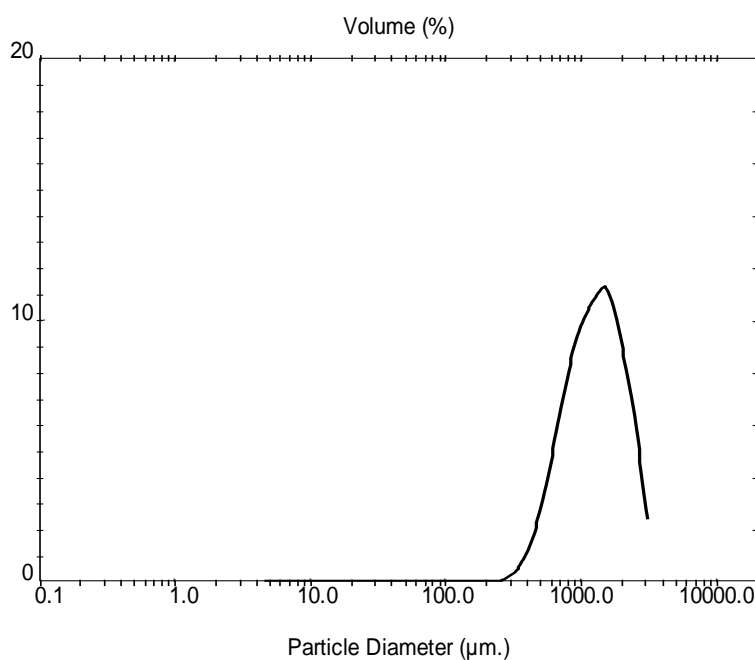
Figure 4.1: Particle size distribution of the biosorbent.

4.2.3   FE-SEM Analysis

The FE-SEM images of the flax shives-based biosorbent are shown in Figure 4.2. As can be seen, the surface of the biosorbent is heterogeneous, and the majority of the pores seem to be large pores (> 100 nm) at the corresponding magnifications in the images. Mesoporous structure inside these pores and also on the outer surface of the biosorbent can be also seen in Figure 4.2-D. Similar porous structure was observed in previous studies for biosorbents such as canola meal.[69] The biosorbent is different from most conventional adsorbents such as molecular sieves and alumina, which have a high mesoporous-microporous volume.
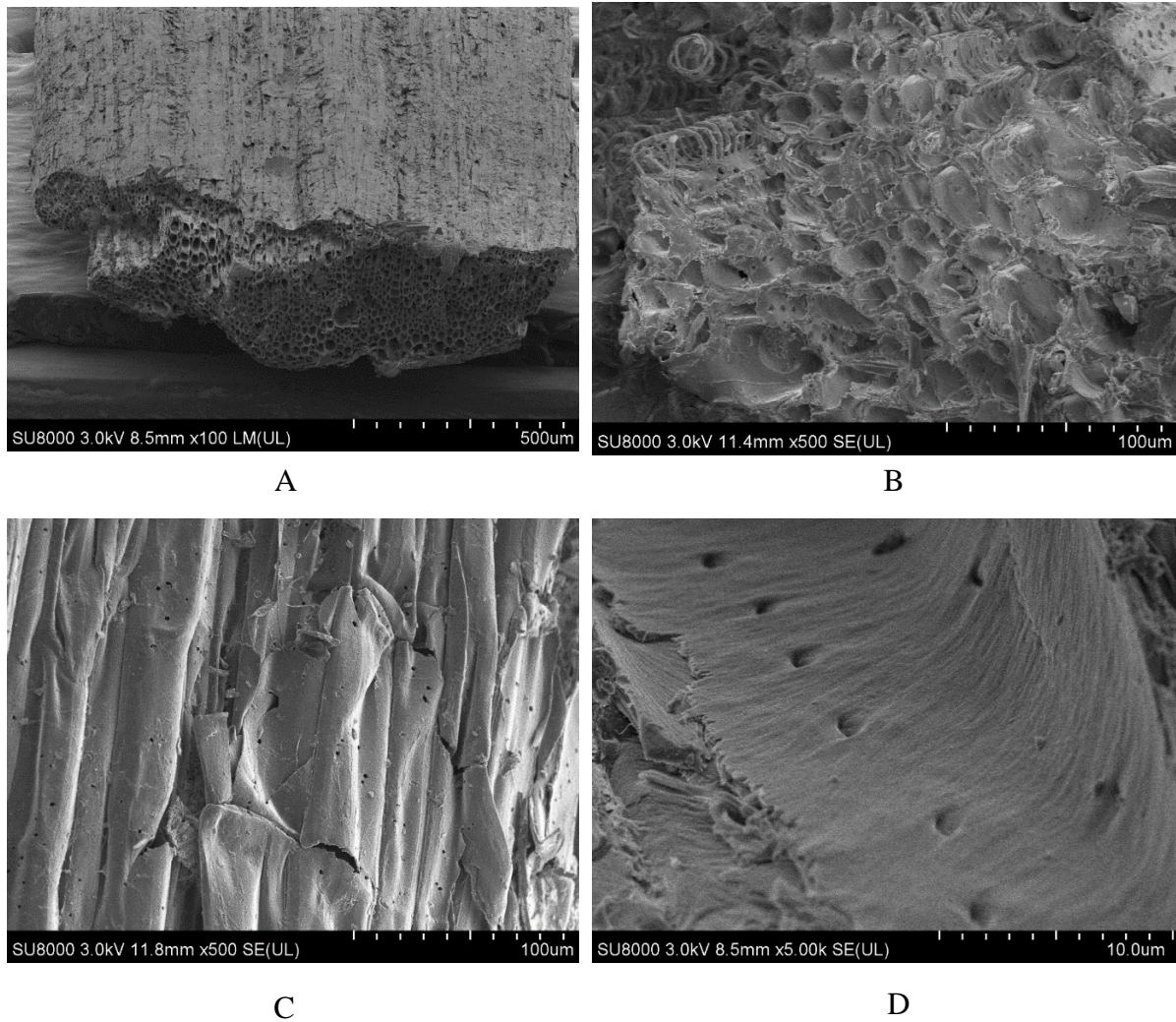
Figure 4.2: SEM images of used flax shives; A: The morphology of a piece of shive; B: The porous structure of flax shives; C: Small pores on the surface of flax shives; D: Small pores and the mesoporous parts of flax shives.

4.2.4 Specific Surface Area and Porous Structure

Large pores with different diameters were seen in SEM images of flax shives particles. In general, they look macroporous. To quantitatively determine this property, the BET surface area, micropore volume (pores smaller than 2 nm), mesopore (pores in the range of 2 – 60 nm), and macropore volume (pores in the range of 60 – 100 nm) of the biosorbent were measured as 1.34 ± 0.07 m^2/g, 0 cm^3/g, 0.0022 ± 0.0008 cm^3/g, and 0.0010 ± 0.0008 cm^3/g, respectively.[7] The average pore width of mesopores was 6.16 ± 1.03 nm. Hence, the flax shives biosorbent in this work is essentially non-porous as the micropore volume is zero and the mesopore volume is substantially low.

4.2.5 XPS Analysis

Figure 4.3 shows the XPS wide scan spectrum of flax shives. The results demonstrated that carbon, oxygen, nitrogen, calcium, and magnesium atoms presented on the surface of the biosorbent. According to this figure, 85.6 % of the atoms on the surface were carbon, which was one of the main compositions of cellulose, hemicellulose and lignin in flax shives. The next atom was oxygen (8.6%), which exist in hydroxyl groups of the aforementioned components and carboxyl groups in a small amount of protein in flax shives. Nitrogen (2.8%) is likely an element of amine groups in protein molecules. Calcium and magnesium atoms on the surface presented in the form of MgO and $CaCO_3$, which were observed in ashes of most biomass.
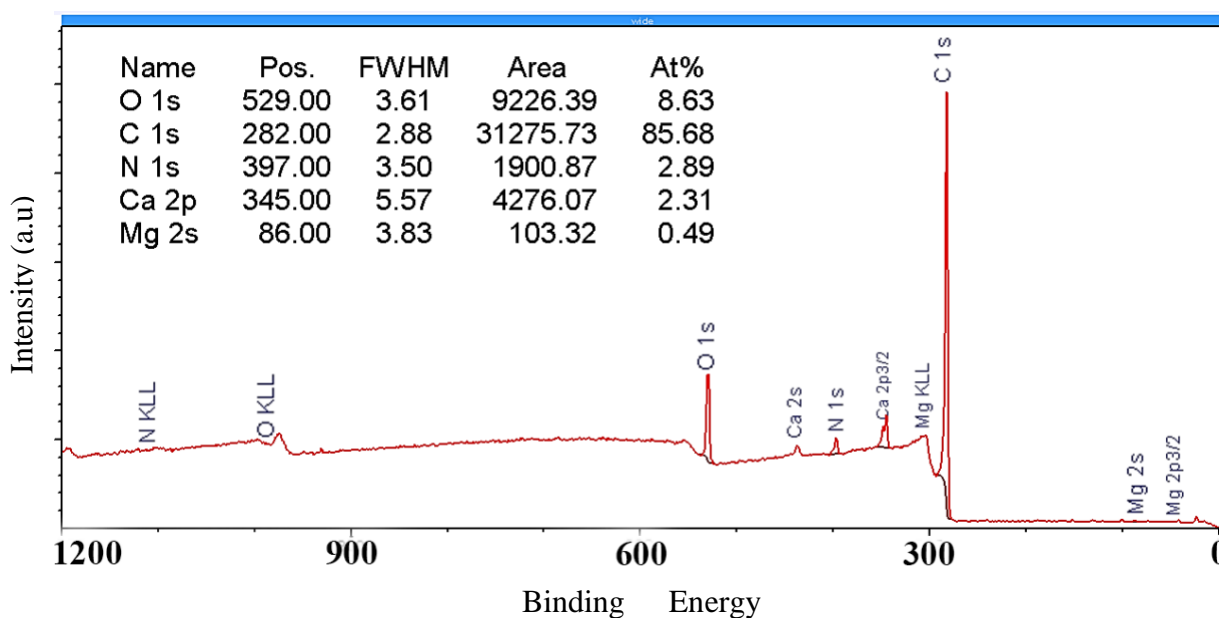
Figure 4.3: XPS spectrum of the biosorbent - wide scan (1200 – 0 eV); FWHM: Full width at half max; At%: Percentage of atoms on the sufrace.

High resolution carbon C 1s and oxygen O 1s spectra are shown in Figure 4.4. These peaks were deconvoluted using CasaXPS software. As identified in the C 1s spectrum, most carbon atoms on the surface (62%) presented in the forms of C-C and C-H, which were the main bonds in cellulose, hemicellulose, lignin, and protein existing in the flax shives. Importantly, the rest total of ~ 38% carbon atoms were in the forms C-OH and C-O-C (29.7%), O-C=O (4.8%), and C=O (3.6%). These chemical structures on the surface of the biosorbent are polar and exist in hydroxyl, carboxyl and other polar groups of the above-mentioned components in flax shives. Such polar groups can sorb polar water molecules. In addition, 1%

carbon atoms were identified in the form of $(CO_3)^{2-}$ (ash) at the binding energy (BE) of 289.5 eV (Figure 4.4-B) on the spectrum of C 1s.[94-97]

Name	Pos.	FWHM	Area	%Area		
C-C, C-H	285.00	1.11	41943.03	62.61		
C-OH, C-O-C	286.60	1.42	18716.06	27.92		
C=O	288.00	0.79	2393.98	3.57		
O-C=O	288.70	1.03	3239.86	4.83		
(CO3)2-	289.50	0.84	714.66	1.07		

Name	Pos.	FWHM	Area	%Area	%StDev	Ratio
O 1s Lattice Oxides	530.20	2.18	11825.87	56.71	0.00	1.00
O 1s Hydroxides, Defect Oxides, Organic	531.58	2.08	6254.45	29.99	0.00	0.53
O 1s Water, Organic	533.95	1.60	434.18	2.08	0.00	0.04
O 1s MgO	529.88	1.50	2340.26	11.22	0.00	0.20

Figure 4.4: High resolution C 1s and O 1s scans. A: Deconvoluted C 1s peak, approximately 28% of the carbon atoms were in the form of alcohols (C-OH); B: Deconvoluted O 1s peak, 53% of oxygen atoms were presented in the form of hydroxides.

The spectrum of O 1s shows that most oxygen atoms on the surface were present in the form of lattice oxides (56.7%), followed by hydroxides and organics (30%). The results are consistent to those of the C 1s spectrum that oxygen existed in polar groups. Inbound water peak (BE=533 eV) (1%) was also detected.[96,98,99]

In addition, MgO was identified at the binding energy (BE) of 529 eV on the spectrum, which may contribute to the ash contents reported in Table 4.1.[96] Furthermore, the oxygen peak in the form of $(CO_3)^{2-}$ in $CaCO_3$ is at the same binding energy as that of lattice oxides (530 eV),

thus the two cannot be distinguished; as such, $CaCO_3$ may also exist and contribute to the ash contents. In conclusion, the XPS results suggest that the surface of the biosorbent has abundant hydroxyl and carboxylic, which can account for the water vapor (polar molecules) sorption from natural gas (non-polar components).

4.2.6 FT-IR Analysis

To further characterize the major functional groups of the biosorbent, FTIR analysis was performed using the fresh biosorbent and the re-used biosorbent (after 70 complete adsorption-desorption cycles) to investigate any change in the surface properties. The FT-IR spectra of flax shives are shown in Figure 4.5. First of all, the spectra of fresh and re-used biosorbents are similar. The peak positions are the same; the detected peaks on the surface correspond to carboxyl, hydroxyl, lignin, and inbound water on the surfaces of both the biosorbents. As can be seen in the spectra, the peaks of carboxyl and hydroxyl groups (1029 and 3334 cm^{-1}) were detected. Flax shives contain 53.2% cellulose, 13.6% hemicellulose, and 20.5% lignin, and 3% protein, which contain carboxyl and hydroxyl groups.[7] The prominent peak of C-O stretching at 1029 cm^{-1} related to the wide dimer OH band around 3334 cm^{-1} representing the O-H stretching, vibrations, and hydrogen bonding.[92] The bands between 800 – 500 cm^{-1} are typical C-H bend and =CH out of plane, which is related to the medium intensity C-C stretching peak around 2140 cm^{-1}.[99] The peak of 5-ring C=C stretching at 1608 cm^{-1} and that of the C-C in ring at 1506 cm^{-1} indicate a small amount of lignin on the surface, which is probably linked to hemicellulose.[92,100] The bands ranged from 1400 to 1000 cm^{-1} are typical C-O and O-C-O stretching and bending vibrations. These functional groups appear to be a part of cellulose and hemicellulose structure. Moreover, the intense signal around 1650 cm^{-1} indicates adsorbed moisture or inbound water.[101] A silane peak was observed at 2365.81 cm^{-1} in the fresh biosorbent spectrum, which indicates the presence of SiO_2 on the surface (ash). It is worth noting that some materials show a carbon dioxide adsorption peak around 2365 cm^{-1} as well, in which case this peak is combined with that of SiO_2 and cannot be distinguished. The above identified carboxyl and hydroxyl groups are polar and have a potential for water binding based on electrostatic forces (dipole or quadropole interactions). Thus, the hydrophilicity of the flax shives could be as a result of cellulose, hemicellulose and small amount of protein in the material.

In addition, it is noted that the peak intensities are slightly lower in the spectrum of the re-used biosorbent, which is probably a result of non-uniformity in the samples (fresh and

reused biosorbents) taken for the FT-IR analysis as a small amount was taken from a large batch that was packed in the column. The biosorbent was stable after water vapor sorption and desorption and their degradation was insignificant. The reusability was confirmed by repeated experiments where saturated biosorbent was regenerated at a temperature no higher than 50°C and under vacuum, and has been re-used for over 70 cycles of water sorption and desorption without deterioration (the data is reported in the next chapter). The biosorbent were continuously used for the experiments at the next stage of the research. Besides, the surface structure of flax shive particles was analyzed using the SEM images, which demonstrated no significant change or degradation after numerous water vapor sorption-desorption cycles.[7] It is understood that the FT-IR analysis in this work tends to provide qualitative data. Quantitative analysis in the regards could form an area of future investigation.
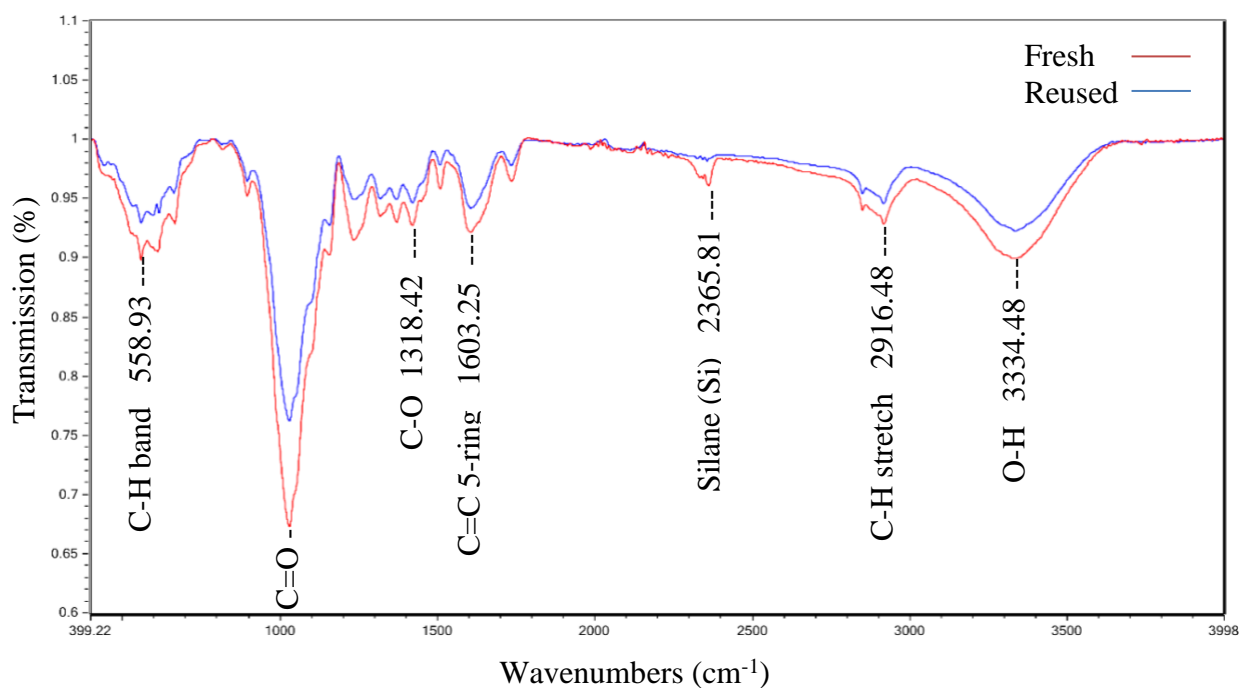
Figure 4.5: FT-IR spectra of the fresh and reused (after 70 complete water adsorption-desorption cycles) flax shives biosorbents

Another controversial discussion topic on biosorbents is their practicality in industrial applications and the effect of diversity in the source and supply line. In this section, another biosorbent was developed from oat hulls, which are a similar natural material to flax shives. Oat hulls were similarly characterized and their properties were compared with those of flax shives. The same single-column and dual-column sorption experiments were repeated for the adsorption of methane, carbon dioxide, nitrogen, and water vapor by oat hulls. Then, the results are compared to those of flax shives and commercial adsorbents.

4.3 Characterization of Biosorbent Developed from Oat Hulls

In a similar procedure to that was used for flax shives, oat hulls were oven dried, ground, and sieved by Canadian Standard Sieves Series (Combustion Engineering Canada Inc.). The biosorbents with the particle size distributions of 0.425 – 1.18 mm, and 1.18 – 3 mm were used for the experiments without further physical or chemical treatment. All the characterization experiments were similarly performed to determine the properties of oat hulls as a new biosorbent.

4.3.1 Main Properties

Oat hulls are also an example of lignocellulose materials, which are composed of cellulose, hemicellulose, lignin and protein. Oat hulls are composed of 37.0 % cellulose, 34.9 % hemicellulose, 7.1 % lignin, 4.6 % ash, 2.2 % fat, and 5.2 % protein (reported by the supplier, Richardson Mills). Research suggests that cellulose and hemicellulos increase the hydrophilicity of surface by imparting suitable surface functional groups unto the surface of biosorbents[8,9,92,93]. It is hypothesized that oat hulls can selectively sorb water vapor from natural gas since water is a polar molecule, and methane is nonpolar.

4.3.2 FE-SEM Analysis

FE-SEM can provide useful information about the morphology and porous structure of the biosorbent. Several images were taken at various magnification shown in Figure 4.6. As can be seen in Figure 4.6, the surface of the biosorbent is rough, heterogeneous, and comprised of large pores visible at the magnifications tested in this work. The shape of pore is slit. Mesopores and transition pores can be also observed inside the larger pores and at some other parts on the surface. These observations indicated that water sorption mechanism is likely to be mostly sorption by surface functional groups than capillary condensation or diffusion[5,9,32,33,69,102]. Similar porous structure was observed in previous studies for similar biosorbents such as canola meal[69]. These results show that the biosorbent is different from most conventional adsorbents such as molecular sieves and alumina having mesoporous-microporous structure and pores in the range of angstrom[5,32].
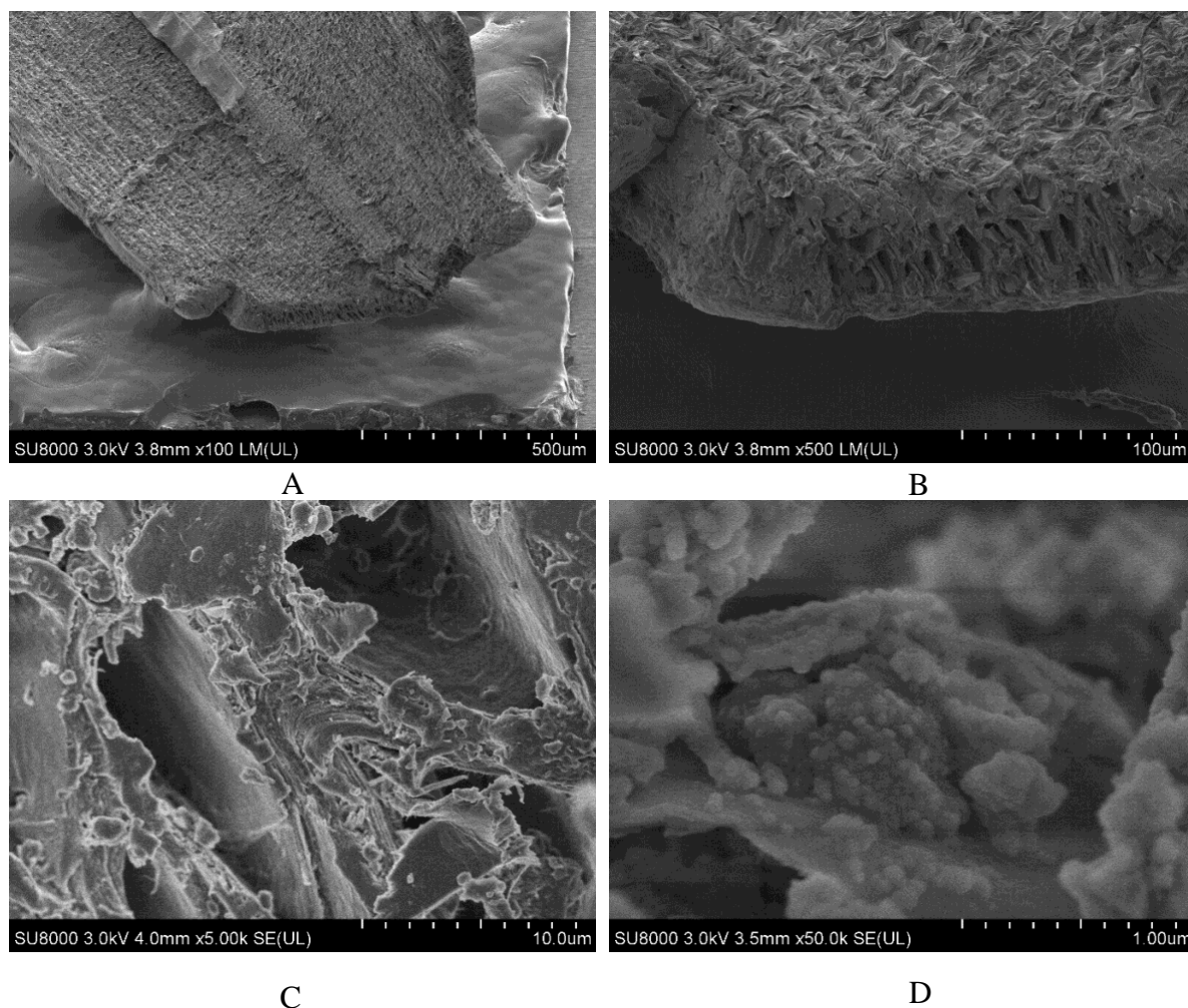
Figure 4.6: : SEM images of oat hulls; A: The morphology of a piece of oat hulls; B: The porous structure of oat hulls- large slit pores; C: Heterogeneity of the structure having small and large pores; D: Transition pores and mesopores in nanometer rage inside the larger pores.

4.3.3   Specific Surface Area and Porous Structure

The standard BET and DFT experiments were performed using the Micromeritics ASAP 2020 device, and the specific surface area, average pore width, average micropore volume, and average mesopore volume were determined. Values of 0.21 ± 0.09 m^2/g, 66.74 ± 0.58 nm, zero, and 0.0036 ± 0.0009 cm^3/g were obtained for the specific surface area, average pore width, average micropore volume, and average mesopore volume, respectively. Similar to other raw biosorbents such as flax shives, oat hulls are essentially non-porous and their specific surface area is very low even though the water sorption capacity was reasonably good. As mentioned before, the functional groups are very likely to be responsible for the water vapor sorption and the high sorption capacity of the biosorbent[10]. Pore size distribution of oat hulls is reported in the supporting data.

4.3.4 XPS Analysis

According to the XPS results, the surface of the biosorbent is covered with carbon, oxygen, nitrogen, and silica atoms. Figure 4.7 shows the survey scan (wide scan) of the sample. According to this figure, over 85 % of the atoms on the surface are carbon. The presence of nitrogen atoms on the surface is because of protein in oat hulls (low amounts). Silica presented in the form of SiO_2 (ash).

Name	Pos.	FWHM	Area	At%	%StDev
O 1s	530.00	3.41	16258.80	13.43	0.00
C 1s	283.00	2.77	35190.11	85.17	0.00
N 1s	398.00	2.75	784.90	1.06	0.00
Si 2p	100.00	3.63	118.13	0.35	0.00
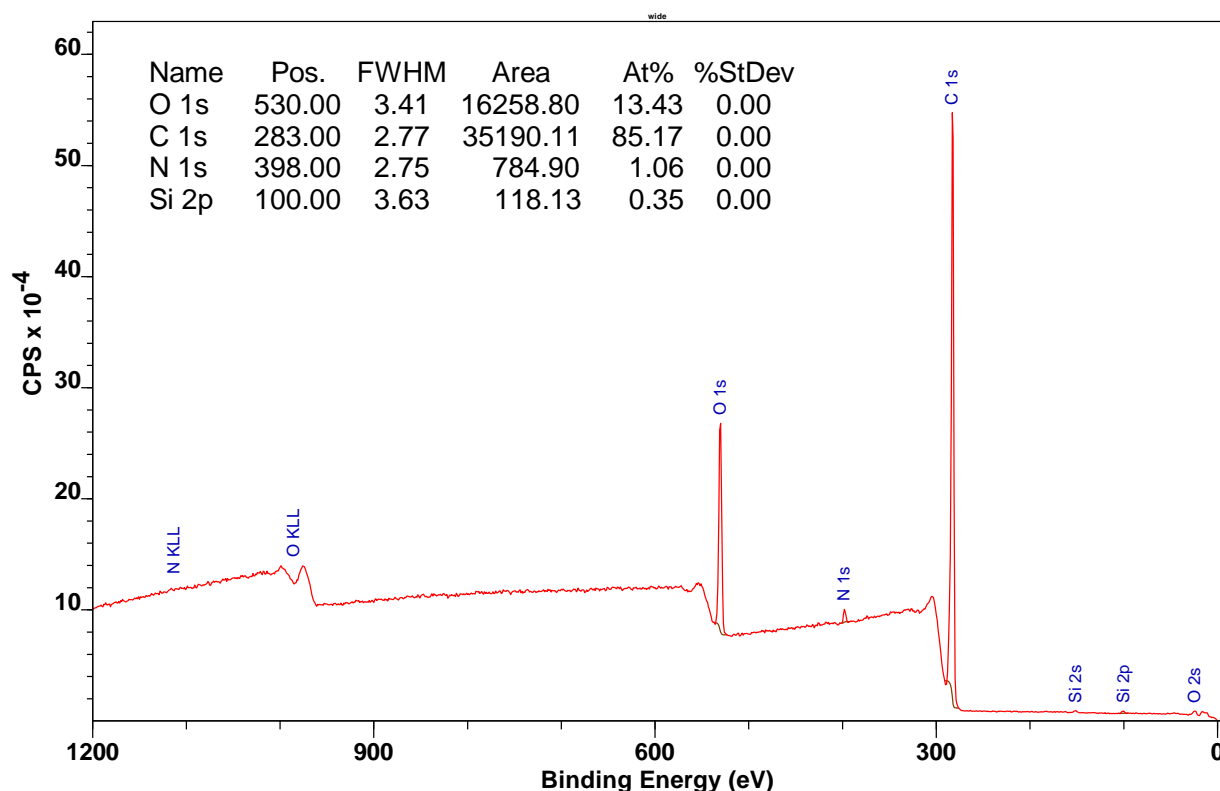
Figure 4.7: XPS spectrum of oat hulls- wide scan (1200 – 0 eV); FWHM: Full width at half max; At%: Percentage of atoms on the sufrace

High resolution oxygen O 1s and carbon C 1s spectra are shown in Figure 4.8. CasaXPS software was used to deconvolute these peaks. As can be seen, almost half of the oxygen atoms on the surface present in the form of hydroxides (48.62%), which can effectively adsorb water vapor. Around 49% of oxygen atoms on the surface present in the form of lattice oxides with a typical bonding energy of 529.9 eV, which are bonded to either carbon or silica[94-97]. Furthermore, a very low amounts of sorbed/inbound water was also observed in the O1s spectrum.

As for the carbon atoms, most carbon atoms on the surface obviously present in the form of C-C and C-H. However, ether, ester, and ketone peaks observed on the surface can

provide useful information about the surface functional groups. According to Figure 4.8-A, 20.78% of hydroxides (out of 48.46% seen in the O1s spectrum) are bonded to carbon atoms or present in the form of ether groups. Carbonyl peak (285.43 eV) suggests the presence of carboxylic acid functional group on the surface of the biosorbent. Ester peak was observed at 286.63 eV, which is also related to the C-OH groups and the hydroxides in the O1s peak[96,98,99]. Overall, the XPS results shows that the surface of the biosorbent is covered with carboxylic acid and hydroxyl functional groups, which can sorb water vapor (polar molecules) from natural gas (non-polar). Therefore, based on the results of SEM and XPS analyses, it is likely that water sorption by the oat hulls based biosorbent is largely as a result of these surface functional groups.

The image contains two XPS spectra plots (A and B).

Plot A (O 1s):

Name	Pos.	FWHM	Area	%Area	%StDev
O 1s Lattice Oxides	529.95	1.71	17052.85	49.72	0.00
O 1s Hydroxides, Defect Oxides	531.25	1.69	16624.14	48.46	0.00
O 1s Water, Organics	532.65	1.16	624.26	1.82	0.00

Plot B (C 1s):

Name	Pos.	FWHM	Area	%Area	%StDev
C 1s C-H, C-C	282.63	1.21	63967.92	72.74	0.00
C 1s C-OH, C-O-C	284.03	1.82	18284.10	20.78	0.00
C 1s C=O	285.43	0.70	770.62	0.88	0.00
C 1s O-C=O	286.63	1.41	4934.29	5.60	0.00

Figure 4.8: High resolution C 1s and O 1s scans; A: Deconvoluted O 1s peak; B: Deconvoluted C 1s

4.4   Chapter Summary

In this chapter, the important properties of both biosorbents were determined and reported. The results suggest that flax shives and oat hulls are similar in many aspects such as composition, porous structure, and surface functional groups. Flax shives and oat hulls are classified as lignocellulose materials mainly composed of cellulose, hemicellulose and lignin. Both biosorbents had zero micropore volume and very low mesopore volume. Their surface area was low (<10 m^2/g). The results of XPS and FT-IR analyses showed that their surface was covered with abundant hydroxyl and carboxyl functional groups. These important results guided the next steps of this research project and were used in modeling sections to fill the knowledge gaps regarding the water vapor sorption mechanism by the biosorbents.

Chapter 5. Sorption of Water Vapor, Methane, and Carbon Dioxide by the Biosrobents

This chapter presents the sorption of natural gas main components by biosorbents developed from flax shives and oat hulls, and the effects of process operating parameters on the sorption capacities. Various experiments were performed using the single-column apparatus. Furthermore, the reusability of the biosorbents was investigated. An analysis was also performed on the length of mass transfer zone under various operating conditions. Lastly, an optical microscopy procedure was implemented to visualize the transport of water molecules inside the flax shive particles to acquire more information on the mass transfer phenomena. It is to note that gas dehydration by lignocellulose materials could be involved in adsorption and/or absorption. Considering the nature of the biosorbents used in this work (flax shives and oat hulls), water removal by the biosorbents could be more reasonably considered to be sorption, which may include adsorption and absorption. This is a scientific term that has been widely used in the literature for the sorption of water vapor by cellulose, hemicellulose, pectin, and similar biopolymers, which are the main components in the composition of biosorbents and similar bio-based materials. Thus, this term "sorption" and its respectively derived term "sorb", and so on are used when discussing water vapor, and the term "adsorption" is used when talking about other nonpolar gases such as methane and nitrogen.

5.1 Capability of Flax Shives for Natural Gas Dehydration

To investigate the capability of flax shives for dehydration of natural gas, methane, the major component of natural gas, was used. Firstly, methane adsorption by biosorbent was investigated. The whole column was packed with 231 g of flax shives. A feed gas stream comprised of carrier gas helium, and methane was sent to the column under the conditions of 101-500 kPa, 24-50 °C, 2-4 L/min, and feed methane 10-50 v/v %. Gas chromatography was used to measure the concentration of methane in the feed and the effluent gas. The experimental results showed that the concentration of methane in the effluent gas was the same as that in the feed gas, demonstrating methane adsorption by the biosorbent was negligible.

Afterwards, the dehydration of humid methane (binary system) was investigated. The column was filled with 27.3 grams of flax shives in this experiment. Figure 5.1 shows a representative concentration history of water vapor in the effluent during the sorption process. The humid gas had a water molar fraction of 0.0082 ± 0.0001 (100% humid), which was fed to the column at 35 °C, 300.0 kPa, and carrier gas (helium) flowrate of 2 L/min. Methane mole

41

fraction in the feed gas was 0.26. As can be seen in this figure, the product gas exiting the column had been dry during the first hour of the experiment; afterward, the water breakthrough point was reached (defined as the point where the water content in the effluent equals to 1% of that in the inlet stream in this work.) and the water vapor concentration in the outlet gradually increased to the saturation point. Concentration of methane at the outlet is also plotted over time, which remained same as that of feed during the experiment as it was not adsorbed by flax shives. The results demonstrated that the flax shive-based biosorbent had a high selectivity for water sorption and successfully dehydrated methane.
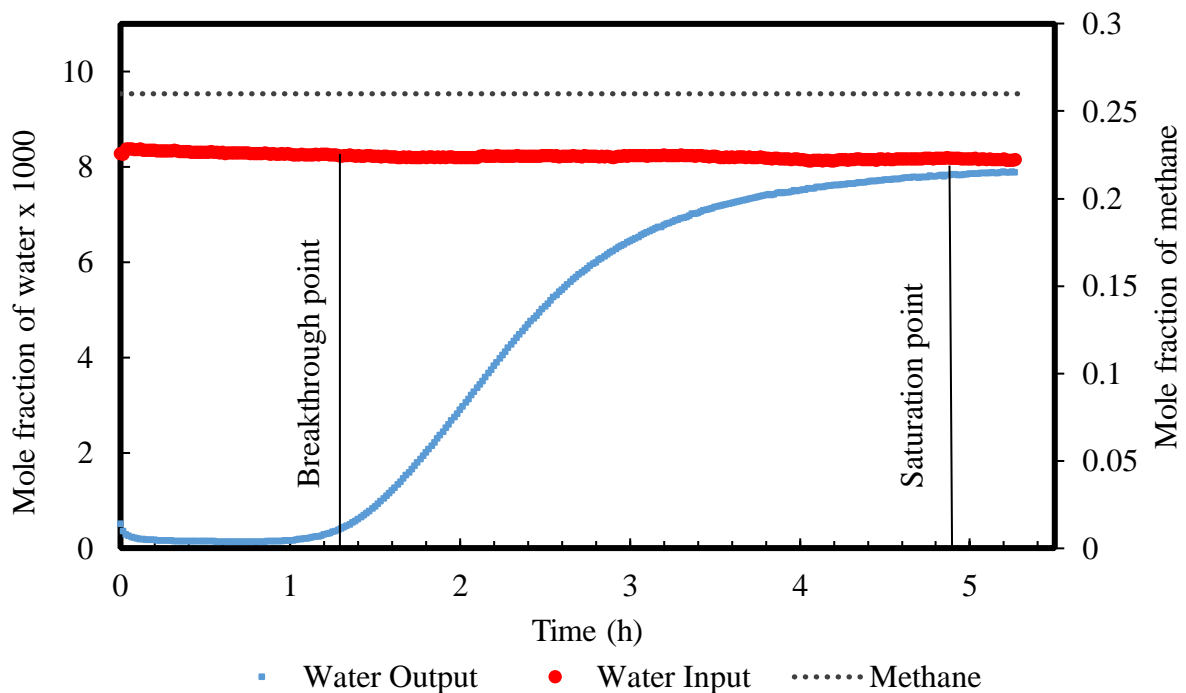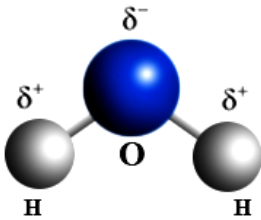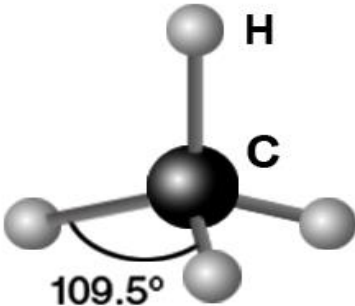
Figure 5.1: Water concentration histories in the effluent during the sorption experiment;Concentration of methane is at the outlet of the column; average standard deviation of all water input and output mole fraction data points is 0.05×10^{-3}; 300 kPa, 35 °C, 2 L/min.

Methane is a non-polar molecule (Table 5.1). Previous results demonstrated that most biomass materials had affinity to polar molecules as a result of their hydrophilic surface.[8,9,93] In this work, hydroxyl, carboxyl, and additional polar groups on the surface of the biosorbent identified by the XPS and FT-IR analyses could be responsible for water vapor sorption.

Table 5.1: Molecular structures of water and methane[91].

| Effective diameter = 2.75 Å | Effective diameter = 3.98 Å |

In addition, experiments were also carried out to investigate the adsorption of nitrogen and carbon dioxide. Again, the adsorption of nitrogen and carbon dioxide was negligible. The hypothesis of this research project was confirmed, that is the effective water sorption by the biosorbent and negligible adsorption of non-polar gases such as methane, nitrogen, and carbon dioxide. The results are reasonable because the above mentioned small nonpolar gases molecules are usually adsorbed in micropores based on the micropore diffusion mechanism,[5,33] and the micropore volume of flax shives is close to zero. Thus, adsorption of such non-polar gases molecules are negligible. Other commercial adsorbents such as silica gel, molecular sieves, activated alumina, and carbon molecular sieves have micropores in the scale of angstrom, which favors effective adsorption of the above mentioned non-polar gases. It was reported that effective pore diameter and surface polarity of adsorbents are the critical parameters affecting the sorption of a gas molecule. Small molecules such as methane, nitrogen, and carbon dioxide were usually adsorbed in micropores as a result of the micropore diffusional activation energy.[5,33] This diffusional activation energy is related to the difference between the molecules' effective diameter and effective pore diameter of adsorbents. The lower this difference, the higher the diffusional activation energy and the adsorption.[5] The characterization results showed that flax shives were essentially non-porous as the micropore volume was almost zero, which may explain why nonpolar molecules such as methane with an effective pore diameter of 3.98 Å could not be adsorbed in micropores by micropore diffusional forces; while polar functional groups were available on the surface of the biosorbents for the water sorption (polar molecules). Two forces are involved in water sorption in mesopores and macropores: 1) dispersion forces (van der Waals); 2) electrostatic forces (dipole and quadropore interactions).[33] Both forces could be involved in the water sorption by flax shives. Water sorption on polar surfaces with hydroxyl functional groups are mainly based on

electrostatic forces and hydrogen bond.[5,33] More discussions on the surface polarity and water sorption by flax shives are made in Chapter 6.

Therefore, the biosorbent seems to be a promising sorbent for the dehydration of natural gas and other non-polar gases. Based on the achieved results, the system was systematically investigated and the results are presented below. The water vapor sorption capacity of flax shives at various operating conditions are reported in Table 5.2. These mass balance calculations (Eq. 3.1) were performed using the breakthrough curve data according to the method illustrated in Chapter 3. According to this full factorial design table, 48 experiments were performed in random order, and each experiment was repeated twice to determine the averages and standard deviations. It is useful to compare the water vapor sorption capacity of flax shives with that of commercial adsorbents and other biomass-based sorbents, which may provide insights on the sorption mechanisms. Flax shives are mainly composed of cellulose, hemicellulose, and lignin. Lignin is known for its hydrophobicity; hence, cellulose and hemicellulose are likely responsible for moisture sorption. Newns et al.[103] and Olsson et al.[104] reported a water vapor sorption capacity of 0.29 g/g and 0.42 g/g for pure cellulose and hemicellulose at atmospheric pressure, 20 °C, and 90% relative humidity (RH), respectively. For a reasonable comparison, the experiment conditions in gaseous systems should be relatively similar. Hence, the water vapor sorption capacity of flax shives at atmospheric pressure, 24 °C, and 100% RH was determined (breakthrough curve is shown in Figure 5.2). Note that the water sorption capacity of 0.04 g/g at atmospheric pressure and 24 °C that is reported in Table 5.2 was for a feed gas with a water mole fraction of 0.0098, which was a design constrain of the full factorial design. As was mentioned before, 0.0098 was the maximum water mole fraction at 300 kPa and 24 °C that has to be considered the same for other levels of the design parameters according to the factorial design procedure. As can be seen in Figure 5.2, the mole fraction of water at 100% RH, atmosphere pressure, and 24 °C is around 0.0243. Under these conditions, the water vapor sorption capacity of flax shives was 0.57 g/g. Table 5.3 compares the water vapor sorption capacity of commercial adsorbents and some biomass-based adsorbents. Pectin has a sorption capacity of 0.108 g/g.[105] Protein, which also presents in other biomass materials, can sorb moisture to some extent.[106,107]

Table 5.2: Summary of data obtained from the full factorial experiments – flax shives biosorbent; q is the water vapor sorption capacity; the flow rates are the total gas flow; the mole fractions are for water vapor corresponding to the humidity level of the feed gas.

ID	T (°C)	P (kPa)	Flowrate (L/min)	Mole Frac.	q (g/g) run 1	q (g/g) run 2	Average	Standard Deviation
1	24	300.0	2	0.0098	0.903	0.894	0.898	0.006
2	24	300.0	2	0.0083	0.568	0.502	0.535	0.047
3	24	300.0	2	0.0068	0.384	0.408	0.396	0.017
4	24	300.0	4	0.0098	0.858	0.862	0.860	0.003
5	24	300.0	4	0.0083	0.503	0.541	0.522	0.027
6	24	300.0	4	0.0068	0.367	0.356	0.361	0.008
7	24	101.3	2	0.0098	0.050	0.048	0.049	0.002
8	24	101.3	2	0.0083	0.042	0.041	0.041	0.001
9	24	101.3	2	0.0068	0.041	0.040	0.041	0.001
10	24	101.3	4	0.0098	0.053	0.054	0.054	0.001
11	24	101.3	4	0.0083	0.048	0.045	0.047	0.002
12	24	101.3	4	0.0068	0.038	0.037	0.038	0.001
13	35	300.0	2	0.0098	0.221	0.234	0.227	0.010
14	35	300.0	2	0.0083	0.206	0.208	0.207	0.001
15	35	300.0	2	0.0068	0.163	0.204	0.183	0.029
16	35	300.0	4	0.0098	0.236	0.238	0.237	0.001
17	35	300.0	4	0.0083	0.207	0.198	0.202	0.006
18	35	300.0	4	0.0068	0.174	0.167	0.170	0.005
19	35	101.3	2	0.0098	0.037	0.036	0.037	0.001
20	35	101.3	2	0.0083	0.041	0.035	0.038	0.004
21	35	101.3	2	0.0068	0.028	0.029	0.029	0.001
22	35	101.3	4	0.0098	0.037	0.035	0.036	0.001
23	35	101.3	4	0.0083	0.034	0.032	0.033	0.001
24	35	101.3	4	0.0068	0.035	0.032	0.034	0.002

The achieved water sorption capacity of flax shives was 0.57 g/g (100 % RH, 101.3 kPa and 24° C), which is much higher than that of commercial adsorbents for dehydration purposes that have been used in natural gas industry under approximately similar experimental conditions, e.g. silica gel (0.35-0.5 g/g), molecular sieves (0.21-0.26 g/g), and alumina (0.25-0.33 g/g).[91]
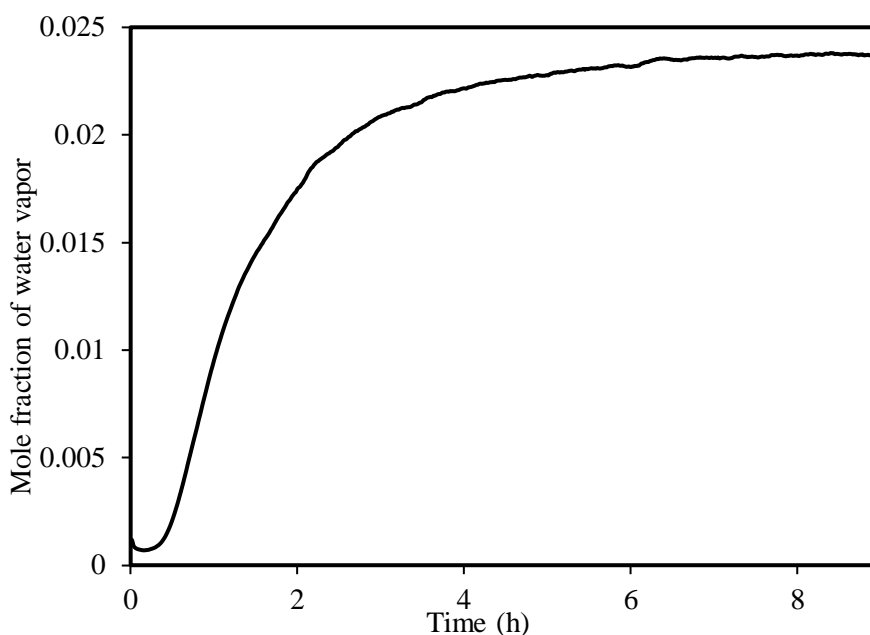
Figure 5.2: Breakthrough curve at 101.3 kPa, 24 °C, 100% humid feed gas, and feed flow rate of 2 L/min.

The maximum achieved water sorption capacity for flax shives in this work was 0.90 g/g at 100 % RH, 300 kPa and 24 °C. Such high sorption capacities were reported for advanced synthetic materials such as a SiO_2-CaCl_2 Sol−Gel composite, which could sorb 1 grams of water per grams of adsorbents[73]. To compare the sorption capacity of flax shives under pressure with those of silica gel and molecular sieves, a few experiments were performed under the same conditions using a similar apparatus and data collection systems for a reasonable comparison. Commercial silica gel (Sigma-Aldrich, 5 mm beads, USA) and molecular sieve 3A (EMD Millipore, 5 mm beads, Ontario, Canada) particles were dried in oven at 105 °C for 24 hours. The column was filled with 105.5 grams of silica gel, which occupied the same height in the column as that in the flax shives experiments (8 cm), and the other operating conditions were the same as well. In a similar experiment, 108.3 grams of oven-dried molecular sieves were packed in the column with a layer height of 8 cm, and the water vapor sorption capacity at 100 % RH, 300 kPa and 24 °C was determined. The water vapor sorption capacities of 1.24 g/g and 0.59 g/g were obtained for silica gel and molecular sieves, respectively. Afterwards, the particles were regenerated under vacuum at 24 °C. Then, the same experiment was repeated and the water vapor sorption capacities of 0.79 and 0.21 g/g were obtained for silica gel and molecular sieves, respectively. A few important observations worth discussing. Firstly, the pressure has a dramatic effect on the water vapor sorption capacity of silica gel, molecular sieves, and flax shives. The water vapor sorption capacity of flax shives increased from 0.57 to 0.9 g/g by increasing the pressure from 101.3 kPa to 300 kPa. Such substantial increases

46

may be a result of a change in the water vapor sorption mechanisms (e.g. multilayer), which is later discussed in the isotherm modeling chapter. Secondly, the regeneration of silica gel and molecular sieves at 24 °C was not effective as their actual operating sorption capacity was reduced from 1.24 to 0.79 g/g and 0.59 to 0.21 g/g, respectively. The silica gel and molecular sieves particles in the first experiment were dried for 24 hours in oven at 105 °C. It is probable that water molecules that were sorbed in the micro-meso porous structure of silica gel and molecular sieves could not be easily desorbed at 24 °C under vacuum and a flow of carrier gas, while high temperatures in oven (under no flow of any gas) were effective in regenerating the particles and removing moisture from their porous structure under suitable thermodynamic and mass transfer conditions. Additionally, the molecular sieves bed was regenerated at 50 °C and vacuum after the second experiment, and the same water sorption experiment was repeated to investigate the effect of the regeneration temperature. The water vapor sorption capacity of molecular sieves in the third experiment was 0.3 g/g, which is higher than that of the second experiment (0.21 g/g) where the particles were regenerated at 24 °C. Similar results were reported for oat hulls in the literature.[10,108,109] It is worth noting that two different batches of flax shives and two different batches of oat hulls were investigated in this work as well, which are summarized in Table 5.3. More details are reported in section 5.8.3.

Speaking about the dehydration of natural gas, it is known that natural gas contains methane, carbon dioxide, nitrogen, water vapor, and small amounts of other components. In natural gas dehydration using a sorption process, water vapor is preferred to be selectively separated from the main component methane and other gaseous species. It was so far shown in this chapter that the flax shives biosorbent did not substantially sorb non-polar gases such as methane, carbon dioxide, and nitrogen, while the conventional adsorbents adsorb methane, nitrogen, and carbon dioxide to some extent (low to moderate selectivity).[7] Furthermore, the biosorbent was regenerated at 25 °C without additional heating and the desorption rate was fast. Taking these excellent properties into account, the biosorbent-based flax shives could have key applications in natural gas dehydration and the drying of other non-polar gases.

Table 5.3: Water vapor sorption capacity of different biosorbents; q: water vapor sorption capacity; H_2O/EtOH is a mixture of ethanol and water vapor; RH is relative humidty; B1: batch of flax shives from SWM international; B2: batch of flax shives from Research Biolin; B7: batch of oat hulls 2017; B8: batch of oat hulls 2018.

Material	Conditions (P, T and Feed Concentration)	q (g/g)	Reference
Flax shives (B1)	101.3 kPa, 24 °C, 36% RH	0.04	This work
Flax shives (B1)	101.3 kPa, 24 °C, 100% RH	0.57	This work
Oat hulls	101.3 kPa, 24 °C, 36% RH	0.13	This work
Raw canola meal	243 kPa, 100 °C, 5 wt % H_2O/EtOH	0.02	9
Protein extracted canola meal	243 kPa, 90 °C, 5 wt % H_2O/EtOH	0.02	8,9
Cornmeal	243 kPa, 90 °C, 5 wt % H_2O/EtOH	0.04	106
Cornmeal	243 kPa, 90 °C, 5 wt % H_2O/EtOH	0.02	107
Oat hulls	135 kPa, 108 °C, 43 wt % H_2O/EtOH	0.13	109
Pectin	101.3 kPa, 29 °C, 90% RH	0.11	105
Corn starch	101.3 kPa, 25 °C, 93% RH	0.4	110
Potato starch	101.3 kPa, 25 °C, 93% RH	0.51	110
Flax shives (B1)	300 kPa, 24 °C, 100% RH	0.9	This work
Flax shives (B2)	300 kPa, 24 °C, 100% RH	0.53	This work
Oat hulls (B7)	300 kPa, 24 °C, 100% RH	0.63	This work
Oat hulls (B8)	300 kPa, 24 °C, 100% RH	0.9	This work
Silica gel	101.3 kPa, 15-25 °C, 80-90% RH	0.3-0.5	5,32,91
Molecular sieves 3A	101.3 kPa, 15-25 °C, 80-90% RH	0.21-0.26	5,32,91
Silica gel	300 kPa, 24 °C, 100% RH	0.79-1.24	This work
Molecular sieves 3A	300 kPa, 24 °C, 100% RH	0.21-0.59	This work
$CaCl_2$ – Activated carbon composite	101.3 kPa, 25 °C, 30% RH	0.52	111
SiO_2−$CaCl_2$ Sol−Gel composite	101.3 kPa, 25 °C, 85% RH	1	73

5.2 Effects of Operating Parameters on Water Sorption by Flax Shives

The effects of key operation parameters including temperature, pressure, feed concentration, and gas flow rate on the water sorption were systematically investigated using a full factorial experimental design. Table 3.3 shows the levels considered for the parameters.

The experimental results were analyzed using SPSS (Statistical Package for Social Science) software in order to determine the main effects of the factors (operating parameters) on the water sorption capacity of the biosorbent and the interactions among these factors. A significance level of $\alpha = 0.05$ was considered. The detailed results are reported in Table 5.4. Overall, under the tested conditions in this work, it was shown that pressure had the most significant effect on the water vapor sorption capacity. Temperature and mole fraction were the second and third important factors, respectively. The water vapor sorption capacity increased with increasing pressure, and/or feed water content, while it decreased with increasing temperature showing the water sorption could be exothermic. The interaction among temperature, pressure, and feed water content were all significant. This was determined by the thermodynamics of water vapor sorption in this system. Total gas flow rate did not have any effects on equilibrium water sorption as expected, but it may have affected the mass transfer coefficients, which is discussed in chapter 7.

Table 5.4: Statistical analysis of the full factorial experiment design – Flax shives.

Tests of Between-Subjects Effects

Dependent Variable: sorption capacity, q (g/g)

Source	F-Test	Significance Level	Partial Estimated Squared
Temperature	3957	0	0.99
Pressure	12773	0	1
Flowrate	5.3	0.08	0.57
Mole fraction	701	0	0.99
Temperature * Pressure	3559	0	0.99
Temperature * Flowrate	3.4	0.14	0.46
Temperature * Mole fraction	448.5	0	0.99
Pressure * Flowrate	6.8	0.06	0.63
Pressure * Mole fraction	621.4	0	0.99
Flowrate * Mole fraction	0.42	0.68	0.17
Temperature * Pressure * Flowrate	5.1	0.09	0.56
Temperature * Pressure * Mole fraction	418.4	0	0.99
Pressure * Flowrate * Mole fraction	0.9	0.64	0.19

The values of partial estimated squared shown in Table 5.4 represents the proportion of total variance with respect to each factor in the experimental design in the ANOVA method. They were used to determine which factor had the most significant effect on the water sorption capacity, and interactions among the factors. The closer the value of partial estimated squared to one, the higher the contribution of the factor to the dependable variable. According to the analysis, pressure, temperature, and mole fraction of water had significant effects on the sorption capacity because their partial estimated squared values are close to 1. In addition, their significance levels are lower than $\alpha = 0.05$. Pressure had the most significant effect on the sorption capacity. Temperature and mole fraction were the second and third important factors, respectively. The effect of volumetric flow rate was not statistically significant at the tested range (significance level larger than $\alpha = 0.05$).

5.3   Water Vapor Desorption from Flax Shives and the Cycle of the Process

Desorption step significantly affects the performance of a swing sorption process. Sorbents are expected to be regenerated rapidly at minimum operating cost. To investigate the pressure swing sorption process (single column system), two steps of a cycle, sorption at a higher pressure and desorption at a lower level, were operated. The carrier gas was nitrogen for both the processes. In this preliminary experiment, the sorption step was operated at 24 °C, 300 kPa, and 2 L/min, while the desorption step was executed at 24 ºC, 46 kPa absolute, and 3 L/min. Figure 5.3 shows the column histories during these cycle steps in one column.

In a general dual-column PSA process, there are four steps in each cycle. Each bed experiences pressurization, sorption at high pressure, depressurization, and desorption at low pressure (vacuum). In industry, cycle time can be from a few seconds to a few minutes depending on the type of process, in which beds usually do not reach complete equilibrium/saturation or regeneration. However, in this preliminary experiment, both the sorption and desorption steps continued till equilibrium and almost full regeneration, respectively, in order to obtain the complete operation data. To further clarify, the equilibrium is when the RH of outlet gas almost reached to that of the humid feed gas (100% RH) and regeneration was considered complete when the measured RH in the outlet gas reached almost zero (same as the dry carrier gas sent into the column during regeneration). Thus, Figure 5.3 shows the histories of one column up to nearly complete saturation and complete regeneration points. It can be seen that the desorption rate on average was much faster than the sorption rate at room temperature (31 hours of sorption and 2.5 hours of desorption). It is critical that the

column is sufficiently regenerated during a specific cycle time; otherwise, the accumulation of water vapor in the column over time would lead to a premature breakthrough in the PSA process, and natural gas could not be sufficiently dehydrated. In an industrial PSA process, the bed temperature is sometimes increased to increase the desorption rate; however, in this work biosorbents were regenerated at a fast rate at room temperature without external heating, which demonstrated the advantages of using the biosorbents for the PSA process, which was further demonstrated in cyclic dual-column experiments in Chapter 6.
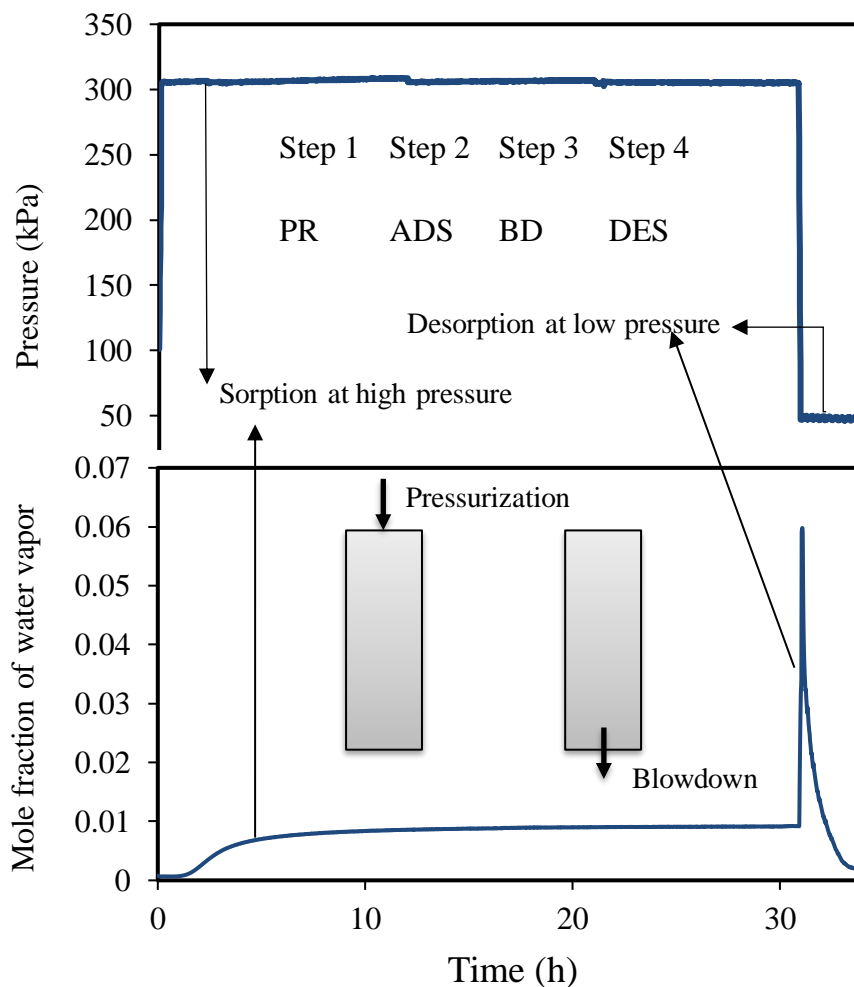
Figure 5.3: Column histories during the sorption-desorption cycle steps at 24 °C; PR: Pressurization; ADS: sorption at high pressure (300 kPa); BD: Blowdown; DES: Desorption under vacuum (46 kPa).

5.4 Reusability of Flax Shives in Repeated Sorption/Desorption Cycles

Biosorbents are expected to dehydrate natural gas during their lifetime with negligible deterioration and loss of their properties. To investigate this aspect, the performance of the biosorbent has been evaluated for 70 sorption-desorption cycles in the single column system. Furthermore, the thermal stability of the biosorbents was also investigated using the TGA analysis.

Figure 5.4 shows the breakthrough curves of water sorption by the fresh, 2nd time used, and 70th time used biosorbents in three experiments under same conditions. The 70th experiment was performed after all the experiments in the full factorial design and additional experiments for isotherms (see Table 5.2). As can be seen, the breakthrough curves overlapped with one another. The achieved water sorption capacities are similar, the average of which had a small standard deviation shown in Figure 5.5. The slight difference among the breakthrough curves could be a result of uncontrollable environmental disturbances. Therefore, the performance of the biosorbent was stable and the results were repeatable. Investigation on the effect of aging over a longer period of time would be necessary in future research.
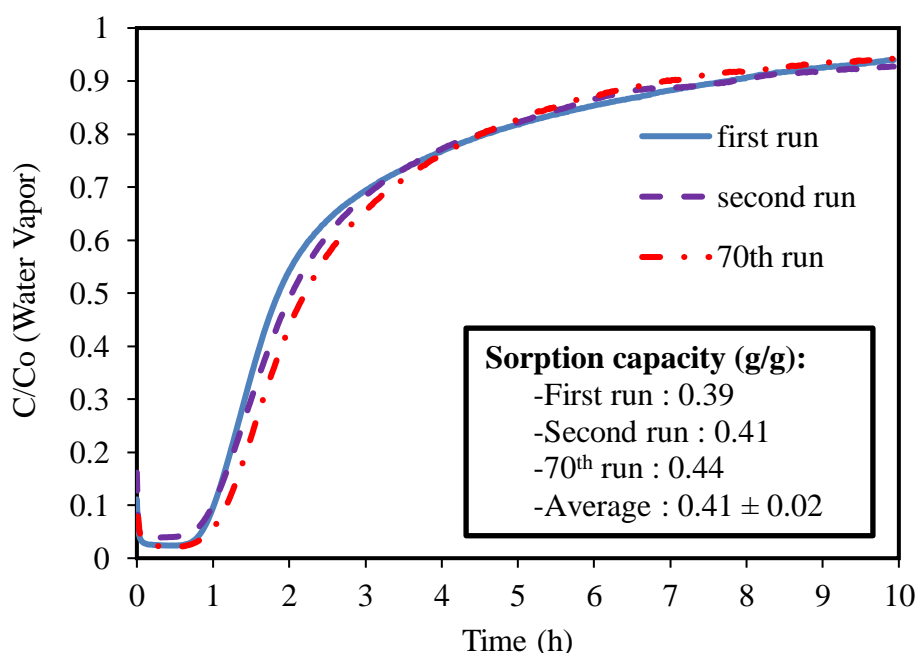
Figure 5.4: Reusability of flax shives for water vapor sorption; Dimensionless concentration of water vs. time; experiment ID in the design table 5, 300 kPa, 24 °C, and flow rate 4 L/min.

The thermogravimetric analysis (TGA) was also performed to determine the thermal stability of the biosorbent. The TGA results are presented in Figure 5.5. According to this figure, flax shives started to decompose at around 200 °C. The sharp blue peak indicates the

decomposition of cellulose at around 380 °C.[112] These temperatures are much higher than the operating temperatures of the PSA process using the biosorbents (24 to 50 °C) in this work, which confirmed that flax shive biosorbent is stable and suitable for dehydrating natural gas.
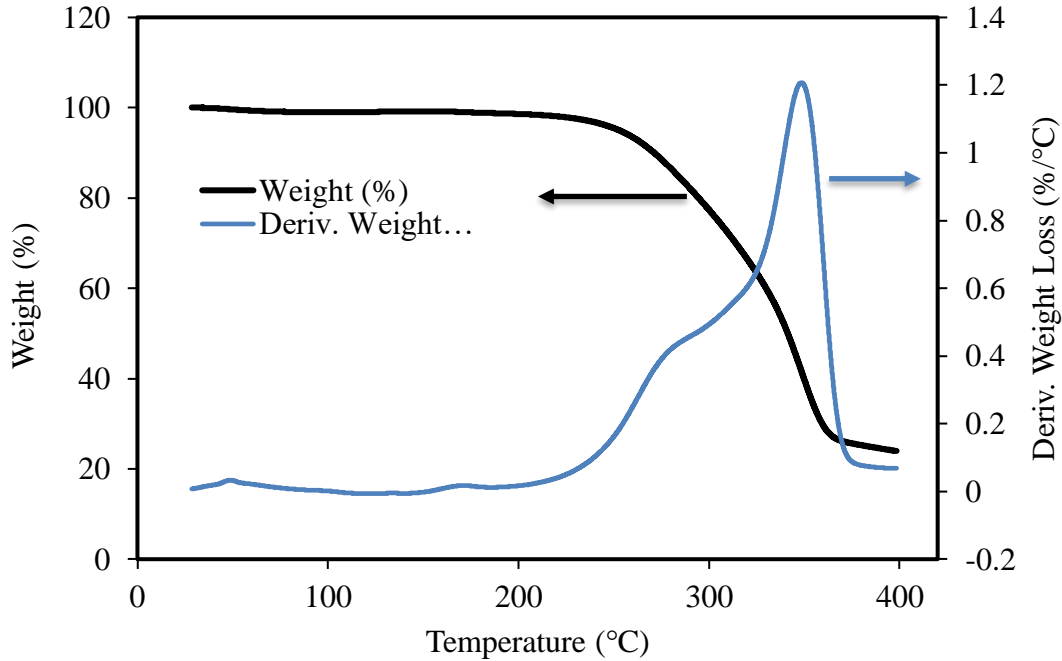
Figure 5.5: TGA results of flax shives; Sample weight loss as a result of thermal degradation and pyrolysis was measured over time as the temperature was gradually increased.

5.5   Mass Transfer Zone in the Flax Shives Layer in the Column

Information about mass transfer zone is important for the design and scale-up of PSA operations. The length of mass transfer zone plays a critical role in the design and operation of PSA systems, which can be determined using breakthrough curves and the following equation[5]:

$$MTZ = 2 \times H \times \left(1 - \frac{\int_0^{t_b} \left(1 - \frac{C}{C_o} \right) dt}{\int_0^{t_s} \left(1 - \frac{C}{C_o} \right) dt} \right) \tag{5.1}$$

where *MTZ* is the length of mass transfer zone, *H* is the height of the column packed with adsorbents, t_b is the breakthrough time, and t_s is the stoichiometric time. Stoichiometric time is the time that divides the mass transfer zone into equal areas.

Eq. 5.1 was used to calculate the length of mass transfer zone using the breakthrough curves obtained at various operating conditions. The representative breakthrough curves for determining the length of mass transfer zone are shown in Figure 5.6. The values are

summarized in Table 5.5. In this work, the breakthrough point for water was defined to be the point where C/C_0 of water vapor equals to 0.01 and equilibrium or saturation point was considered to be the point where C/C_0 of water vapor equals to 0.95; where C is the concentration in the outlet and C_0 is the concentration in the inlet.[5]

Table 5.5: Length of mass transfer zone (MTZ) calculated at various operating conditions.

Pressure (kPa)	Temperature (°C)	Flow rate (L/min)	Particle Size (mm)	MTZ (cm)
300	24	2	0.425 -1.18	10.81 ± 0.11
300	24	4	0.425 -1.18	11.59 ± 0.09
300	35	2	0.425 -1.18	7.09 ± 0.08
300	35	4	0.425 -1.18	8.02 ± 0.11
101.3	24	2	0.425 -1.18	8.49 ± 0.02
101.3	24	4	0.425 -1.18	11.49 ± 0.03
101.3	35	2	0.425 -1.18	8.18 ± 0.06
101.3	35	4	0.425 -1.18	9.23 ± 0.04
300	24	4	0.425 -1.18	10.3 ± 0.11
300	24	4	1.18 – 3.0	9.60 ± 0.09

The ability to predict the length of mass transfer zone under changing conditions in a PSA process is critical. In this work, it was observed that the length of mass transfer zone increased with an increase in the total gas flow rate, which is likely a result of increasing Reynolds number and the residence time of water molecule in the column. On the other hand, the length of mass transfer zone decreased with increasing temperature. This observation could be because of an equilibrium effect (different isotherms) as well as the effect of temperature on molecular diffusion. The effect of pressure was different at low and high temperatures, which is likely a result of the different sorption mechanisms as discussed in the isotherm study in Chapter 6 (monolayer and multilayer sorption mechanisms). Pressure simultaneously affects the equilibrium and transport phenomena in the packed bed, which might have an interacting effect on the length of MTZ. Serbezov studied the mass transfer in a packed bed of biosorbents based on tea wastes for the adsorption of chromium (VI) and also reported an increase in the length of mass transfer zone with an increase in the flow rate and pressure; however, the author

did not report the results obtained at various temperatures.[113] Dynamic modeling of PSA process can provide detailed information on this subject, which is the topic of another chapter.
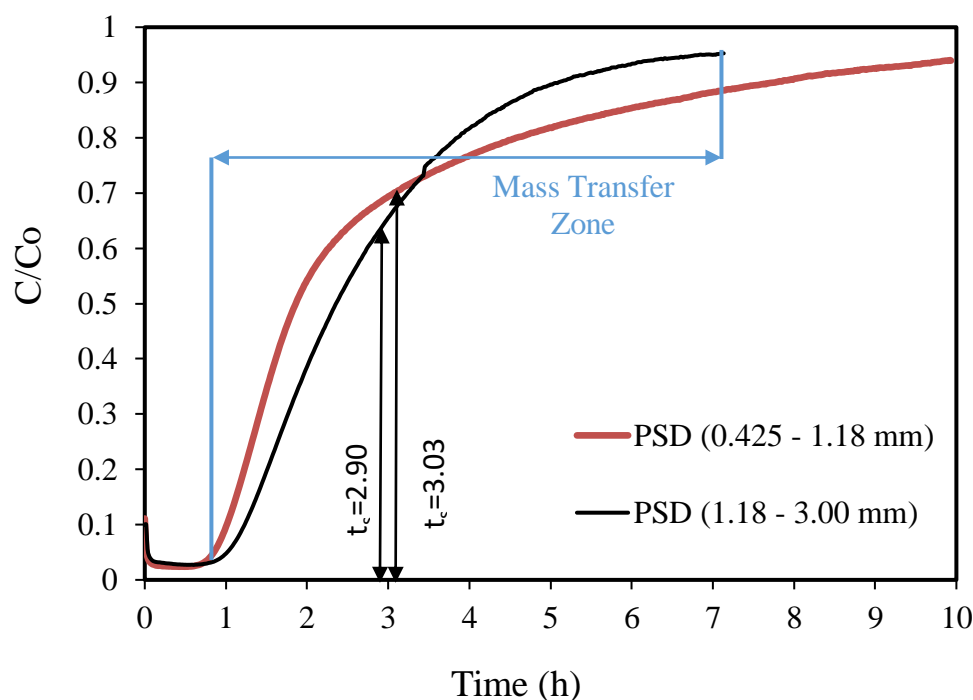
Figure 5.6: Representative breakthrough curves, and length of mass transfer zone. t_b is breakthrough time; t_s is the stoichiometric time; conditions: 300 kPa, 24 °C, feed water mole fraction: 0.0098, and flow rate: 4 L/min.

The effect of biosorbent particle size on the length of mass transfer zone was also evaluated using two different particle size ranges (0.425-1.18 mm, and 1.18-3.00 mm). The results show that the length of mass transfer zone is insignificantly affected by the particles size under the experimental conditions (300 kPa and 24 °C).

A low pressure drop in the range of 2.9 – 5.8 kPa was observed in the above-mentioned experiments. Tajallipour et al. reported a low pressure drop of 2.1-3.4 kPa for canola meal.[9] Pressure drop was reduced to 1.8 kPa when biosorbents with particle size distribution of 1.18 – 3.00 mm were packed in the column. Using the Ergun equation, a value of 0.32 was calculated for the bed voidage at 300 kPa. The bed voidage is lower than the values reported for packed bed of spherical particles (0.4 or higher) as a result of the cylindrical shape of flax shives.[5] Activated alumina particles have a rough cylindrical shape similar to that of the flax shives particles and Neufeld et al.[114] and Rimpel et al.[115] reported bed voidage values of 0.25 and 0.34 for activated alumina, which are close to the values obtained for flax shives in this work.

5.6 Analysis of Water Vapor Sorption by Flax Shives Using Optical Microscopy

Optical microscopy imaging provides information on the dynamic of water transport through the biosorbent particles. In this work, the water sorption (adsorption and absorption) by the biosorbent was monitored over time using dyed water (Figure 5.7). After the addition of the dyed water, the water molecules marked by the dye diffused into individual flax shive particles. The water sorption occurred mainly along the longitudinal walls of the shive cells, with reliance on water cohesion to fill the shive structure (supplementary video is available). As water travelled through the shive's structure, the cells were not filled in a clear pattern. Upon the addition of the shive particle from one of the longer sides, the water molecules travelled preferentially along a parallel route to the side and unevenly across the cells (Figure 5.7-B). This observation could be as a result of non-uniformity in the cell structures seen under FE-SEM as well as differences in structural makeup of individual cells. These results are preliminary and the effect of parameters such as surface tension, viscosity, and dye concentration/type need to be analyzed in future work.
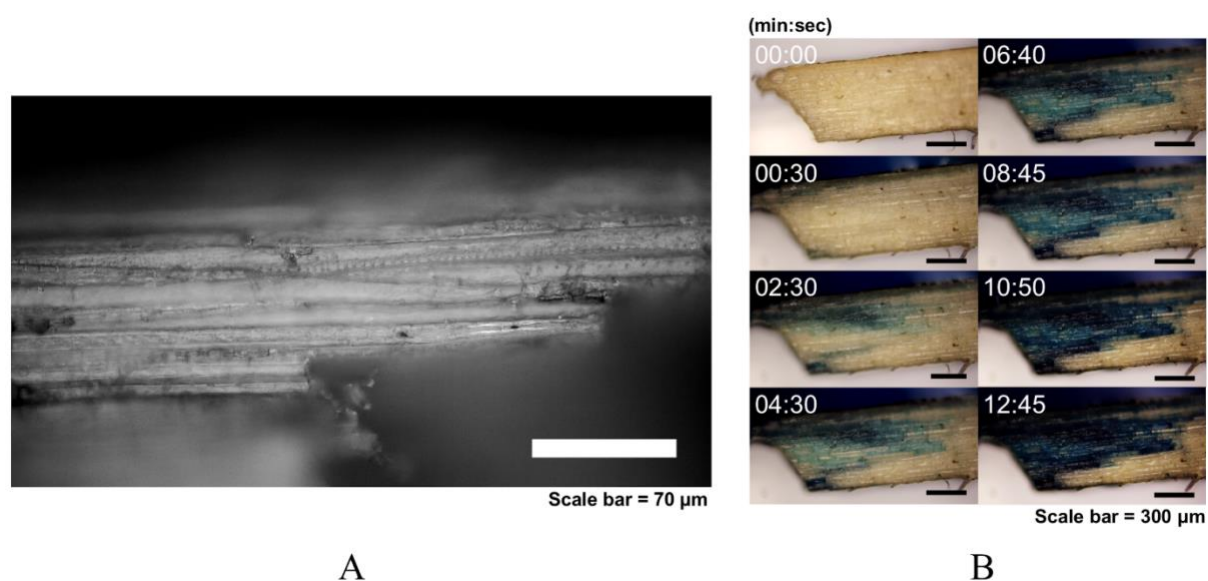
Figure 5.7: Optical microscopy images of flax shives; A: A representative optical image of a flax shive particle (Scale bar, 70 μm). B: Time lapse images of a flax shive particle upon the addition of 5% v/v blue dye. Images were captured using a 10x objective (Scale bar, 300 μm).

Though this observation was performed by monitoring the liquid water within the flax shive particles, the results does provide insights on the water vapor sorption. Working with water vapor at microscopic scale or nanoscale is very challenging as most equipment operate at an ultimate vacuum; thus, introducing humidity is impossible. It would be of interest to

further investigate water vapor sorption in future studies through advanced imaging technologies.

5.7 Performance of Oat Hulls and Biosorbents from Different Batches

5.7.1 Natural Gas Dehydration Using Oat Hulls

In this section, another commonly available agricultural byproduct, oat hulls, was investigated for gas dehydration. The objective was to analyze similarities or differences of this class of materials, which are mainly composed of cellulose and hemicellulose. Similar to flax shives, the developed biosorbents from oat hulls were first analyzed for the adsorption of methane, carbon dioxide, and nitrogen. The column was packed with 40 grams of oat hulls. Numerous experiments at various pressures and total gas flow rates were performed and it was confirmed that the adsorption of nonpolar gases by oat hulls was negligible, which was expected because the properties of oat hulls are very similar to those of flax shives. Next, moisture sorption was analyzed at various conditions according to a full factorial experimental design. Since the total gas flow rate did not have any effect on the water sorption by flax shives, the effect of total gas on the moisture sorption by oat hulls was firstly investigated. The results showed that its effect was negligible; hence, it was not considered as a level in the factorial design and flow rate of 3 L/min was considered for all experiments.

Figure 5.8 shows concentration histories of a methane dehydration experiment at 100 % RH, 300 kPa and 24 °C. As can be seen in this figure, dry gas was collected from the bottom of the column at the beginning of the experiment; afterwards, the water vapor concentration in the outlet had gradually increased and reached to that of the feed gas. Methane was not adsorbed by the biosorbent and its mass flow throughout the experiment is shown, which indicates the high selectivity of the biosorbent. The mole fraction of methane in this experiment was 0.37 and the carrier gas was helium. The first sample for GC analysis was taken about 10-15 seconds after the start of adsorption experiment, and the concentration of methane was the same as that of the feed. If there was any methane adsorption within these few seconds, it was beyond the detectable limit of the GC; however, that amount of methane adsorbed is negligible compared to 19 hours of water vapor sorption.
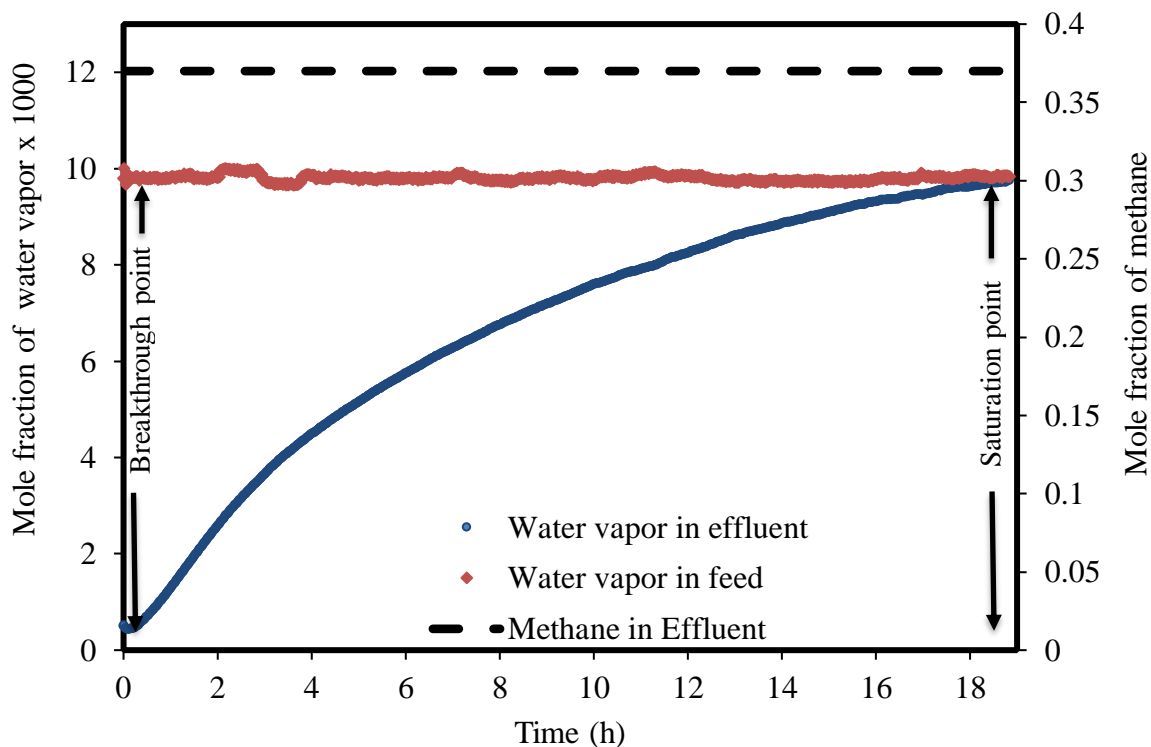
Figure 5.8: Concentration histories during the sorption experiment; 300 kPa and 24 °C; flow rate 3 L/min; Average standard deviation of all water input and output mole fraction data points is 9.47×10^{-5}.

The results of the full factorial experimental design is reported in Table 5.6. Statistical analysis was performed using the same procedure illustrated in the previous chapters and the results were similar to those obtained for flax shives (details in the supporting data). Total pressure had the most significant effect on the sorption capacity (partial estimated squared value of 0.9) followed by temperature, and then mole fraction of water vapor in the feed.

Table 5.6: Results of full factorial experimental design – oat hulls - Sorption capacities (q)

T: temperature; P: total pressure; C: water vapor mole fraction; SD: standard deviation

ID	T (ºC)	P (kPa)	C	q average (mg/g)	SD
1	24	300.0	0.0098	630	6
2	24	300.0	0.0049	200	3
3	24	101.3	0.0098	128	4
4	24	101.3	0.0049	59	8
5	35	300.0	0.0098	187	5
6	35	300.0	0.0049	90	10
7	35	101.3	0.0098	43.4	0.8
8	35	101.3	0.0049	23.8	0.8

5.7.2 Water Vapor Desorption and Reusability of Oat Hulls

In this section, similar desorption experiments were performed to compare the desorption properties of oat hulls with those of flax shives. To investigate the water desorption from oat hulls, an experiment was performed at 300 kPa, 24 °C, 3 L/min total gas flow rate, and 100% humid feed gas. Desorption step was performed under a pressure of 47 kPa absolute and 24 °C, and the flow rate of carrier gas (nitrogen) during sorption was 1.5 times of the feed gas flow rate during the sorption step (4.5 L/min), which was recommended for many PSA systems in industry[5,33]. The flow rate 4.5 L/min was measured at the vacuum pressure (47 kPa). Similar to the results reported for flax shives, oat hulls were effectively regenerated at room temperature without external heating and almost the same water vapor sorption capacity was obtained for duplicated experiments. To investigate the reusability of the biosorbent, the first experiment using fresh biosorbent (experiment 4 in Table 5.6) was repeated after 50 sorption-desorption cycles in the single column system; then, the sorption capacity and the dynamic behavior of the system were compared. These results are shown in Figure 5.9 that shows the dimensionless breakthrough curve for these three experiments. It can be noticed that the measured water vapor sorption capacities and the dynamic behavior of the system were similar. The slight difference among the breakthrough curves is because of noises and uncontrollable environmental disturbances in the system. Overall, the results suggest that oat hulls could be effectively regenerated without external heating and be used in numerous cycles with negligible degradation, similar to the results achieved for flax shives.
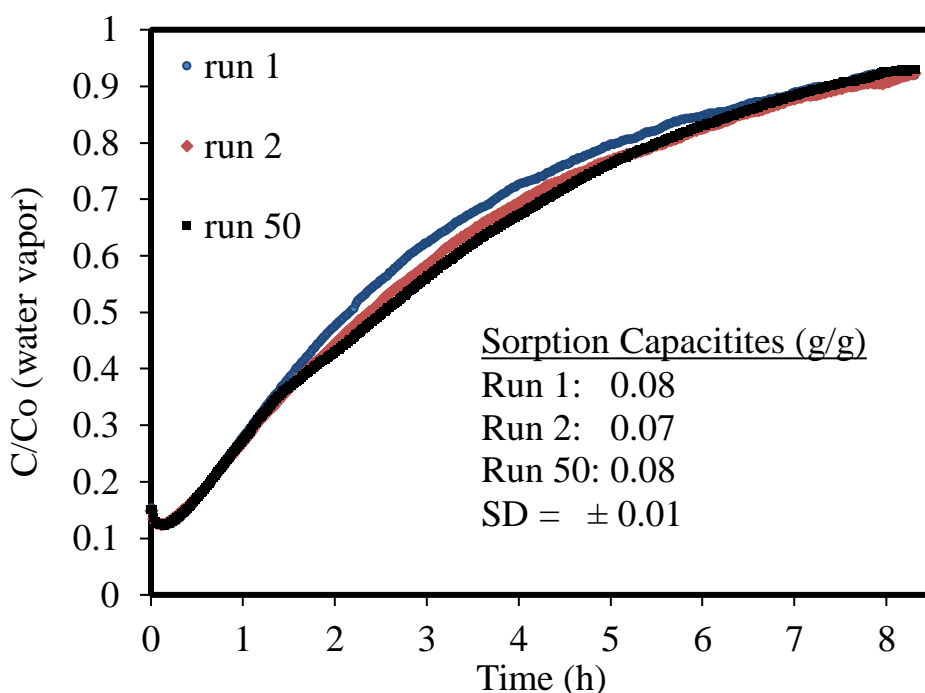
Figure 5.9: Reusability of oat hulls for natural gas dehydration; Dimensionless concentration of water vs. time; experiment ID in the design table, 300 kPa, 24 °C, RH 25%, and flow rate 3 L/min.

TGA experiment was also performed to investigate the thermal stability of the biosorbent (Figure in the supporting data). According to the results, the oat hulls started to decompose at a temperature around $210 °C$. This temperature is much higher than the operating temperatures of the PSA process for natural gas dehydration (35 to $40 °C$); hence, there would be no issues in this process using the biosorbent. The weight change at the beginning of the experiment is as a result of drying of sample (inbound moisture or adsorbed moisture from atmosphere while the sample was loading on the device). In terms of thermal stability, flax shives and oat hulls are also similar.

5.7.3 Performance of Biosorbents from Different Batches and Sources

To investigate the effects of different batches and sources of feedstocks on gas dehydration, a new batch of flax shives (2018) was acquired from Biolin Research Inc. Saskatoon, and two batches of oat hulls (2017 and 2018) from Richardson Milling, Saskatoon. The results showed that the new batch of flax shives and both batches of oat hulls did not adsorb substantial amounts of nonpolar gases. They were able to selectively sorb water vapor and successfully dehydrate the gases. Figure 5.10 exemplifies the results by showing the breakthrough and regeneration curves of the flax shives batch provided by Biolin Research Inc.

In addition, it can be seen in the figure that the biosorbent were effectively regenerated at room temperature at fast rates similar to the first batch.
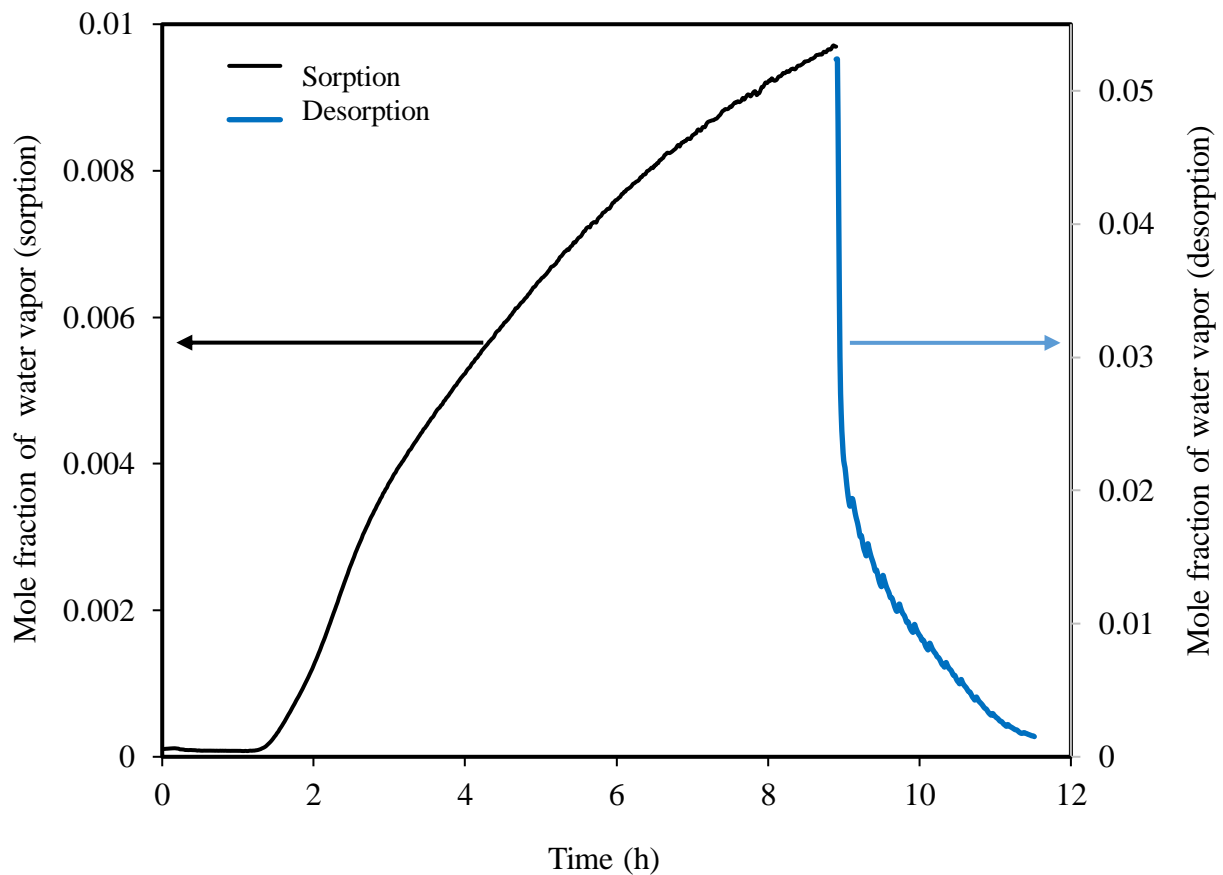
Figure 5.10: Concentration histories during the sorption and regeneration of the flax shives batch supplied by Biolin Research; sorption at 300 kPa and 24 °C; gas flow rate 4 L/min and water mole fraction in feed was 0.0098; desorption time (2.5 h) was much lower than the sorption time (8.9 h).

The sorption capacity of the biosorbents achieved at the same experimental conditions are summarized in Table 5.7. The second batch of flax shives showed a lower sorption capacity compared to the first batch, while the trend was opposite for the first and second batches of oat hulls. It seems that different batches and sources of the materials led to different water sorption capacity. However, all of the evaluated materials had adequate water sorption capacity. In addition, the regeneration properties of biosorbents are critical and were the reason behind the success of the PSA process for natural gas dehydration. The columns and cycle time could be properly designed to contain the mass transfer zone in the column during the PSA process.

Table 5.7: Water vapor sorption capacity of two different batches of flax shives and oat hulls; all the sorption capacity values are maximum values achieved in g/g under same experimental conditions.

Flax shives SWM (2017)	Flax shives Biolin research (2018)	Oat hulls batch 2017	Oat hulls batch 2018
0.90 ± 0.01	0.57 ± 0.02	0.63 ± 0.01	0.90 ± 0.02

The composition of flax shives SWM and oat hulls batch 2017 were reported by the manufacturer, but the composition of other batches were unknown. In a few failed attempts to measure the composition of all four batches, some unknown sugar compounds were observed, which could not be quantified using the equipment and facilities available. Hence, no conclusions are made here. Determining the correlation between the water vapor sorption capacity and the composition of the biosorbents could form a research objective for future study. Overall, the main research objective in this chapter was to demonstrate the gas dehydration capability of flax shives and oat hulls as two examples of biosorbents developed from agricultural byproducts. The results confirmed that flax shives and oat hulls are similar and both demonstrated successful performance and excellent properties for water sorption and gas dehydration.

5.8   Chapter Summary

In this chapter, the single-column system was used to investigate natural gas dehydration using biosorbents. Started with single-component feed gases, the sorption capacity of natural gas components including water vapor, methane, nitrogen, and carbon dioxide was determined. The results showed that the biosorbents developed from flax shives and oat hulls were highly selective to water vapor and did not adsorb substantial amounts of nonpolar components such as methane and carbon dioxide. The two materials had water sorption capacities up to 0.9 g/g at 300 kPa and 24 °C. They were easily regenerated by dropping the absolute pressure to ~40 kPa, which is much economically favorable than the vacuum levels used in other VSA processes in industry. Flax shives showed a stable performance in 70 sorption-desorption cycles and no significant degradation was observed, while oat hulls performance was stable up to 50 cycles. Both of the materials can be used continuously. Among the main operating parameters, pressure had the most significant effect followed by temperature. The length of mass transfer zone at various operating conditions were determined and reported as well. The performance of the biosorbents from different batches and sources was also investigated and compared with those of commercial adsorbents used in dehydration

industries. Two batches of flax shives and two batches of oat hulls were analyzed and both had acceptable water sorption capacities and selectivities. Moreover, all batches of biosorbents were easily regenerated at room temperature at fast rates without any external heating. Furthermore, an optical microscopy imagery method was used provide further information on the water transport and the sorption phenomenon in the flax shives particles. The results achieved in the chapter are the foundation for further investigation reported in the following chapters of this dissertation.

Chapter 6.   Equilibrium of Water Sorption by the Biosorbent

In this chapter, the presented sorption isotherm theories in Chapter 2 were applied to analyze the experimental equilibrium data in order to obtain information about the fundamentals of the water sorption process and its underlying mechanisms. A number of isotherm models were fitted on the equilibrium data, each of which provided new pieces of information about the sorption characteristics. In addition, the water sorption mechanism is discussed and compared to that of similar bio-based materials reported in the literature. As seen in previous chapters, flax shives and oat hulls are similar in terms of properties and water sorption performance; therefore, this chapter only presents the results using flax shives as a model material and the details in regard to the equilibrium of oat hulls can be found in the papers published by the author of this thesis. The flax shives samples used in this chapter were the batch of 2017 provided by SWM international. It is to note that gas dehydration by lignocellulose materials could be involved in adsorption and/or absorption. Thus, the term "sorption" and its respectively derived term "sorb", and so on are used where applicable in this chapter when discussing water vapor in this thesis. This term has been widely used in the literature for water sorption by similar materials composed of cellulose and hemicellulose. The term "adsorption" is used when discussing the nonpolar gases such as methane, carbon dioxide, nitrogen, and helium.

6.1   Equilibrium Data of Water Vapor Sorption

The experimental water sorption equilibrium capacities of flax shives were determined at various operating conditions in accordance to the full factorial experimental design. The isotherms at 300 kPa and 24 $^{\circ}$C was nonlinear, while those at other conditions tested in this work were almost linear. The experimental data are presented in Figure 6.1. As temperature was increased, the water sorption capacity decreased, while the water sorption capacity increased with increasing total pressure within the tested range. These observations are typical of an exothermic phenomenon; however, the change in the isotherm type suggest a significant difference in the water vapor sorption mechanisms under different conditions. More analyses in the regard were performed and reported later in this chapter. As can be seen in Figure 6.1, the effect of total pressure on the equilibrium isotherms is more significant than the effect of temperature. Moreover, the effect of temperature on the isotherm at 101.3 kPa was less significant than its effect at 300 kPa. These observations are in harmony with the statistical analysis reported in Chapter 5. A considerable increase in the water sorption capacity was observed at 300 kPa when the temperature decreased from 35 to 24 $^{\circ}$C. Furthermore, the

magnitude of this increase had a rising trend with increasing water vapor mole fraction to the point that the isotherm type also changed to a nonlinear form.
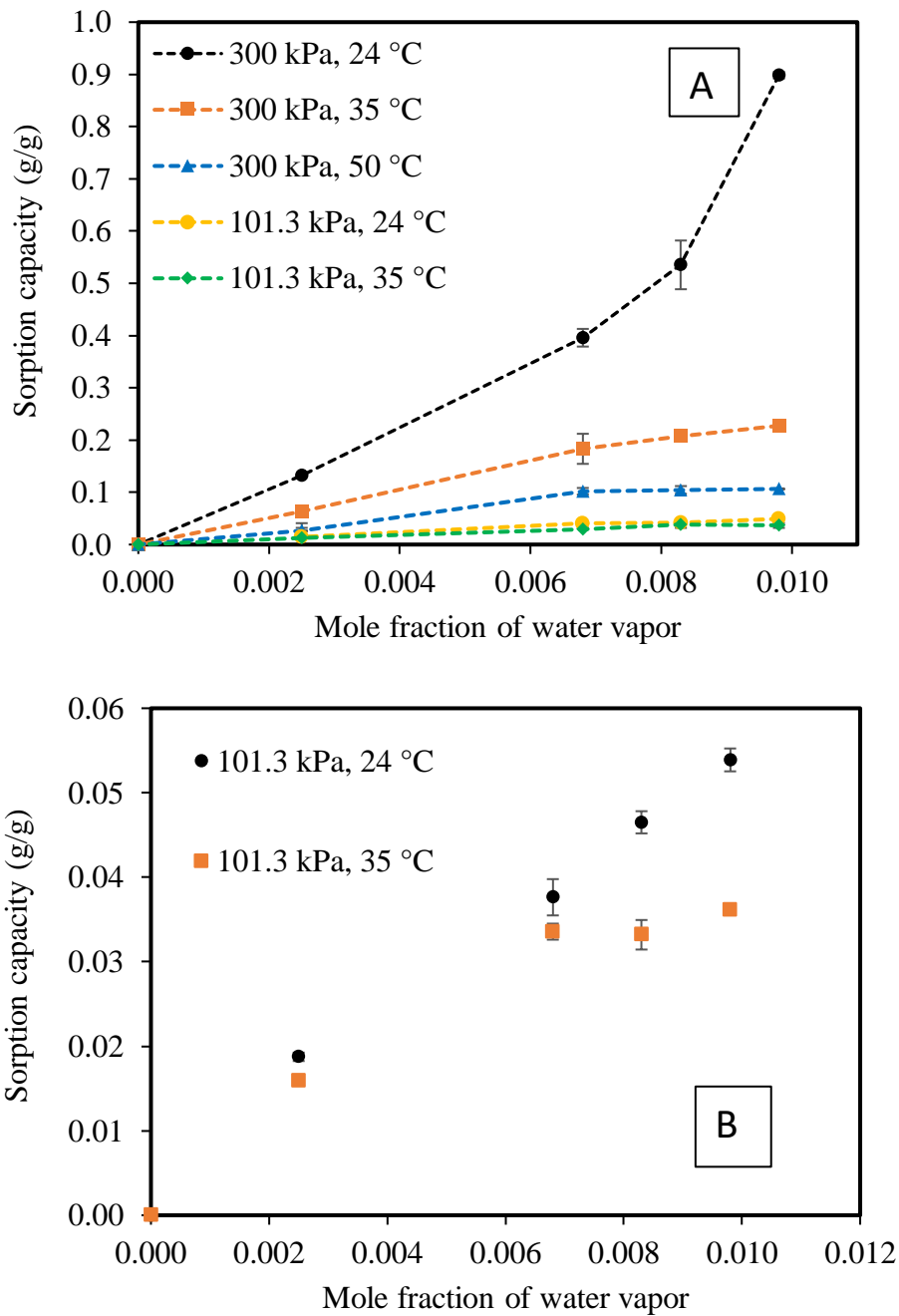
Figure 6.1: Water vapor sorption equilibrium data of flax shives obtained at different temperatures and pressures. A: Effects of total pressure and temperature on sorption isotherms; B: Zoom-in isotherms obtained at 101.3kPa and 24-35ºC. Error bars represents standard deviations.

In the following sections, the isotherm modeling results are reported and discussed. The goodness of fit was assessed and the model coefficients were analyzed and compared to the values reported in the literature for water vapor sorption.

6.2 Isotherm Modeling

As described in the above section, the equilibrium water vapor sorption data was determined in the pressure and temperature ranges of 101.3 – 300 kPa and 24 – 50 °C. Only the isotherm at 300 kPa and 24 °C was nonlinear, while the other isotherms were almost linear. Thus, the modeling results are presented in two sections of non-linear and linear isotherms.

6.2.1 Non-linear Isotherm

6.2.1.1 Redhead Model

The Redhead model has two fitting parameters and is suitable for isotherms type II and type III isotherms. The model and its description were provided in Chapter 2 and Eq. 2.4. It was used in this work to determine the monolayer water sorption capacity of flax shives using the isotherm at 300 kPa and 24 °C. The modeling results are presented in Figure 6.2, and Table 6.1. It can be observed that the Redhead model simulated the isotherm reasonably well. All experimental data points were within the 95% confidence intervals, and a reasonable R squared value was achieved. According to Table 6.1, the monolayer water sorption capacity was 0.009 mol/g, which is the same as the value obtained from the GAB model to be described later.
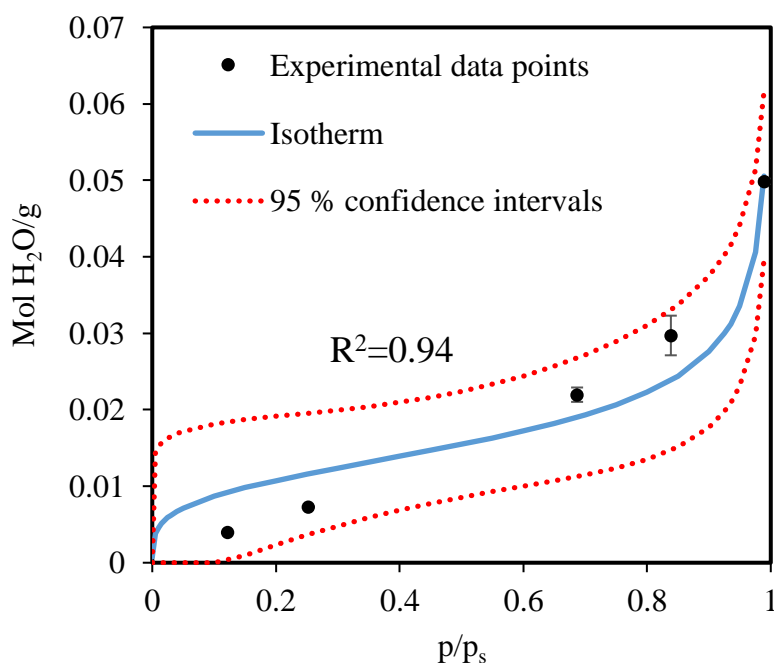
Figure 6.2: Redhead isotherm fitted on the experimental data points at 300 kPa and 24 °C.

Table 6.1: Summary of the nonlinear isotherm modeling results; SSE: sum of squared errors.

Redhead Model					
P (kPa)	T(ºC)	n	$q_{m \, (mol/g)}$	SSE	R^2
300	24	3.8	0.009	$9.3E^{-05}$	0.96

GAB Model					
P (kPa)	T(ºC)	$q_{m \, (mol/g)}$	c_a (pa)	k (pa^{-1})	SSE	R^2
300	24	0.009	9.14	0.83	$9.5E^{-06}$	0.99

The estimated water vapor monolayer sorption capacity seems reasonable and is within the range of values reported in the literature for similar bio-based sorbents. As can be seen in Table 6.2, the monolayer sorption capacities in the range of 0.04 – 0.31 g/g were reported for the water vapor sorption by various materials, where the monolayer sorption capacity of flax shives (0.16 g/g) falls within this acceptable range.

Table 6.2: Comparison of the water vapor monolayer sorption capacities of several sorbent materials.

Material	T (°C)	$q_{m \, (g/g)}$	Isotherm Model	Reference
Flax shives	24	0.16	GAB, Redhead	This work
Canola meal	100	0.11	GAB	9
Pectin	29	0.11	BET	105
Corn flour	22	0.08	GAB	118
Pineapple peel	25	0.31	GAB	118
Walnut peal	25	0.04	GAB	118
Zeolite	25	0.13	Langmuir	64

6.2.1.2   GAB Model

The GAB model has three fitting parameters and can provide information on the excess heat of water sorption in addition to the monolayer water sorption capacity. The model was presented through Eq. 2.1 in Chapter 2. It was used in this work for three reasons: 1) to separately determine the monolayer water sorption capacity and compare the estimated value with that from the Redhead model; 2) to determine the excess heat of water sorption; and 3) to

enhance the goodness of model fitting because the R^2 of the Redhead model was 0.94. The GAB model (Eq. 2.1) was applied to simulate the nonlinear water sorption isotherm at 300 kPa and 24 °C very well with a R^2 value of 0.99, as can be seen in Figure 6.3. The experimental data points were also within the 95 % confidence intervals of the model fitting line. The optimal model parameters are summarized in Table 6.1. The monolayer water sorption capacity estimated using this model is the same as that predicted using the Redhead model.
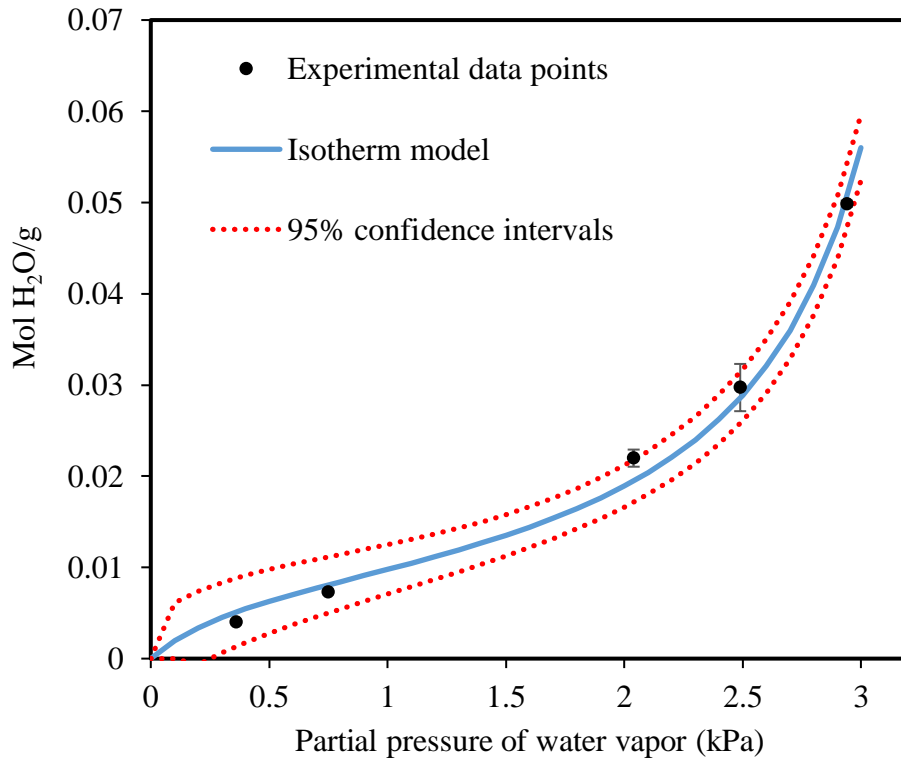
Figure 6.3: GAB isotherm fitted on the experimental data points at 300 kPa and 24 °C.

The value of k representing the surface affinity of the biosorbent towards water vapor is around 0.83 Pa^{-1}, which is higher than the values obtained for conventional adsorbents in the literature (0.6 to 0.7).[32] This high value indicates the slightly stronger attraction of water molecules towards the surface of the biosorbent at 300 kPa and 24 °C.

6.2.2 Linear Isotherms

6.2.2.1 Linear Model

As for the simplest form of sorption isotherms (Eq. 2.7 in Chapter 2), the fitting results regarding the linear isotherm model are shown in Figure 6.4 and Table 6.3. As can be noticed, the linear isotherm was able to simulate the experimental equilibrium data with satisfaction. The value of Henry constant (sorption equilibrium constant) decreased with increasing temperature and decreasing total pressure. The values obtained at different temperature and pressure were used to determine the standard heat of water vapor sorption later.

Table 6.3: Summary of linear isotherm modeling results; SSE: sum of squared errors.

Fowler-Guggenhein Model						
P (kPa)	**T(ºC)**	**b (pa^{-1})**	**c$_{FW}$**	**w (J/mol)**	**SSE**	**R^2**
300	35	0.052	0.010	6.40	3.4E^{-04}	1.00
300	50	0.043	0.012	8.33	3.3E^{-01}	0.98

Linear Model				
P (kPa)	**T(ºC)**	K_L (**mmol/g.kPa**)	**SSE**	**R^2**
300	35	4.55	1.39	0.99
300	50	2.27	1.73	0.94
101.3	24	3.07	0.11	0.99
101.3	35	2.26	0.11	0.93
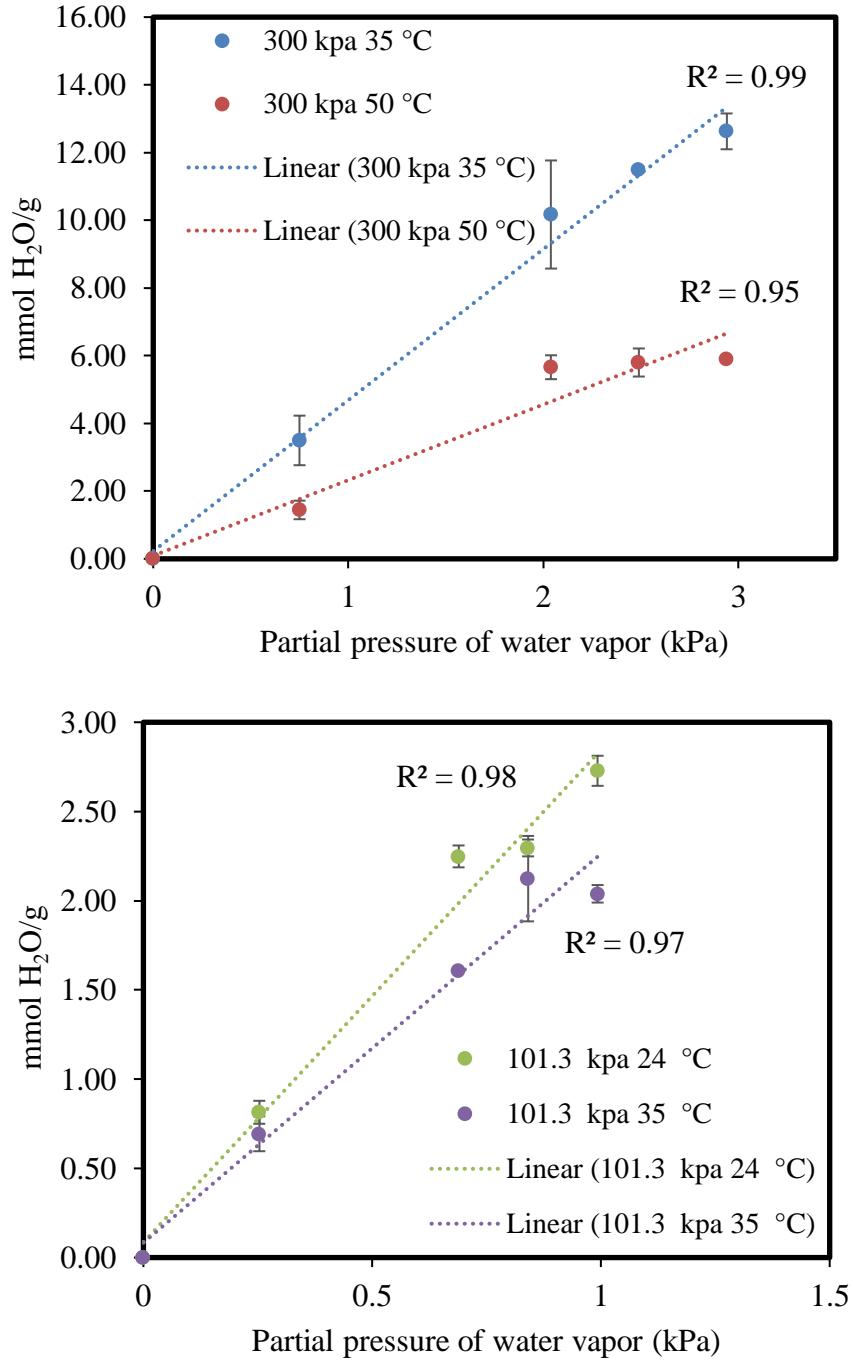
Figure 6.4: Linear isotherms fitted on the experimental data at various operating conditions.

6.2.2.2 Fowler-Guggenhein Model

The Fowler-Guggenhein (F-G) model (Eq. 2.5 in Chapter 2) was used in this work in addition to the linear isotherm to determine the lateral interactions among the sorbed molecules on the surface. This model can also demonstrate whether two-dimensional condensation took place during the water vapor sorption. The surface affinity of water towards the surface can be determined by this model as well. The fitted isotherm is shown in Figure 6.5. The results demonstrated that the G-F model similarly provided satisfactory prediction for the isotherms obtained at elevated temperatures 35, and 50 °C. The regressed model parameters are summarized in Table 6.3.

It can be noticed in the modeling results that the surface affinity (sorption equilibrium constant) towards water vapor, represented by the value of b, slightly decreased with increase in the temperature. The results again confirmed that water sorption was exothermic. Thus, at elevated temperatures, both surface affinity and sorption capacity decreased. In addition, the value of c_{FW} was 0.01, which is smaller than 4, indicating that no two-dimensional condensation took place in the system operated at 35 and 50 °C.[32]

The lateral interaction parameters (w) were calculated using Eq. 2.6 presented in Chapter 2 and are listed in Table 6.3 as well. A value of 4 was used for the water's coordination number, which was calculated from molecular dynamic simulations.[32] In this work, the values of w are all positive, indicating attraction between sorbed water molecules on the surface. The lateral interactions also slightly increased with increasing temperature in the tested range, which seems to be a result of higher internal energy and more collisions among atoms on the surface; however, this change was not significant within the tested range in the experiments. The attraction forces among water molecules sorbed onto the surface of flax shives (6 – 8 J/mol) are much lower than the van der Waals weak forces (400 – 4000 J/mol) and hydrogen bonds such as HO-H⋯OH_3^+ (18,000 J/mol).[119] Water molecules in liquid state (condensed water on surface) are held together by hydrogen bond.[119] Therefore, the results suggest that the sorbed water vapor molecules on the surface of flax shives were not in liquid or condensed state; rather low density physisorption. In the case of strong interaction among the sorbed water molecules on the surface, the density of sorbed phase suddenly raises to high densities, which leads to the two-dimensional condensation phenomenon.[32] Overall, the F-W modeling results conclusively suggest that water sorption by flax shives under the tested

conditions (dilute system) is exothermic physisorption with Henry behavior at very dilute concentrations.
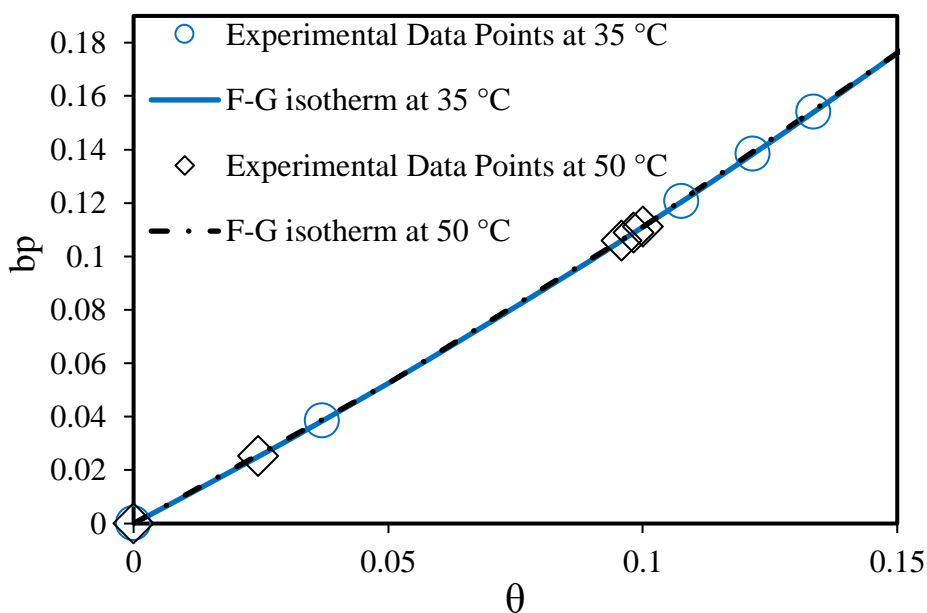
Figure 6.5: F-G isotherm fitted on the experimental data points at 35 and 50 °C; flow rate 2 L/min.

6.3 The Heat of Water Sorption

The heat of sorption not only acts as an indicator of the strength of the interaction between an adsorbate and a solid sorbent, but also provides information on the sorption mechanism. In this work, the isotherm modeling results were further used to determine the standard heat of water sorption. The respective equations are presented in Chapter 2. The heat of water sorption based on different isotherm models was determined for comparison. First, the standard heat of sorption was determined by the van't Hoff's equation (Eq. 2.8 in Chapter 2) using the linear isotherm coefficients. The estimated standard heat of sorption (ΔH) at 300 kPa and 101.3 kPa were -39 and -21 kJ/mol, respectively. Flax shives mainly contain cellulose, hemicellulose, and lignin, all of which have abundant polar groups such as hydroxyls, Ph-OH (Ph: phenol), carboxyls and so on. According to Steiner[120], the enthalpies of the hydrogen bonds formed between these groups and water molecules are in the range of 25-34 kJ/mol. The obtained values of the heat of water sorption in this work are within this range. Therefore, the results provides an evidence that water sorption by the biosorbent could be through hydrogen bonding between water molecules and the polar groups such as hydroxyls, Ph-OH, carboxyls, and additional polar groups on the surface. In addition, the similar standard heat of water sorption by canola meal[9] and molecular sieves 3A[5] were reported as -32.11 and -45.95 kJ/mol,

respectively. According to these references, these materials also contain functional groups such as carboxyl, hydroxyls, and additional polar groups. Hydrogen bonds can also form between those groups and water molecules. As such, the heat of sorption is similar to those obtained in this work.

Second, the excess heat of liquefaction was calculated based on the GAB modeling results using Eq. 2.2. It is the amount of released energy per mole of water vapor sorbed on the second or any subsequent layers on the surface of sorbent during the multilayer sorption. According to the multilayer sorption theory, it takes more energy for the molecules in the second and subsequent layers to desorb from the sorbed phase into the gas phase compared to the first layer (monolayer).[32] A value of -0.45 kJ/mol was determined for the excess heat of liquefaction for sorption at 300 kPa in this work. Values around -0.25 kJ/mol were reported for the excess heat of liquefaction in the literature for most cases such as the adsorption of nitrogen and hydrocarbons by various types of zeolites.[32] Therefore, the model predictions for the case of flax shives seem reasonable. One of the main assumptions of the GAB model is that the heat of sorption on the second layer is less than the heat of liquefaction.[32] The isotherm obtained at 300 kPa and 24 °C in this work was non-linear (type II like) suggesting a multilayer sorption mechanism, and this excess heat is released when second or subsequent layers of water are sorbed onto the first layer.

6.4   Mechanisms of Water Vapor Sorption by Flax Shives

As described above, the equilibrium water sorption data of flax shives demonstrated linear or non-linear isotherms at various operating conditions indicating different water vapor sorption mechanisms. Specifically, the water vapor sorption equilibrium data was determined in the pressure and temperature ranges of 101.3 – 300 kPa and 24 – 50 °C in this work and all the isotherms demonstrated linear or almost linear behavior except for the only isotherm obtained at 300 kPa and 24 °C, which was nonlinear (type II like) and corresponded to the maximum achieved water vapor sorption capacity within the tested range. To elaborate on the mechanisms of water vapor sorption for each type of the isotherms, i.e. linear and non-linear isotherms, this section further analyzes the results achieved in this work with relevant discussions with respect to the adsorption/sorption theories and similar results reported in literature.

6.4.1 Linear Isotherms

In general, a linear isotherm with a low heat of sorption in a dilute system indicates a physical sorption process with Henry's law behavior. Under the experimental conditions in this work, the system was very dilute (molar fraction of water vapor was 0.0098 at max). The surface affinity of water vapor towards the surface of flax shives under the tested region was within the range reported for physisorption $(0.4 - 0.5$ pa^{-1})[5,60,65,75]. Furthermore, the estimated two-dimensional condensation coefficient (c_{FW}) in the F-G model was smaller than 4, which indicates no two-dimensional condensation under the tested conditions.[5] According to Ruthven[5], the heat of sorption in chemisorption is typically higher than 2 or 3 times the latent heat of evaporation. Considering the latent heat of water evaporation (-40.8 kJ/mol), the estimated values of heat of sorption in this system are in the range of -39 to -21 kJ/mol indicating that water vapor sorption by flax shives is physisorption under the tested conditions. Furthermore, it was reported by Ruthven[5] that chemisorption is monolayer only and possible over a wide range of temperature, while physisorption is monolayer or multilayer and only significant at relatively low temperatures. Physisorption is rapid and reversible in contrast to chemisorption that is activated and may be slow and irreversible. The results of sorption-desorption cycles presented in Chapter 5 and 6 of this thesis showed that the water vapor sorption by the biosorbent was fast, reversible, and more significant at a lower temperature such as 24 °C in comparison with the results in the range of 35-50°C. In addition, the negative sign of the heat of sorption obtained in this work also confirmed that the water sorption is exothermic. As such, water vapor sorption by flax shives demonstrated the nature of physisorption at the tested conditions in this work.

In addition, the results of FT-IR and XPS and additional characterization of the flax shives presented in Chapter 4 shows that the biosorbent mainly contains cellulose, hemicellulose, and lignin, which have abundant polar groups such as hydroxyls, Ph-OH, carboxyls, and so on. The electrostatic forces are involved here and hydrogen bond can form between these polar groups and water molecules. This was supported by that the heat of water sorption in this system was in the range of 21-39 kJ/mol, which is similar to the hydrogen bond enthalpy values reported in the literature for hydroxyls, Ph-OH, and carboxyls and water molecules (25-34 kJ/mol)[120]. Hydrogen bonding is considered to be complex interactions, which may be contributed from electrostatics, polarization, van der Waals, charge transfer, dispersion, exchange repulsion, and combination of any of them[120]. The energy of most of these interactions is in the energy range of physiosorption.

Based on the experimental and modeling analysis results achieved in this work, it could be collectively suggested that the water vapor sorption by flax shives for the case of linear isotherms obtained under the operation conditions could be exothermic, and physiosorption in nature. The water vapor could be sorbed on the functional groups such as hydroxyls, Ph-OH, and carboxyls on the surface of the biosorbent through hydrogen bonding or additional interaction with similar energy levels. Oat hulls and other similar lignocellulose materials may have similar mechanisms of water vapor sorption.

6.4.2   Non-linear isotherm

The non-linear isotherm and the observed change in the behavior of the water vapor sorption system requires close scrutiny. The non-linear isotherm was obtained at the lowest temperature 24 °C and highest total pressure 300 kPa within the tested conditions. According to Figure 6.1, as the temperature was decreased from 35 and 24 °C, the two isotherms generated at 300 kPa drastically changed; the water vapor sorption capacity of flax shives increased from 0.2 to 0.9 g/g at 100 % RH and 0.19 to 0.5 g/g at ≈80 % RH, respectively. This increase is considerably significant compared to the changes in the other isotherms at 101.3 kPa. In addition, the isotherm changed from linearity to nonlinear (a type II like) isotherm indicating that multilayer sorption took place (water sorption capacity increases sharply when the relative pressure p/p_s increases to 1), which suggests a fundamental change in the sorption mechanism.

First, the sorption mechanisms were analyzed from the perspective of flax shives composition. As mentioned before, flax shives are mainly composed of cellulose, hemicellulose, and lignin. Newns et al.[103] and Olsson et al.[104] reported a water vapor sorption capacity of 0.29 g/g and 0.42 g/g for pure cellulose and hemicellulose at atmospheric pressure, 20 °C, and 90 % relative humidity (RH), respectively. The term of sorption was used to indicate that water uptake could be by adsorption and absorption. Both the isotherms of pure cellulose and hemicellulose are type II similar to that of flax shives. Flax shives contain 53.2 wt % cellulose and 13.6 wt % hemicellulose that are bonded to each other in a very complex matrix along with lignin and other compounds. The measured sorption capacity under similar experimental conditions was 0.57 g/g. Therefore, the results indicate that the complex structure of cellulose, hemicellulose, and other components such as lignin, protein, and fat of flax shives may have contributed to the moisture sorption.

According to Newns et al., "During the successive sorption on the lower limb there will be a tendency for the water first to cluster in the more accessible regions of the cellulose

structure, and then for interchain bonds to break and be replaced by water-cellulose bonds."[103] The authors observed two different stages of moisture sorption with increasing relative humidity, where more moisture was sorbed in the second stage of sorption. They attributed this observation to inner structural changes with a smaller stress being placed on the interchain bonds in order to accommodate more water molecules[103]. It is possible that flax shives sorbed large amounts of water vapor by a collective interaction and interchain bond minor reformations of cellulose, hemicellulose, and other compounds at higher RH ranges.

Second, the mechanisms were analyzed from the perspective of surface functional groups. As discussed in the above section for the possible mechanisms for the linear isotherms, water sorption was exothermic and physiosorption in nature. The water vapor could be sorbed on the functional groups such as hydroxyls, Ph-OH, and carboxyls on the surface of the biosorbent through hydrogen bonding or additional interactions. Such interactions are expected to also play important roles for the first layer water sorption on the functional groups of cellulosic components of the flax shives surface for the type II isotherm in the discussion.

Olsson et al.[121] used an advanced in-situ FT-IR study of moisture sorption by cellulose and hemicellulose. They recorded the spectra of cellulose and hemicellulose online during moisture sorption in wide range of relative humidity (RH), and identified the water sorption mechanisms and the main bonds between the functional groups and the water molecule. In addition, the authors compared their spectra over a wide range of relative humidity with that of pure liquid water. According to the authors, "water bounds directly by hydrogen bonds to the OH groups of the cellulose and the hemicelluloses, and this would explain why no such peak is observed for free water."[121] They further added that the peak at 3200 cm^{-1} directly associated with the hydrogen bonding of water molecules with the OH groups in cellulose and hemicellulose, and the peak at 3600 cm^{-1} was associated with more loosely bond water.[121] Furthermore, the peaks at 1325 cm^{-1} were considered to be associated with carboxylic acid COO^{-} groups and water sorption by such groups. According to the authors, "The adsorption of water probably affects the vibration of the O(3)H…O hydrogen bond, which stiffens the cellulose chain and is important for the stress transfer along the chain."[121]

In regards to analysis of the second and subsequent layer water sorption, as discussed earlier, the analysis of the heat of water vapor sorption revealed that indicated the heat of sorption is less than the heat of water liquefaction, which is in accordance with the GAB model assumption discussed in the Chapter 2. In addition, Anderson[32] reported that in some cases the

released heat was much higher than the heat of liquefaction, which was attributed to either capillary condensation or two-dimensional condensation with high sorbed-phase density at higher surface loadings as a result of high adsorption energy of the surface. Flax shives have negligible micropores, thus capillary condensation is not feasible. Considering the above-mentioned excess heat value, the energy levels of interactions on the second and subsequent layer of water sorption are within the range of hydrogen bonding formed with water molecules[120].

Olsson et al.[121] also observed that the multilayer moisture uptake by cellulose took place at RH levels up to 80%. These observations are in harmony with the flax shives data obtained in this work. The characterization results showed that the surface of flax shives has abundant hydroxyl and amounts of carboxylic acid functional groups, and the water vapor sorption capacity significantly increased at RH values higher than 80 %, as seen in Figure 6.1. Based on the results of Olsson et al.[121], it could be suggested that multilayer water sorption by hydroxyl and carboxylic acid functional groups were activated at a higher RH range and caused a considerable increase in the water sorption capacity of flax shives.

Third, this matter is analyzed from the perspective of swelling and structural change. The moisture content of gas in the gas dehydration experiments was very low (0.98 mol % at max), which reduces the possibility of swelling. Liquid water in high concentrations is likely to create a high enough driving force for swelling. Olsson et al.[121] noted that the structure of cellulose is very crystalline and sorbs the least amount of water vapor compared to hemicellulose, glucomannan, kraft, and pectin. In a similar study by Olsson et al.[104], a mechanical spectroscopy method was used to determine the softening and glass temperature of hemicellulose. The authors reported an apparent activation energy of 400 to 500 kJ/mol for hemicellulose to exhibit a true glass transition at high humidity levels at room temperature. Such a level of energy was not available to activate the softening and glass temperature of hemicellulose in flax shives under the experimental conditions. In another work on pectic substances, Bettelheim et al.[105] concluded that large changes in the entropy are required in swelling polymers such as pectic substances. Using X-ray diffraction methods, they showed that the crystallinity of the polymer increased with moisture sorption. According to the authors, "Values of −ΔH for adsorption greater than the enthalpy of condensation of water vapor indicate that hydrogen bonding between water and polymer is stronger than in liquid water."[105] It was analyzed in section 7.3 that the heat of water sorption by flax shives was less than the heat of water liquefaction (-40.8 kJ/mol) and the energy levels of interactions on the second

and subsequent layer of water sorption are within the energy range of hydrogen bonding with water molecules[120]. Therefore, strong energies to change the crystallinity of flax shives structures were not available under the tested conditions in this work. Overall, it could be suggested that flax shives particles are not likely to significantly swell under the experimental conditions.

In summary, the discussions in this section suggest that the complex structure of cellulose, hemicellulose, and other components such as lignin, protein, and fat may have contributed to the moisture sorption. The water vapor sorption by flax shives for the case of linear isotherms obtained under the operation conditions could be monolayer, exothermic, and physiosorption in nature. The water vapor could be sorbed on the functional groups such as hydroxyls, Ph-OH, and carboxyls on the surface of the biosorbent through hydrogen bonding or additional interaction with similar energy levels. For the case of the non-linear isotherm with multilayer water sorption, the first layer sorption could be mainly through the similar sorption mechanisms as described for the linear isotherms. For the second and subsequent layer water sorption, it could be through water-water interaction with low sorbed-phase density with energies lower than the heat of liquefaction or normally condensed water. The results of water sorption and characterization of oat hulls are similar to those of flax shives. Their water sorption mechanisms are expected to be similar to those of flax shives.

6.5   Chapter Summary

The water sorption equilibrium, isotherm modeling, and mechanisms were investigated in this chapter. The solid-gas equilibrium data was determined in the pressure and temperature ranges of 101.3 – 300 kPa and 24 – 50 °C. Linear and non-linear isotherms were observed; only the isotherm at 300 kPa and 24 was non-linear and resembled a type II isotherm, while the rest of isotherms were linear. Two isotherm models, Redhead and GAB, were successfully fitted on the non-linear isotherm and the monolayer water sorption capacity, surface affinity of water toward the flax shives, and the excess heat of water sorption based on the GAB were determined. Linear isotherm and F-G isotherm models were well fitted on the linear isotherms, and the Henry constant and the lateral interaction forces among the sorbed water molecules on the surface were determined. The monolayer water sorption capacity was 0.16 g/g, which was within the range reported for similar bio-based materials in the literature. The surface affinity of flax shives towards water vapor was also 0.83 pa^{-1} based on the GAB isotherm model, which was slightly higher than the values reported in the literature. According to the F-G modelling

results, the lateral interactions among the sorbed water molecules was in the range of 6 – 9 J/mol, which is not strong and do not suggest a high density or two-dimensional sorption. Using the Henry constant determined from the linear isotherm modeling results, the standard heat of water sorption was estimated as -24 to -39 kJ/mol, which indicates that water sorption by flax shives was exothermic and the heat is consistent with the enthalpies of hydrogen bonding between water molecules and the hydroxyl, Ph-OH, and carboxyl functional groups. Afterwards, based on the collective data obtained in this work, the possible mechanisms of water sorption by flax shives were discussed from different perspectives of composition, surface functional groups, and structural changes. It was suggested that the water vapor sorption by flax shives for the case of linear isotherms obtained under the tested operation conditions could be monolayer, exothermic, and physiosorption in nature. The water vapor could be sorbed on the functional groups such as hydroxyls, Ph-OH, and carboxyls on the surface of the biosorbent through hydrogen bonding or additional interaction with similar energy levels. For the case of the non-linear isotherm with multilayer water sorption, the first layer sorption could be mainly through the similar sorption mechanisms as described for the linear isotherms, while mechanism for the second and subsequent layer water sorption could be water-water interaction with low sorbed-phase density. In addition, absorption may also take place. The in-depth investigation of water sorption mechanisms is necessary.

Chapter 7.   Kinetic Study of Water Sorption by the Biosorbents

This chapter investigated the kinetic of water sorption by flax shives. The experimental water breakthrough curves presented in this chapter were obtained by performing water vapor sorption in the single column system. The mathematical model presented in Chapter 2 was fitted on the experimental data to determine the mass transfer coefficients. As seen in the previous chapters, flax shives and oat hulls were similar; hence, the kinetic of water sorption by this class of material is illustrated here using flax shives as a model material. The details of oat hulls can be found in the published papers by the author of the thesis. The flax shives samples used in this chapter were the batch of 2017.

7.1   Introduction

The kinetic modeling of sorption systems has been classified based on the nature of the mass transfer front, nature of equilibrium relationship, heat transfer conditions (isothermal or non-isothermal), concentration levels of adsorbate components (trace and non-trace systems), and complexity of kinetic model. The water sorption equilibrium of flax shives was investigated in Chapter 6. The breakthrough experiments were performed under isothermal conditions to study the effect of various operating parameters on the kinetic of the system. Dehydration systems are essentially trace systems as water vapor presents only in very low concentrations of the feed (maximum molar percentage of 0.98% corresponding to 100% RH) as shown in the previous chapters. Speaking of the complexity of kinetic models, the assumption regarding the mass transfer resistance is key here. Assuming no mass transfer resistance is the simplest form of the kinetic model as instantaneous equilibrium is assumed at all points in the sorption columns.[33] Assuming two individual mass transfer resistances results in a complex mathematical problem where coupled PDE equations need to be solved for the external fluid film resistance plus intraparticle diffusion and two internal diffusional resistances (macropore and micropore). As mentioned in Chapter 2, the model considering the total resistance of mass transfer by lumping both external and internal mass transfer is a simplified but adequate and popular model to provide reasonable description of most practical systems where an overall (lumped parameter) mass transfer coefficient was assumed, which is known as the linear driving force (LDF).[33]

Flax shives particles were characterized and their water sorption dynamic performance in dehydration was experimentally investigated and presented in Chapters 4, 5 and 6. Based on the obtained data, the above mentioned LDF kinetic model is suitable based on the conditions

of the system. Flax shives were almost non-porous; hence, the lumped mass transfer resistance essentially describes the external film mass transfer resistance, which is caused by the thin stagnant film of fluid (gas mixture) surrounding the flax shives particles contained in the column bed.[33] Many parameters including the properties of gas in the hydrodynamic boundary layer, particle radius, particle diffusion coefficient, surface diffusion, and the intraparticle voidage can effect this process.[33] Depending on the dehydration process, the film mass transfer coefficient of water vapor in different gas mixtures (e.g. air or natural gas) could be different. In addition, flax shives are essentially non-porous and the intraparticle diffusion effects can be neglected. Their particle shape is almost cylindrical or needle shape. That said, it is critical to investigate the kinetic of water sorption by flax shives in this chapter and compare the results with those reported in the literature.

7.2 Modeling the Water Sorption Kinetic

The water sorption kinetic was investigated at various total pressures, temperatures, and gas phase flowrates. To analyze the kinetic data of water sorption in the packed column system, the mass balance equation (Eq. 2.9) for water vapor in the column and the LDF kinetic model (Eq. 2.11) were solved together with the initial and boundary conditions (Eq. 2.10) discussed in Chapter 2. The model equations were fitted on the set of experimental water vapor breakthrough data obtained in Chapter 5 and the model parameters (mass transfer coefficients) were estimated. The optimal values were obtained using the Line-Search optimization routine in ASPEN Adsorption. The isotherm parameters and important properties of the biosorbent reported in Chapter 6 were used here. The GAB isotherm model was used for the data following the non-linear isotherm and the linear isotherm for the rest because they provided better simulation results for the respective isotherm data. Table 7.1 is a summary of the parameters related to the kinetic modeling.

Table 7.1: Parameters used in the modeling.

Bed voidage	0.32
Height of biosorbent layer	8 cm
Internal diameter of biosorbent layer	5 cm
Average particle size	1.01mm
Bulk density	155.2 kg/m^3
True density	1350 kg/m^3

The kinetic model was successful in predicting the behavior of the system. Figure 7.1 shows the goodness of fit of the water breakthrough curves at various pressure. As can be seen, the models predicted the breakthrough curves very well. The model predictions are close to the experimental data and acceptable R squared values were achieved for all experiments. The total mass transfer coefficients together with other modeling results are presented in Table 7.2.
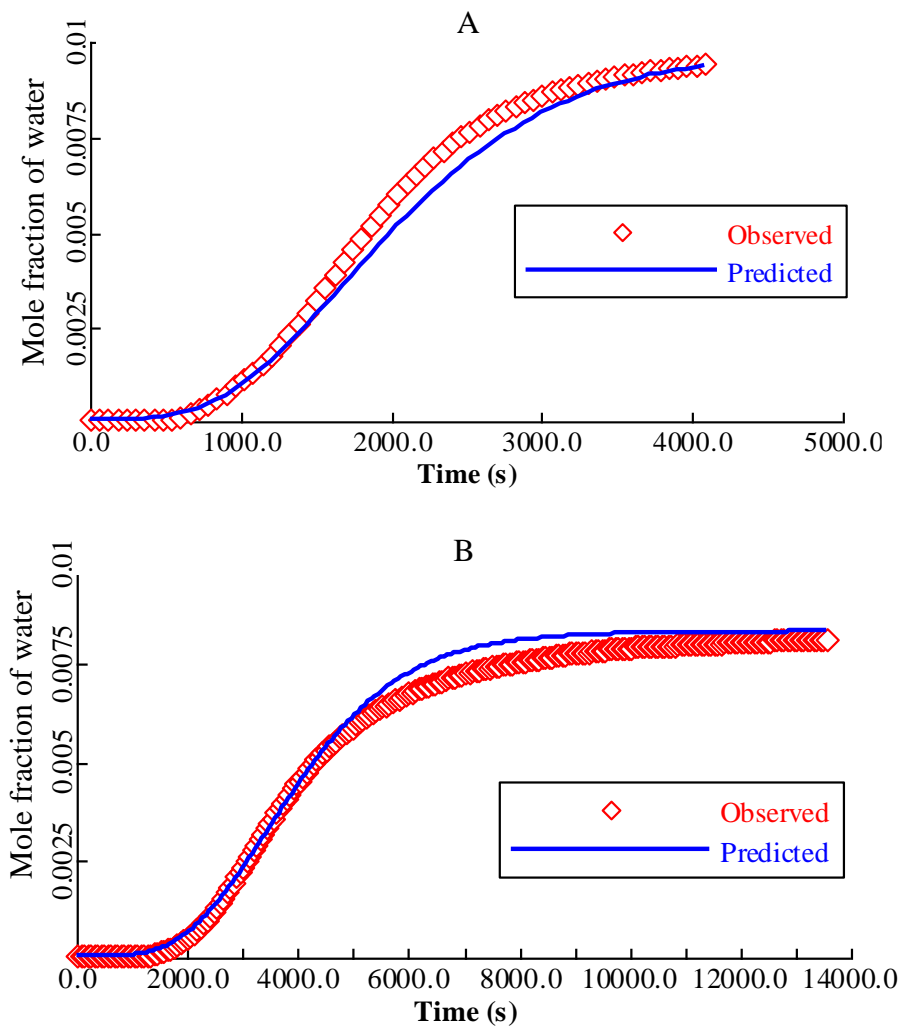
Figure 7.1: Examples of models' prediction of the breakthrough curves; A: 300 kPa, 50 °C, 4 L/min, Y=0.0098, B: 101.3 kPa, 24 °C, 2 L/min, Y=0.0098; R^2 was 0.98 for both.

The effect of temperature on the water vapor breakthrough curves and the total experimental time at 300 kPa, 4 L/min, and feed water mole fraction of 0.0098 is shown in Figure 7.2. The models could correctly predict the behavior of the system at various temperatures. At 24, 35, and 50 °C, the corresponding estimated mass transfer coefficients were 9.43×10^{-4}, 5.40×10^{-3}, and 1.21×10^{-2} s^{-1}, respectively, as shown in Table 8.2. The effect of temperature on the mass transfer coefficient will be further analyzed by statistical analysis in following section.
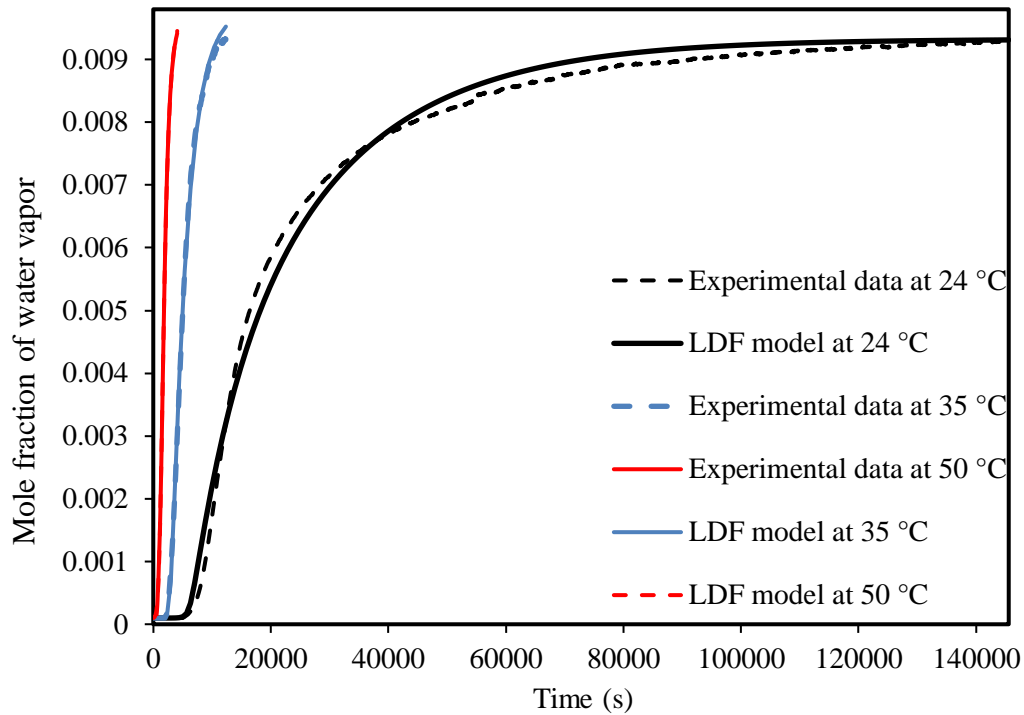
Figure 7.2: Breakthrough curves at three different temperatures predicted using the LDF model; 300 kPa, 4 L/min, and mole fraction of water: 0.0098.

The modeling results of the water breakthrough curves at various gas flow rate are presented in Figure 7.3. The model also reasonably well simulated the experimental data. The total mass transfer coefficients are also presented in Table 8.2. It is shown that the total mass transfer coefficient increased from 8.24×10^{-4} to 9.43×10^{-4} (s^{-1}) as the gas flowrate increased from 2 L/min to 4 L/min at 300 kPa and 24°C.
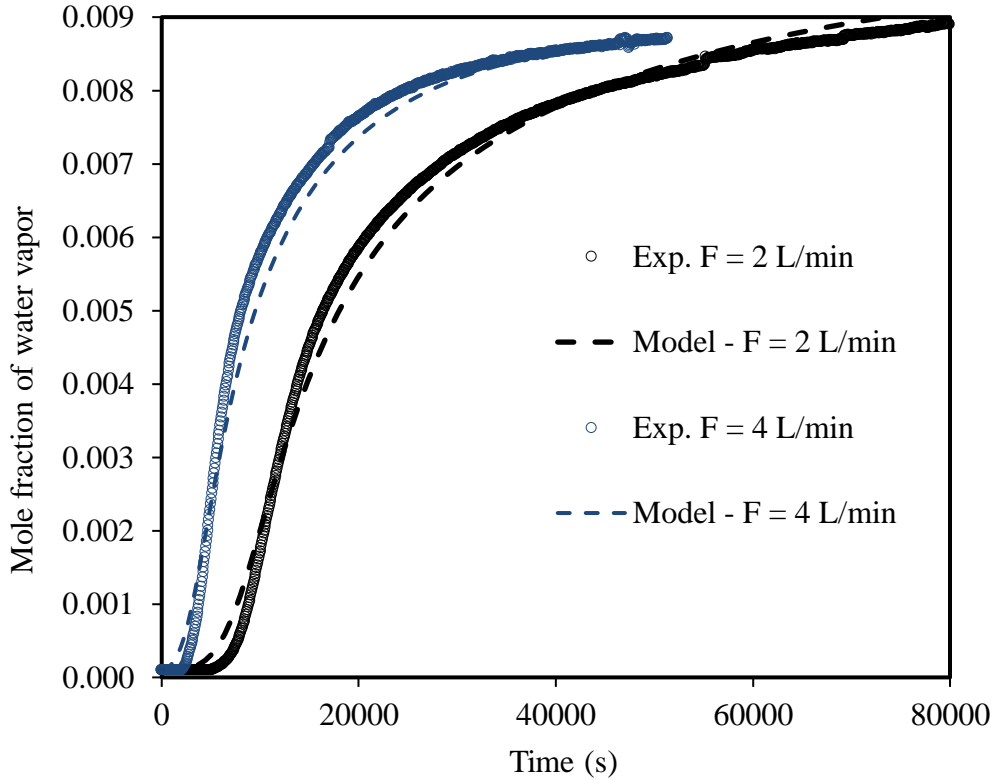
Figure 7.3: Breakthrough curves at two different flow rates predicted using the LDF model; 300 kPa, 24 °C and 100 % RH feed gas.

Table 7.2: Mass transfer coefficients obtained from the linear driving force model; P is total pressure; T is temperature; F is total gas flow rate; K_{LDF} is the mass transfer coefficient; and SSE is sum of squared residual errors in the curve fitting, R^2 is coefficient of determination; the mole fraction of water vapor in the feed gas was 0.0098 for all the data in this table.

T (ºC)	P (kPa)	F (L/min)	K_{LDF} (s⁻¹)	SSE	R^2
24	300	2	8.24×10^{-4}	1.54×10^{-5}	0.99
24	300	4	9.43×10^{-4}	6.60×10^{-4}	0.99
24	101.3	2	1.41×10^{-2}	5.40×10^{-4}	0.98
24	101.3	4	1.56×10^{-3}	7.80×10^{-4}	0.98
35	300	2	5.40×10^{-3}	1.10×10^{-6}	0.97
35	300	4	6.46×10^{-3}	3.36×10^{-4}	0.99
35	101.3	2	2.20×10^{-2}	3.90×10^{-5}	0.98
35	101.3	4	3.10×10^{-2}	4.40×10^{-4}	0.98
50	300	4	1.21×10^{-2}	5.60×10^{-5}	0.98

It is useful to compare the estimated mass transfer coefficients of flax shives with those of other materials reported in the literature. As can be noticed in Table 7.3, the K_{LDF} values obtained in this work (8.2×10^{-4} – 3.1×10^{-2} s⁻¹) are slightly higher than those reported in the

literature within the range of $1 \times 10^{-5} - 1 \times 10^{-3}$ s^{-1} depending on the experimental conditions. Specifically, at 300 kPa, flax shives in this work has a K_{LDF} value of 8.2×10^{-4} s^{-1} which is higher than that of CaCl$_2$ – Al$_2$O$_3$ composite 4×10^{-5} s^{-1}. At the atmospheric pressure or close value, the values of K_{LDF} (1.4×10^{-2} – 3.1×10^{-2} s^{-1}) of flax shives is higher than those of zeolites, biochar, and bitumen coal (1×10^{-3} – 6.7×10^{-3} s^{-1}), plant materials such as canola meal, corn meal, and oat hulls (2.8×10^{-3} – $4.3 \times \times 10^{-3}$ s^{-1}), polymeric adsorbent 1.8×10^{-5} – 4.7×10^{-5} s^{-1}, and desiccants CaCl$_2$ – Al$_2$O$_3$ and silica gel (9.5×10^{-5} – $1.3 \times \times 10^{-4}$ s^{-1}).

These results were reported under different conditions for materials that are significantly different. For instance, water vapor sorption by zeolites, silica gel, and similar porous materials could be mostly intraparticle diffusion controlled in contrast to flax shives, oat hulls, and cornmeal that are almost non-porous materials. In addition, the isotherm types and equilibrium behaviors of these materials are completely different in most cases. For example, water sorption isotherms of zeolite NaX , zeolite NaMgX , and zeolite NaX/MgCl$_2$ were highly favorable Langmuir type[122], while isotherms type II and V were reported for several materials composed of cellulose, hemicellulose, and pectin.[103,104,121] The linear driving force model with lumped mass transfer resistance considers the collective effects of external film and intraparticle diffusion (macropore and micropore) mass transfer resistances.[33] However, this coefficient most probably represents the external film transfer resistance in the case of flax shives as the material contains negligible mesopores. In addition, it can be seen in Table 7.2 that the K_{LDF} for flax shives at 300 kPa and 24 °C (type II isotherm) was 8.24×10^{-4} s^{-1}, which is lower than the values at other conditions (linear isotherm) in the range of 1.4×10^{-2} – 3.1×10^{-2} s^{-1}. In multilayer water sorption, the mass transfer resistances in the stagnant gas in the boundary layer and in the sorbed phase could be higher than the mass transfer resistances in the monolayer water sorption in ideal dilute systems (linear isotherm). In theory, the thickness of hydrodynamic boundary layer increases with increasing pressure of the ambient (free) stream in a Laminar flow regime.[123] Moreover, the amount of sorbed moisture on the surface in the sorbed phase could affect the hydrodynamic boundary layer and its properties could be different from those of the boundary layer on the surface of dry material. The effects of equilibrium and mass transfer are highly coupled in water sorption. Yan et al.[122] also reported the entanglement of water loading, equilibrium type, and the diffusional mass transfer in zeolite NaX. Sultan et al.[124] reported different trends in the mass transfer resistance with respect to temperature and partial pressure of water at different surface loading because the isotherm was type V. In type V isotherms, monolayer and multilayer sorption are dominant

at lower surface loadings, while other phenomena such as micropore filling are more dominant at higher surface loadings.[32,122] Type V and type III isotherms are similar except with regard to a maximum plateau in type V isotherm at relative pressures approaching one.[32] Same case applies to type II and type IV isotherms. They also reported that in some cases, the total amounts of sorbed water was higher than the micropore volume of the material, which result in an unstable sorption performance in repeated sorption/desorption cycles.[122,124] In the following sections, the effects of operating parameters are investigated and compared with the results reported in the literature.

Table 7.3: Comparison of mass transfer coefficents; Linear driving force model.

Material	Conditions (P, T and Feed Concentration)	K_{LDF} (s^{-1})	Reference
Flax shives	300 kPa, 24 °C, 100 RH % or 0.98 mol %	8.2×10^{-4}	This work
Flax shives	101.3 kPa, 24 °C, 0.98 mol %	1.4×10^{-3}	This work
Raw canola meal	243 kPa, 110 °C, 9.8 mol % H_2O/EtOH	4.0×10^{-3}	9
Cornmeal	101.3 kPa, 82 °C, 5.1 % RH	2.8×10^{-3}	125
Oat hulls	135 kPa, 110 °C, 55 mol % H_2O/EtOH	4.3×10^{-3}	109
Biochar	101.3 kPa, 23 °C, 2 mol % H_2O /N_2	1×10^{-3}	126
Bituminous coal	101.3 kPa, 25 °C, 93% RH	1×10^{-3}	127
Zeolite NaX	101.3 kPa, 28.8 °C, 93% RH	2.5×10^{-3}	122
Zeolite NaMgX	101.3 kPa, 29.6 °C, 93% RH	1×10^{-3}	122
Zeolite NaX/$MgCl_2$	101.3 kPa, 29.9 °C, 93% RH	6.7×10^{-3}	122
$CaCl_2$ – Al_2O_3 composite	101.3 kPa, 25 °C, 70 % RH	9×10^{-5}	128
$CaCl_2$ – Al_2O_3 composite	300 kPa, 25 °C, 70 % RH	4×10^{-5}	128
$CaCl_2$ and synthetic coal Sibunit composite	101.3 kPa, 25 °C, 70 % RH (air drying)	13.3×10^{-5}	128
Silica gel/LiCl composite	101.3 kPa, 20 °C, 70% RH	9.5×10^{-5}	129
PS-II polymer-based adsorbent	101.3 kPa, 20 °C, 45% RH	1.8×10^{-5}	124
PS-II polymer-based adsorbent	101.3 kPa, 50 °C, 48% RH	4.7×10^{-5}	124

Figure 7.4 were drawn using the estimated marginal means to visualize the effect of the operating parameters and the data provided Table 7.2 According to these figures, the K_{LDF} increased with increasing temperature and flowrate and decreasing total pressure within the tested conditions.

A

B
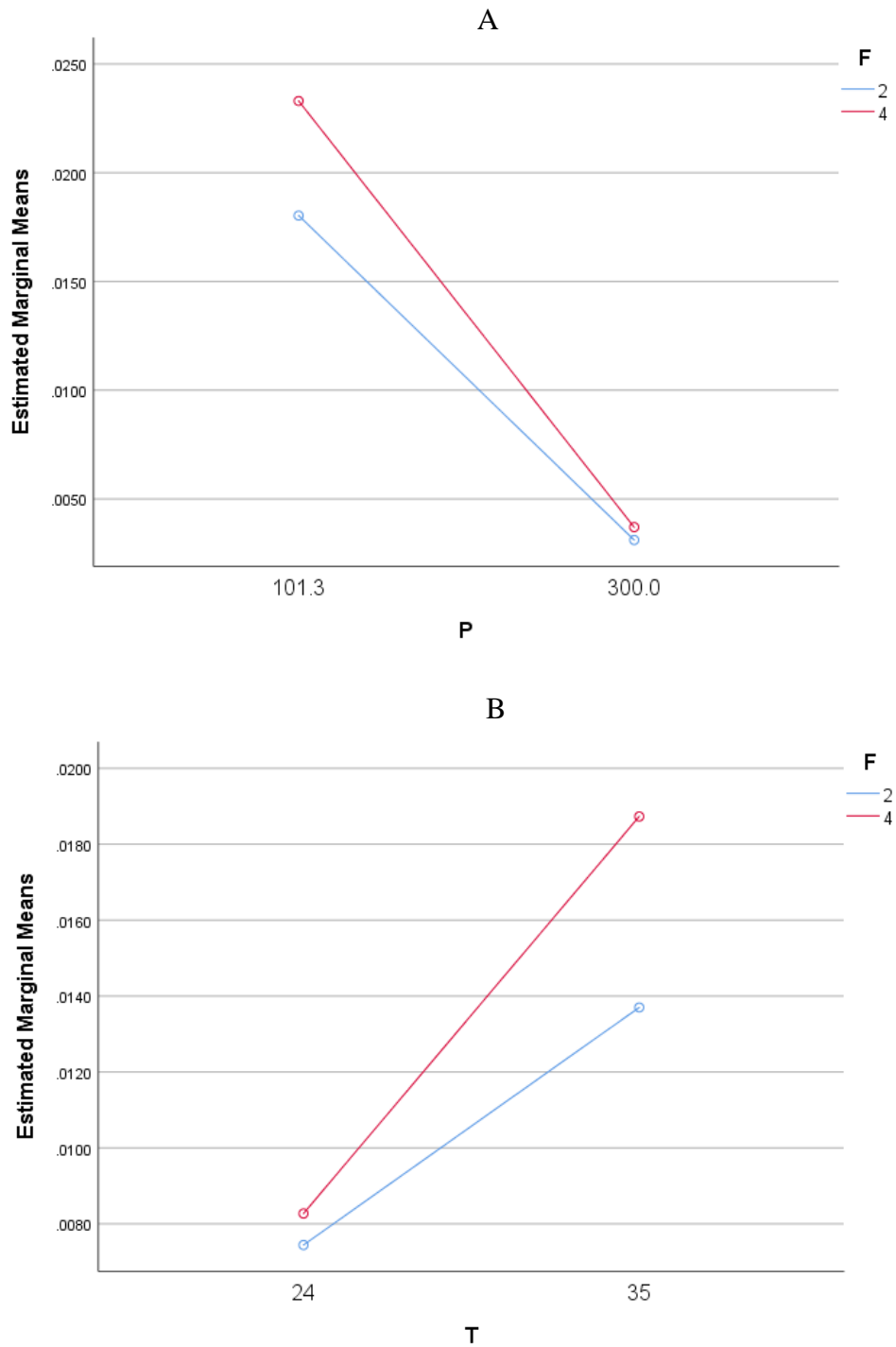
Figure 7.4: Effects of operating parameters on the estimated marginal means of K_{LDF}; P is total pressure kPa; T is temperature °C; and F is flow rate L/min.

7.3   Effect of Operating Parameters on the Mass Transfer Coefficient

The reported data in previous chapters collectively demonstrated that flax shives were almost non-porous and the intraparticle diffusion effects on the water sorption process is not very significant; hence, the lumped mass transfer represented by the value of K_{LDF} most probably describes the external film mass transfer resistance, which is caused by the thin stagnant film of fluid (gas mixture) surrounding the flax shives particles contained in the column bed.[33] Therefore, the operating parameters simultaneously affected the hydrodynamic boundary layer around the flax shives particles, the water sorption equilibrium, and the sorbed phase. In this section, these effects are analyzed based on the obtained kinetic modeling data and existing knowledge on the hydrodynamic boundary layer.

The estimated marginal means shown in Figure 7.4 can assist comprehending the effects of the operation parameters and the values of K_{LDF} provided in Table 7.2. As shown in Figure 7.4-A, the K_{LDF} values decreased with increasing total pressure within the tested range. According to the theory, the thickness of boundary layer increases with increasing pressure.[123] Therefore, the increasing pressure could have increased the thin stagnant film of fluid (gas mixture) surrounding the flax shives particles; thus the overall transfer resistance increased. Even though heat is released during water sorption, which may enhance the mass transfer rate, it is likely that its impact did not overcome that of the pressure under the operation conditions. The boundary layer depends on the Reynolds and Nusselt numbers as well as the geometry of the particles, which is complicated. In addition, it was shown before that the water sorption capacity was higher at higher total pressure. Particularly, the isotherm changed from linearity to type II like indicating multilayer water sorption mechanism when pressure was increased from 101.3 kPa to 300 kPa (24 °C). In multilayer water sorption, the mass transfer resistances in the stagnant gas in the boundary layer and in the sorbed phase could be higher than the mass transfer resistances in the monolayer water sorption in ideal dilute systems (linear isotherm). Overall, the thickness of hydrodynamic boundary layer around flax shives particles could have increased with increasing pressure and caused a higher overall mass transfer resistance.[32,123]. Tajallipor et al.[9] also reported decreasing K_{LDF} with increasing pressure for ethanol dehydration using canola meal. Similarly, Ostrovskii et al.[128] observed decreasing mass transfer coefficients with increasing pressure in the range of 1 − 7 bar for water sorption by calcium chloride composites.

According to Figure 7.4-B, the values of K_{LDF} increased with increasing temperature in the tested range. At higher temperatures, the heat transfer coefficient increases and gas viscosity decreases, which consequently increase the Reynolds and Nusselt numbers. As such, the thickness of the hydrodynamic boundary layer is likely decreased; and consequently increased the mass transfer coefficient. Similar results were reported for water sorption by oat hulls[109] and canola meal[9]. Charrière et al.[127] also observed increasing K_{LDF} values with increasing temperature in water sorption by coal. However, in another work on water sorption by cornmeal, Chang et al.[125] reported no significant increase of K_{LDF} value in the temperature range of 82 – 100 °C.

With regards to the effect of gas flowrate, Figure 8.4 shows that the value of K_{LDF} increased with increasing gas flow rate. From the equilibrium standpoint, the gas flow rate does not affect the equilibrium sorption capacity. In theory, the thickness of hydrodynamic boundary layer decreases with increasing flow rate and ambient (free) stream velocity in a Laminar flow regime[123], which may have reduced the overall mass transfer resistance. The Reynolds number for the gas flow through the flax shives bed under different operating conditions was analyzed. The Reynolds numbers at 300 kPa and 24 °C were 6.61 (flow rate 2 L/min) and 37.28 (flow rate 4 L/min), while the Reynolds numbers at 101.3 kPa and 24 °C were 6.22 (flow rate 2 L/min) and 12.38 (flow rate 4 L/min). The flow through packed bed is Laminar when Reynolds number is smaller than 1 and is turbulent when Reynolds number is larger than 100.[123] The flow is transitional when the Reynolds number is in the range of 1 – 100. It can be seen that the flow regime transitioned toward the threshold Reynolds number of turbulent regime with increasing gas flow rate, which might have affected the hydrodynamic boundary layer and the overall mass transfer resistance. In a similar work on ethanol dehydration by canola meal, Tajallipor et al.[9] also reported increasing K_{LDF} with increasing flow rate. Simo et al.[130] reported increasing K_{LDF} with increasing flow rate in ethanol dehydration by zeolite.

7.4   Desorption Rate

Desorption rate is critical in a PSA process. The biosorbent bed must be sufficiently regenerated in a cycle time; otherwise, moisture would accumulate in the bed causing a premature breakthrough.[3,33,113] Desorption rate must be at least equal to or higher than the rate of sorption in a cycle. In Chapter 5, a method was used to approximately determine the average rate of sorption and desorption in the biosorbent. In this chapter, the linear driving force model was used to determine the mass transfer coefficient during the desorption step. Same equations

(Eq. 2.9 and 2.11) were used except that the initial conditions in the bed where the feed water mole fraction (C_{in}) was zero (dry gas is used for regeneration). The molar flow rate and pressure of the regeneration gas was accordingly adjusted in the simulation. As for the flax shives layer in the column, the biosorbent bed was saturated with water vapor after the end of the sorption experiments and this condition was the initial condition for the desorption step. The fitted desorption curves were shown in Figure 7.5 and the mass transfer coefficients at 24 °C and   35 °C were 9.8×10^{-3} s^{-1} and 1.1×10^{-1} s^{-1}, respectively. As can be noticed, the model could correctly predict the desorption curves as well. The deviations in the experimental data are probably because of the fluctuations in the vacuum pump used during the desorption process. The values of mass transfer coefficients for the desorption process were much higher than those of sorption process in the order of $10^{-5} – 10^{-2}$ s^{-1} depending on the experimental conditions (see Table 7.2), confirming desorption speed is much faster that sorption, which is favored in industrial application of the process. Thus these results are in harmony with those reported in Chapters 5 and 6. In summary, the desorption rates were fast and the biosorbent had excellent regeneration properties, which makes it a suitable material for gas dehydration in a PSA process.
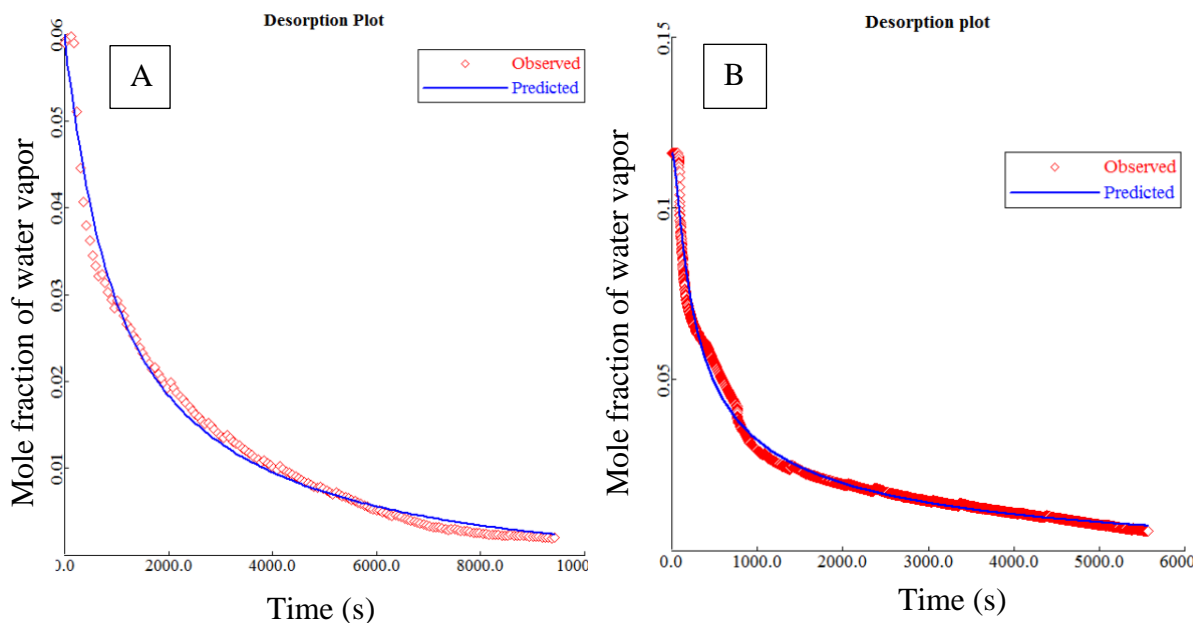
Figure 7.5: Desorption plots predicted by the LDF model; 47 kPa absolute, A: 24 °C, K$_{LDF}$ = 9.8×10^{-3} s^{-1}; B: 35 °C, K$_{LDF}$ =1.1×10^{-1} s^{-1}.

7.5   Chapter Summary

In this chapter, the linear driving force (LDF) model was used to simulate the experimental breakthrough curves of water sorption by flax shives (batch of 2017). The model successfully simulated the experimental water breakthrough curves. The LDF mass transfer coefficients at

various operating conditions were determined and analyzed. The K_{LDF} values obtained in this work ($8.2 \times 10^{-4} - 3.1 \times 10^{-2}$ s^{-1}) are slightly higher than those reported in the literature within the range of $1 \times 10^{-5} - 1 \times 10^{-3}$ s^{-1} depending on the experimental conditions. The effect of operating parameters on the mass transfer coefficient was further determined and discussed. The mass transfer coefficient increased with increasing flow rate, increasing temperature, and decreasing total pressure. The mass transfer coefficient during the water desorption under vacuum was also determined. The results showed that the water desorption rate was much faster than the sorption rate under the tested conditions. Overall, the results of this chapter provide important information on the kinetic of water sorption by flax shives.

Chapter 8.   The Performance of Biosorbents in a Cyclic Process

In this chapter, the performance of biosorbents was investigated using a dual-column pressure swing sorption system based on the results achieved in the previous chapter using the single-column system. A simulated natural gas with conditions similar to a field natural gas was prepared and the performance of the process using the biosorbents for natural gas dehydration was studied. Different types of pressure swing cycles were used in the experiments at atmospheric pressure and moderate pressure to investigate the effect of process parameters such as cycle time on the efficiency of the process. It is to note that the term "sorption" and its respectively derived term "sorb", and so on are used where applicable in this chapters associated with the results and discussion about water vapor in this thesis. The term "adsorption" is used when discussing the nonpolar gases such as methane, carbon dioxide, nitrogen, and helium.

8.1   Dual Column Cyclic Experiments with Flax Shives

Biosorbents used in this work are flax shives, which were supplied from Schweitzer-Mauduit Canada, Inc., Winkler, Manitoba. In the dual-column experiments, both columns were filled with flax shives having a particle size distribution of 0.425 – 1.18 mm. They were oven-dried at 105 °C for 24 hours before packing (Figure 8.1). Ultra-High Purity (5.0) N_2 gas was purchased from Praxair Canada and used as carrier gas for the experiments. In Chapter 5, it was confirmed that flax shives did not adsorb substantial amounts of methane and carbon dioxide and had almost 100% selectivity towards water vapor; therefore, because of safety issues, nitrogen gas was used in the experiments as the representative of nonpolar gases.

Figure 8.1: Picture of flax shives used in the dual- column experiments.

8.1.1 Medium-Pressure Experiments

In this section, cyclic pressure swing experiments were performed based on the six-step cycle illustrated in Chapter 3. The detailed experimental conditions are given in Table 8.1. The columns were operated under an adiabatic condition. These columns were equipped with a jacket that was maintained at a vacuum of 1 µHg throughout the experiment to minimize heat loss to the environment. The column flanges were covered by a heat insulation material to avoid heat loss from the columns' inlet and outlet.

Table 8.1: Feed gas conditions for dual-column experiment with flax shives; volumetric flows are at the corresponding pressure level; carrier gas was nitrogen.

Temperature	$29.9 \pm 0.2\,°C$
Pressure	300 kPa
Feed gas flow rate (V_F)	3 L/min
Feed gas humidity (water vapor mole fraction)	100% (0.0098 ± 0.0002)
Regeneration gas flow rate (V_R)	$\dfrac{V_R}{V_F} = 1.5$
Vacuum level during regeneration	39 kPa absolute

Water histories in the feed and product gases: The 100% humid gas was fed from the top, while dry product gas was draw from the bottom; whereas the columns were regenerated counter-currently from the bottom in order to avoid product contamination with water vapor (see the supplementary information for details). A cycle time of 10 minutes was considered. The pressure equalization time was 5 seconds. A normal building vacuum was used to regenerate the columns (39 kPa absolute). The PSA process was run for 85 cycles until a full T-size nitrogen gas cylinder was dehydrated (5002 liters at 300 kPa). The volumetric flow rate of feed gas (V_F) and regeneration gas (V_R) were 3 and 4.5 L/min, respectively. The ratio of $\frac{V_R}{V_F} = 1.5$ was considered in this experiment, which is commonly used in dehydration systems.[33] The feed gas temperature was controlled at 29.9 ± 0.2°C, which is the usual temperature of sweet gas in natural gas plants[4], and the mole fraction of water vapor in the feed gas was 0.0098 ± 0.0002 (100% relative humidity). The mole fraction of water vapor in the feed gas and product gases was recorded every second throughout the experiment using a data acquisition system. Figure 8.2 shows the water vapor history throughout this experiment. As can be seen, the feed mole fraction was controlled at 0.0098 and dry gas was collected as the

product throughout the 85 cycles. This experiment confirmed that this PSA process can effectively dehydrate nitrogen, methane, carbon dioxide, and other nonpolar gases.
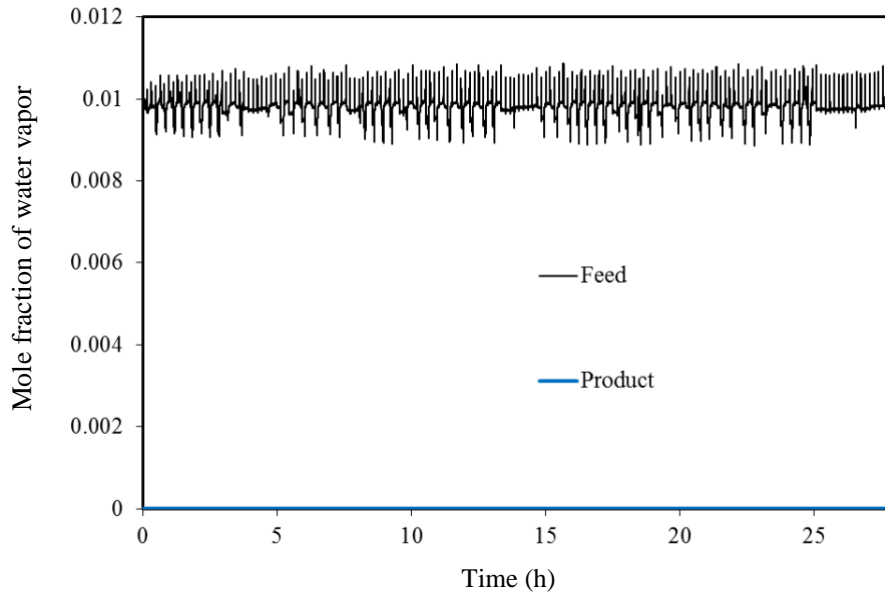
Figure 8.2: Water vapor history throughout the experiment (85 cycles) –temperature 29.9 °C; pressure 300 kPa; vacuum 39 kPa; V_F 3 L/min; 100 % humid feed gas; V_R/V_F = 1.5.

Pressure and temperature histories: Cyclic pressure and temperature histories during two cycles are shown in Figure 8.3. During this cyclic operation, each column runs at 300 kPa for 10 minutes followed by a 5 second pressure equalization where both columns reach an equal pressure of about 170 kPa; then, the column is depressurized and kept under a vacuum of 39 kPa for another 10 minutes. Two temperature sensors were installed to record the temperature of the biosorbent layer at the top and bottom of the columns. As can be seen, the temperature at the top of the column (where humid feed gas was sent) increased during the pressurization and sorption steps because of the heat of water vapor sorption, while it decreased during the pressure equalization and regeneration steps as a result of the heat of water vapor desorption. The temperature history of the column provides valuable information about the performance of the system, which is discussed in detail in the following sections.
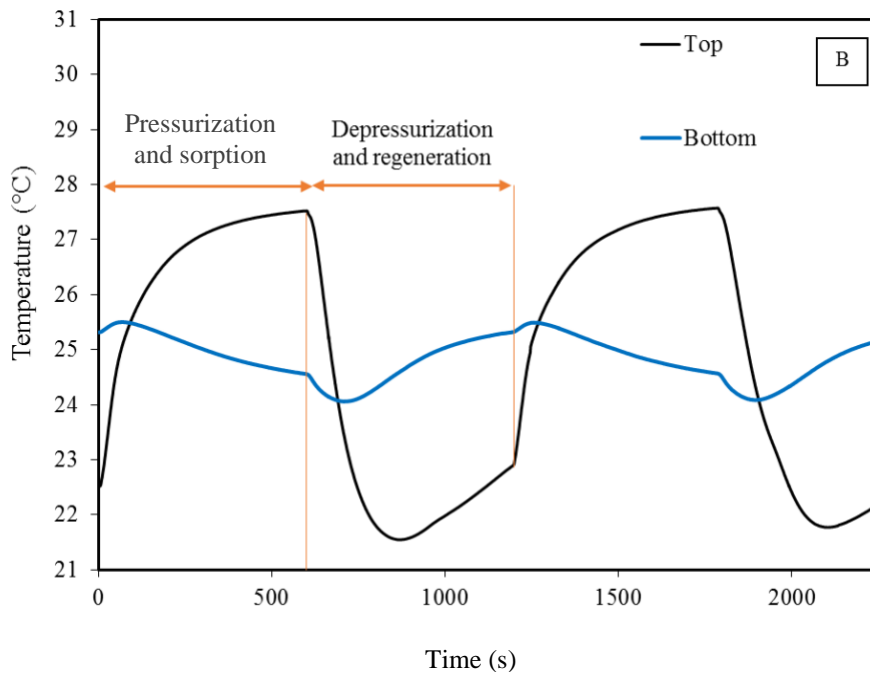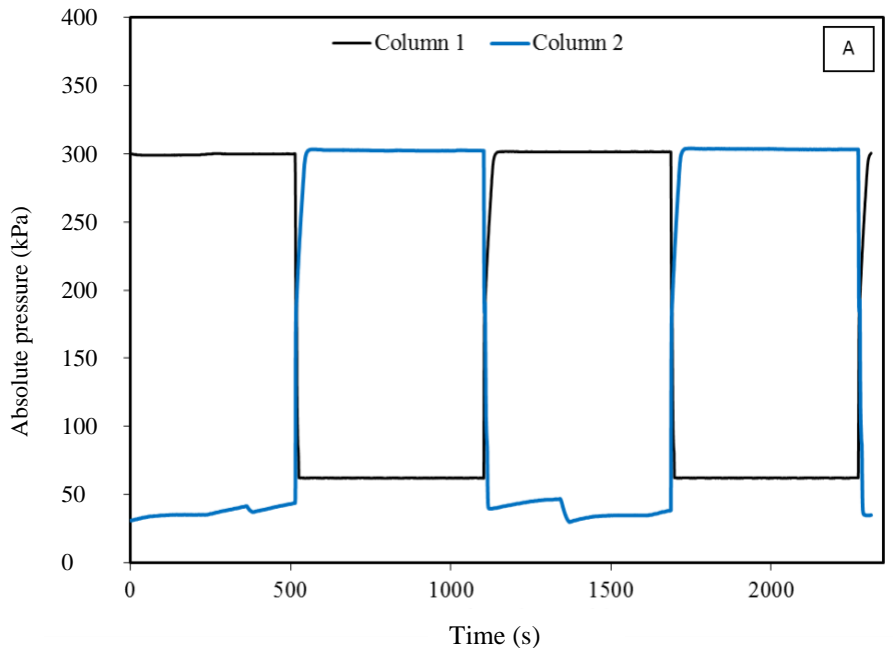
Figure 8.3: Cyclic pressure and temperature (solid phase) histories (two cycles) - temperature 29.9 °C; pressure 300 kPa; vacuum 39 kPa; V_F 3 L/min; 100 % humid feed gas; $V_R/V_F = 1.5$.

Figure 8.4 shows the detailed analysis of the column temperature history during a cycle. As can be noticed, the temperature at the top of the column sharply increased as a result of the heat of sorption during the pressurization and sorption steps. In the meantime, the temperature at the bottom of the column slowly decreased as a result of heat transfer to the column wall. This observation also confirms that the mass transfer zone (MTZ) was at the top of the column and far away from the column's outlet. According to results reported in Chapter 5 at isothermal

condition, the length of mass transfer zone at 24 and 35 °C was 10.8 and 7.09 cm, respectively.[7] Under adiabatic condition, the length of mass transfer zone changes over time with varying temperature during a cycle; however, it is likely to be within the range mentioned above. Furthermore, the total height of the biosorbent bed in the column (51 cm) was much higher than the length of mass transfer zone in this experiment, which ensured the breakthrough point was not reached in this cyclic operation. Afterward, the temperature at the top and bottom of the column suddenly decreased as a result of the pressure equalization and depressurization steps (Joule-Thomson effect).[5] It is worth clarifying that the Joule-Thomson effect is a phenomenon in the gas phase and the solid temperature shown here changed as a result of the heat transfer from gas to solid. Next, the temperature at the top continued to decrease because of the heat of desorption (MTZ was at the top of the column, see Figure 8.4), while the temperature at the bottom gradually increased since the warm regeneration gas (N_2) at 29.9 °C was being sent from the bottom of the column (counter-current) that was already colder. Finally, the temperature at the top and bottom slightly increased as a result of the pressure equalization and pressurization steps; then, this cycle repeats.

The critical observation here was the temperature history at the top during the regeneration step (Figure 8.4-A, between 800 to 1150 seconds). As can be seen in Figure 8.4-A, the regeneration gas was being sent from the bottom of the column at 29.9°C and the only reason for the temperature drop in the column is the heat of desorption. The temperature at the top decreased from 27.5 to 20.6 °C in the period of 600-800 seconds; then, it started to increase to about 22.5 °C. This observation confirms that the biosorbents were substantially regenerated after 6-7 minutes, and a cycle time of 10 minute was sufficient for this PSA process. This observation and the temperature history had been repeatedly seen in all 85 cycles throughout the experiment as shown in Figure 8.5 and Figure 8.6. The process can continue to operate in such cycles. Furthermore, moisture holdup in the column at the end of the experiment (85 cycles) was determined later by RH measurements to confirm that the beds were completely regenerated in every cycle at such low temperatures and regeneration for 6-7 minutes was adequate. Dry carrier gas (nitrogen) was sent into the column and the humidity of the output gas was recorded. This property of the biosorbent is unique and makes it an excellent sorbent for dehydration and drying applications. It is worth noting that the regeneration in this work was at about 30°C while temperatures about 300 – 400 °C were required to regenerate some commercial adsorbents such as molecular sieves.[5,33] The process developed in this work can significantly reduce energy consumption and costs.
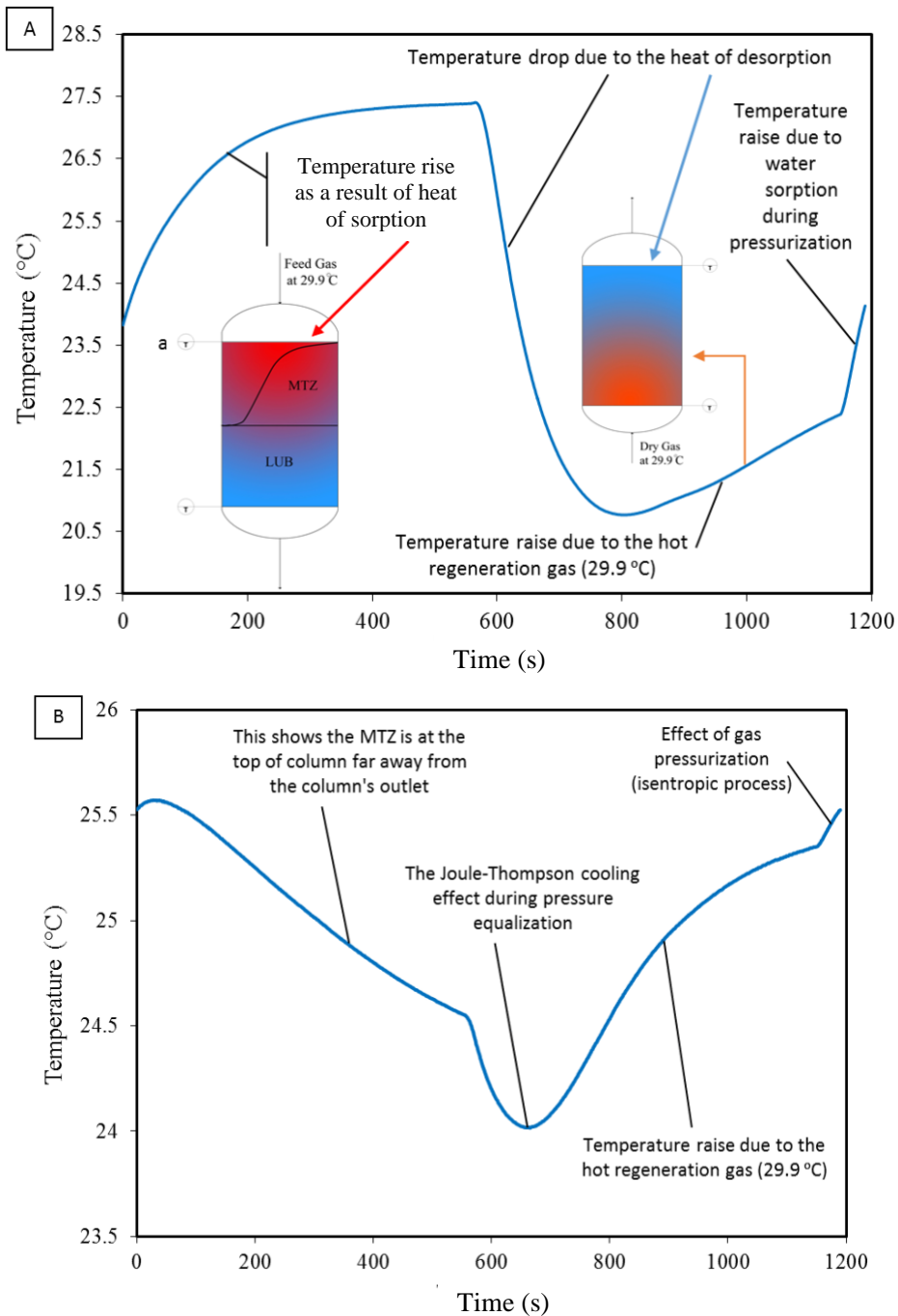
Figure 8.4: Detailed analysis of column temperature history during a cycle using flax shives temperature 29.9 °C; pressure 300 kPa; vacuum 39 kPa; V_F 3 L/min; 100 % humid feed gas - $V_R/V_F = 1.5$; A: Temperature at the top of the column; B: Temperature at the bottom of the column; MTZ: mass transfer zone; LUB: length of unused bed.

The average temperature values from the sensors at the top and bottom of each column were calculated and showed in Figure 8.5, which demonstrate a stable behavior where no heat accumulation can be seen after 85 cycles. Average temperatures were considered to represent any temperature fluctuation at both ends of the columns. This shows the columns were

97

sufficiently regenerated and a cycle time of 10 minutes worked well. An increasing trend would suggest an unsteady and insufficient regeneration in every cycle.[5,33]

Figure 8.5: Cyclic temperature history during the PSA process using flax shives- temperature 29.9 °C; pressure 300 kPa; vacuum 39 kPa; V_F 3 L/min; 100 % humid feed gas; $\frac{V_R}{V_F} = 1.5$; the temperature values were not shown for better figure visibility; each temperature wave (maximum to minimum values and vice versa) is about 600 seconds.

Figure 8.6 again shows the overlapped temperature history of the column during different cycles. As can be seen, the temperature histories during cycle numbers 18, 35, 60, and 76 were similar, which shows the stable performance of the biosorbent and the PSA process. The slight differences were a result of uncontrollable environmental noises and fluctuations in the feed gas flow rate. It is also worth mentioning that the accuracy of the temperature sensors used was 0.3 °C (systematic errors).
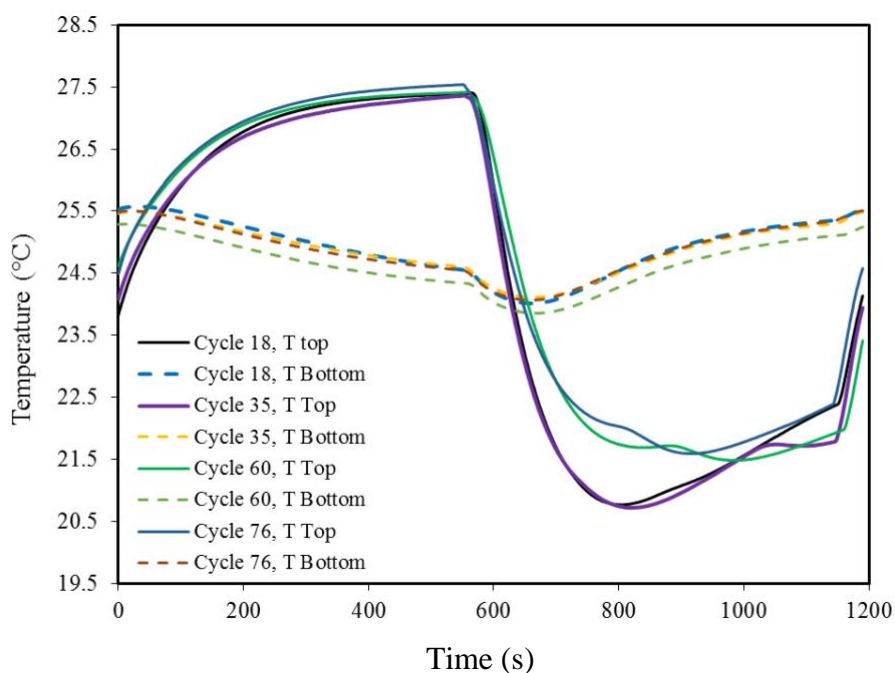
Figure 8.6: Comparison of temperature history in different cycles throughout the experiment - temperature 29.9 °C; pressure 300 kPa; vacuum 39 kPa; V_F 3 L/min; 100 % humid feed gas; $V_R/V_F = 1.5$.

Water holdup: The water holdup in the column was determined after 85 cycles (experiment termination) to ensure that the columns were sufficiently regenerated. For that, dry gas (N_2) was sent into the column from the top and the mole fraction of water in the outlet of the column was measured using the RH sensors while the column was under vacuum. No moisture was detected and the temperature history did not show a significant reduction. As can be seen in Figure 8.7, the temperature at the top of the column slightly decreased (within about 1°C); and after a minute, it increased because of the heating effect of the warmer inlet dry nitrogen gas (29.9 °C). This slight temperature drop in Figure 8.7 was caused by the desorption heat of the amount of water vapor sorbed during the pressurization before stopping the experiment (about a minute to pressurize the column).
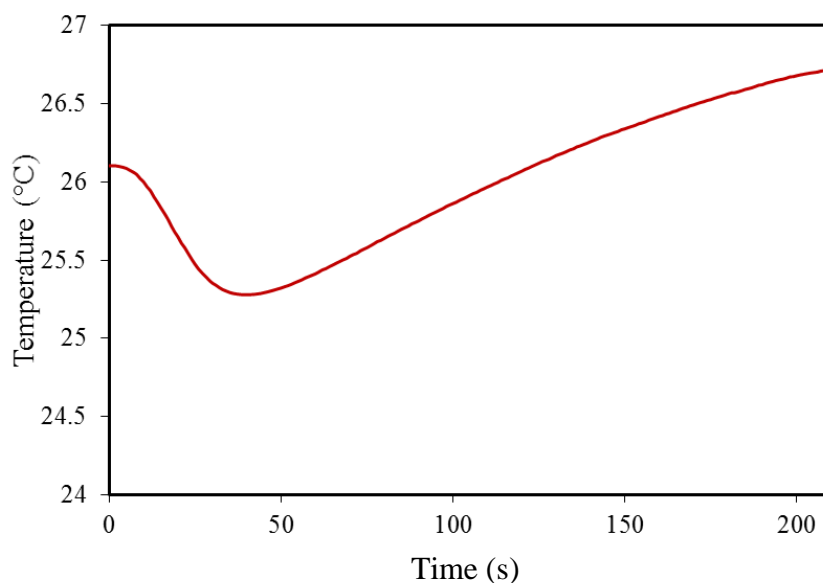
Figure 8.7: Temperature history during the determination of water holdup in bed after 85 cycles - V_R/V_F = 1.5.

Reduction of $\frac{V_R}{V_F}$ ratio: In addition, the experiment illustrated above was repeated with a regeneration gas volumetric flow rate to feed gas volumetric flow rate of one ($\frac{V_R}{V_F} = 1$). This volumetric ratio must be equal or larger than one in order to remove all the sorbed moisture from the biosorbent bed.[5] According to Ruthven[33], equal gas volume is at least required during the regeneration step at its corresponding pressure (or vacuum level) in a given cycle time to carry out the desorbed moisture from the column, which was accumulated in the column during the sorption step at its corresponding pressure (typically higher than that of the regeneration step). In industry, a standard ratio of 1.5 is usually considered (same as the experiment discussed above). However, in this section, the same experiment was repeated with a volumetric ratio of one to improve the product gas recovery of the PSA process and investigate if a stable process is feasible under these conditions. Similar to the previous experiment, this experiment was also run for 85 cycles and a stable performance was observed. Similar results were achieved and the performance of the system was as good as the previous experiment when $\frac{V_R}{V_F} = 1.5$ as can be seen in the product composition and other column histories shown in Figure 8.8 to Figure 8.9.
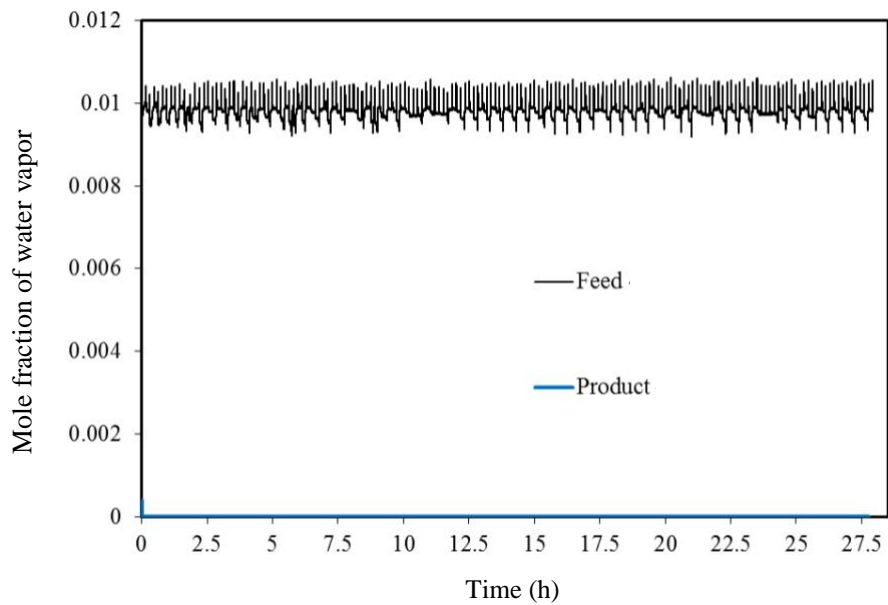
Figure 8.8: Water vapor history throughout the experiment (85 cycles) –Flax shives-temperature 29.9 °C; pressure 300 kPa; vacuum 39 kPa; V_F 3 L/min; 100 % humid feed gas; $V_R/V_F = 1$.

The temperature history during the regeneration was similar to what was observed in the previous experiment. The temperature raise after 7-8 minutes during the regeneration indicates that the bed was completely regenerated even with the volumetric flow rate of $\frac{V_R}{V_F} = 1$. Moreover, this temperature history was repeatedly seen throughout all the cycles, which shows the stable operation of the process.
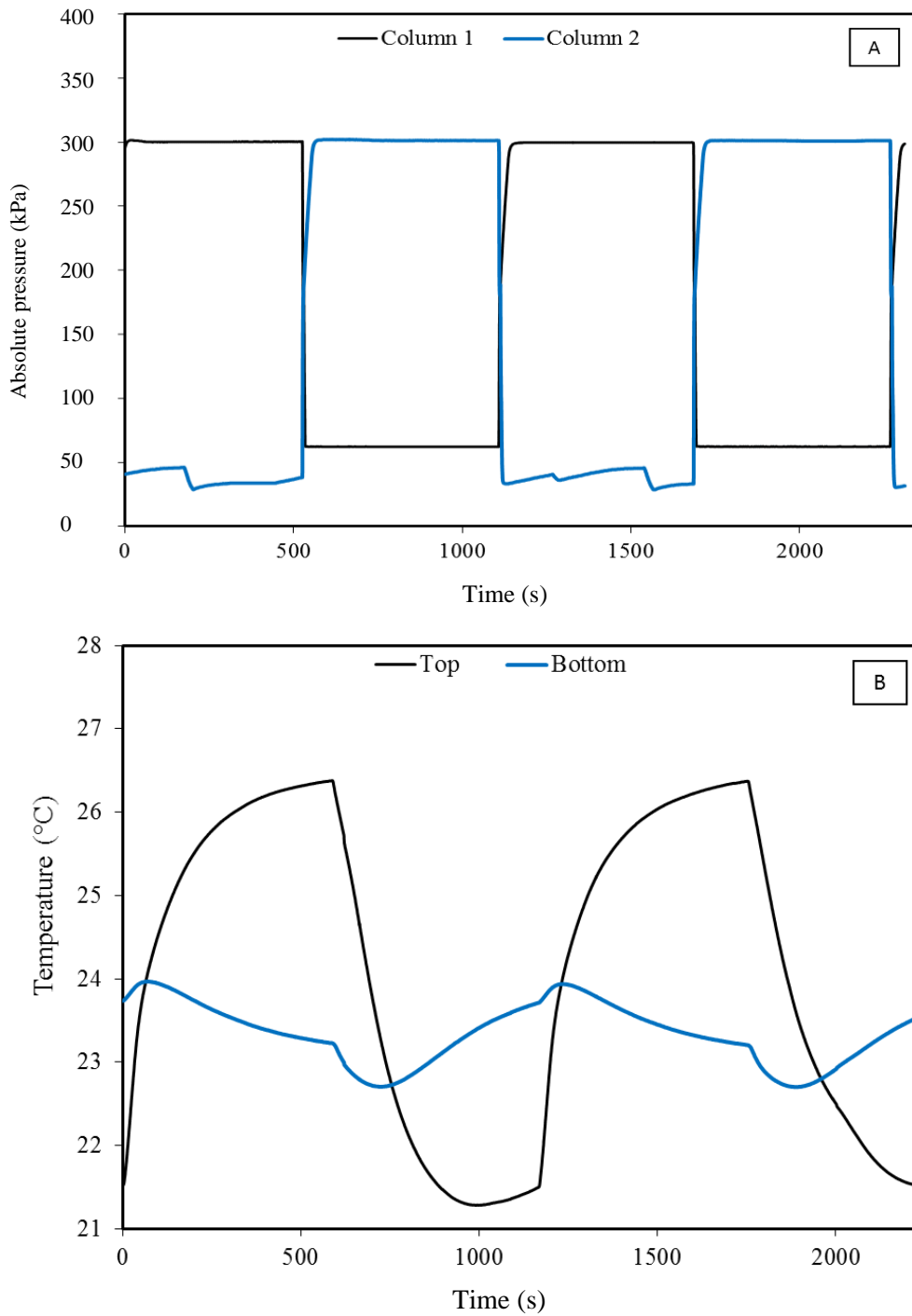
Figure 8.9: Cyclic pressure (A) and temperature (B) histories (two cycles) – Flax shives-temperature 29.9 °C; pressure 300 kPa; vacuum 39 kPa; V_F 3 L/min; 100 % humid feed gas; $V_R/V_F = 1$.
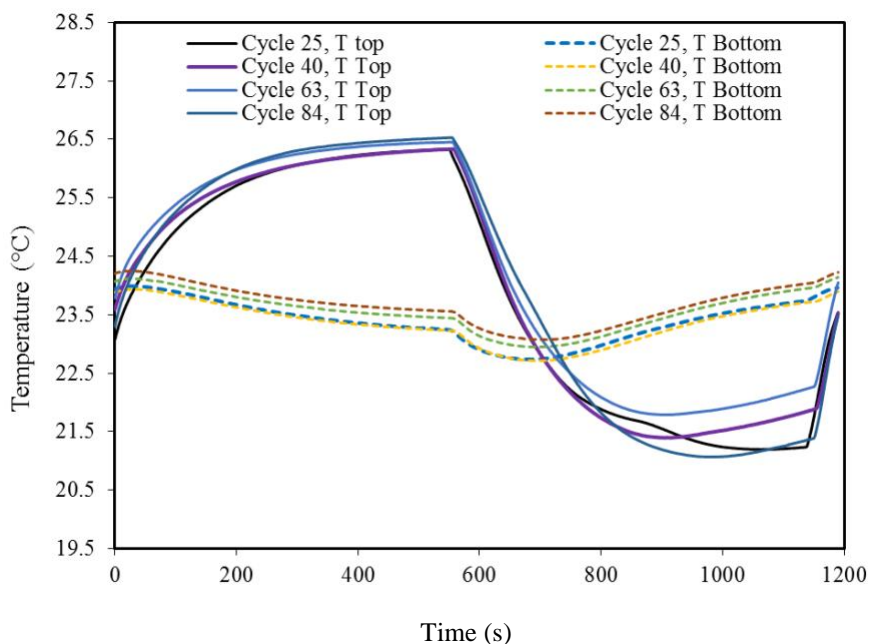
Figure 8.10: Comparison of temperature history in different cycles throughout the experiment-Flax shives - temperature 29.9 °C; pressure 300 kPa; vacuum 39 kPa; V_F = 3 L/min; 100 % humid feed gas; V_R/V_F = 1.

Figure 8.10 compares the temperature histories of the column in different cycles and Figure 8.11 shows that the process reached a stable condition as the average temperature of top and bottom of the column was almost identical during the experiment even when $\frac{V_R}{V_F} = 1$.

Similar to the previous experiment, the moisture holdup in the column after 85 cycles was determined and no moisture was detected in both columns. This reduction in the volumetric flow rate of the regeneration gas significantly may improve the economics of the process since the regeneration gas needs to be compressed and recycled.
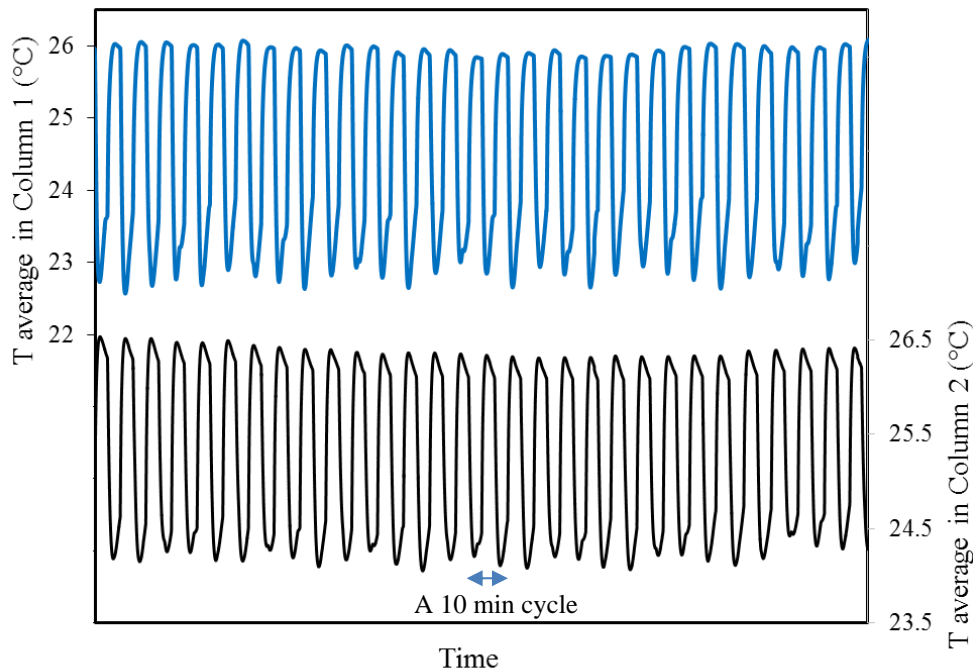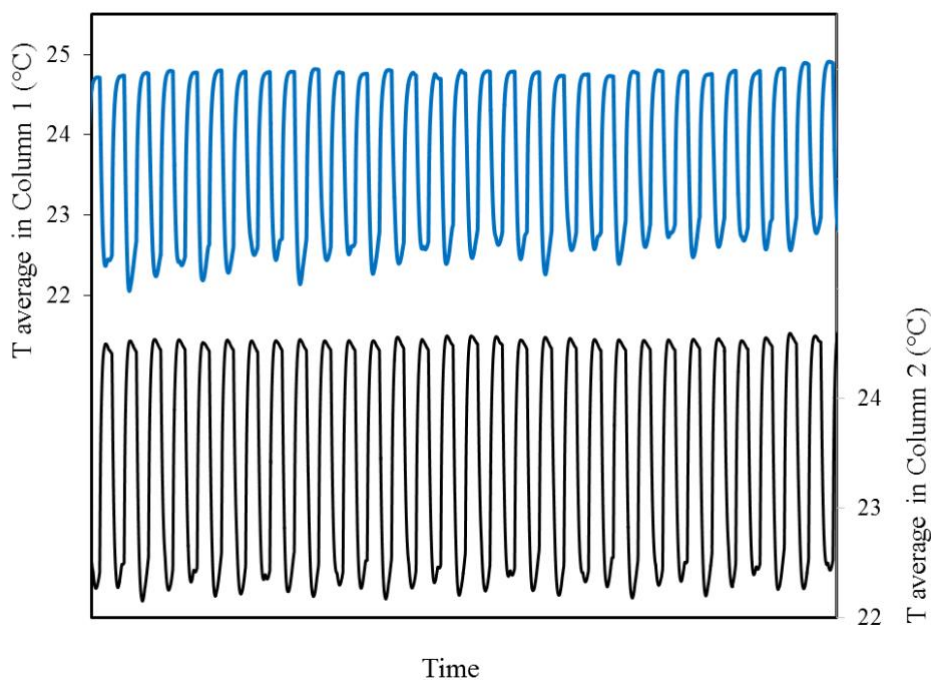
Figure 8.11: Cyclic temperature history during the PSA process using flas shives - temperature 29.9 °C; pressure 300 kPa; vacuum 39 kPa; V_F 3 L/min; 100 % humid feed gas; $V_R/V_F = 1$; the time values were not shown for better figure visibility; each temperature wave (maximum to minimum values and vice versa) is about 600 seconds.

8.1.2   Atmospheric-Pressure Experiments

Gas pressurization is energy intensive and costly, especially in the case of natural gas where multi-staged compressors and intercoolers are required. Similarly in air drying processes, atmospheric air has to be compressed before entering the PSA process.[33] In order to save energy and reduce processing costs, experiments were performed in this section to investigate whether the PSA process using the biosorbent is feasible at atmospheric pressure for dehydration (water sorption). If it is successful, this atmospheric PSA process has a potential for drying of air and biogas in addition to natural gas. It can also be integrated with carbon capture technologies in upstream processes to selectively dry the gas because the presence of moisture in the gas usually decreases the performance of adsorbents in the carbon dioxide caption system.[18]

To begin with, a dual-column experiment at atmospheric pressure was conducted based on the four step cycle illustrated in Chapter 3 where a normal building vacuum (39 kPa) was used during the regeneration step. A volumetric ratio of $\frac{V_R}{V_F} = 1$ and a cycle time of 10 minutes were considered. The feed gas was 100% humid with a temperature of 29.4 °C. This experiment was not successful and breakthrough point was reached in the second cycle. It was also

observed that water vapor was condensed in the column during the regeneration step and liquid water in the outlet wet the RH sensors. The water condensation was a result of the low volumetric flow rate of the regeneration gas, which could not carry out all the desorbed moisture from the column; as a result, excess water was condensed.

To address that, the experiment was conducted at the same conditions but with a volumetric ratio of $\frac{V_R}{V_F} = 1.5$. This result was successful; however, the performance of the system was not as good as the medium-pressure (300 kPa) experiments. As can be seen in Figure 8.12, the breakthrough point was reached in the first three cycles; and then, the process achieved a stable performance of generating dry gas for about 44 cycles. This observation can also be clearly seen in the cyclic temperature history of the columns (Figure 8.13). The temperature of columns increased over time and eventually reached a stable profile. The situation where the breakthrough point reached in the first few cycles can be explained based on the sorption-desorption rates discussed in the previous chapters (higher desorption rates obtained at higher temperatures); therefore, as the temperature of columns increased after a few cycles, the biosorbent in the columns were effectively regenerated as a result of a higher desorption rate. It is worth noting that the breakthrough point occurring at the beginning of the experiment can be simply avoided by heating the column during the startup prior to starting the cyclic operation.
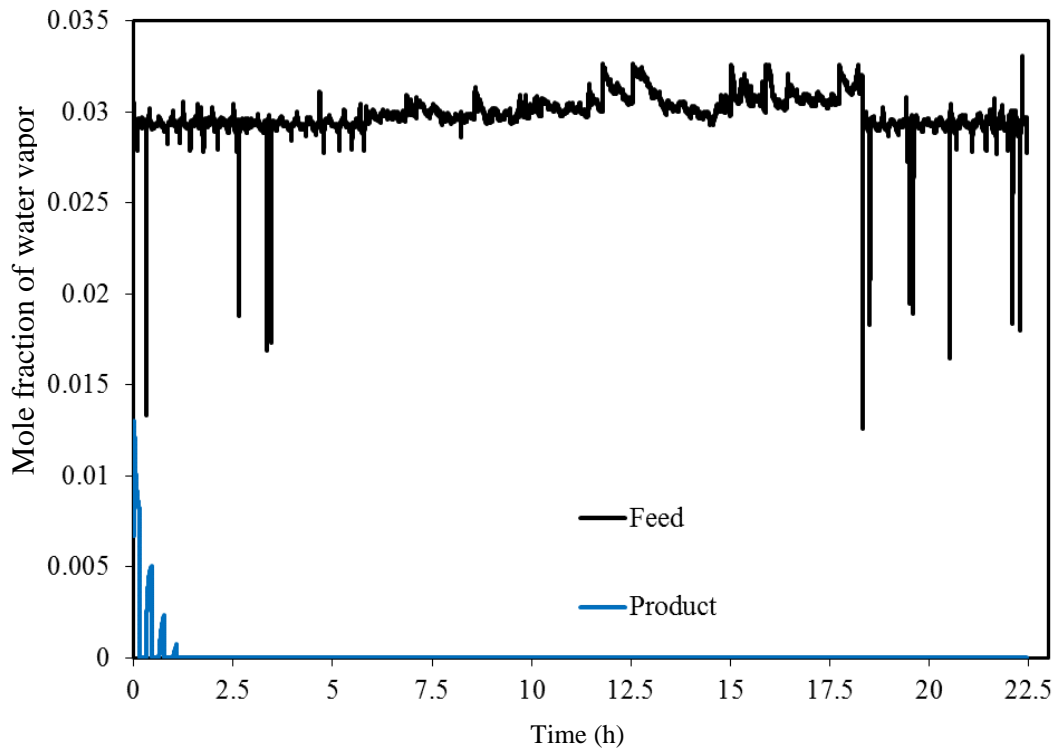
Figure 8.12: Water vapor history throughout the experiment using flax shives –temperature 29.4 °C; pressure 101.3 kPa; vacuum 39 kPa; V_F = 3 L/min; 100 % humid feed gas; V_R/V_F = 1.5.
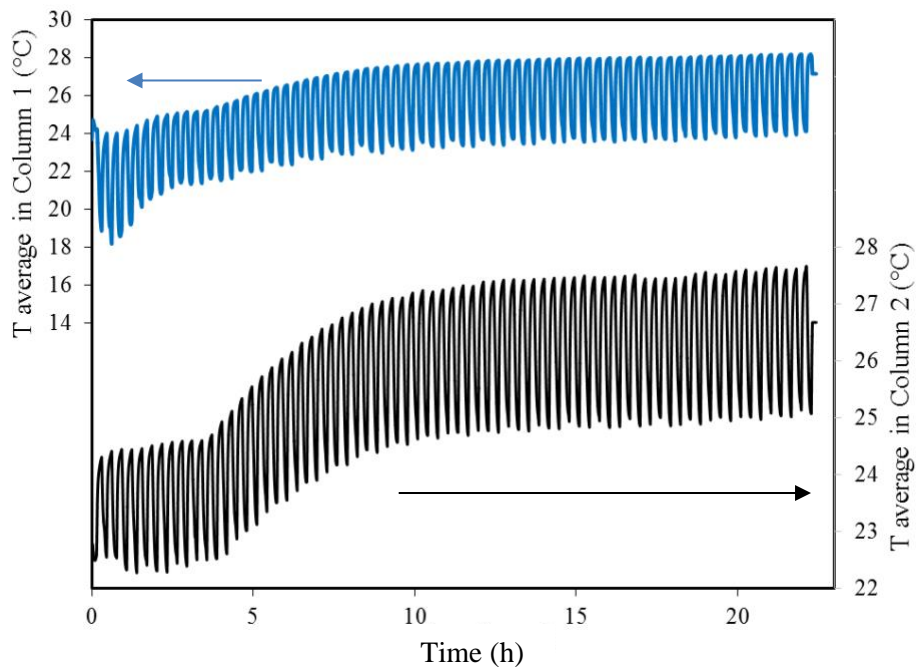
Figure 8.13: Cyclic temperature history during the experiment using flax shives – temperature 29.4 °C; pressure 101.3 kPa; vacuum 39 kPa; V_F 3 L/min; 100 % humid feed gas; V_R/V_F = 1.5.

106

Based on the results presented above, the effect of vacuum level on the cyclic process was further studied. In this experiment, a vacuum pump that can provide a vacuum level of 3 µHg was used to regenerate the columns. The other conditions were the same as the previous experiment. As can be seen in Figure 8.14, though the breakthrough point reached in the first cycle, the process reached a stable performance of producing dry gas. Figure 8.15 further shows that the cyclic temperature history of the column did not demonstrate an increasing trend as that of the previous experiment; in fact, the temperature history demonstrated a decreasing trend as a result of more effective regeneration steps and reached a stable situation. Detailed temperature histories are available in the supporting information.
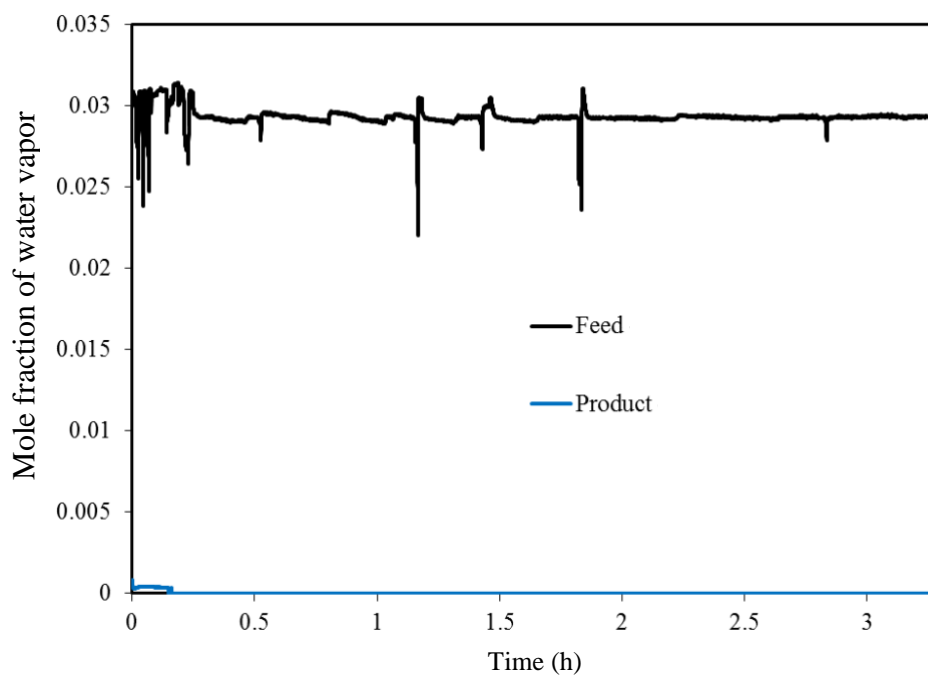
Figure 8.14: Water vapor history throughout the experiment –Flax shives– sorption at 101.3 kPa; Regeneration at 3 µHg using a vacuum pump; temperature 29.4 °C; V_F 3 L/min; 100 % humid feed gas; $V_R/V_F = 1.5$.
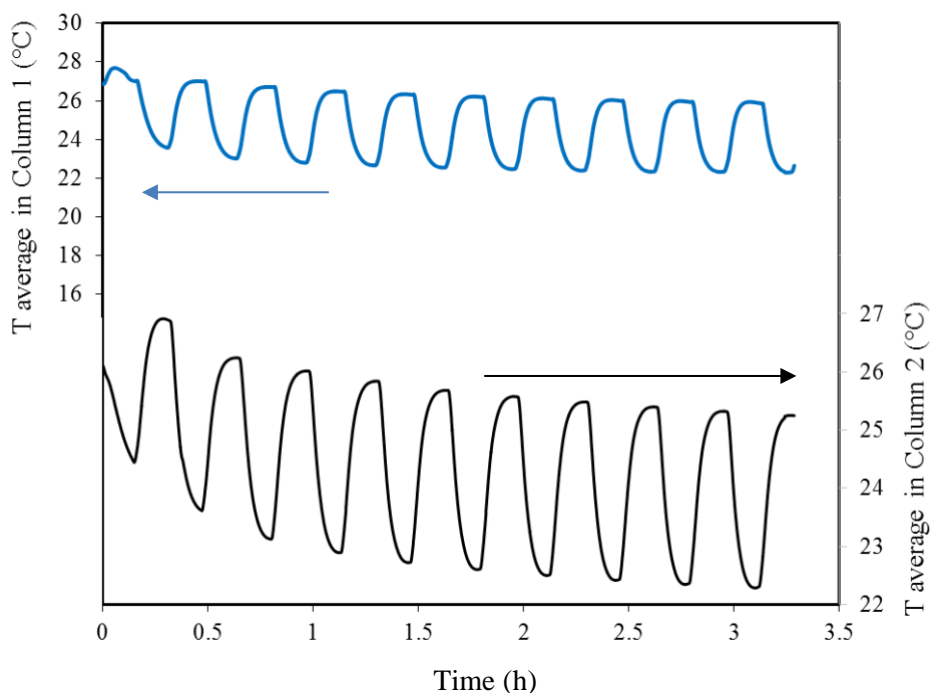
Figure 8.15: Cyclic temperature history of the experiment - sorption at 101.3 kPa; Flax shives- Regeneration at 3 µHg using a vacuum pump; ; temperature 29.4 °C; V_F 3 L/min; 100 % humid feed gas; $V_R/V_F = 1.5$.

The above results suggest that the PSA process can operate at atmospheric pressure as well and gas dehydration is possible under these conditions. This process was successful as a result of the excellent regeneration properties of the biosorbent (fast desorption rates at room temperature without external heating). Atmospheric PSA operation was not successful using other commercial adsorbents such as molecular sieves.[4,5,33] Attempts were made to use hot gas or electrical rods (installed inside the columns) to heat the solid adsorbents inside the column during the regenerations step to increase the regeneration rate. Using a vacuum pump is effective for desorption when the atmospheric pressure is used for water sorption to ensure effective gas dehydration in the PSA cycles. A vacuum level in the range of $39 - 1.33 \times 10^{-4}$ kPa (1µHg) is workable for this process. However, it is necessary to evaluate the cost of using a high level vacuum for desorption and the cost of operating water sorption at a high pressure in order to make the optimal design of the operation conditions, which are dependent on various conditions such as the feed gas condition and the chemical plant. There is no single best design for all scenarios.

8.2 Technical Discussions

In this section, several important topics about the PSA process are discussed that significantly affect the economics, feasibility, and life cycle of the process. To be more specific,

liquid carry over to the sorption columns, the lifetime of the biosorbents, and the effect of very high pressures on the dehydration performance of biosorbents may challenge the practicality of the process for the natural gas dehydration industry. These topics are concisely discussed here with the support of the data presented in this chapter.

8.2.1   Effect of Liquid Water Carry-Over and Self-Regulation of the Process

Liquid carry-over is one of the industrial problems reported for the TSA process.[4] This problem can lead to a premature breakthrough and insufficient dehydration of natural gas. Sometimes, the process needs to be shut down to replace the whole adsorbent bed with fresh dry adsorbents.[4,33] An expensive complex knock-out drum is typically designed and installed to separate any liquid from the natural gas prior to the dehydration unit. This knock-out drum is expensive because of higher liquid residence time, lower design terminal velocity, thicker mist eliminator, and longer vapor disengagement height, all of which are to reduce the liquid carry over.[3] Commercial adsorbents such as molecular sieves are sensitive to liquid water and cannot effectively sorb moisture from gas when they are wet[4,5]; therefore, this problem needs to be prevented. In this work, the experiments were performed using the wet biosorbent. The results showed that the biosorbent was not sensitive to liquid carry-over and the process was able to self-regulate and successfully produce dry gas. Figure 8.16 shows the RH of the output gas and the temperature histories at the top and bottom of the column with the wet biosorbents. As can be seen in Figure 6.16-A, the product gas was insufficiently dehydrated at the beginning of the cyclic experiment. However, after about 30 cycles, dry gas was achieved without any external heating. This observation showed the self-regulating and excellent regeneration properties of the biosorbent. Figure 8.16-B further illustrates the self-regulation of the process. The temperature at the top and bottom of the column were measured over time. As can be seen, the temperature at the top of the column increased over time because of the heat of sorption (feed gas was sent from the top) and then reached a stable level. In the meantime, the temperature at the bottom sharply decreased to low temperatures as 3 °C as a result of the heat of water desorption (regeneration was performed counter-currently). In every cycle, the bed was further regenerated and the temperature at the bottom had increased over time. This temperature increase at the bottom could be a result of heat conduction in solid from the top of the column to the bottom as well as the decreasing amounts of water that were desorbed in every cycle as the bed became drier over time.
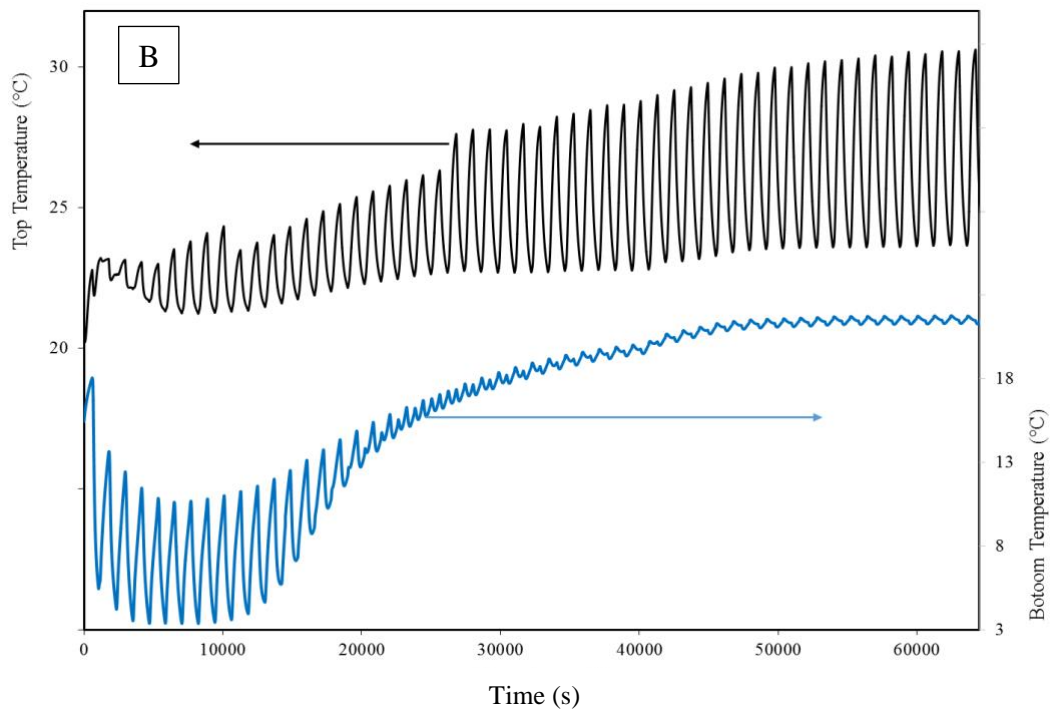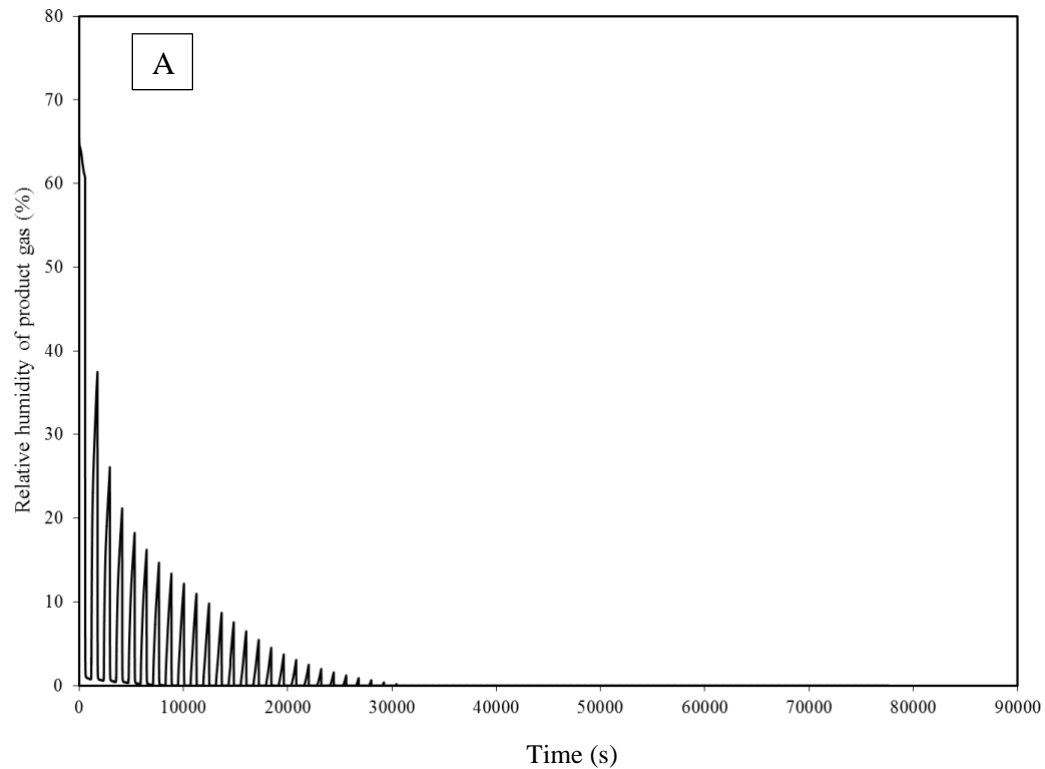
Figure 8.16: The effect of water carry-over and self-regulating response of the system using flax shives to liquid water carry over; A: breakthrough point reached for 30 cycles and the system self-regulated itself and then reached a steady-state operation; B: The significant temperature drop to 3 °C was as a result of the heat of water desorption while the system was self-regulating itself in order to reach a steady-state condition - temperature 29.4 °C; pressure 300 kPa; vacuum 39 kPa; V_F 3 L/min; 100 % humid feed gas; $V_R/V_F = 1.5$.

110

It can be noticed in Figure 8.16 that the temperature at the bottom started to rise at $t \cong 30000$, where the RH of the product gas reached zero in Figure 8.16; and then reached a stable value of about 20 °C, which was the initial temperature of the bed at the beginning of the experiment. This self-regulation of the PSA process is a result of the excellent regeneration properties of the biosorbent and fast rates of desorption, which were analyzed in previous chapters. That being said, in the case of liquid carry-over in industry, the PSA process using biosorbents can be simply controlled without a process shut down.

8.2.2   Lifetime of the Biosorbents

It has been documented that the glycol solutions in the glycol that are used in the TEG dehydration systems lose their properties over time as a results of continuous temperature fluctuations in the close loop between the absorber column and the distillation column.[3,4,29] Similarly, solid adsorbents continuously experience temperature fluctuations in the TSA process, which result in a loss in their adsorption properties over time. No solid data on the exact lifetime of conventional adsorbent in the natural gas dehydration units could be found in the literature.

The results presented in this chapter confirmed that the PSA process can dehydrate nonpolar gases at atmospheric and medium-pressures. A critical question that must be answered is the lifetime of the biosorbent in this process. It was shown in Chapter 5 that the biosorbent showed negligible degradation after experiencing 70 full sorption-desorption cycles under isothermal conditions (complete saturation and regeneration).[7] In this chapter, the biosorbent showed a stable performance in 450 cycles in a continuous dual-column PSA process under adiabatic conditions and can continue to operate for more cycles. Flax shives are a natural material and can degrade over time if stored in a wet environment; however, in a PSA process, they are periodically dried within the PSA cycles at a temperature range of 19 to 40 °C. Furthermore, the surface chemistry of the flax shives was investigated over time (70 sorption-desorption cycles). The results showed that the surface properties were not substantially changed. Taking these results into consideration, it can be predicted that the biosorbent can effectively work in the PSA process with negligible degradation for a relatively long time. However, future pilot scale studies are required to substantiate this aspect with data. In Chapter 9, the capital and operating costs of the PSA process were compared with those of the TSA and TEG process including more discussions in the regard.

8.2.3   Process Performance at Higher Pressures

Another critical question that needs to be answered regarding the PSA process is the effect of particularly high pressures of natural gas operations (3000 to 6500 kPa). Because of safety issues, the dehydration performance of the flax shives at such pressures could not be investigated in this work. The maximum operating pressure possible in the lab-scale setup was 500 kPa (5 bar). The concentration history of this experiment at 500 kPa (5 bar) and 24 °C is shown in Figure 8.17. The feed gas was 100% humid having a flow rate of 3 L/min. A water vapor sorption capacity of 0.88 g/g was achieved, which is still very good compared to commercial adsorbents such as molecular sieves. Again, the adsorption of methane, carbon dioxide, and nitrogen was negligible at 500 kPa. Methane, carbon dioxide, and nitrogen adsorption at pressures up to 6000 kPa will be investigated once a safe setup is available when funding is available. No solid conclusions, however, can be made here without data. In the case of methane adsorption by flax shives at higher pressures, the PSA process would still work with some modifications of the cycle steps as a result of the excellent regeneration properties of the biosorbent.
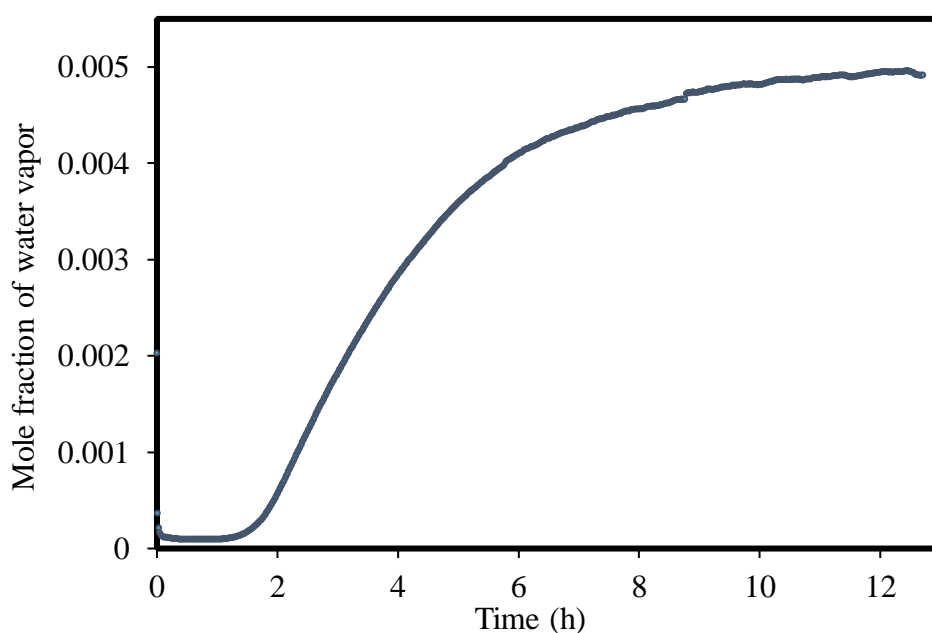
Figure 8.17: Water vapor history in the outlet of column packed with flax shives at 500 kPa and 24 °C; flow rate 3 L/min; 100% humid feed gas.

8.3   Dual Column Cyclic Experiments with Oat Hulls

These experiments with oat hulls were performed to investigate similarities and differences in the cyclic performance of the process with oat hulls and flax shives as the

biosorbents. In these experiments, both columns were filled with oat hulls. The particle size distribution of oat hulls was 1.18 – 3 mm and they were oven-dried at 105 °C for 24 hours before packing (Figure 8.18). Similar to the flax shives experiments, Ultra-High Purity (5.0) N_2 gas was purchased from Praxair Canada and used for the experiments. In the experiments in these section with oat hulls, the experimental conditions (sections 8.1.1 and 8.1.2) and feed gas composition were identical to those used in the flax shives experiment (Table 8.1). The only difference is the biosorbent material.

Figure 8.18: Photo of oat hulls used in the dual-column experiments.

8.3.1.1   Medium-Pressure Experiments

Water histories in the feed and product: Based on the results achieved in the dual-column cyclic experiments with flax shives, the process based on the six-step cycle worked with both $\frac{V_R}{V_F}$ of 1.5 and 1 (regeneration gas to feed gas volumetric flow rate ratios); therefore, the oat hulls experiments were started with the volumetric ratio of 1 and the experiment with the volumetric ratio of 1.5 was not performed because of the success of the first experiment. Figure 8.19 shows the water vapor history throughout this experiment. As can be seen, the results are similar to those achieved with flax shives; the feed mole fraction was controlled at 0.0098 and dry gas was collected as the product throughout the 85 cycles. This experiment confirms that oat hulls can effectively dehydrate nitrogen, methane, carbon dioxide, and other nonpolar gases in a pressure swing sorption process.
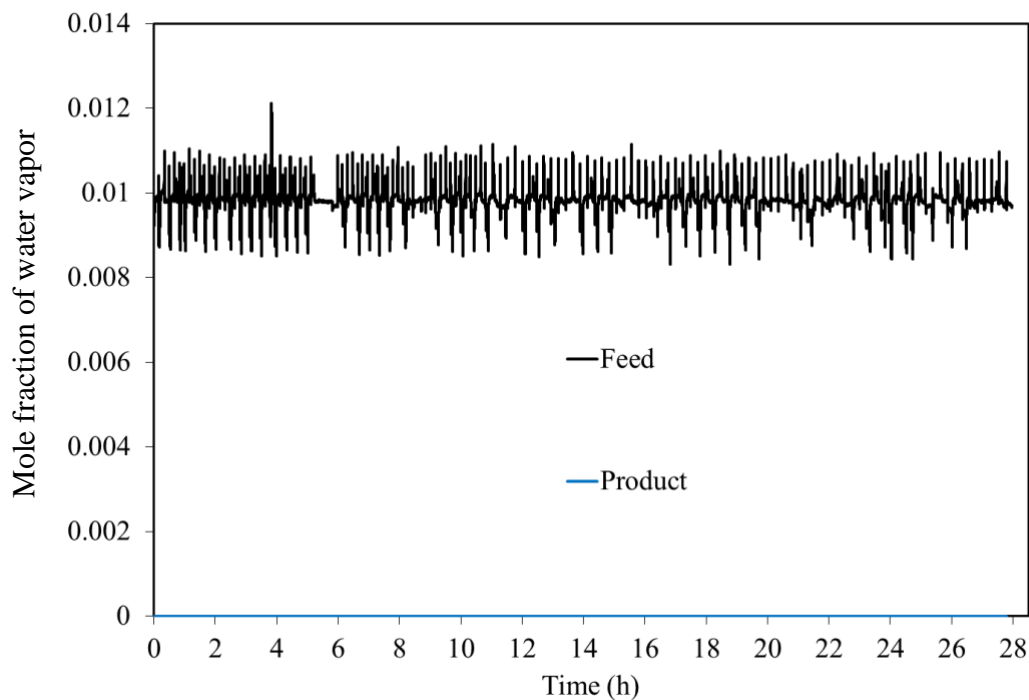
Figure 8.19: Water vapor history throughout the dual-column experiment using oat hulls (85 cycles) - temperature 29.9 °C; pressure 300 kPa; vacuum 39 kPa; V_F 3 L/min; 100 % humid feed gas; $V_R/V_F = 1$.

Cyclic Temperature and Pressure Histories: Cyclic pressure and temperature histories during two cycles in this experiment are shown in Figure 8.20, which are again similar to those achieved with flax shives. During this cyclic operation, each column run at 300 kPa for 10 minutes followed by a 5 second pressure equalization where both columns reached an equal pressure of approximately 170 kPa; then, the column was depressurized and kept under a vacuum of 39 kPa for another 10 minutes. Two temperature sensors were installed to record the temperature of the biosorbents at the top and bottom of the column. As can be seen, the temperature changes during the cycle steps are quite similar to those achieved in the experiments with flax shives, which were expected as these two biosorbents are rather similar.
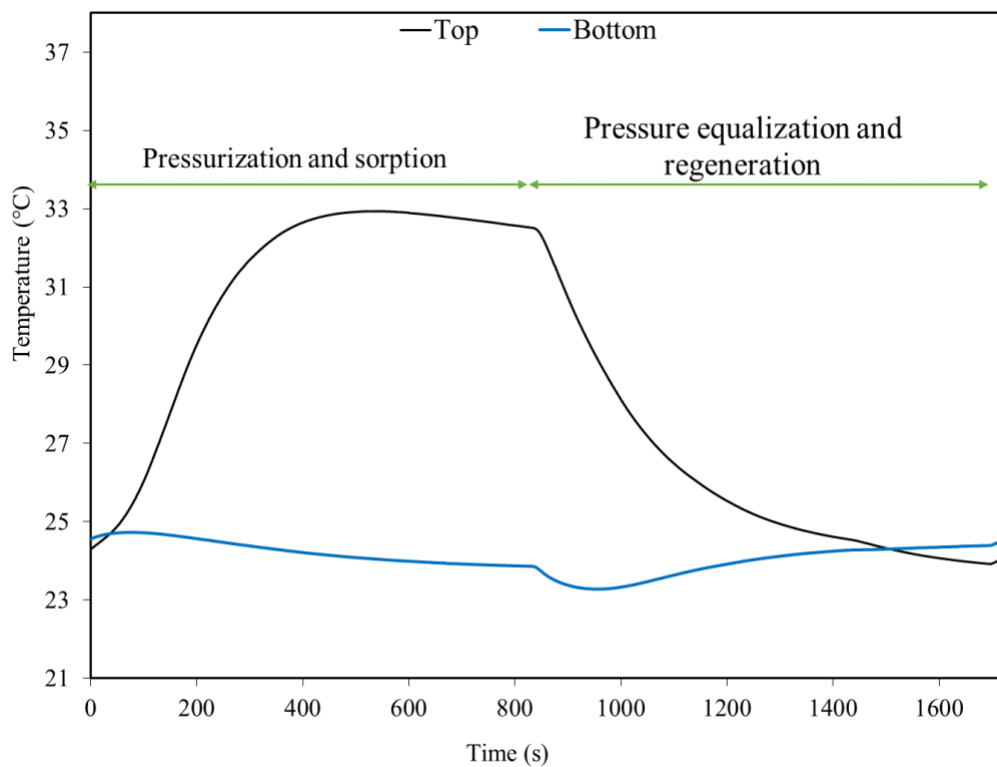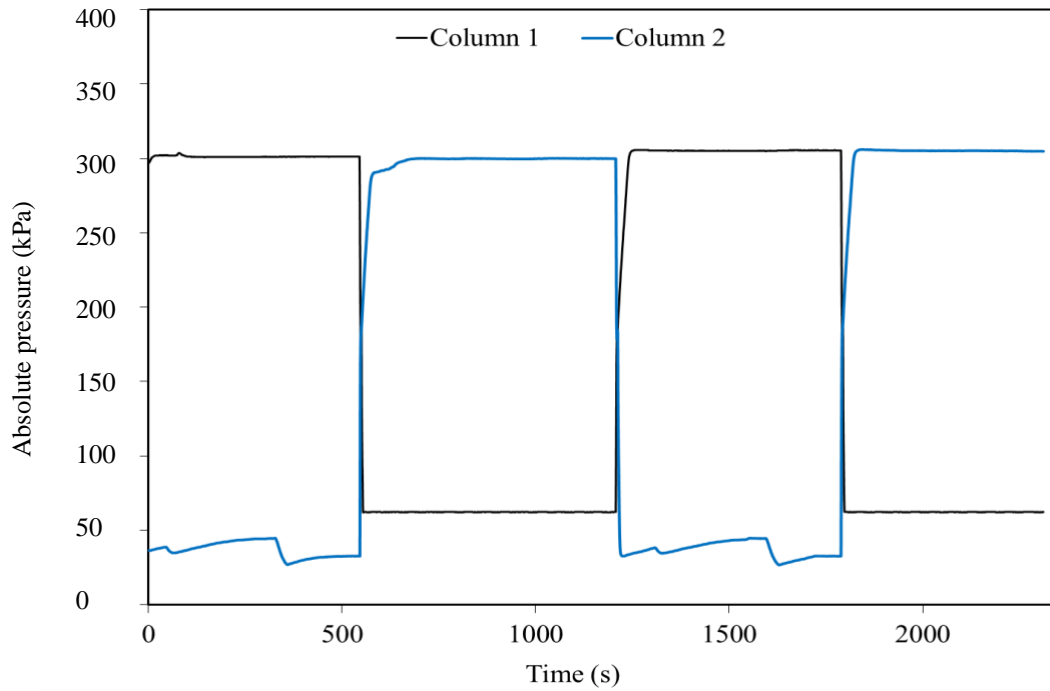
Figure 8.20: Cyclic pressure and temperature histories (two cycles); oat hulls - temperature 29.9 °C; pressure 300 kPa; vacuum 39 kPa; V_F 3 L/min; 100 % humid feed gas; $V_R/V_F = 1$.

The average temperature of column (top and bottom) showed a stable behavior and no heat accumulation or increasing trend was seen after 85 cycles. This shows the columns were sufficiently regenerated and a cycle time of 10 minutes worked well.

115
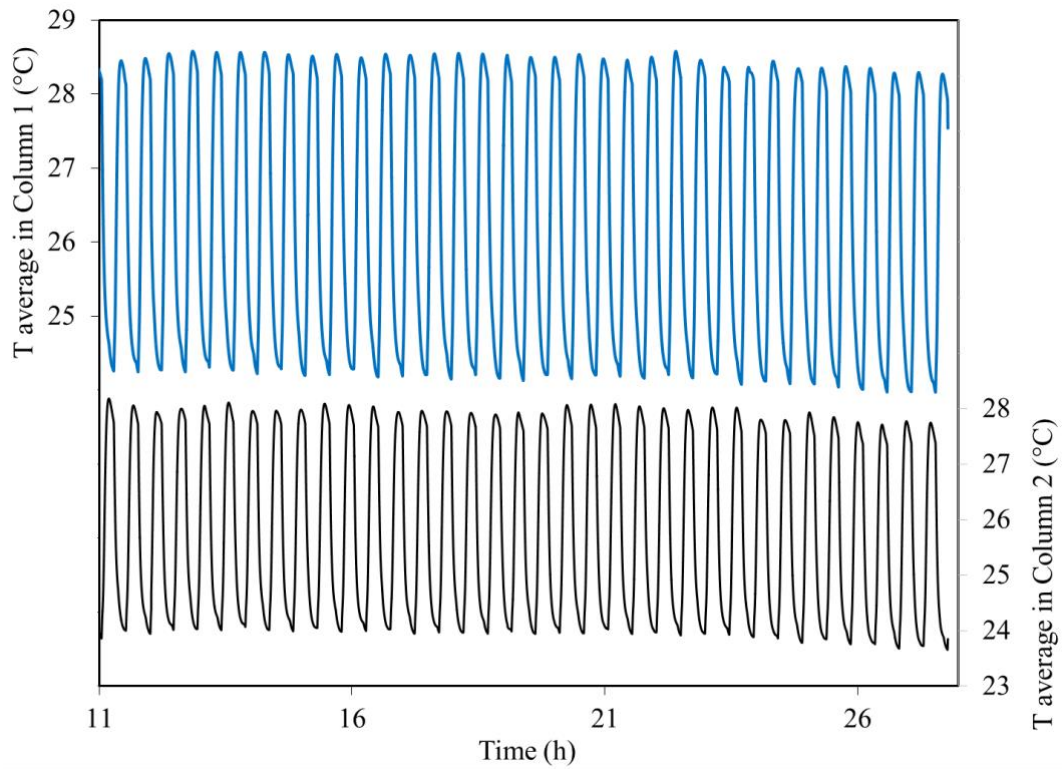
Figure 8.21: Cyclic temperature history during the PSA process; oat hulls temperature 29.9 °C; pressure 300 kPa; vacuum 39 kPa; V_F 3 L/min; 100 % humid feed gas; $V_R/V_F = 1$.

Figure 8.22 similarly shows the overlapped temperature history of the column during different cycles. As can be seen, the temperature histories during cycle 2, 9, 21, and 32 were almost identical, which shows the stable performance of oat hulls and stable behavior of the process.
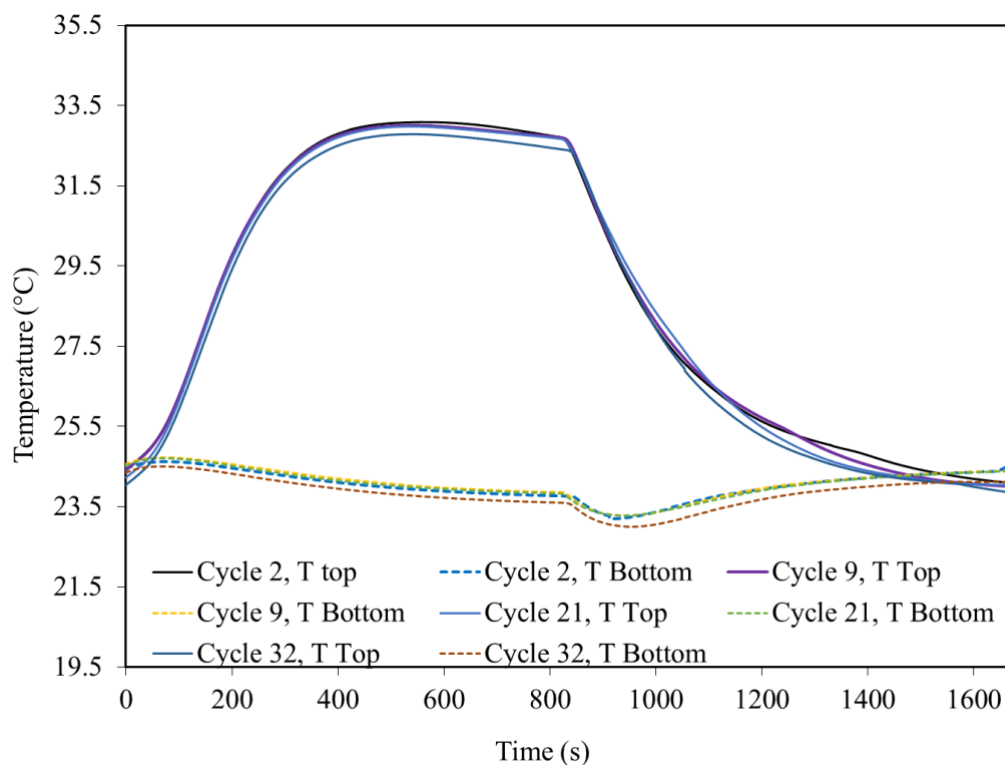
Figure 8.22: Comparison of temperature history in different cycles throughout the experiment - temperature 29.9 °C; pressure 300 kPa; vacuum 39 kPa; V_F 3 L/min; 100 % humid feed gas; $V_R/V_F = 1$.

Water Holdup: The water holdup in the column was determined after 85 cycles (experiment termination) in a similar procedure to that in the flax shives experiments to ensure that the columns were sufficiently regenerated. Dry gas was sent into the column from the top and the mole fraction of water in the outlet of the column was measured over time using the RH sensors while the column was under vacuum. Very low amounts of moisture were detected in the outlet for a short amount of time and the temperature history showed a slight reduction. As can be seen in Figure 8.23, the humidity at the outlet dropped to zero after about a minute and the temperature gradually increased as a result of the heating effect of the warmer inlet gas at 29.9 °C. Overall, this shows that the columns were essentially regenerated after 85 cycles as a result of suitable properties of oat hulls. Indeed, oat hulls and flax shives showed a similar promising performance in gas dehydration in the pressure swing sorption process.

117
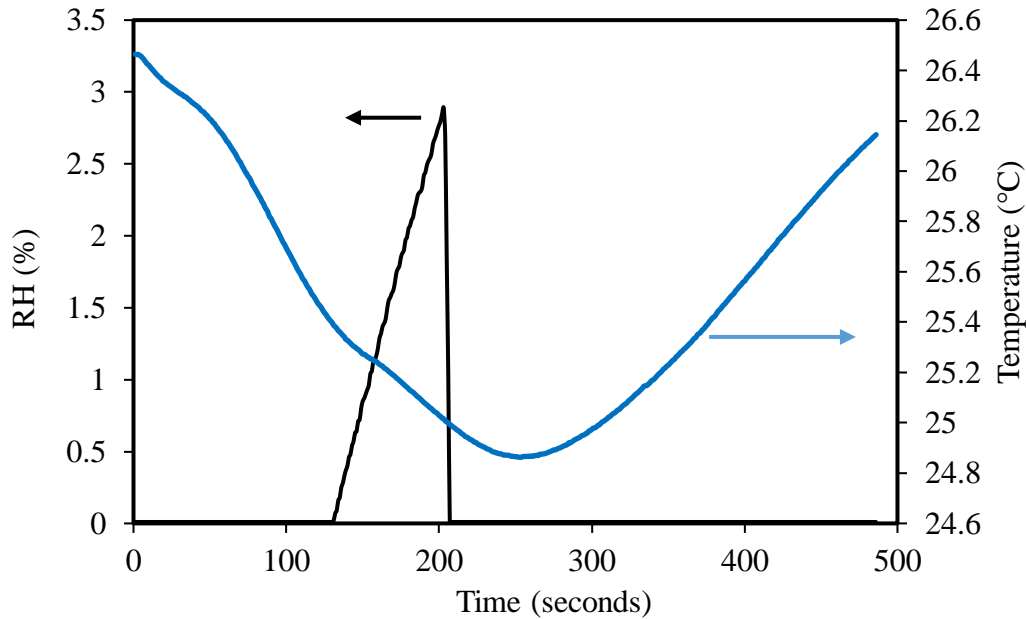
Figure 8.23: Temperature history during the determination of water holdup in the oat hulls bed after 85 cycles - temperature 29.9 °C; pressure 300 kPa; vacuum 39 kPa; V_F 3 L/min; 100 % humid feed gas; $V_R/V_F = 1$.

8.3.1.2   Atmospheric-Pressure Experiments

Two experiments at atmospheric pressure were performed based on the four-step cycle; one with a normal vacuum (≈39 kPa absolute) and one with a vacuum pump (3 µHg). The volumetric flow ratio was $\frac{V_R}{V_F} = 1$. This experiment was successful; however, the performance of the system was not as good as the medium-pressure experiments. As can be seen in Figure 8.24, breakthrough point was reached in the first eight cycles; and then, the process reached a stable condition and dry product gas was achieved. Figure 8.25 better illustrates the transition of the process from the startup to stable conditions. The temperature of columns increased over time and reached a stable profile. Similar results were observed in the experiments with flax shives.

118
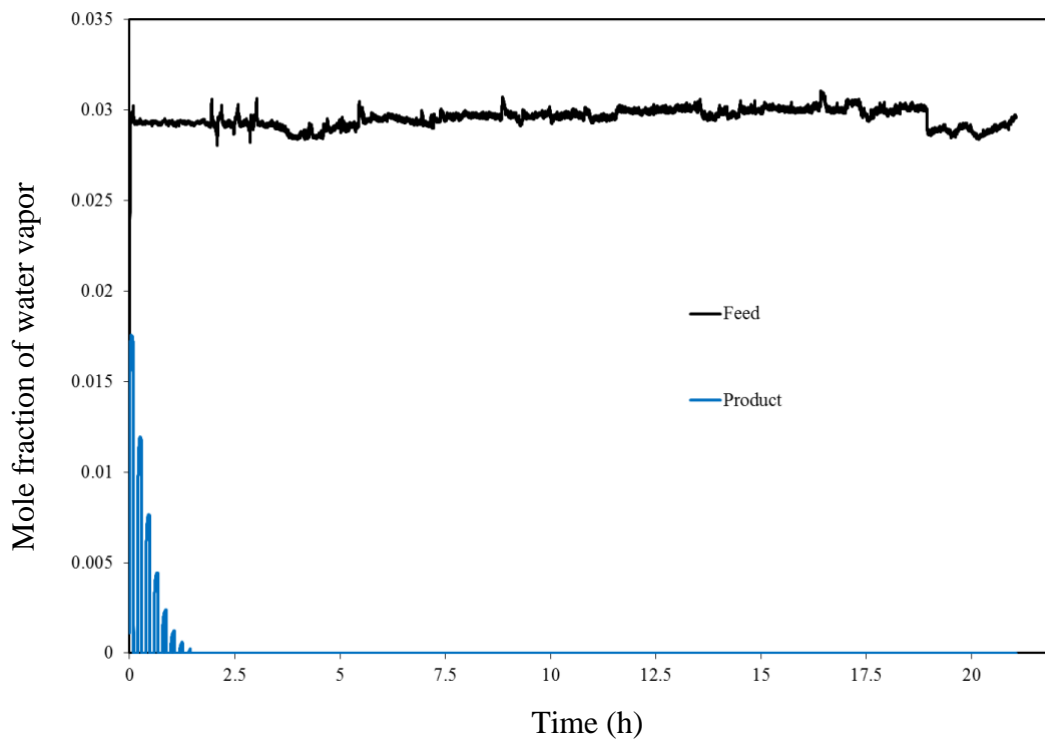
Figure 8.24: Water vapor history throughout the experiment – oat hulls; temperature 29.9 °C; pressure 101.3 kPa; vacuum 39 kPa; V_F 3 L/min; 100 % humid feed gas; $V_R/V_F = 1$.
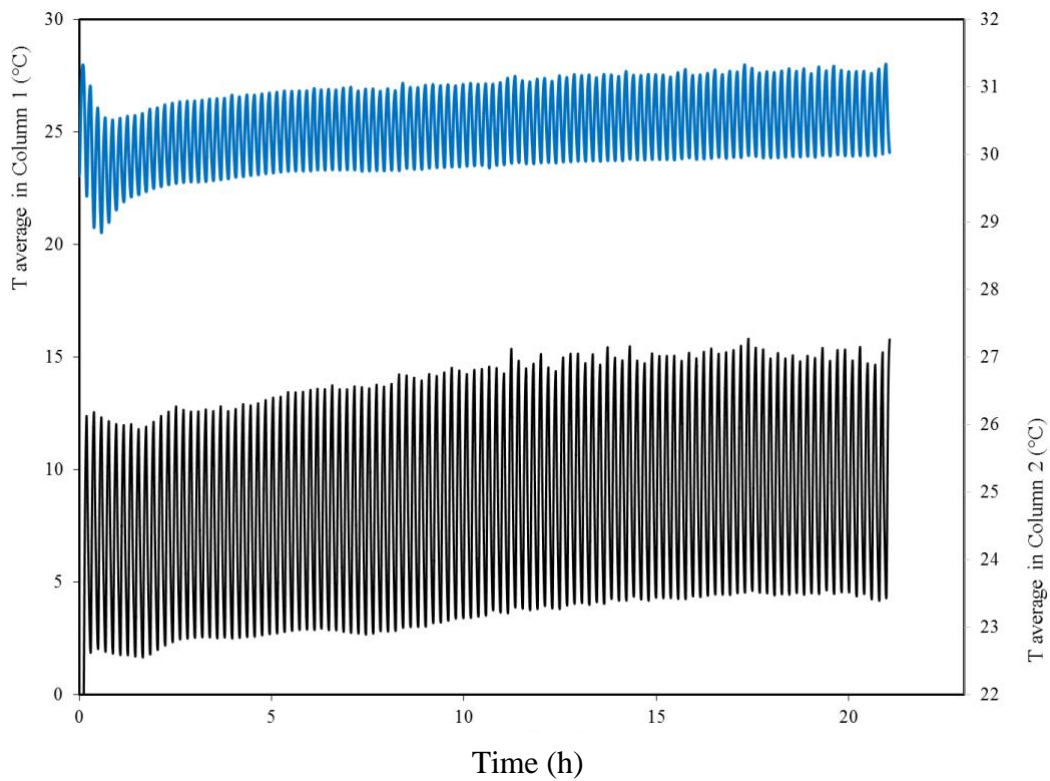
Figure 8.25: Cyclic temperature history during the experiment – oat hulls temperature 29.9 °C; pressure 101.3 kPa; vacuum 39 kPa; V_F 3 L/min; 100 % humid feed gas; $V_R/V_F = 1$.

119

In the next experiment, a vacuum pump capable of providing a vacuum level of 3 µHg was used to regenerate the columns, while other experimental conditions remained the same. A stronger vacuum could improve the regeneration of oat hulls and prevent the issues observed in the previous experiment. According to Figure 8.26, breakthrough point was reached only in the first cycle; afterward, the process reached a stable condition. The temperature history of the columns was much more stable compared to that of the first experiment (Figure 8.27). The vacuum level had the same effect on the performance of flax shives, which again shows the similarity in the properties and performance of oat hulls and flax shives.
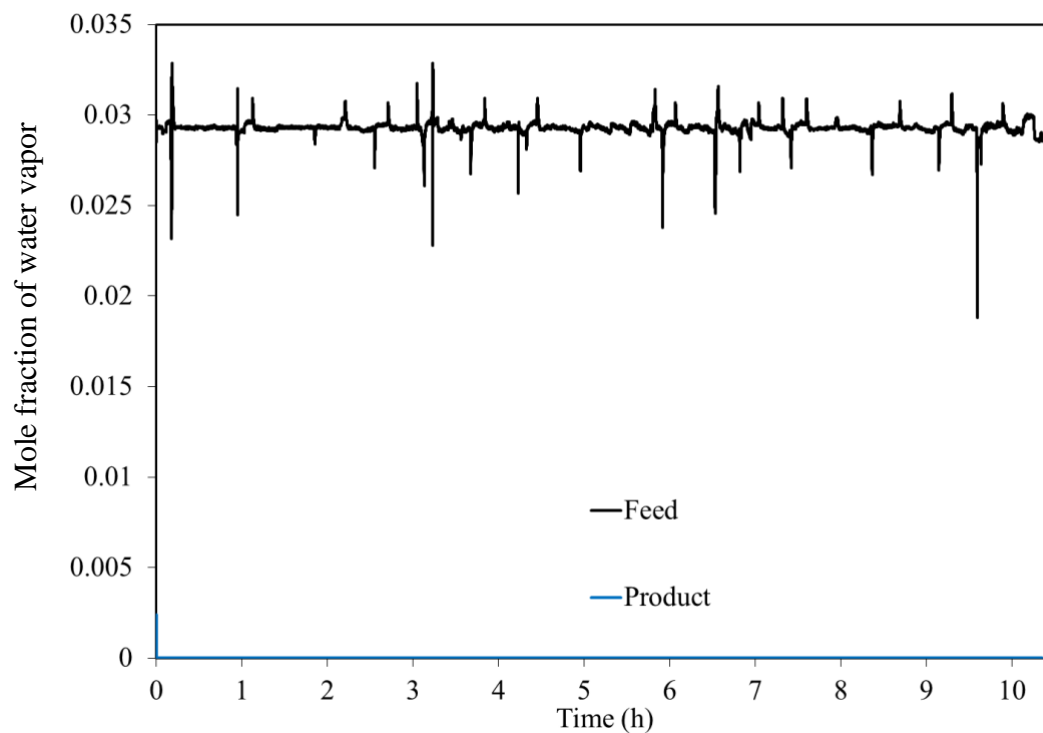
Figure 8.26: Water vapor history throughout the experiment – oat hulls; sorption at 101.3 kPa; Regeneration at 3 µHg using a vacuum pump; temperature 29.9 °C; V_F 3 L/min; 100 % humid feed gas
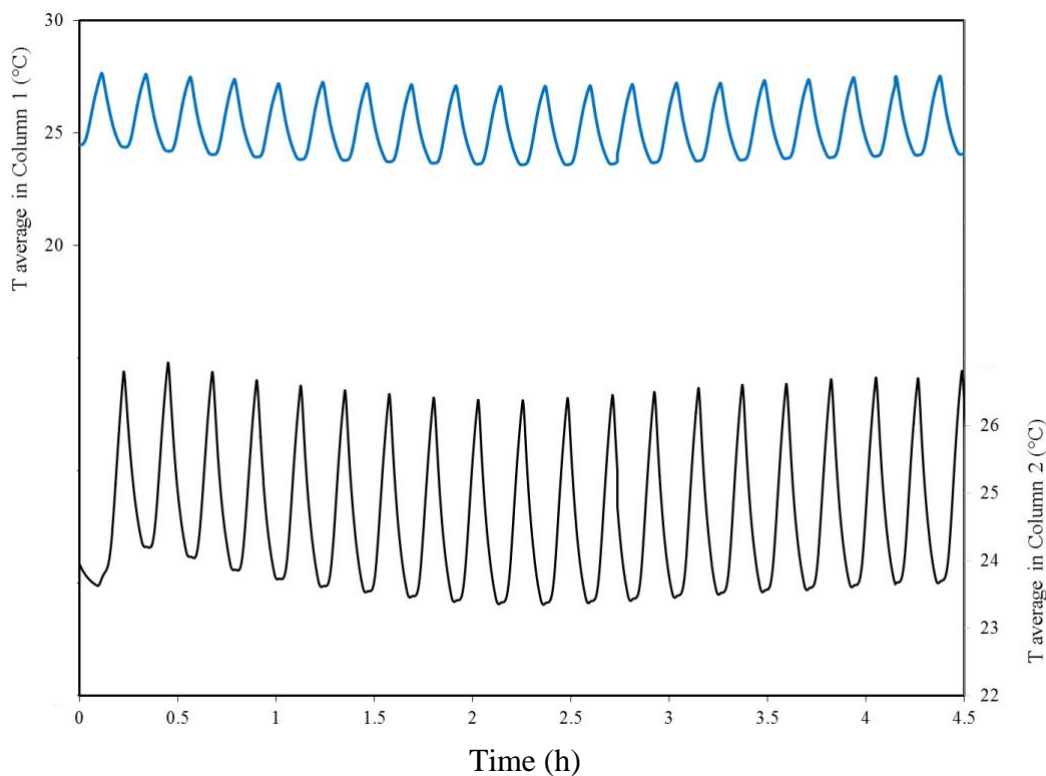
Figure 8.27: Cyclic temperature history of the experiment – oat hulls; sorption at 101.3 kPa; Regeneration at 3 µHg using a vacuum pump; temperature 29.9 °C; V_F 3 L/min; 100 % humid feed gas; $V_R/V_F = 1$.

Collectively, these results of dual-column cyclic experiments with both flax shives and oat hulls suggest that the natural gas dehydration process using biosorbents is effective at atmospheric and pressurized conditions. This success was a result of the excellent regeneration properties of the biosorbent (fast rates at lower temperatures without external heating). The biosorbents can be developed from similar inexpensive biomass materials similar to flax shives or oat hulls and their treatment process is also cost-effective.

8.3.1.3 Effect of Cycle Time and Vacuum Level on the PSA Process

It was demonstrated in Chapter 5 that the gas flow rate did not have a substantial on the sorption capacity of flax shives; however, the length of mass transfer zone slightly increased with increasing total gas flow rate. Similar trend was seen in other works.[18,116,117] This increase in the length of MTZ does not affect the cyclic performance of the process as it was seen that MTZ was far away from the column's outlet. In addition, the increase in the length of MTZ was not significant. As seen in the flax shives experiments, a 100% increase in the gas flow rate increased the length of MTZ from 10.8 to 11.4 cm at 24 °C.[7] This increase was even smaller at higher temperatures. Furthermore, the columns are usually overdesigned (height to

diameter ratios of 2 to 4); therefore, the length of unused bed (LUB) is usually bigger than the length of MTZ (extra adsorbents in the column).[33] Moreover, a higher gas flow rate improves the regeneration of adsorbents since more moisture (desorbed water) can be carried out of the bed in each cycle.[5] The analysis of temperature histories during the cyclic operation in this chapter demonstrated that a cycle time of 7-8 minutes was sufficient to regenerate the biosorbent beds; therefore, a longer cycle time would not be advantageous for this PSA process. It results in further propagation of the mass transfer and heat transfer front towards the end of the column and more significant temperature fluctuations in the columns, which is disadvantageous for the biosorbent (Figure 8.28). As can be observed in the figures below, various cycle times from 6 to 20 minutes were investigated during an experiment and dry product was achieved. The temperature histories were slightly changed, which was expected. The height of packed bed was much higher than the length of MTZ and the MTZ never reached the outlet of the column (breakthrough point).
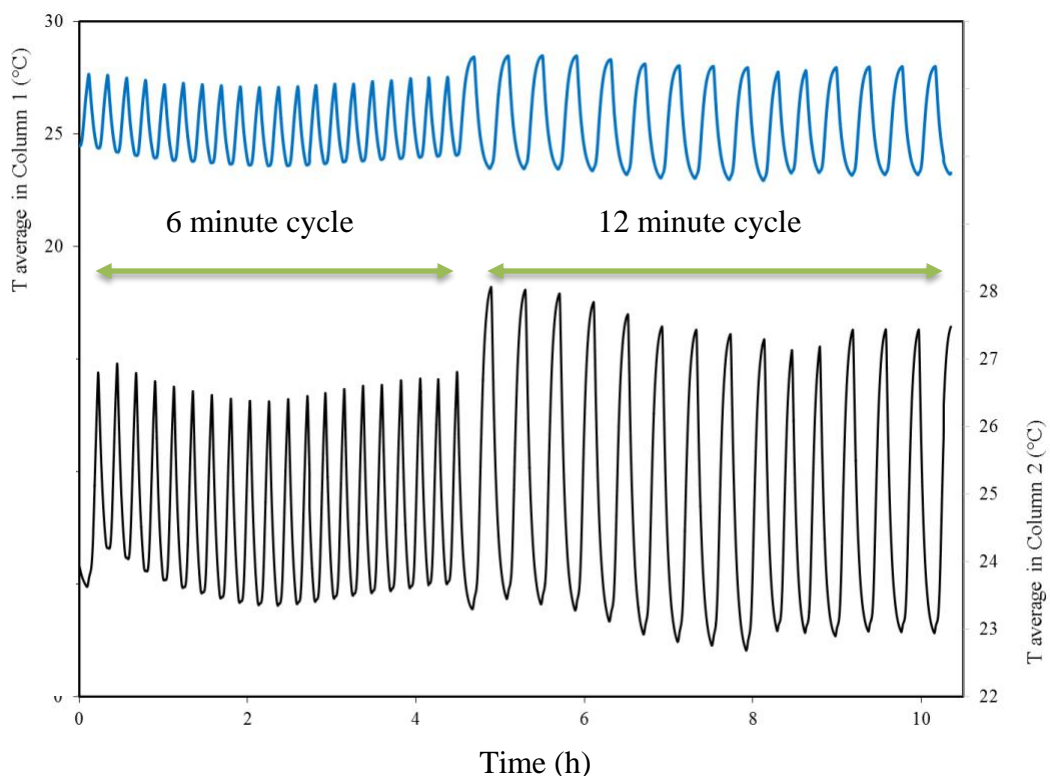
Figure 6.28-A and B: Effect of cycle time on the cyclic temperature profile; oat hulls sorption at 101.3 kPa; Regeneration at 3 µHg using a vacuum pump; temperature 29.9 °C; V_F = 3 L/min; 100 % humid feed gas; $V_R/V_F = 1$; A: effect of doubling the cycle time; Figure B and C are magnified at different times.
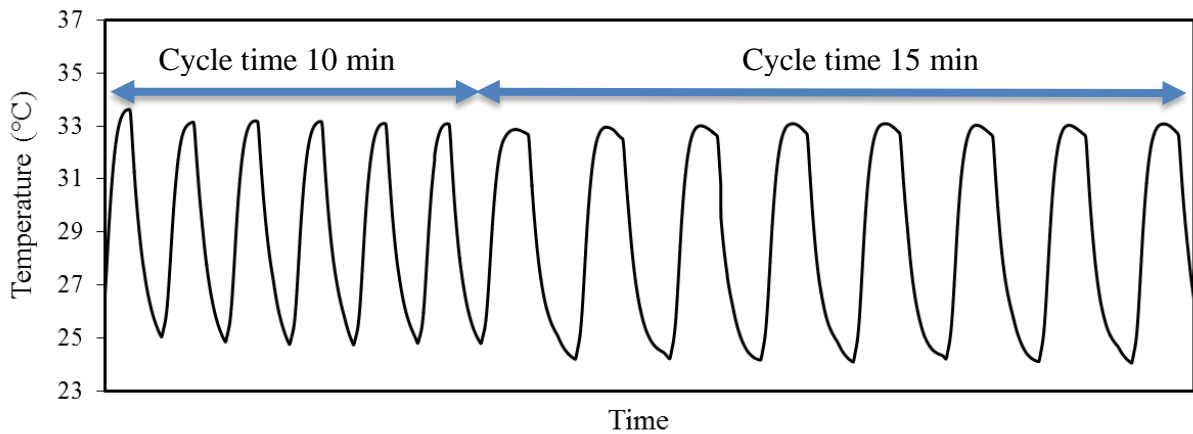
B
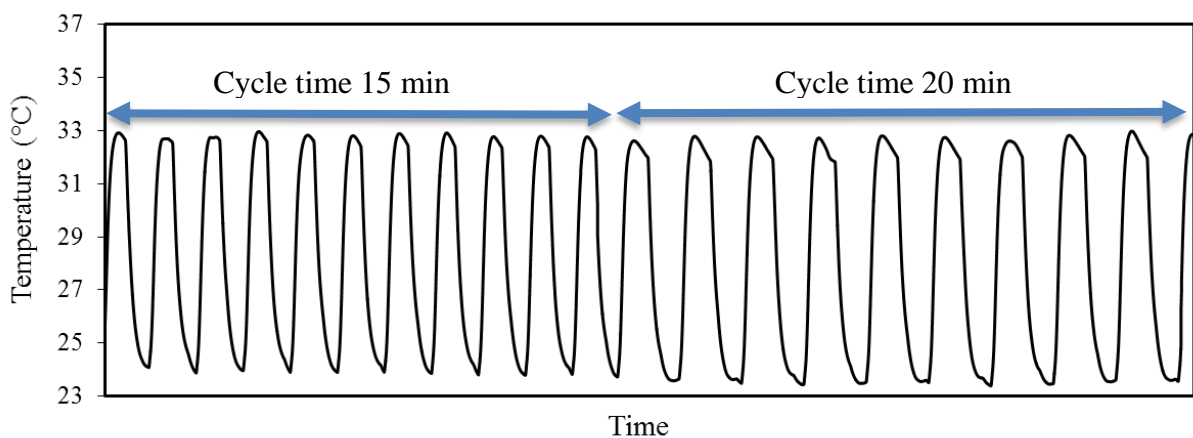
C

Figure 8.28: Effect of cycle time on the cyclic temperature profile; oat hulls – sorption at 101.3 kPa; Regeneration at 3 µHg using a vacuum pump; temperature 29.9 °C; $V_F = 3$ L/min; 100 % humid feed gas; $V_R/V_F = 1$;A: effect of doubling the cycle time; Figure B and C are magnified at different times.

8.4 Application of Biosorbents in Air Drying

In order to investigate the capability of the developed PSA process for drying of an additional gaseous system, air drying experiments were further performed using oat hulls as a model material in the dual-column PSA process operating based on the four-step cycle. Dry air is an essential utility in many industries. According to Statistics Canada, the average annual humidity of air in Saskatchewan is around 61 % RH. As for the conditions of feed gas (air) in this experiment, this average humidity was assumed and the process was designed to operate at atmospheric pressure without further gas compression for drying and with a typical cost-effective building vacuum for the regeneration of the columns. The temperature of gas after solid filtering is reported to be around 26-27 °C. For the experiments, a cylinder of

123

compressed air (laboratory grade 3.5, Praxair, Canada) was used, which was humidified using the humidifier column developed in this work. Its relative humidity was adjusted at ≈ 61 % using a PID controller. The specific experimental conditions are reported in Table 8.2. This experiment was performed right after the dual-column experiments using the same batch of oat hulls that was used in the previous experiments in section 8.3 (after about 150 cycles).

Table 8.2: Feed gas conditions for dual-column experiment with oat hulls – Air drying.

Temperature	$26.9 \pm 0.4\,℃$
Pressure	101.3 kPa
Feed gas flow rate (V$_F$)	4.5 L/min
Feed gas humidity (water vapor mole fraction)	61 % (0.0191 ± 0.0005)
Regeneration gas flow rate (V$_R$)	$\dfrac{V_R}{V_F} = 1$
Vacuum level during regeneration	39 kPa absolute

The results were quite similar to those obtained in the atmospheric experiments illustrated in the previous sections. As can be seen in Figure 8.29 and Figure 8.30, dry product was successfully achieved and the temperature/pressure histories were similar to those achieved in the previous experiments using flax shives and oat hulls for drying nitrogen as the model gas. The operation of the process was stable. Such observation was expected as the biosorbents adsorb negligible amounts of non-polar gases such as nitrogen and oxygen molecules in the air. The major differences of the operation conditions between this experiment and those described in the previous sections of this chapter were the relative humidity of the feed and temperature of the feed gas. The results demonstrated that the dual-column PSA process developed in this work with the biosorbent is also promising in the drying non-polar gases. In future research, the lifetime of the biosorbents and frequency of refilling the columns with fresh biosorbents should be investigated.
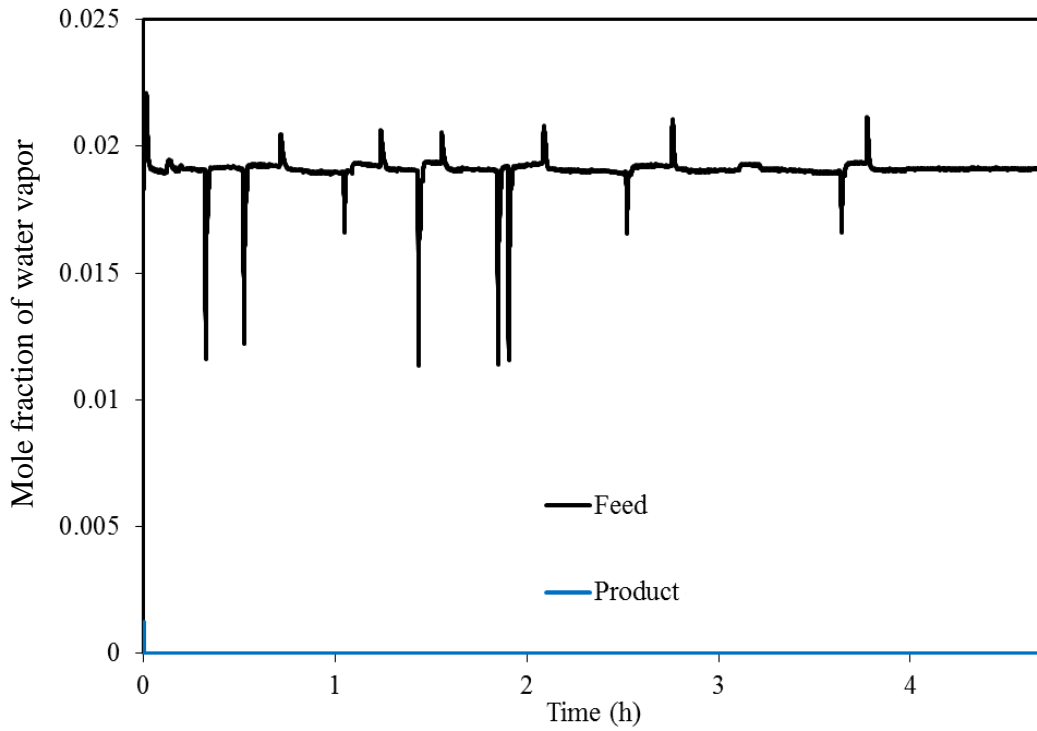
Figure 8.29: Air drying using oat hulls – the composition of product gas in the first 5 hours of the experiment; temperature 26.9 °C; pressure 101.3 kPa; vacuum level 39 kPa; air humidity 61 %;feed flow rate 4.5 L/min; $V_R/V_F = 1$.
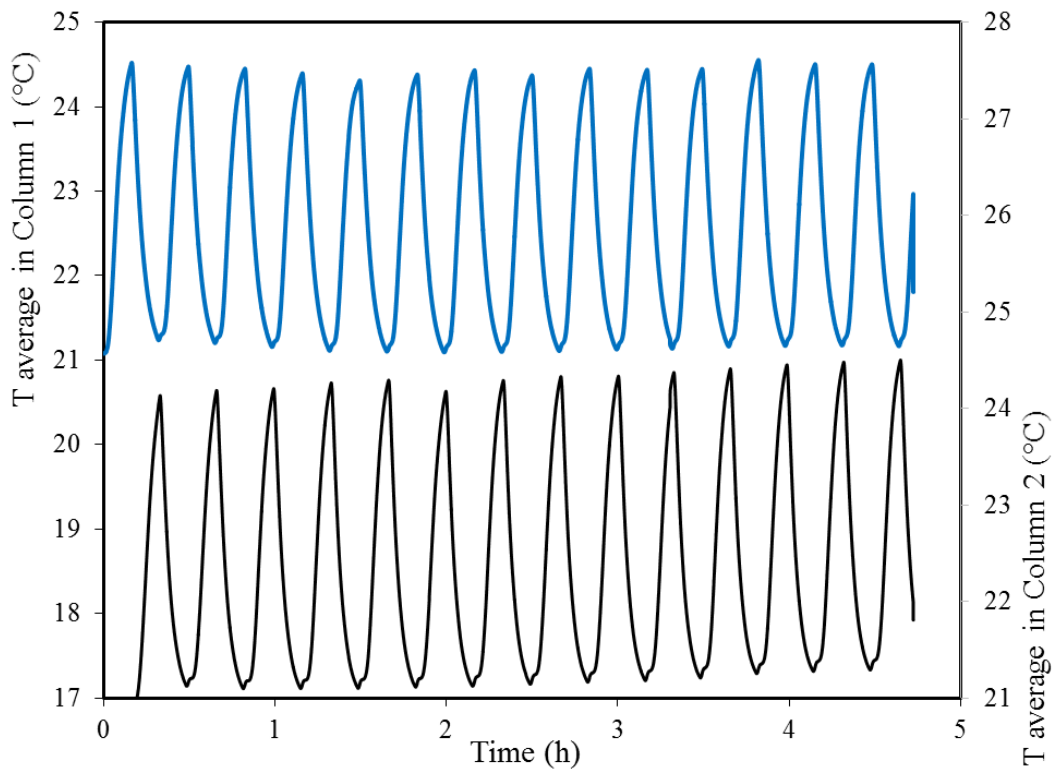
Figure 6.30-A: Air drying using oat hulls – Temperature (A) history of the columns in a few cycles during the experiment;
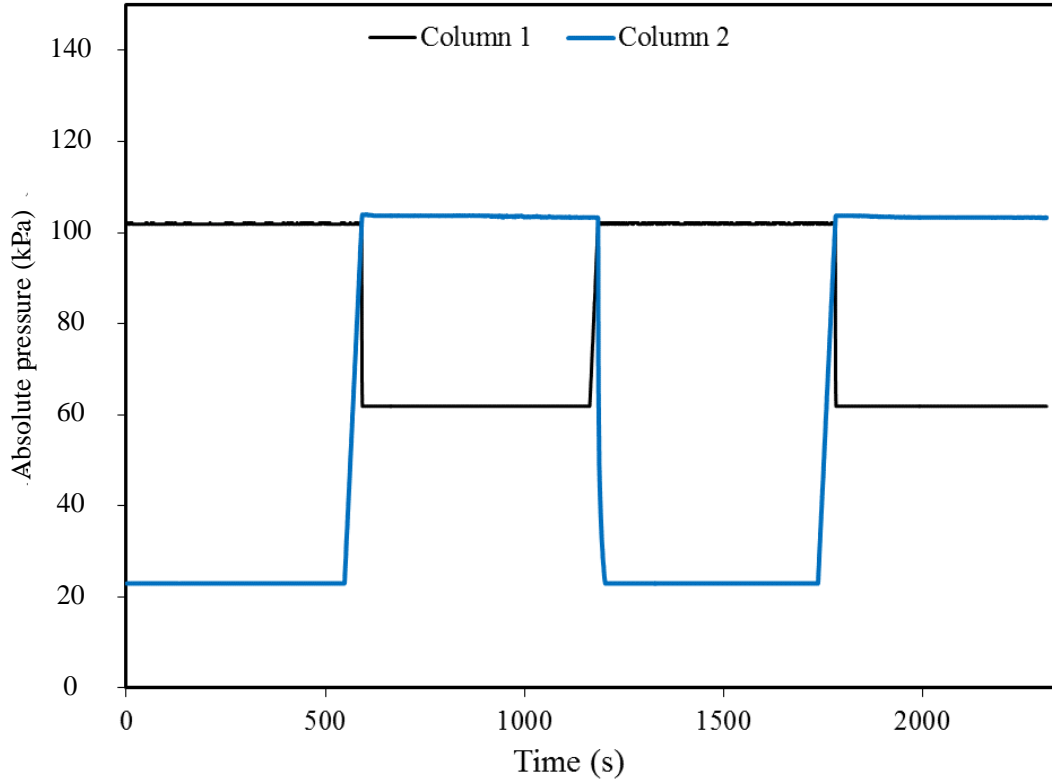
B

Figure 8.30: Air drying using oat hulls – pressure (B) history of the columns in a few cycles during the experiment; temperature 26.9 °C; pressure 101.3 kPa; vacuum level 39 kPa; air humidity 61 %; feed flow rate 4.5 L/min; $V_R/V_F = 1$.

8.5   Chapter Summary

In this chapter, the research objective was to demonstrate the capability of biosorbents for gas dehydration in a cyclic dual-column operation. Both flax shives and oat hulls were used in the experiments. The six-step cycle was used in the experiments at 300 kPa, while the four-step cycle was used in the experiments at atmospheric pressure. A simulated natural gas was used in the experiments where nitrogen gas was the carrier gas. The performance of the system was analyzed based on the product gas and the cyclic temperature/pressure histories of the two columns. All the experiments at 300 kPa and 101.3 kPa were successful and dry product gas was achieved. Flax shives and oat hulls were collectively used in more than 450 cycles each to produce dry gas. The temperature/pressure histories showed a stable oscillating trend throughout the cycle steps without any sign of water accumulation or breakthrough point. The biosorbents were effectively regenerated using a normal building vacuum (39 kPa absolute) and without external heating during the regeneration step. The effects of vacuum level (as low as 3 µHg absolute), regeneration gas to feed gas volumetric ratio (1-1.5), and cycle time (6 – 20 minutes) were investigated as well. The performance of the process at 300 kPa was

superior to that at 101.3 kPa. The results demonstrated increasing performance with increasing regeneration gas to feed gas volumetric ratio and decreasing vacuum level during the regeneration step. A significant achievement was the improved product gas recovery as the process successfully work with a regeneration gas to feed gas volumetric ratio of 1, which was a result of the fast regeneration of biosorbents under vacuum without external heating at temperatures below 40 °C. As for the biosorbents, flax shives and oat hulls have similar compositions and properties, and their dehydration performance was similar in these experiments. In addition, the performance of the dual-column process in air drying using the biosorbents at atmospheric pressure based on the four-step cycle was investigated. The experiment was successful and demonstrated the excellent performance of the process. In summary, the research objective of this chapter was substantiated by abundant data and the potential of the process and the biosorbents for the drying of non-polar gases including natural gas and air in the industry was demonstrated.

Chapter 9.   Life Cycle Assessment of Adsorbent Production Units

In this chapter, a life cycle assessment was performed on the production process of biosorbents from flax shives and that of molecular sieves 3A. The environmental damages and footprint of these two adsorbent manufacturing processes were then analyzed. The results provided some insights on how the environmental damages caused by biosorbents production stand compared to other commercial adsobents.

9.1   Introduction

Over the past decades, a great deal of research has been focused on the development of processes and novel adsorbents for gas dehydration.[5,7,10,11,18,113,116,117] Several high-performance adsorbents were developed from agricultural wastes such as barley straw[21,22,131], oat hulls[10,132], canola meal[6,8,9,24,67,68], and flax shives[66,80,112,132], and their sorption properties were investigated for both wastewater treatment and gas/alcohol dehydration applications. Nonetheless, these studies were limited to lab scale and no pilot-bench scale studies including economic analysis have been performed. An exception is a recent techno-economic study by Kong et al. comparing conventional and stripping gas dehydration processes.[133] They concluded that stripping gas dehydration process had a higher annual net profit; however, they did not present robust data about the capital cost. For instance, they did not report the total amount of TEG required for the process based on the close system volume. Techno-economic analysis is of great importance for engineering applications and process design and has been extensively used and applied to various systems.[7,134-138] The results showed that some processes were not economically feasible even though the experimental results were promising.

In addition to the techno-economic analysis, life cycle assessment (LCA) has been widely used to investigate the life cycle of various adsorbents and catalysts developed for different applications and their impact on the environment.[139-141] Several studies reported on the production of bioethanol and compared the impact of various processes and system parameters on the environmental impact categories.[131,136,140,142] Spatari et al. conducted a LCA to examine the environmental implications of the production and use of ethanol in automobiles in Ontario, Canada.[143] They investigated several scenarios and their results suggest greenhouse gas (GHG) emissions could be 25-35% lower than those in 2010. Nguyen et al. performed a LCA on a similar ethanol production plant in Thailand and investigated the effect of location and biomass feedstock.[142] In another study, Pierobon et al. performed a LCA on the production of biomass-based jet fuel with activated carbon and lignosulfonate as co-products.[144] This study

showed that their alternative jet fuel production from slash piles has a lower impact on local pollution and global warming. Several review papers were published on the production of ethanol and fuels from biomass as a result of its popularity and rapid growth in industry.[139,145] Others investigated environmental impacts of combined power cycle power systems operating based on biomass gasification using LCA.[141]

Limited LCA reports are available on adsorbents used for gas dehydration, especially biomass-derived adsorbents. In this chapter, a life cycle assessment was performed using SimaPro to compare the environmental impact of molecular sieves production (the common adsorbent for gas dehydration) and the biosorbent developed for the new PSA process. This chapter provides some insights on the environmental damages caused by adsorbent production processes.

9.2   Life Cycle Assessment

9.2.1   Assumptions and Methodology

9.2.1.1   Goal and Scope of the Study

SimaPro version 7.2 was used to perform a life cycle assessment (LCA) in this work and both Ecoinvent and USL CI databases were used. The assessment method was Impact 2002+, which is a commonly used method for similar LCA.[146,147] The goal of this LCA was to compare the impacts of two adsorbents used in the natural gas dehydration swing adsorption processes, commercial molecular sieves 3A and the biosorbent based on flax shives, on the environment. The scope of this LCA was from the synthesis of the adsorbents to their packing in the adsorption columns for use. The actual dehydration processes were not included in the scope of the LCA analysis because of detailed information on the TEG system was not available to complete the data inventory of the LCA analysis. The LCA analysis of the dehydration process is an expensive and time consuming project, which could be a separate project alone. The main focus in this work was the development of biosorbent.

9.2.1.2   Functional Units and Data Inventory

Two functional units were considered in this study. Firstly, the functional unit was one ton of the adsorbents to compare their effects on the environment alone. The second functional unit was 10.45 ton/h of natural gas production, which was the capacity of Alberta natural gas plant. The data inventory is shown in Table 9.1. The processes for the production of molecular

sieves and the biosorbent are shown in Figure 9.1. Numerous patents were published on the production of molecular sieves.[59,148-151] The commonly reported synthesis method for the production of molecular sieves 3A was considered in this LCA.

Table 9.1: Data inventory for the LCA; adsorbents production processes; MS: molecular sieves.

Molecular Sieves 3A		The Biosorbent	
Process Inventory	Input data	Process Inventory	Input data
Transportation, Lorry truck (feeds)	Total of 121 km for 920 kg of Al_2O_3 and 48 kg of Kaolin clay	Transportation, Lorry truck (feed)	650 km for 1,430 kg of raw flax shives
MS reactor (Industrial mixing vessel and spheronizer machine, Laksa Inc. ME 1000)	Power = 1,431,000 kJ	Sieving (Zeus industrial sieving machine, FTI-0800)	Power = 15,840 kJ
Drying (kiln rotary dryer)	Power = 323,280 kJ Natural gas = 213 kg Air = 3010 kg	Drying (kiln rotary dryer)	Power = 323,280 kJ Natural gas = 213.2 kg Air = 3010 kg
Heat treatment and activation (Conveyor belt furnace, SECO/Warwick, MBC-18112)	Power = 3,150,000 kJ		
Transportation, Lorry truck (product)	3,186 km		

*The data inventory is based on 1 function unit input.

It was assumed that the molecular sieves are produced in Ontario, Canada and shipped to Alberta (natural gas plant location) because it would be cheaper to supply the required feedstock from the nearby manufacturers in Ontario. Kaolin clay and aluminum oxide were produced by New Directions Aromatics (Mississauga, Ontario) and Caswell Canada (Palmerston, Ontario), respectively. These two chemicals were shipped to the Caledon Laboratory Chemicals molecular sieves production plant in Georgetown (Halton Hills), Ontario. These transportation inputs in SimaPro were considered as heavy truck (Lorry) land transportation. Afterwards, the final molecular sieves product was transported to Alberta by road. Similarly, raw flax shives were transported to Alberta from Saskatoon and the raw material was processed into biosorbent on site in the natural gas plant in Alberta; hence, the only transportation required is the raw material from Saskatoon to Alberta. Ground flax shives were provided by the fiber processing units; therefore, no milling/grinding step is required in the process. Moreover, flax shives are assumed as a waste/byproduct from the agricultural industry and it is not harvested or produced specifically for the biosorbent production. This waste material is typically burnt or used as horse bedding. Only the handling process is

considered in flax shives on their contribution to the environmental impact for this LCA study; however, molecular sieves were produced specifically for this dehydration application and the environmental impacts of feed streams were considered in the LCA.
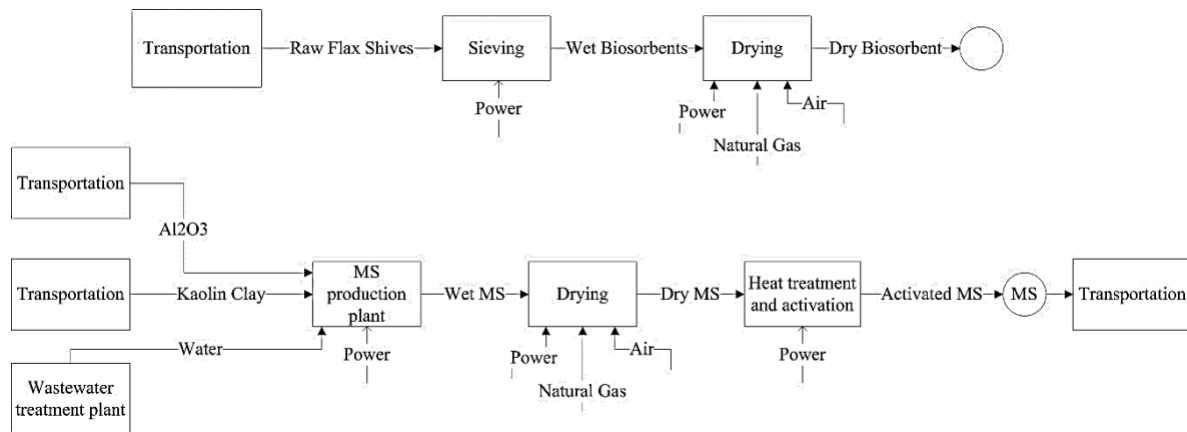
Figure 9.1: Block diagram of adsorbents production systems; MS: molecular sieves.

The power consumption for the industrial machines was estimated using the data provided by the manufacturers such as the capacity, feed rate, and power consumption. The rotary kiln dryer power and natural gas consumptions were estimated using the handbook of industrial drying.[152] Furthermore, aluminum oxide and kaolin clay were imported from the SimaPro Ecoinvent database and all supplies required to produce these chemicals such sodium hydroxide, aluminum hydroxide, and Bauxite as well as the gas emissions and other waste streams were considered in the LCA based on the impact assessment method models.

9.2.1.3 Life Cycle Impact Assessment and Impact Categories

In this LCA, three different indicators, single score, characterization, and damage assessment were used to study and compare the impact of molecular sieves and flax shives biosorbent on the environment. Basically, the substance contributing to an impact category is multiplied by a characterization factor, which expresses the relative contribution of the substance, while the damage assessment indicator, which is a relatively a new step in impact assessment, combines a number of midpoint impact category indicators into four damage categories: human health, ecosystem quality, climate change, and resources (Figure 9.2).[146,147] Human Health is expressed as the number of year life lost and the number of years lived disabled, which are combined as Disability Adjusted Life Years (DALYs). Ecosystem quality is expressed as the loss of species over a certain period of time.[146] The impacts of resources accounted the energy consumed from mineral and non-renewable energy. The LCA impact assessment method combines the inventory and impact calculations into one impact factor

using the IMPACT 2002 standardized weighing factors; therefore, this single score (Pt) serves as an easy starting point to assess two products or processes based on their environmental impacts.[147] The higher the single score, the higher the negative impact on the environment.

Human Health	Ecosystem Quality	Climate Change	Resources
•Carcinogens •non-Carcinogens •Respiratory inorganics •Ionizing radiation •Ozone layer depletion •Respiratory organics	•Terrestrial ecotoxicity •Aquatic ecotoxicity •Terrestrial acid/nutri •Land occupation •Aquatic acidification •Aquatic eutrophication	• Global warming	• Non-renewable energy • Mineral extraction

Figure 9.2: Damage assessment categories based on IMPACT 2002+ method.

9.2.2   Results and Discussions

The single score assessment method simplifies all the environmental impacts into one single parameter using a model and is useful for the illustration of the assessment results to non-experts in LCA. According to the single scores, in all categories, molecular sieve production has a higher impact on the environment and the total score for molecular sieves is 10.85 times larger than that of the biosorbent. Figure 9.3 better illustrates and compares the impact assessment of the two adsorbents. As can be seen, the molecular sieves production has a much larger impact in all categories. Non-renewable energy, global warming, and respiratory inorganics impact categories seem to have the biggest contributions among the other impact categories for both adsorbents. This observation is a result of the consumption of natural gas for power production as well as in the Kiln drying units in both processes. Carbon dioxide (global warming impact category) and SO_x/NO_x (respiratory inorganics impact category) emissions resulted from the production of 1 ton of biosorbent were much lower than those results from the production of 1 ton of molecular sieves.

Figure 9.3: Comparing 1 ton 'biosorbent' with 1 ton 'molecular sieves, 3A'; Method: IMPACT 2002+ V2.06 / IMPACT 2002+ / Single score / Excluding infrastructure processes; Pt: single score point.

The characterized LCA results are shown in Table 9.2 where the numerical values for each impact category are listed. Similarly, the production of molecular sieves has a much higher impact on the environment from all midpoint impact categories.

Table 9.2: Characterized LCA comparison results; functional unit 1 ton.

Impact category	Unit	Biosorbent production	Molecular sieves production
Carcinogens	kg C_2H_3Cl eq	4.2	79.8
Non-carcinogens	kg C_2H_3Cl eq	2.8	228.2
Respiratory inorganics	kg PM2.5 eq	0.34	3.29
Ionizing radiation	Bq C-14 eq	510	18,664
Ozone layer depletion	kg CFC-11 eq	$3.65E^{-05}$	0
Respiratory organics	kg C_2H_4 eq	0.13	1.08
Aquatic ecotoxicity	kg TEG water	20,249	312,976
Terrestrial ecotoxicity	kg TEG soil	12,802	91,454
Terrestrial acid/nutri	kg SO_2 eq	10.7	85.2
Land occupation	m^2 org.arable	0.28	1.79
Aquatic acidification	kg SO_2 eq	1.9	18.8
Aquatic eutrophication	kg PO_4 P-lim	0.03	0.37
Global warming	kg CO_2 eq	308	3,212
Non-renewable energy	MJ primary	4341.68	45,467
Mineral extraction	MJ surplus	0.18	1,321

It is a good practice to use different LCA indicators to validate the results; therefore, damage assessment indicator was also used and the results are shown in Figure 9.4. As can be seen, the damages caused by the production of one ton of the biosorbent are less than 15% of those caused by the molecular sieves production. Therefore, the biosorbent is environmentally friendly.
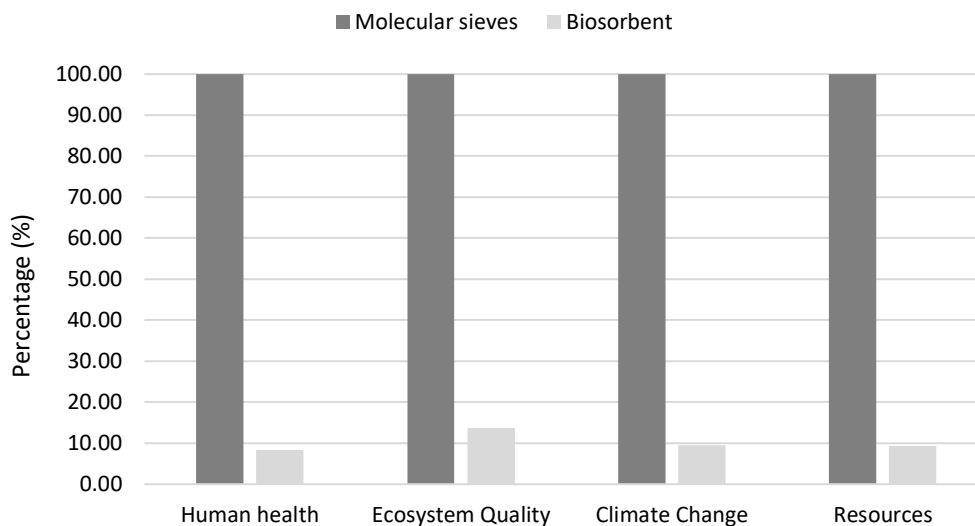
Figure 9.4: Comparing 1 ton 'biosorbent' with 1 ton 'molecular sieves, 3A';Method: IMPACT 2002+ V2.06 / IMPACT 2002+ / Damage Assessment / Excluding infrastructure processes; the percentages of damage categories are relative to molecular sieves that is 100%.

Figure 9.5 compares the contribution of each impact category for both the molecular sieves and the biosorbent based on one functional unit. According to the results for molecular sieves, the transportation, aluminum oxide, and electricity consumption were the main contributors to the environmental damages, while the transportation had the highest contribution to most environmental impacts for the biosorbent production. These findings show that the other processing inputs had insignificant environmental impacts compared to those of molecular sieves. To produce aluminum oxide, Bauxite ores are extracted and chemically and physically treated in several mineral processing units such as crush milling, chemical reactor, filtering, cooing and crystallization, and drying. Electricity, natural gas, water, and several chemicals are used in these unit operations, which resulted in the environmental impacts shown in Figure 9.5 in order to produce aluminum oxide. Biomass is known for its handling and transportation costs and LCA results show that most environmental damages are also caused by the transportation of the biosorbent.
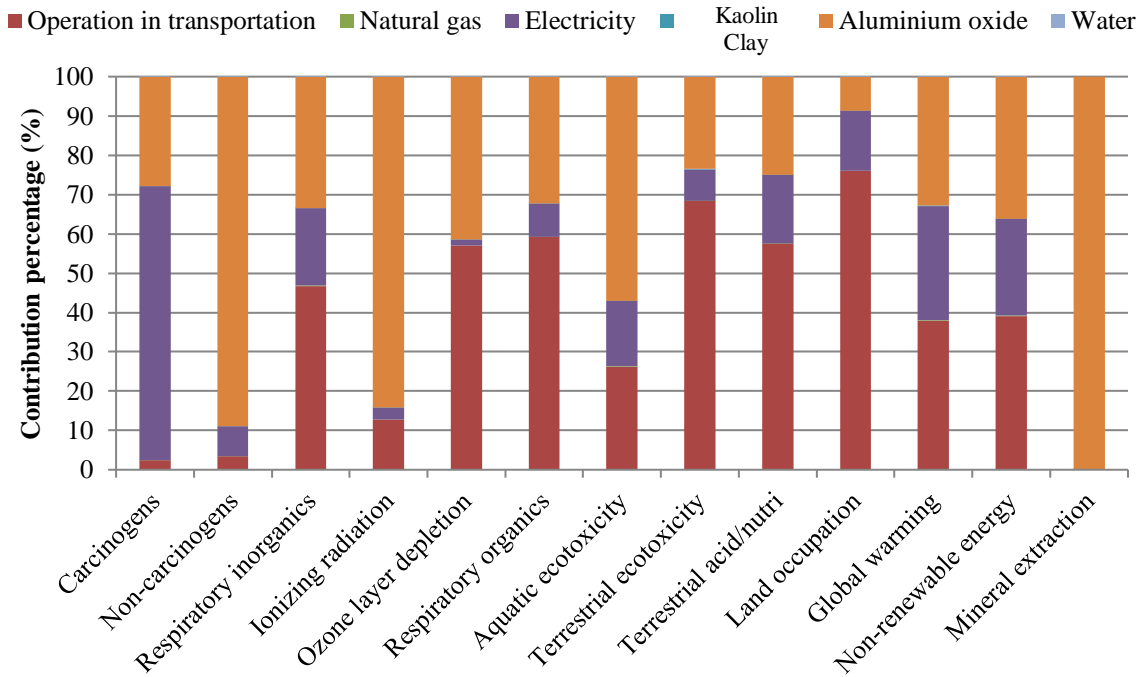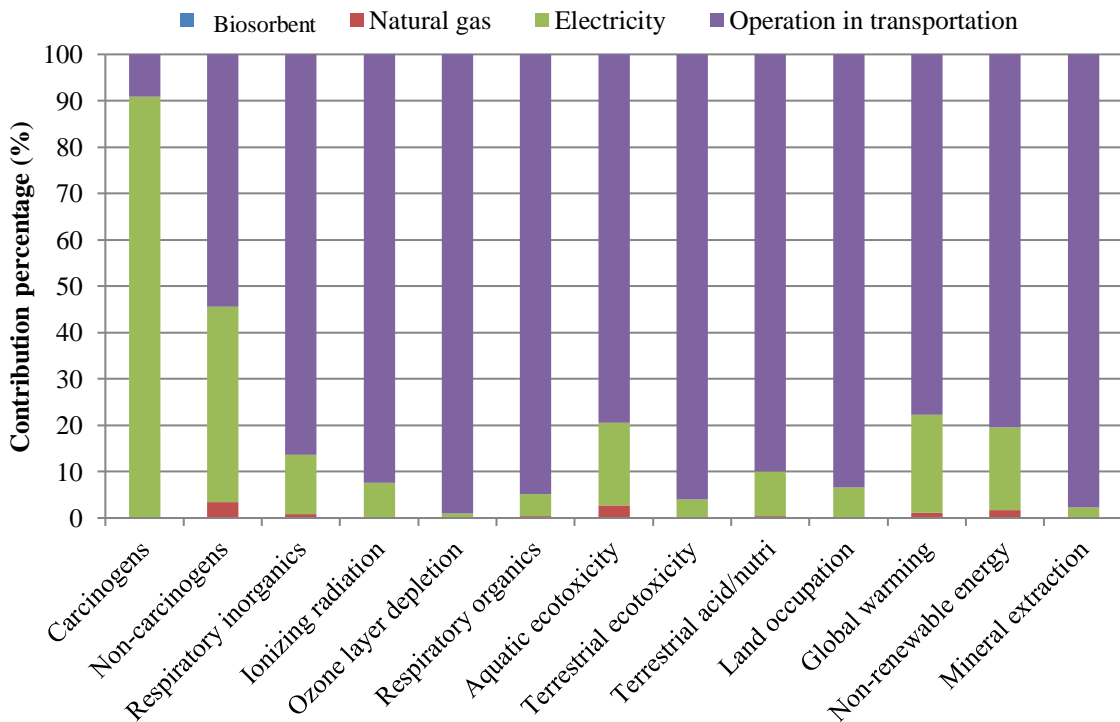
Figure 9.5: Comparing the contributions of processing inputs on the impact categories; Method: IMPACT 2002+ V2.06 / IMPACT 2002+ / Damage assessment / Excluding infrastructure processes; A: molecular sieves; B: the biosorbent.

For a reasonable comparison, however, the total mass of adsorbents required for a specific natural gas plant needs to be considered in the LCA. According to differences in the

packing density of the two materials, 1.67 ton of the biosorbent and 0.72 ton of molecular sieves were required for the PSA units to dehydrate the Alberta natural gas. This difference is because of their packing density. That being said, the single scores based on a functional unit of 1.45 ton/h of humid natural gas were determined (the biosorbent and molecular sieves considering the total mass required are 1.67 and 7.82, respectively). The single point results based on this new functional units are shown in Figure 9.6. It can be seen that the biosorbent production is still more environmentally friendly.
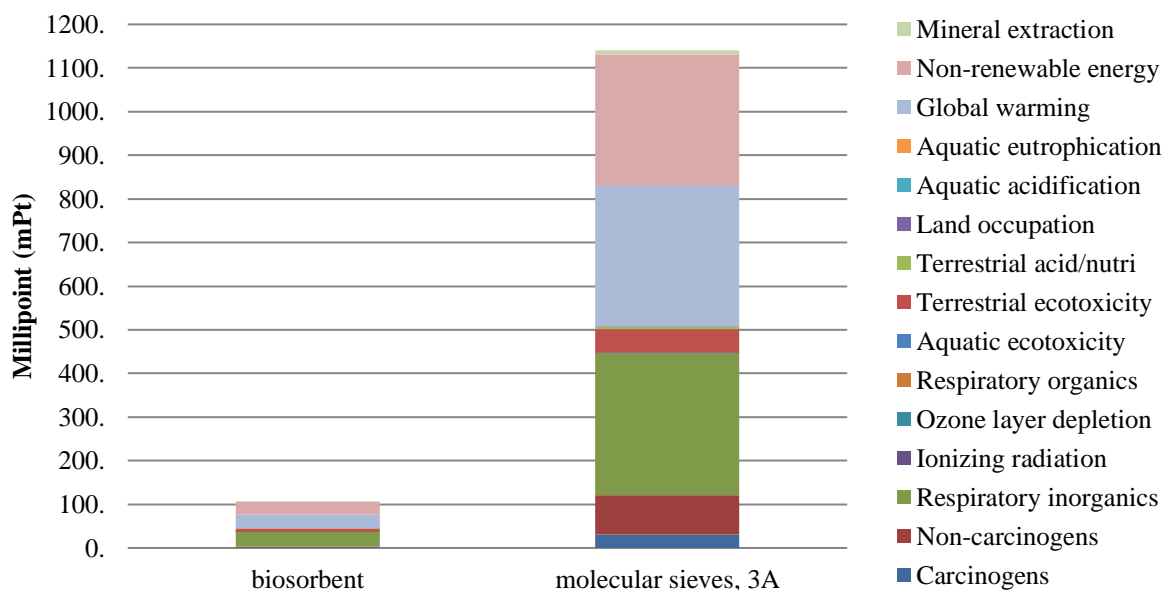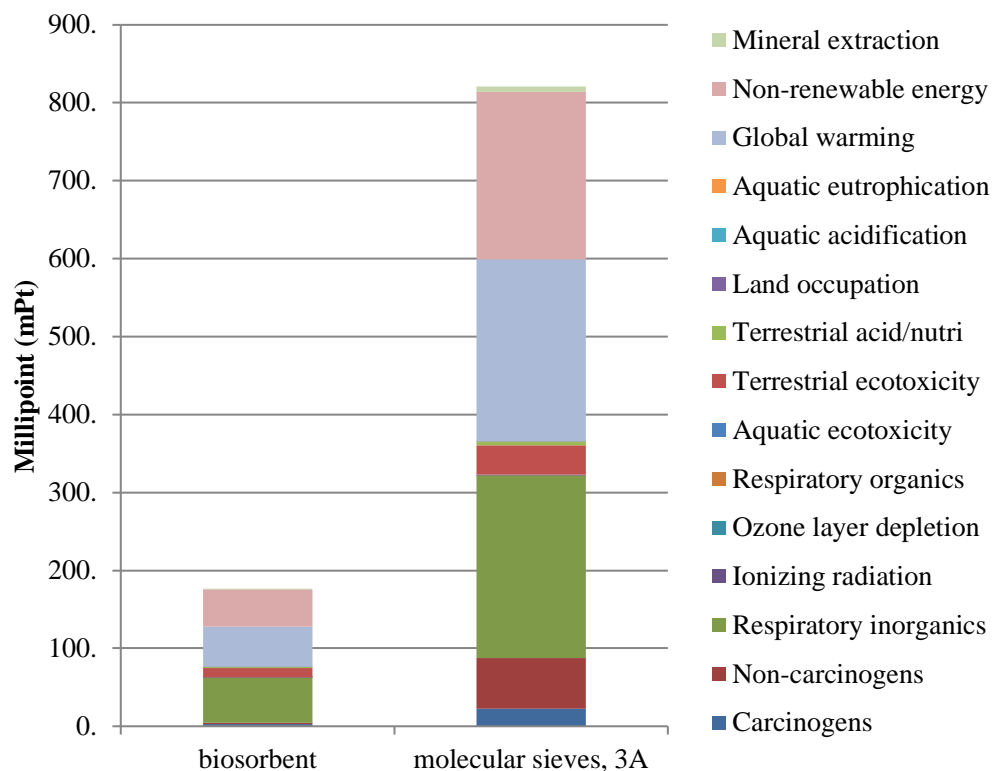

Figure 9.6: Comparing 1.67 ton 'biosorbent' with 0.72 ton 'molecular sieves, 3A'; Method: IMPACT 2002+ V2.06 / IMPACT 2002+ / Single score / Excluding infrastructure processes; mPt: millipoint.

Therefore, based on the LCA results, it can be concluded that the biosorbent production has a much lower impact on the environment. In addition, the process seems economically favorable and has a better public image as a result of the conversion of agricultural wastes into useful materials and creation of a market for agricultural industries.

9.3 Chapter Summary

This chapter was focused on the LCA of the adsorbents used in the process. A LCA was performed to compare the environmental impact of adsorbent production: one ton of molecular sieves 3A (that is commonly used in the TSA process) and one ton of the biosorbent developed from flax shives. The results suggest that the environmental impacts of molecular sieves production were 10.85 times higher than those of the biosorbent based on the single scores. The major impact categories were GHG emissions, non-renewable energy sources, and respiratory inorganics. In other words, both the PSA process and the biosorbent production had much lower negative impacts on the environment. Overall, the PSA process for natural gas dehydration using the biosorbent seems promising in terms of performance and environmental impacts. Industrial collaboration and pilot-scale experiments in future to further develop this process would be very valuable.

Chapter 10. Conclusions, Significant Contributions, and Recommendations

In this research, cost-effective and efficient biosorbents were successfully developed from agricultural residues, flax shives and oat hulls as model materials, for natural gas dehydration in a pressure swing sorption process. This research project conducted a wide scope of investigation covering from the fundamental water sorption characteristics and mechanisms to life cycle assessment. The important properties of the biosorbents (oat hulls and flax shives) were determined and the PSA process was engineered based on these properties. The high water vapor sorption capacity, selectivity, and easy regeneration at fast rates without external heating were the three key properties of the biosorbents that rendered the natural gas dehydration in a PSA process feasible. These three main properties solved the operating issues in the temperature swing adsorption process in regard to high energy requirements and cost. The stability of the biosorbent was investigated given the limited time and resources in laboratory. The flax shives-based biosorbent dehydrated the gas for 450 cycles in the bench-scale dual column system with a stable performance, and no degradation was observed in its properties. The same batch of the biosorbent can be further used. Experiments at room temperature showed that the PSA process can dehydrate nonpolar gases such as air and biogas at atmospheric pressure and room temperature as well, which could be other applications of the process using the biosorbents in industry. To study the effect of biosorbent feedstocks, two different batches of flax shives and oat hulls were analyzed and compared. Their water vapor sorption capacity was different, which may be because of their compositions; however, both batches demonstrated sufficient water vapor sorption capacity, high water vapor selectivity, and high desorption rates at room temperature without external heating. Furthermore, the life cycle assessment suggests that the negative environmental damages caused by the PSA process using the biosorbent were much lower than those of other applied processes in industry. The PSA process for natural gas dehydration seems promising and the author looks forward to pilot studies in future to further investigate this technology.

The water sorption isotherm studies were also performed. The solid-gas equilibrium data was determined in the pressure and temperature ranges of 101.3 – 300 kPa and 24 – 50 °C. Two types of isotherms were observed; only the isotherm at 300 kPa and 24 was non-linear and the rest isotherms were linear. Two isotherm models, Redhead and GAB, were successfully fitted on the non-linear isotherm and the monolayer water sorption capacity, surface affinity of water toward the flax shives, and the excess heat of water sorption based on the GAB were determined. Linear isotherm and F-G isotherm models were well fitted on the

linear isotherms and the Henry constant and the lateral interaction forces among the sorbed water molecules on the surface were determined. Using the Henry constant determined from the linear isotherm modeling results, the standard heat of water sorption was estimated as -24 to -39 kJ/mol, which indicates that water sorption by flax shives was exothermic and the heat is consistent to the enthalpies of hydrogen bonding between water molecules and the hydroxyl, Ph-OH, and carboxyl groups. The collective isotherm data and surface characterization of flax shives suggested that hydrogen bonding with the above-mentioned functional groups was likely the water sorption mechanism. In the case of linear isotherms, water sorption was monolayer, exothermic, and physiosorption in nature, while multilayer water sorption occurred in the case of type II like isotherm where the first layer sorption was likely similar to that of the linear isotherms and the second and subsequent layer water sorption could be water-water interaction with low sorbed-phase density. The biosorbents were almost 100% selective to water vapor and did not sorb other nonpolar gases such as methane, carbon dioxide, and nitrogen because of the polar surface functional groups and macroporous structure of the biosorbents. The commercial adsorbents have a microporous/mesoporous structure and can adsorb small nonpolar molecules such as methane, while the micropore/mesopore volume of the biosorbent was almost zero.

A kinetic model was successfully used to determine the linear driving force mass transfer coefficients, which were compared to those of other applied adsorbents in industry. The LDF mass transfer coefficients at various operating conditions were determined and analyzed. The K_{LDF} values obtained for flax shives in this work ($8.2 \times 10^{-4} - 3.1 \times 10^{-2}$ s^{-1}) are slightly higher than those reported in the literature within the range of $1 \times 10^{-5} - 1 \times 10^{-3}$ s^{-1} depending on the experimental conditions. The effect of operating parameters on the mass transfer coefficient was further determined and discussed. The mass transfer coefficient increased with increasing flow rate, increasing temperature, and decreasing total pressure. The mass transfer coefficient during the water desorption under vacuum was also determined. The results showed that the water desorption rate was much faster than the sorption rate under the tested conditions, which is one of the advantages of biosorbents to commercial adsorbents.

The limitations of this study were safety because high pressure experiments with natural gas (3000 to 6000 kPa) could not be performed with the setup available and the experiments were limited to a pressure of 500 kPa. However, the sorption mechanism and statistical analysis results based on the factorial experimental design suggest that the PSA process is likely to work effectively at higher pressures. Yet, this hypothesis can only be confirmed with solid

experimental data. Another limitation of this study was the lifetime of the biosorbent. Molecular sieves, for example, is replaced with a fresh batch in industry every 6 to 7 years. No data was produced in this research project to predict the lifetime of the biosorbents for such a long period of time. Finally, the modeling work in this project all have their own limitations and assumptions to simplify the solution. Best attempts were made whenever possible to report all the data with uncertainty and to report the systematic and human errors in the experiments. The parameters predicted from the models should be used as initial estimations based on the readers discretion. The author highly recommends to follow up this work by running pilot-scale experiments at high pressures for a longer period of time to determine the lifetime of the biosorbents, and to evaluate the performance of the system at pressures in the range of 3000 to 6000 kPa. It is worth investigating whether the biosorbent can also sorb hydrogen sulfide because it is a polar molecule that is likely to be sorbed by the polar functional groups on the surface of the biosorbent.

Publications, Patents, and Conferences

1. US Patent WO 2019075578A1, International Application (PCT), Published on 25 April, 2019, "DEHYDRATION USING BIOSORBENTS IN MODIFIED PRESSURE SWING ADSORPTION"

2. Ghanbari, S.; Niu, C. H. Characterization of a High-Performance Biosorbent for Natural Gas Dehydration, Energy & Fuels. 2018, 32, 11979.

3. Ghanbari, Saeed, and Catherine H. Niu. "Characteristics of Oat Hull Based Biosorbent for Natural Gas Dehydration in A PSA Process." Journal of Natural Gas Science and Engineering, 61 (2019): 320-332.

4. Ghanbari, S.; Diaz, A. M.; Park, J.; Kang, H.; Niu, C. H. Equilibrium and heat of water vapor adsorption on the surface of natural lignocellulose materials, Chemical Engineering Research and Design. 2019, 147, 18.

5. Ghanbari, S.; Niu, C. H. Equilibria of lignocellulose biosorbents for gas dehydration, Separation and Purification Technology. 2019, 227, 115668.

Conferences:

1) Ghanbari, S & Niu, C. H. Water Adsorption Properties of Flax Shives and Their Potential for Natural Gas Dehydration. Presented at the 67th Canadian chemical engineering conference, Edmonton, AB, 22-25 October, 2017.

2) A. Aghababaei, Niu, C. H., Ghanbari, S, Drying air using oat hull based adsorbent, Presented at the 67th Canadian chemical engineering conference, Edmonton, AB, 22-25 October, 2017.

3) Ghanbari, S & Niu, C. H., Analysis of pressure swing adsorption process using biosorbents for dehydration of natural gas. Presented at the 68th Canadian chemical engineering conference, Toronto, ON, 28-31 October, 2018.

References

(1)	Sun, Q.; Li, H.; Yan, J.; Liu, L.; Yu, Z.; Yu, X. Selection of appropriate biogas upgrading technology-a review of biogas cleaning, upgrading and utilisation, Renewable and Sustainable Energy Reviews. **2015**, *51*, 521.

(2)	Eimer, D. *Gas treating: absorption theory and practice*; John Wiley & Sons, 2014.

(3)	Kidnay, A. J.; Parrish, W. R.; McCartney, D. G. *Fundamentals of natural gas processing*; CRC Press, 2011; Vol. 218.

(4)	Mokhatab, S.; Poe, W. A. *Handbook of natural gas transmission and processing*; Gulf professional publishing, 2012.

(5)	Ruthven, D. M. *Principles of adsorption and adsorption processes*; John Wiley & Sons, 1984.

(6)	Baylak, T.; Kumar, P.; Niu, C. H.; Dalai, A. Ethanol dehydration in a fixed bed using canola meal, Energy & Fuels. **2012**, *26*, 5226.

(7)	Ghanbari, S.; Meda, V.; Conceptual Design and Feasibility Study of a Multi-Feed Integrated Biomass Conversion System, Advances in Agricultural Science. **2018**, *6*, 01.

(8)	Ranjbar, Z.; Tajallipour, M.; Niu, C. H.; Dalai, A. K. Water removal from ethanol vapor by adsorption on canola meal after protein extraction, Industrial & Engineering Chemistry Research. **2013**, *52*, 14429.

(9)	Tajallipour, M.; Niu, C.; Dalai, A. Ethanol Dehydration in a Pressure Swing Adsorption Process Using Canola Meal, Energy & Fuels. **2013**, *27*, 6655.

(10)	Ghanbari, S.; Niu, C. H. Characteristics of Oat Hull Based Biosorbent for Natural Gas Dehydration in A PSA Process, Journal of Natural Gas Science and Engineering. **2018,** 61, 320-332.

(11)	Netusil, M.; Ditl, P. Comparison of three methods for natural gas dehydration, Journal of Natural Gas Chemistry. **2011**, *20*, 471.

(12)	Carter, J.; Wyszynski, M. The pressure swing adsorption drying of compressed air, Chemical Engineering Science. **1983**, *38*, 1093.

(13)	Grande, C. A.; Blom, R. Dual pressure swing adsorption units for gas separation and purification, Industrial & Engineering Chemistry Research. **2012**, *51*, 8695.

(14)   Santos, M. n. P.; Grande, C. A.; Rodrigues, A. r. E. Pressure swing adsorption for biogas upgrading. Effect of recycling streams in pressure swing adsorption design, Industrial & Engineering Chemistry Research. **2010**, *50*, 974.

(15)   Kacem, M.; Pellerano, M.; Delebarre, A. Pressure swing adsorption for CO_2/N_2 and CO_2/CH_4 separation: comparison between activated carbons and zeolites performances, Fuel Processing Technology. **2015**, *138*, 271.

(16)   Babicki, M. L., Keefer, B. G., Gibbs, A. C., IaCava, A. I., & Fitch, F. (2006). *U.S. Patent No. 7,037,358*. Washington, DC: U.S. Patent and Trademark Office.

(17)   Yang, B.; Xu, E. L.; Li, M. Purification of coal mine methane on carbon molecular sieve by vacuum pressure swing adsorption, Separation Science and Technology. **2016**, *51*, 909.

(18)   Ho, M. T.; Allinson, G. W.; Wiley, D. E. Reducing the cost of CO_2 capture from flue gases using pressure swing adsorption, Industrial & Engineering Chemistry Research. **2008**, *47*, 4883.

(19)   Santos, J.; Portugal, A.; Magalhaes, F.; Mendes, A. Simulation and optimization of small oxygen pressure swing adsorption units, Industrial & Engineering Chemistry Research. **2004**, *43*, 8328.

(20)   Sun, N.; Okoye, C.; Niu, C. H.; Wang, H. Adsorption of water and ethanol by biomaterials, International Journal of Green Energy. **2007**, *4*, 623.

(21)   Thevannan, A.; Mungroo, R.; Niu, C. H. Biosorption of nickel with barley straw, Bioresource Technology. **2010**, *101*, 1776.

(22)   Thevannan, A.; Hill, G.; Niu, C. H. Kinetics of nickel biosorption by acid‐washed barley straw, The Canadian Journal of Chemical Engineering. **2011**, *89*, 176.

(23)   Niu, C. H.; Volesky, B. Modeling chromium (VI) biosorption by acid washed crab shells, AIChE journal. **2007**, *53*, 1056.

(24)   Niu, C.; Baylak, T.; Wilson, D.; Zhang, M. Pelletisation of canola meal by extrusion–spheronisation for ethanol dehydration, Biomass and Bioenergy. **2014**, *66*, 116.

(25)   Yan, B.; Niu, C. H. Pre-treating biosorbents for purification of bioethanol from aqueous solution, International Journal of Green Energy. **2017**, *14*, 245.

(26)   Yan, B.; Niu, C. H. Modeling and site energy distribution analysis of levofloxacin sorption by biosorbents, Chemical Engineering Journal. **2017**, *307*, 631.

(27)   Kerry, F. G. *Industrial gas handbook: gas separation and purification*; CRC Press, 2007.

(28)   Karimi, A.; Abdi, M. A. Selective dehydration of high-pressure natural gas using supersonic nozzles, Chemical Engineering and Processing: Process Intensification. **2009**, *48*, 560.

(29)   Netušil, M.; Ditl, P. *Natural Gas Dehydration*; INTECH Open Access Publisher, 2012.

(30)   Clinton, P.; Hubbard, R.; Shah, H. In *proceedings of the laurance reid gas conditioning conference* 2008; Vol. 2008, p 393.

(31)   Gandhidasan, P. Parametric analysis of natural gas dehydration by a triethylene glycol solution, Energy Sources. **2003**, *25*, 189.

(32)   Do, D. D. *Adsorption Analysis: Equilibria and Kinetics: (With CD Containing Computer Matlab Programs)*; World Scientific, 1998.

(33)   Ruthven, D. M.; Farooq, S.; Knaebel, K. S. *Pressure swing adsorption*; VCH publishers New York, 1994; Vol. 480.

(34)   BHADRA, S. J. (2007). *Methane-nitrogen separation by pressure swing adsorption* (Doctoral dissertation).

(35)   Skarstrom, C. W. (1960). *U.S. Patent No. 2,944,627*. Washington, DC: U.S. Patent and Trademark Office.

(36)   Hamed, H. H. (2015). Oxygen separation from air using zeolite type 5A. International Journal of Science and Engineering Research, *6*, 597-602.

(37)   De, M. P. G., & Daniel, D. (1964). *U.S. Patent No. 3,155,468*. Washington, DC: U.S. Patent and Trademark Office.

(38)   Teague, K. G.; Edgar, T. F. Predictive dynamic model of a small pressure swing adsorption air separation unit, Industrial & Engineering Chemistry Research. **1999**, *38*, 3761.

(39)   Sircar, S. (1988). High efficiency separation of methane and carbon dioxide mixtures by adsorption. In *AICHE Symposium Series[AICHE SYMP. SER.].* (No. 72).

(40)   Mitariten, M. New technology improves nitrogen-removal economics, Oil & Gas Journal. **2001**, *99*, 42.

(41)   Seery, M. W. (1999). *U.S. Patent No. 5,938,819*. Washington, DC: U.S. Patent and Trademark Office.

(42)   Taveira, A. P. G., & Mendes, A. M. M. (2008). *U.S. Patent No. 7,442,236*. Washington, DC: U.S. Patent and Trademark Office.

(43)   Das, N. K.; Chaudhuri, H.; Bhandari, R. K.; Ghose, D.; Sen, P.; Sinha, B. Purification of helium from natural gas by pressure swing adsorption, Current Science. **2008**, *95*.

(44)   Pahinkar, D. G.; Garimella, S. A novel temperature swing adsorption process for natural gas purification: Part I, model development, Separation and Purification Technology. **2018**, *203*, 124.

(45)   Pahinkar, D. G.; Garimella, S. A novel temperature swing adsorption process for natural gas purification, Part II: Performance assessment, Separation and Purification Technology. **2018**, *204*, 81.

(46)   Moreira, M. A.; Ribeiro, A. M.; Ferreira, A. F.; Rodrigues, A. E. Cryogenic pressure temperature swing adsorption process for natural gas upgrade, Separation and Purification Technology. **2017**, *173*, 339.

(47)   Augelletti, R.; Conti, M.; Annesini, M. C. Pressure swing adsorption for biogas upgrading. A new process configuration for the separation of biomethane and carbon dioxide, Journal of Cleaner Production. **2017**, *140*, 1390.

(48)   Canevesi, R. L. S.; Andreassen, K. A.; da Silva, E. A.; Borba, C. E.; Grande, C. A. Pressure swing adsorption for biogas upgrading with carbon molecular sieve, Industrial & Engineering Chemistry Research. **2018**.

(49)   Yousef, A. M.; Eldrainy, Y. A.; El-Maghlany, W. M.; Attia, A. Upgrading biogas by a low-temperature CO_2 removal technique, Alexandria Engineering Journal. **2016**, *55*, 1143.

(50)   Bhatt, T. S.; Storti, G.; Rota, R. Detailed simulation of dual-reflux pressure swing adsorption process, Chemical Engineering Science. **2015**, *122*, 34.

(51)   Erden, H.; Ebner, A. D.; Ritter, J. A. Development of a Pressure Swing Adsorption Cycle for Producing High Purity CO_2 from Dilute Feed Streams. Part I: Feasibility Study, Industrial & Engineering Chemistry Research. **2018,** *57*(23), 8011-8022.

(52)   Shi, Y. F.; Liu, X. J. Heat and Mass Transport Characteristics of Pressure Swing Adsorption for the Removal of High-Level Moisture along with CO_2 from Air, Industrial & Engineering Chemistry Research. **2018**, *57*, 6464.

(53)   Kim, Y. J.; Nam, Y. S.; Kang, Y. T. Study on a numerical model and PSA (pressure swing adsorption) process experiment for CH_4/CO_2 separation from biogas, Energy. **2015**, *91*, 732.

(54)   Yang, R.; Doong, S. Gas separation by pressure swing adsorption: A pore‐diffusion model for bulk separation, AIChE Journal. **1985**, *31*, 1829.

(55)   De Falco, M.; Basile, A. *Enriched Methane: The First Step Towards the Hydrogen Economy*; Springer, 2015.

(56)   Gandhidasan, P.; Al-Farayedhi, A. A.; Al-Mubarak, A. A. Dehydration of natural gas using solid desiccants, Energy. **2001**, *26*, 855.

(57)   Tagliabue, M.; Farrusseng, D.; Valencia, S.; Aguado, S.; Ravon, U.; Rizzo, C.; Corma, A.; Mirodatos, C. Natural gas treating by selective adsorption: Material science and chemical engineering interplay, Chemical Engineering Journal. **2009**, *155*, 553.

(58)   Herm, Z. R.; Swisher, J. A.; Smit, B.; Krishna, R.; Long, J. R. Metal− organic frameworks as adsorbents for hydrogen purification and precombustion carbon dioxide capture, Journal of the American Chemical Society. **2011**, *133*, 5664.

(59)   Mertens, M. M., & Engels, B. (2004). *U.S. Patent No. 6,685,905*. Washington, DC: U.S. Patent and Trademark Office.

(60)   Wang, Y.; LeVan, M. D. Adsorption equilibrium of carbon dioxide and water vapor on zeolites 5A and 13X and silica gel: pure components, Journal of Chemical & Engineering Data. **2009**, *54*, 2839.

(61)   Jüntgen, H.; Knoblauch, K.; Harder, K. Carbon molecular sieves: production from coal and application in gas separation, Fuel. **1981**, *60*, 817.

(62)   Balköse, D.; Ulutan, S.; Çakıcıoğlu Özkan, F.; Çelebi, S.; Ülkü, S. Dynamics of water vapor adsorption on humidity-indicating silica gel, Applied Surface Science. **1998**, *134*, 39.

(63)   Breck, D. W., & Sieves, Z. M. (1974). Structure, chemistry and use. *Zeolite Molecular Sieves. Wiley, New York*.

(64)   Karimi, S.; Ghobadian, B.; Omidkhah, M.-R.; Towfighi, J.; Yaraki, M. T. Experimental investigation of bioethanol liquid phase dehydration using natural clinoptilolite, Journal of Advanced Research. **2016**, *7*, 435.

(65)   Rudzinski, W.; Everett, D. H. *Adsorption of gases on heterogeneous surfaces*; Academic Press, 2012.

(66)   Borhan, M. S.; Rahman, S.; Hammer, C. Water absorption capacity of flax and pine horse beddings and gaseous concentrations in bedded stalls, Journal of Equine Veterinary Science. **2014**, *34*, 611.

(67)   Dhabhai, R.; Mahaninia, M.; Niu, C. H.; Dalai, A. K. Drying of nonpolar gas in a pressure swing adsorption process using canola meal biosorbents, Asia‐Pacific Journal of Chemical Engineering. **2018**, *13*.

(68)   Dhabhai, R.; Niu, C. H.; Dalai, A. K. Agricultural byproducts-based biosorbents for purification of bioalcohols: a review, Bioresources and Bioprocessing. **2018**, *5*, 37.

(69)   Jayaprakash, D.; Dhabhai, R.; Niu, C. H.; Dalai, A. K. Selective Water Removal by Sorption from Butanol–Water Vapor Mixtures: Analyses of Key Operating Parameters and Site Energy Distribution, Energy & Fuels. **2017**, *31*, 5193.

(70)   Besser, B.; Tajiri, H. A.; Mikolajczyk, G.; Mollmer, J.; Schumacher, T. C.; Odenbach, S.; Glaser, R.; Kroll, S.; Rezwan, K. Hierarchical Porous Zeolite Structures for Pressure Swing Adsorption Applications, ACS Appl Mater Interfaces. **2016**, *8*, 3277.

(71)   Cavenati, S.; Grande, C. A.; Rodrigues, A. E. Adsorption equilibrium of methane, carbon dioxide, and nitrogen on zeolite 13X at high pressures, Journal of Chemical & Engineering Data. **2004**, *49*, 1095.

(72)   Wang, Y.; LeVan, M. D. Adsorption equilibrium of binary mixtures of carbon dioxide and water vapor on zeolites 5A and 13X, Journal of Chemical & Engineering Data. **2010**, *55*, 3189.

(73)   Mrowiec-Białoń, J.; Jarzebski, A. B.; Pajak, L. Water Vapor Adsorption on the SiO_2- $CaCl_2$ Sol− Gel Composites, Langmuir. **1999**, *15*, 6505.

(74)   Desai, R.; Hussain, M.; Ruthven, D. Adsorption of water vapour on activated alumina. I— ‐ equilibrium behaviour, The Canadian Journal of Chemical Engineering. **1992**, *70*, 699.

(75)   Serbezov, A. Adsorption equilibrium of water vapor on F-200 activated alumina, Journal of Chemical & Engineering Data. **2003**, *48*, 421.

(76)   El-Sharkawy, I. I.; Saha, B. B.; Koyama, S.; Ng, K. C. A study on the kinetics of ethanol-activated carbon fiber: theory and experiments, International Journal of Heat and Mass Transfer. **2006**, *49*, 3104.

(77)   Ferreira, D.; Magalhães, R.; Taveira, P.; Mendes, A. l. Effective adsorption equilibrium isotherms and breakthroughs of water vapor and carbon dioxide on different adsorbents, Industrial & Engineering Chemistry Research. **2011**, *50*, 10201.

(78)   Jadhav, R. A.; Agnihotri, R.; Gupta, H.; Fan, L. S. Mechanism of selenium sorption by activated carbon, The Canadian Journal of Chemical Engineering. **2000**, *78*, 168.

(79)   Jribi, S.; Miyazaki, T.; Saha, B. B.; Pal, A.; Younes, M. M.; Koyama, S.; Maalej, A. Equilibrium and kinetics of CO_2 adsorption onto activated carbon, International Journal of Heat and Mass Transfer. **2017**, *108*, 1941.

(80)   Marshall, W. E.; Wartelle, L. H.; Akin, D. E. Flax shive as a source of activated carbon for metals remediation, Bioresources. **2007**, *2*, 82.

(81)   Saha, B. B.; El-Sharkawy, I. I.; Chakraborty, A.; Koyama, S.; Yoon, S.-H.; Ng, K. C. Adsorption rate of ethanol on activated carbon fiber, Journal of Chemical & Engineering Data. **2006**, *51*, 1587.

(82)   Yao, C.; Tien, C. Approximation of intraparticle mass transfer in adsorption processes-I. Linear systems, Chemical Engineering Science. **1992**, *47*, 457.

(83)   Yao, C.; Tien, C. Approximation of intraparticle mass transfer in adsorption processes—II. Non-linear systems, Chemical Engineering Science. **1992**, *47*, 465.

(84)   Teo, H. W. B.; Chakraborty, A.; Kitagawa, Y.; Kayal, S. Experimental study of isotherms and kinetics for adsorption of water on Aluminium Fumarate, International Journal of Heat and Mass Transfer. **2017**, *114*, 621.

(85)   Liu, Y.; Feist, S. D.; Jones, C. M.; Armstrong, D. R. Isopropyl alcohol dehydration by hot gas pressure swing adsorption: experiments, simulations, and implementation, Industrial & Engineering Chemistry Research. **2014**, *53*, 8599.

(86)   Cheng, D.; Peters, E. F.; Kuipers, J. H. Performance study of heat and mass transfer in an adsorption process by numerical simulation, Chemical Engineering Science. **2017**, *160*, 335.

(87)   Ghasemi, N.; Ghasemi, M.; Moazeni, S.; Ghasemi, P.; Alharbi, N. S.; Gupta, V. K.; Agarwal, S.; Burakova, I. V.; Tkachev, A. G. Zn (II) removal by amino-functionalized magnetic nanoparticles: Kinetics, isotherm, and thermodynamic aspects of adsorption, Journal of Industrial and Engineering Chemistry. **2018**, *62*, 302.

(88)   Fedorov, A.; Viskanta, R. Analysis of transient heat/mass transfer and adsorption/desorption interactions, International Journal of Heat and Mass Transfer. **1999**, *42*, 803.

(89)   Sapienza, A.; Santamaria, S.; Frazzica, A.; Freni, A.; Aristov, Y. I. Dynamic study of adsorbers by a new gravimetric version of the Large Temperature Jump method, Applied Energy. **2014**, *113*, 1244.

(90)   Zhong, Y.; Critoph, R.; Thorpe, R.; Tamainot-Telto, Z. Dynamics of $BaCl_2$–NH_3 adsorption pair, Applied Thermal Engineering. **2009**, *29*, 1180.

(91)   Green, D. W.; Perry, R. H. *Perry's Chemical Engineers' Handbook/edición Don W. Green y Robert H. Perry*, 1973.

(92)   Buranov, A. U.; Mazza, G. Extraction and characterization of hemicelluloses from flax shives by different methods, Carbohydrate Polymers. **2010**, *79*, 17.

(93)   Kataoka, Y.; Kondo, T. FT-IR microscopic analysis of changing cellulose crystalline structure during wood cell wall formation, Macromolecules. **1998**, *31*, 760.

(94)   Tan, B. J.; Klabunde, K. J.; Sherwood, P. M. XPS studies of solvated metal atom dispersed (SMAD) catalysts. Evidence for layered cobalt-manganese particles on alumina and silica, Journal of the American Chemical Society. **1991**, *113*, 855.

(95)   Wallart, X.; Henry de Villeneuve, C.; Allongue, P. Truly quantitative XPS characterization of organic monolayers on silicon: study of alkyl and alkoxy monolayers on H− Si (111), Journal of the American Chemical Society. **2005**, *127*, 7871.

(96)   Crist, B. V. (1999). Handbook of the elements and native oxides. *XPS International Inc., Iowa, USA.*

(97)   Zafeiropoulos, N.; Vickers, P.; Baillie, C.; Watts, J. An experimental investigation of modified and unmodified flax fibres with XPS, ToF-SIMS and ATR-FTIR, Journal of Materials Science. **2003**, *38*, 3903.

(98)   Liu, C.-F.; Ren, J.-L.; Xu, F.; Liu, J.-J.; Sun, J.-X.; Sun, R.-C. Isolation and characterization of cellulose obtained from ultrasonic irradiated sugarcane bagasse, Journal of Agricultural and Food Chemistry. **2006**, *54*, 5742.

(99)   Sgriccia, N.; Hawley, M.; Misra, M. Characterization of natural fiber surfaces and natural fiber composites, Composites Part A: Applied Science and Manufacturing. **2008**, *39*, 1632.

(100)   Khan, M. A.; Drzal, L. T. Characterization of 2-hydroxyethyl methacrylate (HEMA)-treated jute surface cured by UV radiation, Journal of Adhesion Science and Technology. **2004**, *18*, 381.

(101)   Freire, C. S.; Silvestre, A. J.; Neto, C. P.; Gandini, A.; Fardim, P.; Holmbom, B. Surface characterization by XPS, contact angle measurements and ToF-SIMS of cellulose fibers partially esterified with fatty acids, Journal of Colloid and Interface science. **2006**, *301*, 205.

(102)   Lü, Y.; Doong, S.-J.; Bülow, M. Pressure-swing adsorption using layered adsorbent beds with different adsorption properties: I—results of process simulation, Adsorption. **2003**, *9*, 337.

(103)   Newns, A. The sorption and desorption kinetics of water in a regenerated cellulose, Transactions of the Faraday Society. **1956**, *52*, 1533.

(104)   Olsson, A. M., & Salmén, L. (2004). The softening behavior of hemicelluloses related to moisture; ACS Publications (book).

(105)   Bettelheim, F. A.; Volman, D. H. Pectic substances—water. II. Thermodynamics of water vapor sorption, Journal of Polymer Science. **1957**, *24*, 445.

(106)   Chang, H.; Yuan, X.-G.; Tian, H.; Zeng, A.-W. Experimental study on the adsorption of water and ethanol by cornmeal for ethanol dehydration, Industrial & Engineering Chemistry Research. **2006**, *45*, 3916.

(107)   Ladisch, M. R.; Voloch, M.; Hong, J.; Bienkowski, P.; Tsao, G. T. Cornmeal adsorber for dehydrating ethanol vapors, Industrial & Engineering Chemistry Process Design and Development. **1984**, *23*, 437.

(108)   Ghanbari, S.; Niu, C. H. Equilibria of lignocellulose biosorbents for gas dehydration, Separation and Purification Technology. **2019**, *227*, 115668.

(109)   Huang, Q.; Niu, C. H.; Dalai, A. K. Production of anhydrous biobutanol using a biosorbent developed from oat hulls, Chemical Engineering Journal. **2019**, *356*, 830.

(110)   Hellman, N. a.; Boesch, T.; Melvin, E. Starch granule swelling in water vapor sorption, Journal of the American Chemical Society. **1952**, *74*, 348.

(111)   Okada, K.; Nakanome, M.; Kameshima, Y.; Isobe, T.; Nakajima, A. Water vapor adsorption of CaCl2-impregnated activated carbon, Materials Research Bulletin. **2010**, *45*, 1549.

(112)   Rentsen, B. Characterization of flax shives and factors affecting the quality of fuel pellets from flax shives Rentsen, B. (2010). *Characterization of flax shives and factors affecting the quality of fuel pellets from flax shives* (Doctoral dissertation, University of Saskatchewan), **2010**.

(113)   Serbezov, A. Effect of the process parameters on the length of the mass transfer zone during product withdrawal in pressure swing adsorption cycles, Chemical Engineering Science. **2001**, *56*, 4673.

(114)   Neufeld, R. D.; Thodos, G. Removal of orthophosphates from aqueous solutions with activated alumina, Environmental Science & Technology. **1969**, *3*, 661.

(115)   Rimpel Jr, A. E.; Camp, D. T.; Kostecki, J. A.; Canjar, L. N. Kinetics of physical adsorption of propane from helium on fixed beds of activated alumina, AIChE Journal. **1968**, *14*, 19.

(116)   Liu, Z.; Green, W. H. Experimental investigation of sorbent for warm CO_2 capture by pressure swing adsorption, Industrial & Engineering Chemistry Research. **2013**, *52*, 9665.

(117)   Yin, C.; Sun, W.; Yang, H.; Zhang, D. Optimization of three-bed VPSA system for biogas upgrading, Chemical Engineering Science. **2015**, *135*, 100.

(118)   Andrade P, R. D.; Lemus M, R.; Pérez C, C. E. Models of sorption isotherms for food: uses and limitations, Vitae. **2011**, *18*, 325.

(119) Markovitch, O.; Agmon, N. Structure and energetics of the hydronium hydration shells, The Journal of Physical Chemistry A. **2007**, *111*, 2253.

(120) Steiner, T. The hydrogen bond in the solid state, Angewandte Chemie International Edition. **2002**, *41*, 48.

(121) Olsson, A.-M.; Salmén, L. The association of water to cellulose and hemicellulose in paper examined by FTIR spectroscopy, Carbohydrate research. **2004**, *339*, 813.

(122) Yan, T.; Li, T.; Xu, J.; Wang, R. Water sorption properties, diffusion and kinetics of zeolite NaX modified by ion-exchange and salt impregnation, International Journal of Heat and Mass Transfer. **2019**, *139*, 990.

(123) Bird, R. B.; Lightfoot, E. N.; Stewart, W. E. *Transport Phenomena*; Wiley, 2002.

(124) Sultan, M.; El-Sharkawy, I. I.; Miyazaki, T.; Saha, B. B.; Koyama, S.; Maruyama, T.; Maeda, S.; Nakamura, T. Water vapor sorption kinetics of polymer based sorbents: Theory and experiments, Applied Thermal Engineering. **2016**, *106*, 192.

(125) Chang, H.; Yuan, X.-G.; Tian, H.; Zeng, A.-W. Experiment and prediction of breakthrough curves for packed bed adsorption of water vapor on cornmeal, Chemical Engineering and Processing: Process Intensification. **2006**, *45*, 747.

(126) Plaza, M. G.; Durán, I. s.; Querejeta, N.; Rubiera, F.; Pevida, C. Experimental and simulation study of adsorption in postcombustion conditions using a microporous biochar. H_2O, CO_2, and N_2 adsorption, Industrial & Engineering Chemistry Research. **2016**, *55*, 6854.

(127) Charrière, D.; Behra, P. Water sorption on coals, Journal Of Colloid and Interface Science. **2010**, *344*, 460.

(128) Ostrovskii, N.; Chumakova, N.; Bukhavtsova, N.; Vernikovskaya, N.; Aristov, Y. I. Modeling of the limiting step of water sorption by composite sorbents of the "calcium chloride in porous matrix" type, Theoretical Foundations of Chemical Engineering. **2007**, *41*, 83.

(129) Zheng, X.; Ge, T.; Wang, R.; Hu, L. Performance study of composite silica gels with different pore sizes and different impregnating hygroscopic salts, Chemical Engineering Science. **2014**, *120*, 1.

(130) Simo, M.; Sivashanmugam, S.; Brown, C. J.; Hlavacek, V. Adsorption/desorption of water and ethanol on 3A zeolite in near-adiabatic fixed bed, Industrial & Engineering Chemistry Research. **2009**, *48*, 9247.

(131) Gabrielle, B.; Gagnaire, N. Life-cycle assessment of straw use in bio-ethanol production: a case study based on biophysical modelling, Biomass and Bioenergy. **2008**, *32*, 431.

(132) Ghanbari, S.; Diaz, A. M.; Park, J.; Kang, H.; Niu, C. H. Equilibrium and heat of water vapor adsorption on the surface of natural lignocellulose materials, Chemical Engineering Research and Design. **2019**, *147*, 18.

(133) Kong, Z. Y.; Mahmoud, A.; Liu, S.; Sunarso, J. Development of a techno‑economic framework for natural gas dehydration via absorption using Tri‑Ethylene Glycol: a comparative study on conventional and stripping gas dehydration processes, Journal of Chemical Technology & Biotechnology. **2019**, *94*, 955.

(134) da Silva, A. R. G.; Errico, M.; Rong, B.-G. Techno-economic analysis of organosolv pretreatment process from lignocellulosic biomass, Clean Technologies and Environmental Policy. **2018**, *20*, 1401.

(135) Rao, M.; Fernandes, A.; Pronk, P.; Aravind, P. Design, modelling and techno-economic analysis of a solid oxide fuel cell-gas turbine system with CO_2 capture fueled by gases from steel industry, Applied Thermal Engineering. **2019**, *148*, 1258.

(136) Sahoo, K.; Bilek, E.; Bergman, R.; Mani, S. Techno-economic analysis of producing solid biofuels and biochar from forest residues using portable systems, Applied Energy. **2019**, *235*, 578.

(137) Yang, S.; Li, B.; Zheng, J.; Kankala, R. K. Biomass-to-Methanol by dual-stage entrained flow gasification: Design and techno-economic analysis based on system modeling, Journal of Cleaner Production. **2018**, *205*, 364.

(138) Zhang, X.; Li, H.; Liu, L.; Bai, C.; Wang, S.; Zeng, J.; Liu, X.; Li, N.; Zhang, G. Thermodynamic and economic analysis of biomass partial gasification process, Applied Thermal Engineering. **2018**, *129*, 410.

(139) Eriksson, O.; Finnveden, G.; Ekvall, T.; Björklund, A. Life cycle assessment of fuels for district heating: A comparison of waste incineration, biomass-and natural gas combustion, Energy Policy. **2007**, *35*, 1346.

(140) Fu, G. Z.; Chan, A. W.; Minns, D. E. Life cycle assessment of bio-ethanol derived from cellulose, The International Journal of Life Cycle Assessment. **2003**, *8*, 137.

(141) Mann, M. K.; Spath, P. L. *Life cycle assessment of a biomass gasification combined-cycle power system*, National Renewable Energy Lab., Golden, CO (US), 1997.

(142)   Nguyen, T. L. T.; Gheewala, S. H. Life cycle assessment of fuel ethanol from cane molasses in Thailand, The International Journal of Life Cycle Assessment. **2008**, *13*, 301.

(143)   Spatari, S.; Zhang, Y.; MacLean, H. L. Life cycle assessment of switchgrass- and corn stover-derived ethanol-fueled automobiles, Environmental Science & Technology. **2005**, *39*, 9750.

(144)   Pierobon, F.; Eastin, I. L.; Ganguly, I. Life cycle assessment of residual lignocellulosic biomass-based jet fuel with activated carbon and lignosulfonate as co-products, Biotechnology for Biofuels. **2018**, *11*, 139.

(145)   Singh, A.; Pant, D.; Korres, N. E.; Nizami, A. S.; Prasad, S.; Murphy, J. D. Key issues in life cycle assessment of ethanol production from lignocellulosic biomass: Challenges and perspectives, Bioresour Technology, **2010**, *101*, 5003.

(146)   Jolliet, O.; Margni, M.; Charles, R.; Humbert, S.; Payet, J.; Rebitzer, G.; Rosenbaum, R. IMPACT 2002+: a new life cycle impact assessment methodology, The International Journal of Life Cycle Assessment. **2003**, *8*, 324.

(147)   Frischknecht, R.; Jungbluth, N.; Althaus, H.-J.; Hischier, R.; Doka, G.; Bauer, C.; Dones, R.; Nemecek, T.; Hellweg, S.; Humbert, S. *Implementation of life cycle impact assessment methods. Data v2. 0 (2007). Ecoinvent report No. 3*, Ecoinvent Centre, 2007.

(148)   Ballman, A. A., Bierlein, J. D., Ferretti, A., Gier, T. E., & Morris, P. A. (1992). *U.S. Patent No. 5,084,206*. Washington, DC: U.S. Patent and Trademark Office.

(149)   Mertens, M. M. W.; Mortier, W. J.; Janssen, M. J.; Van Oorschot, C. M. W.; Verduijn, J. P.; 2005; Washington, DC: U.S. Patent and Trademark Office.

(150)   Pfenninger, A., Odolo-Hitz, S., Weston, K., Kleeb, B., & Jaussaud, D. (2005). *U.S. Patent Application No. 10/939,751*.

(151)   Mertens, M. M. W., Mortier, W. J., Janssen, M. J., Van Oorschot, C. M. W., & Verduijn, J. P. (2005). *U.S. Patent No. 6,974,889*. Washington, DC: U.S. Patent and Trademark Office.

(152)   Mujumdar, A. S. *Handbook of industrial drying*; CRC press, 2006.

Appendices

A1. Water Transport Video

A video showing the water transport in flax shives that was recorded using fluorescence microscopy. Video Link: https://doi.org/10.1016/j.cherd.2019.04.019

A2: The Bench-Scale Pressure Swing Sorption System Built for Gas Dehydration

Figure A.1: Picture of the dual-column PSA setup.

A2.1 Six-step PSA process

The six-step process is described in the following table.

Table A.7: P&ID of the six-step PSA process.

Step 1

Step 2

Step 3

Step 4

Step 5

Step 6
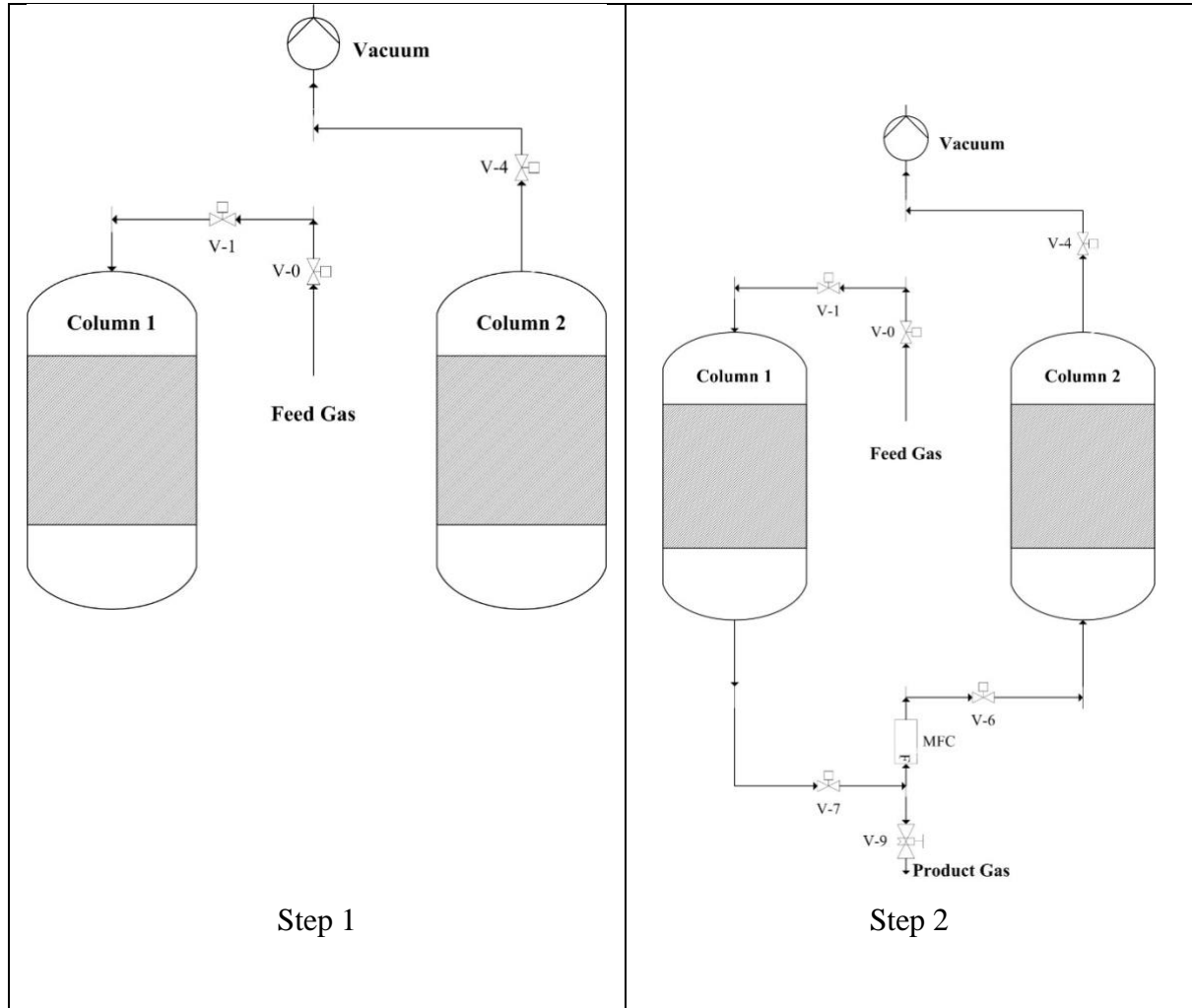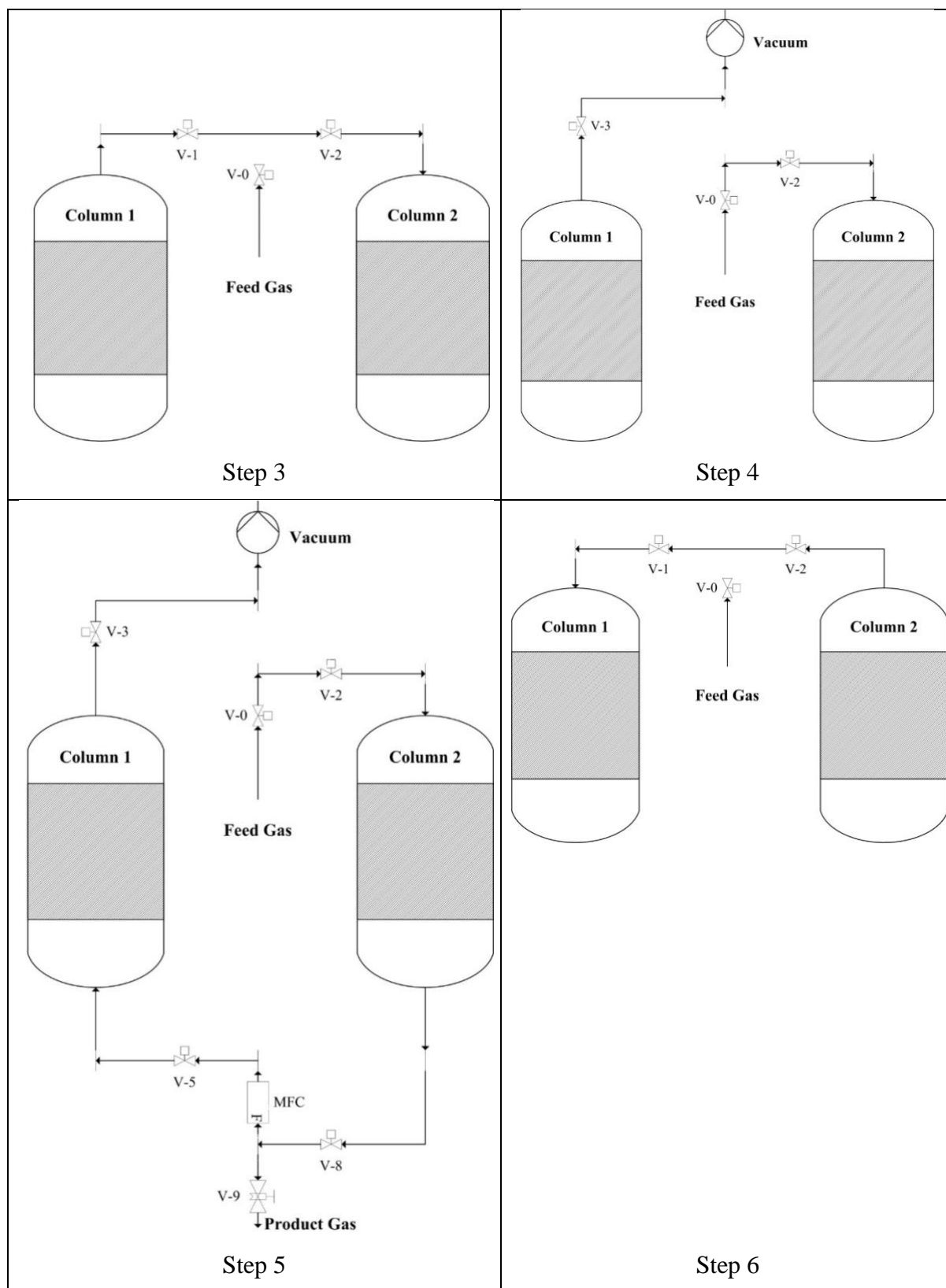
To determine the desorption rate at full bed saturation, the sorption experiment was operated continuously till bed saturation followed by ten minutes of regeneration under vacuum; afterwards, the sorption continued again until the bed was fully saturated. This

experiment was done at 300 kPa, 24 °C, and total flow rate of 4 L/min. The water vapor history in the effluent is plotted in Figure A.2. The mass balance calculations revealed that 8.23 g of water was sorbed during the first 4.6 hours of sorption, while 2.18 g of water was desorbed in the 10 minutes, which results in a desorption rate of 0.22 g/min. It is worthy to mention that the biosorbent was regenerated at 24 °C, while all commercial adsorbents such as molecular sieves were regenerated at temperatures above 200 °C. Moreover, the vacuum used for the regeneration is not expensive (not very low vacuum). These results show the excellent performance of the biosorbent in the PSA process. The biosorbent has not only high selectivity, but also suitable regeneration properties.
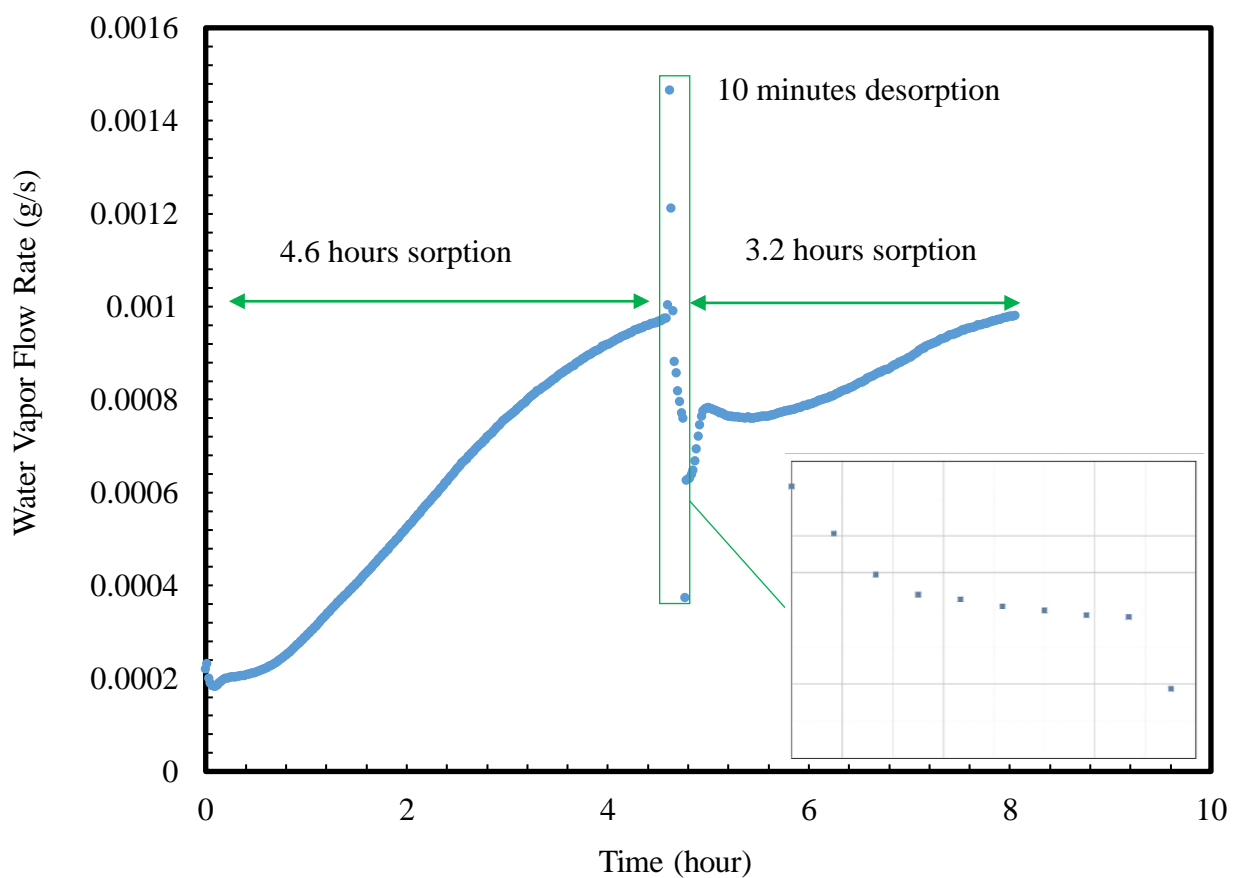
Figure A.2: Sorption – Desorption experiments in 10 minutes cycle time; water vapor history in the effluent.

A3. Atmospheric Dual-Column PSA Experiments by Flax Shives

Some additional figures are presented in this section. Detailed analysis of the temperature history indicates that the columns were partially regenerated during the atmospheric pressure operation as no temperature raise was seen during the regeneration step similar to what was seen in high pressure experiments; however, the process still reached a

157

steady-state condition and could run for more repeated cycles. Similar to other industrial PSA operations, the adsorbent beds are partially saturated and regenerated in every cycle.[33]
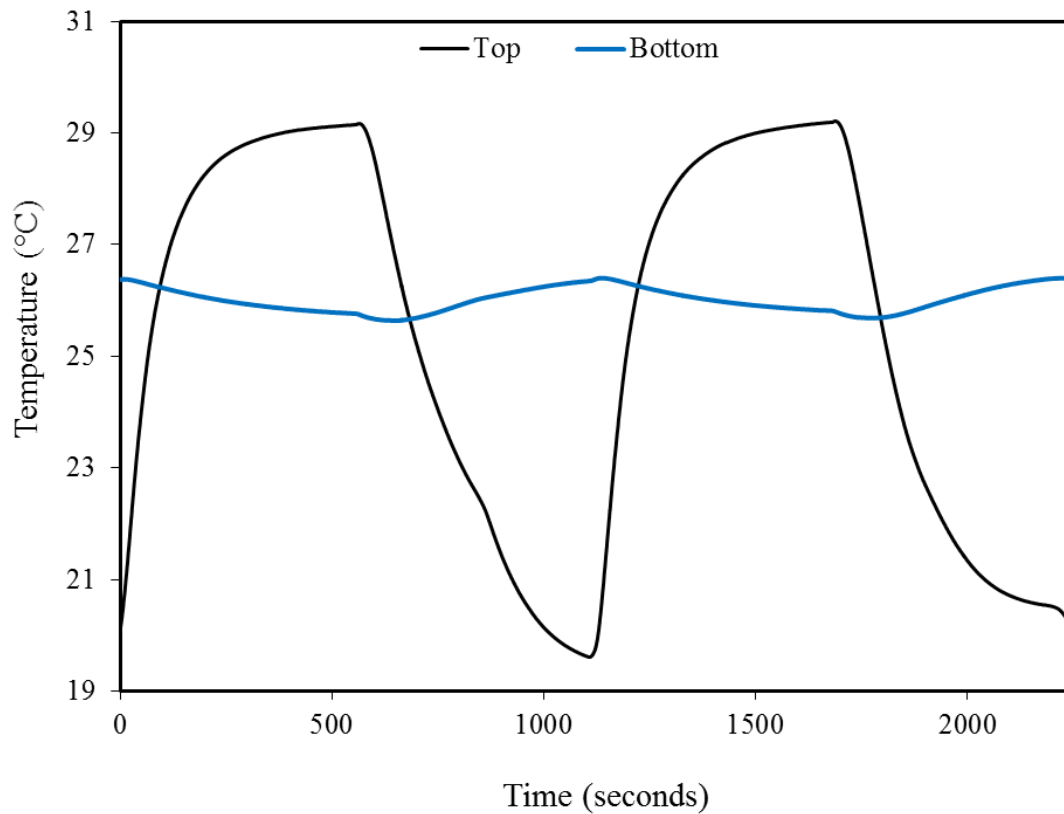
Figure A.3: Temperature history of the sorption column throughout the experiment using flax shives –temperature 29.4 °C; pressure 101.3 kPa; vacuum 39 kPa; V_F 3 L/min; 100 % humid feed gas.

Figure A.4 also shows that the temperature almost reached to a constant level during the regeneration step and then sharply increased once the column was switched from the regeneration step to the sorption step (see Figure A.3).
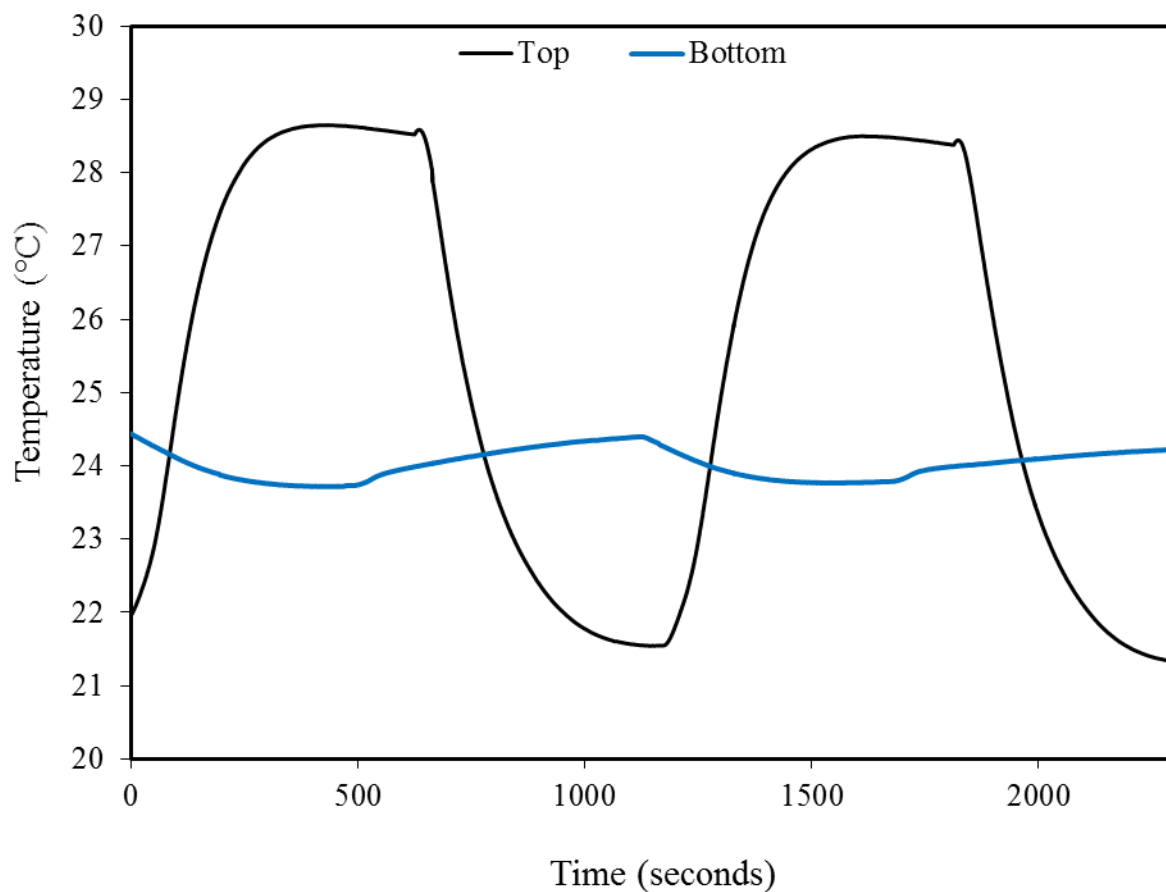
Figure A.4: Temperature history of the column - Water vapor history throughout the experiment using flax shives –temperature 29.4 °C; pressure 101.3 kPa; V_F 3 L/min; 100 % humid feed gas; Regeneration at 3 µHg using a vacuum pump.

A4. Statistical Analysis of Water Sorption Capacity Data by Oat Hulls

*Table A.8: Statistical analysis of the full factorial experimental design –oat hulls (* signifies interactions among factors)*

Tests of Between-Subjects Effects

Dependent Variable: Sorption capacity (g/g)

Factor	F test	Significance level	Partial Estimated Squared
T	5.570	0.02	0.85
P	9.039	0.02	0.90
C	4.698	0.03	0.82
T * P	2.287	0.04	0.69
T * C	1.813	0.04	0.65
P * C	2.380	0.04	0.70

A5. Additional Characterization Results of Oat Hulls
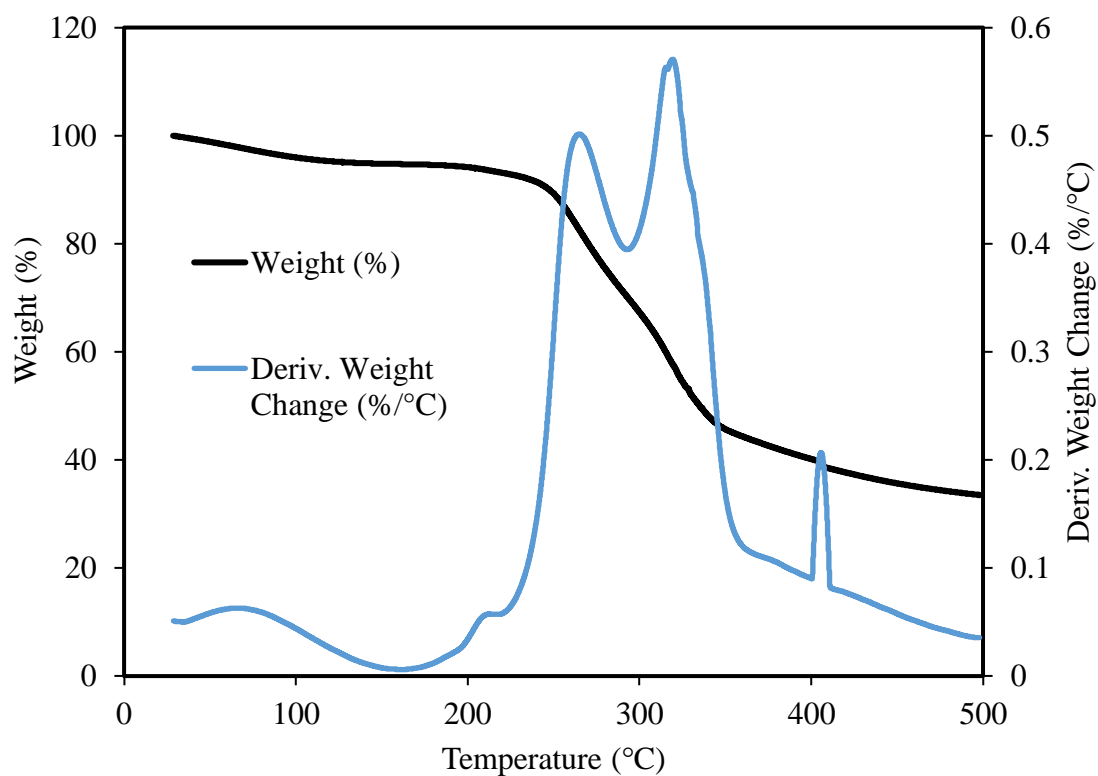
Figure A.5: TGA results of oat hulls.
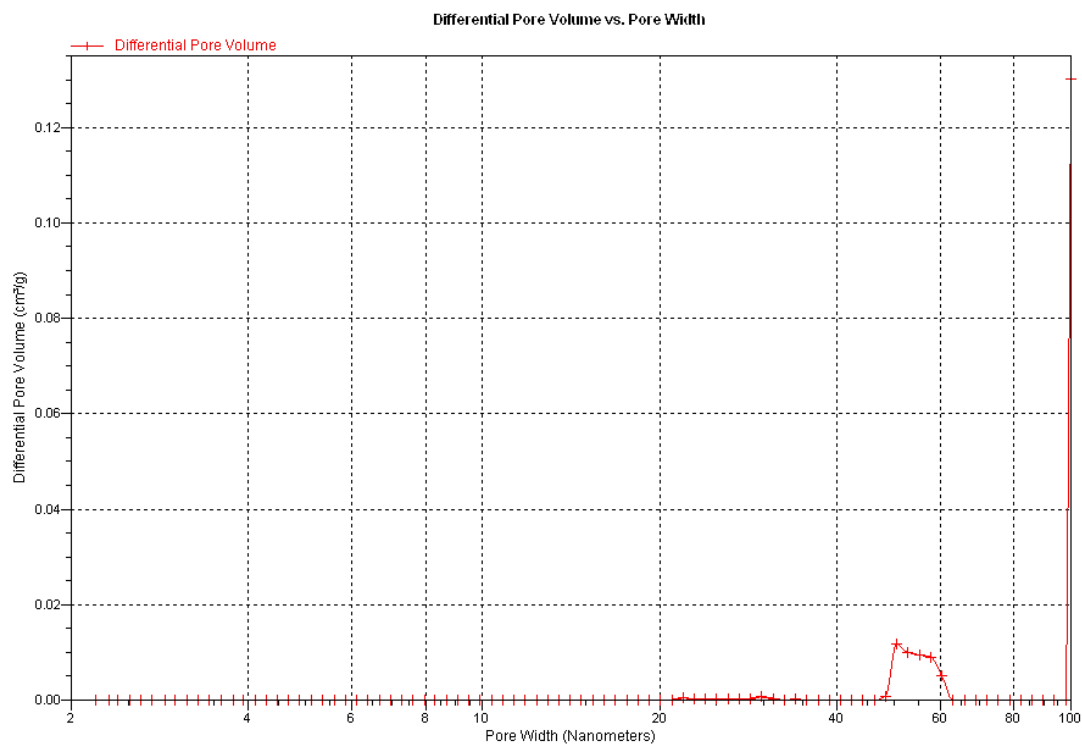
Figure A.6: Pore size distribution of oat hulls based on incremental pore volume obtained from DFT; average pore diameter around 55 nm.
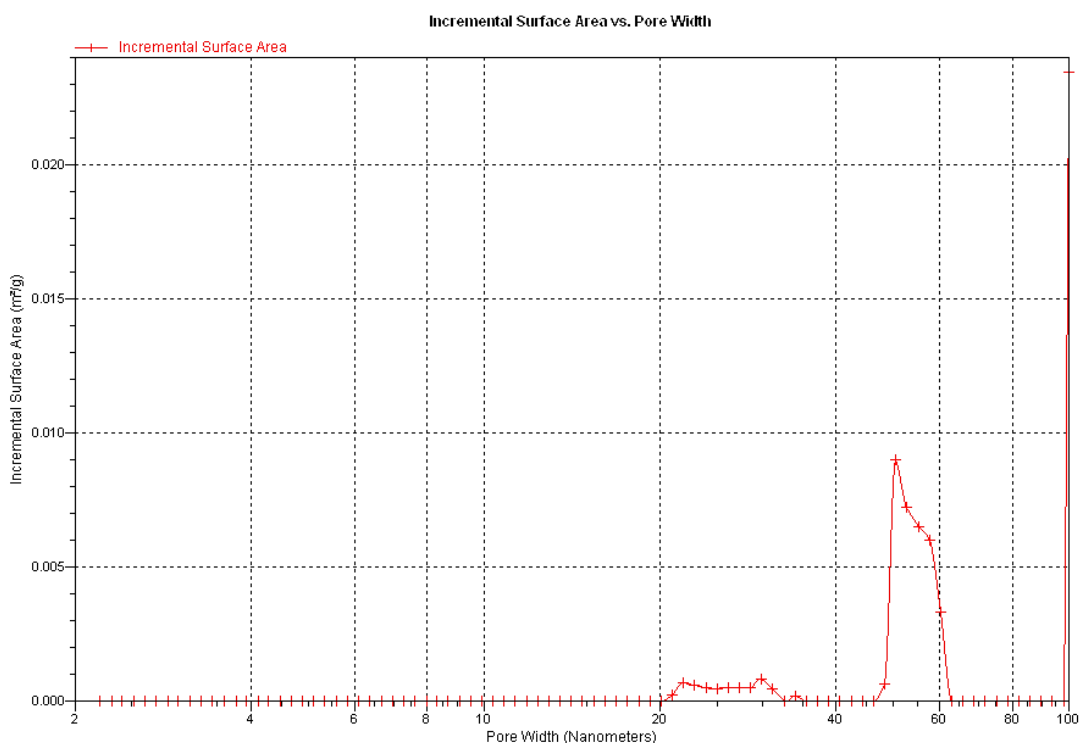
Figure A.7: Pore size distribution of oat hulls based on incremental surface area obtained from DFT; average pore diameter is around 55 nm.

A6: Calculations of Total Amount of Moisture Trapped in the Column's Void Space

The water vapor sorption by the biosorbents was performed in the column packed with a top layer and a bottom layer of glass beads with a total height of 43 cm and a middle layer of biosorbent with a height of 8 cm.

The glass beads (diameter of 3 mm) were purchased from Fisher-Scientific Inc. They are lab grade and recommended by the manufacture for chromatography/adsorption columns. It is reported in the product datasheet that it does not adsorb moisture. To verify this, the whole column (51 cm) of this work was filled with the glass beads to test if they sorb any water vapor. The humid gas (RH 100 %) at 300 kPa and room temperature was sent into the column and the RH at the outlet reached from about zero to 100 % in about 6 seconds (see figure below). The total moisture accumulation during these few seconds in the 51 cm high column fully packed with the glass beads was 0.0011 g. Thus, it is negligible compared with 24.64 g water sorbed by the same column but packed with the 8 cm height flax shives layer and the 43 cm high glass bead layer at the same experimental conditions.
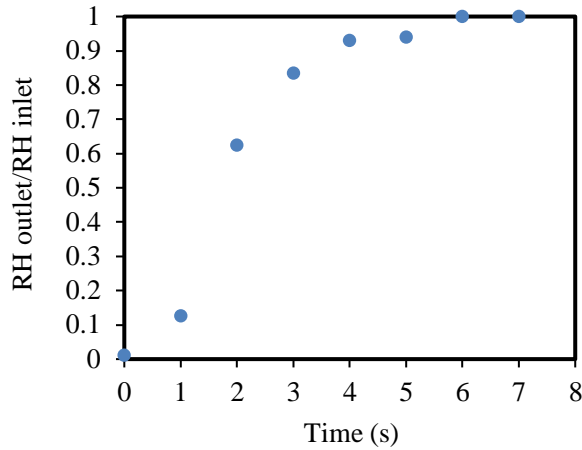
Figure A.8: Water sorption by glass beads.

In the experiment of water accumulating in the void space of glass beads, the column was only filled with glass beads with a height of 43 cm, same as that in the experiments with flax shives (8 cm high) and glass beads (43 cm high). At the beginning of the experiment, the column was pressurized to 300 kPa with the dry carrier nitrogen gas; hence, the void volume of the column was filled with the dry gas. To start the water sorption experiment, humid gas (100% RH, 0.0098 water mole fraction, nitrogen as carrier gas) was sent into the column from the top and gradually replaces the dry gas in the void space of the column until the whole void volume was filled with the humid gas. From this point until the rest of the experiment, the total amount of humid gas accumulating in the void space was constant because the same mass of gas was entering and exiting the column per unit time. In other words, the mass of gas accumulating in the void space of glass beads became constant; otherwise, the pressure of the system would increase over time, which was not the case in this work.

The bed voidage of the glass bead layer was calculated to be 0.4 according to the following correlation reported in the literature (Benyahia, F., & O'Neill, K. E.; 2005) for packed bed of spherical beads.
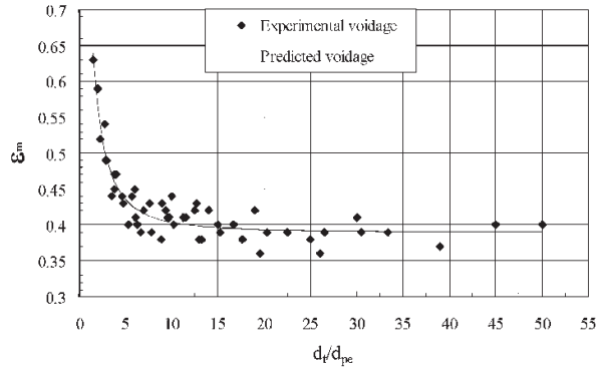
Particle shape	Correlation	Range of d_t/d_p	MCC	SE
Spherical	$0.390 + \dfrac{1.740}{(d_t/d_p + 1.140)^2}$	$1.5 \leq d_t/d_{pe} \leq 50$	0.93	0.015
Solid cylinders	$0.373 + \dfrac{1.703}{(d_t/d_{pe} + 0.611)^2}$	$1.7 \leq d_t/d_{pe} \leq 26.3$	0.96	0.016
Hollow cylinders	$0.465 + \dfrac{2.030}{(d_t/d_{pe} + 1.033)^2}$	$1.9 \leq d_t/d_{pe} \leq 14.5$	0.92	0.020
4-hole cylinders	$0.595 + \dfrac{0.082}{(d_t/d_{pe} + 1.244)^2}$	$1.9 \leq d_t/d_{pe} \leq 8.4$	0.91	0.024

Figure A.9: Bed voidage of particles with different shapes based on experimental data and correlations; d_t is column diameter and d_p is particle diameter (Benyahia, F., & O'Neill, K. E.; 2005).

The calculation results are shown in Table A 4 below. The total volume of the glass bead layer was calculated using the height and diameter of the column. The void volume in the glass bead layer was calculated using the bed voidage multiplying the total volume of the glass bead bed. Then the total amount of the humid gas (carrier plus water vapor) accumulating in this void volume was calculated using the ideal gas law. The total moles of water vapor in the void space was calculated by multiplying the total moles of gas with the molar fraction of water in the gas phase. Thus, the amount of water accumulating in the void space of glass beads was 0.0004 mol equivalent to 0.0073 g.

Table A.4: Calculations of water vapor trapped in the void space of the glass bead layer.

Diameter of the column (D)	5	cm
Heigh of glass bead (GB) layers (H)	43	cm
Bed voidage of GB layer (e)	0.4	-
Cross section area of the column (A)	0.0019	m^2
Total volume of GB layers (A*H)	0.0008	m^3
Void volume of GB layers (A*H*e)	0.0003	m^3
Total mol of gas in GB void space n=PV/RT p=300 kPa, T=24 ˚C	0.0409	mol
Mole fraction of water vapor in gas (x)	0.0098	
Mol of water vapor in void space GB (n*x)	0.0004 or 0.0073	mol g
Total mass of water vapor sorbed by Flax shives (FS) layer during the whole 40 hours of experiment	24.64	g
Percentage of water vapor accumulating in the void space of glass beads layer to that sorbed by the FS layer and the glass bead layer	0.03	%

Similar calculations were done for the water accumulation in the void space of the flax shives layer. As shown in Table A 5, the total mass of water vapor accumulating in the void space of flax shives layer was also very low (0.0011 g). Because water vapor was sorbed by flax shives over time and was transferred from the gas phase to the sorbed phase, this amount of water vapor in the void volume of the flax shives layer is at bed saturation.

Based on the above results, the total mass of water vapor accumulating in the void space of glass beads and flax shives was 0.0083 g, which was 0.03% of 24.64 g of water sorbed by flax shives (40 h) under the same experimental conditions. Thus, the amount of water accumulating in the void space of glass beads and flax shives are negligible in comparison with that sorbed by flax shives.

Table A.5: Calculations of water vapor trapped in the void space of the flax shives layer.

Height of flax shives (FS) layer	8	cm
Bed voidage FS layer	0.32	
Void volume of FS layer	5.02E-05	m^3
Mole of water in FS layer void space	5.98E-05 Or 0.0011	mol g

A7: Additional LCA Data

In this section, the original data calculated using SimaPro software regarding the LCA analysis are reported for interested readers.

Table A.9: Biosorbent production data based on the characterization method.

Impact category	Unit	Total	Natural gas, compressed	Electricity, low voltage	Operation, lorry 3.5-7.5t,
Carcinogens	kg C_2H_3Cl eq	4.2	0.001	3.84	0.38
Non-carcinogens	kg C_2H_3Cl eq	2.8	0.01	1.2	1.54
Respiratory inorganics	kg PM2.5 eq	0.35	0.003	0.04	0.31
Ionizing radiation	Bq C-14 eq	510	0	38.98	471
Ozone layer depletion	kg CFC-11 eq	3.65E-05	2.25E-12	3.36E-07	3.62E-05
Respiratory organics	kg C_2H_4 eq	0.13	E-4	6E-3	0.13
Aquatic ecotoxicity	kg TEG water	2E4	555	3.6E4	1.6E4
Terrestrial ecotoxicity	kg TEG soil	1.3E4	0.13	513	1.3E4
Terrestrial acid/nutri	kg SO_2 eq	10.71	0.05	1.03	9.7
Land occupation	m^2 org.arable	0.29	0	0.02	0.27
Aquatic acidification	kg SO_2 eq	1.88	0.03	0.44	1.4
Aquatic eutrophication	kg PO_4 P-lim	0.03	3.65E-05	0.01	0.02
Global warming	kg CO_2 eq	308	3.7	64.74	240
Non-renewable energy	MJ primary	4342	73.9	774	3494
Mineral extraction	MJ surplus	0.18	0	0.004	0.18

Table A.10: Molecular sieves production data based on the Characterization method.

Impact category	Unit	Total	Operation, lorry 3.5-7.5t	Natural gas, compressed	Electricity, low voltage	Kaolin clay	Aluminum oxide	Water, deionized, at plant
Carcinogens	kg C_2H_3Cl eq	79.8	1.96	0.001	55.6	0.002	22.2	1E-4
Non-carcinogens	kg C_2H_3Cl eq	228	7.8	0.1	17.2	0.001	203	4E-4
Respiratory inorganics	kg PM2.5 eq	3.3	1.5	0.003	0.64	3E-4	1.1	0
Ionizing radiation	Bq C-14 eq	1.9E4	2396	0	564	7.9	1.6E4	3.7
Ozone layer depletion	kg CFC-11 eq	0	2E-4	0	0	0	1E-4	0
Respiratory organics	kg C_2H_4 eq	1.1	0.64	5E-4	0.1	2E-4	0.35	0
Aquatic ecotoxicity	kg TEG water	3.1E5	81785	555	52324	21.5	1.8E5	248
Terrestrial ecotoxicity	kg TEG soil	9.1E4	6.3E4	0.13	7422	11.1	2.1E4	0.3
Terrestrial acid/nutri	kg SO_2 eq	85.1	49	0.05	15	0.008	21.2	4E-4
Land occupation	m^2 org.arable	1.8	1.4	0	0.3	0	0.16	1E-4
Aquatic acidification	kg SO_2 eq	18.8	7.1	0.03	6.3	0.002	5.3	1E-4
Aquatic eutrophication	kg PO_4 P-lim	0.37	0.08	0	0.16	0	0.1	0
Global warming	kg CO_2 eq	3212	1216	3.7	936	0.6	1054	0.03
Non-renewable energy	MJ primary	45467	1.8E5	74	11192	10	16414	0.7
Mineral extraction	MJ surplus	1320	0.9	0	0.06	4E-4	1319	1E-4

Table A.11: Biosorbent production data based on the Damage Assessment method.

Impact category	Unit	Total	Natural gas, compressed	Electricity, low voltage	Operation, lorry 3.5-7.5t
Carcinogens	DALY	1.19E-05	3.71E-09	1.08E-05	1.08E-06
Non-carcinogens	DALY	7.94E-06	2.76E-07	3.34E-06	4.32E-06
Respiratory inorganics	DALY	0.0002	2.03E-06	3.12E-05	0.0002
Ionizing radiation	DALY	1.07E-07	0	8.19E-09	9.89E-08
Ozone layer depletion	DALY	3.84E-08	2.37E-15	3.53E-10	3.8E-08
Respiratory organics	DALY	2.82E-07	1.06E-09	1.34E-08	2.68E-07
Aquatic ecotoxicity	PDF*m^2*yr	1.01	0.03	0.18	0.81
Terrestrial ecotoxicity	PDF*m^2*yr	101	0.001	4.06	97.2
Terrestrial acid/nutri	PDF*m^2*yr	11.14	0.05	1.07	10.01
Land occupation	PDF*m^2*yr	0.31	0	0.02	0.29
Aquatic acidification		-	-	-	-
Aquatic eutrophication		-	-	-	-
Global warming	kg CO_2 eq	307.5	3.7	64.7	239.1
Non-renewable energy	MJ primary	4342	73.9	774	3494
Mineral extraction	MJ primary	0.2	0	0.004	0.18

Table A.12: Molecular sieves production data based on the Damage assessment method.

Impact category	Unit	Total	Operation, lorry 3.5-7.5t	Natural gas, compressed	Electricity, low voltage	Kaolin Clay	Aluminium oxide	Water, deionized, at plant
Carcinogens	DALY	0.0002	5.5E-06	3.71E-09	0.0002	5.04E-09	6.22E-05	3.61E-10
Non-carcinogens	DALY	0.0006	2.2E-05	2.76E-07	4.83E-05	3.4E-09	0.0006	1.11E-09
Respiratory inorganics	DALY	0.002	0.001	2.03E-06	0.0004	2.08E-07	0.0008	1.59E-08
Ionizing radiation	DALY	3.92E-06	5.03E-07	0	1.18E-07	1.66E-09	3.3E-06	7.7E-10
Ozone layer depletion	DALY	3.39E-07	1.93E-07	2.37E-15	5.11E-09	9.95E-11	1.4E-07	1.17E-11
Respiratory organics	DALY	2.3E-06	1.36E-06	1.06E-09	1.94E-07	5.14E-10	7.4E-07	9.63E-12
Aquatic ecotoxicity	PDF* m^2*yr	15.7	4.1	0.03	2.6	0.001	8.9	0.01
Terrestrial ecotoxicity	PDF* m^2*yr	723.4	495	0.001	58.7	0.09	170	0.002
Terrestrial acid/nutri	PDF* m^2*yr	88.6	51	0.05	15.5	0.008	22	4E-4
Land occupation	PDF* m^2*yr	1.9	1.5	0	0.3	2.58E-05	0.2	1E-4
Aquatic acidification		-	-	-	-	-	-	-
Aquatic eutrophication		-	-	-	-	-	-	-
Global warming	kg CO_2 eq	3212	1216	3.7	936	0.64	1055	0.03
Non-renewable energy	MJ primary	45467	17775	73.9	11192	10.1	16414	0.74
Mineral extraction	MJ primary	1320	0.9	0	0.06	4E-4	1319	9.05E-05